B 540
1 MA

T 325
1 MA

# Fabrication and Property evaluation of Jute reinforced Soy flour/Starch Bio-nanocomposites

*A thesis submitted in partial fulfilment of the requirements for the degree of Doctor of Philosophy*

By

**Murshid Iman**

*Registration No. 028 of 2010*

School of Science

Department of Chemical Sciences

Tezpur University, Napaam,

Assam – 784028, India

**December, 2014**

*Dedicated to my beloved Maa & Abba*

तेजपुर विश्वविद्यालय
(केंद्रीय विश्वविद्यालय)

नपाम, तेजपुर - 784 028, असम, भारत

**TEZPUR UNIVERSITY**

( A Central University)

Napaam, Tezpur - 784 028, Assam India

# CERTIFICATE

This is to certify that the thesis entitled "*Fabrication and Property evaluation of Jute reinforced Soy flour/Starch Bio-nanocomposites*" submitted to the School of Science, Tezpur University in part fulfilment for the award of the degree of Doctor of Philosophy in Chemical Sciences is a record of research work carried out by Murshid Iman under my supervision and guidance at Department of Chemical Sciences, Tezpur University, Assam-784028. He has successfully completed the work.

He has fulfilled all the requirements for submitting the thesis for award of the degree of Doctor of Philosophy in Science.

No part of this thesis has been submitted elsewhere for award of any other degree.

(Prof. Tarun K. Maji)

Professor

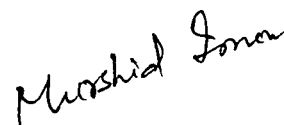Department of Chemical Sciences

Tezpur University

Assam, INDIA - 784028

# Declaration

I do hereby declare that the thesis entitled "**Fabrication and Property evaluation of Jute reinforced Soy flour/Starch Bio-nanocomposites**" is the result of investigations carried out by me in the Department of Chemical Sciences, Tezpur University, India under the guidance of Professor Tarun K. Maji, Department of Chemical Sciences, Tezpur University. In keeping with the general practice of reporting scientific opinions, due acknowledgements have been made wherever the work described is based on the findings of other investigators. It has not been submitted before for any degree or examination at this or any other University.

December, 2014

Tezpur University

Murshid Iman

# Acknowledgement

December, 2014                                                    Murshid Iman
Tezpur University
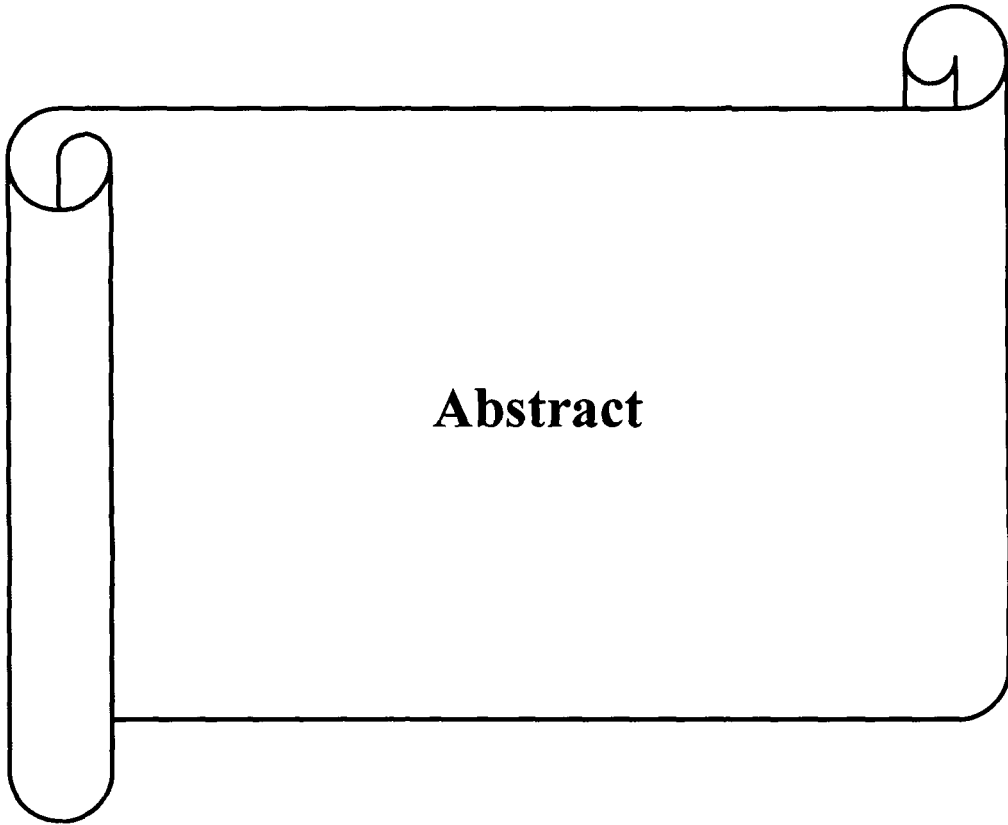
**Abstract**

## ABSTRACT

Current scenario about the conservation of natural resources and recycling has led to the renewed interest concerning biomaterials with the focus on renewable raw materials. The use and removal of traditional composite materials usually made of glass, carbon, aramid fibres being reinforced with unsaturated polyester, epoxy or phenolics are viewed critically due to increasing global awareness and demands of legislative authorities. Therefore, the growing awareness of the pressing need for greener and more sustainable technologies has focused attention on use of bio-based polymers instead of conventional petroleum based polymers to fabricate biodegradable materials with high performance. Another aspect, which is receiving more attention, is the use of alternate resource prior to the use of the conventional materials. The biocomposites prepared by using natural fibres and varieties of natural polymers such as soy flour, starch, gluten, poly(lactic acid) *etc.* have evoked considerable interest in recent years due to their eco-friendly nature. These natural polymers have some negative aspects also. Thus modification by cross linking, grafting, blending and inclusion of nanotechnology provide desired properties and widen the spectrum of applications of bio composites. Biocomposites offer modern world an alternative solution to waste-disposal problems associated with conventional petroleum based plastics. Therefore, the development of commercially viable "green products" for a wide range of application is on the rise. Moreover, using nanotechnology for the synthesis of biocomposites provide improved mechanical properties and thermal stability. In short, the use of bionanocomposites may lead healthier environment owing to its multifaceted advantages over conventional counterparts.

The thesis entitled, "Fabrication and Property evaluation of Jute reinforced Soy flour/Starch Bio-nanocomposites" consists of five chapters. It deals with the fabrication, characterization and property evaluation of some bionanocomposites.

## Chapter 1.  Introduction

This chapter consists of introduction and literature evaluation. In this chapter, the concept of polymer composite and development of bio-nanocomposite have been reviewed. Different types of polymers used in the development process have also been discussed. This chapter briefly contains explicit discussion on the structure and properties of natural polymers such as starch, soy flour (SF) and jute. The properties of different nanofillers like clay, cellulose whisker (CW), ZnO nanoparticles (ZNP), and TiO$_2$ have also been included in this chapter. Thorough literature search pertaining to bio based polymer composite has been done and reported in this chapter.

## Chapter 2.   Experimental Methods

This chapter provides a brief account of the materials used; including the syntheses of the literature reported composites, which has been employed in our subsequent investigation. Also, the characterization methods (including spectroscopic) used are discussed succinctly.

## Chapter 3.   Results and Discussions: Jute based Soy flour nanocomposites

This chapter deals with the result and discussion part. This chapter has been further sub divided into the following four sections.

*Section A: Study on the effect of crosslinker and nanoclay on jute fabric reinforced soy flour bio-nanocomposites.*

In this part of work, SF and glutaraldehyde (GA) have been used as polymer matrix and crosslinking agent respectively. The aim of this study is to prepare and evaluate the various properties of jute based crosslinked SF bio-nanocomposite. The nanocomposites have been prepared by solution induced intercalation method comprising of SF, jute, glycerol, GA, and nanoclay. Glycerol was added as a plasticizer.   The synthesized composites were characterized by various techniques such as scanning electron microscopy (SEM), transmission electron microscopy (TEM), X- ray diffractometry (XRD), Fourier transform infrared spectroscopy (FT-IR), and thermogravimetric analysis (TGA). The exfoliation of clay layers was detected both by XRD and TEM study. FT-IR study showed an interaction between clay, jute and soy flour. The percentage content of GA and nanoclay was found to have profound influence on various physical properties of the composites. The increase in the concentration of GA and nanoclay improved the thermal stability, flame retardancy, dimensional stability and most importantly the mechanical properties of the prepared composite.

*Section B: Study on the effect of cellulose whisker and nanoclay on jute fabric reinforced soy flour bio-nanocomposites.*

In this part of investigation a practical procedure for extracting CW from ordinary filter paper by acid hydrolysis has been developed. The extracted CW alone and in combination with nanoclay were used as reinforcing agents for the preparation of bio-nanocomposites based on jute fabric and GA cross-linked SF. The formation of nanocomposites was confirmed by various physicochemical and spectroscopic techniques, and by DFT studies. The results of the various analyses suggest a strong interfacial interaction

between the filler and the matrix. The properties of nanoparticle-filled SF/jute nanocomposites were compared with those of unfilled composites. Furthermore, the mechanical strength, thermal stability, flame retardancy, and dimensional stability of the filled composites were found to be better than those of the unfilled composites, allowing the processing of high-performance bio-nanocomposites.

**Section C: Study on the effect of TiO₂ and nanoclay on jute fabric reinforced soy flour bio-nanocomposites.**

In this part, preparation of bio-nanocomposites consisting of SF, jute, glycerol, GA, TiO₂ and nanoclay by solution induced intercalation method are discussed. Efforts were made to study the various properties like mechanical, thermal, flame retardancy, water resistance, biodegradation etc. of the synthesized bio-nanocomposites. The distribution of silicate layers of nanoclay within the nanocomposites was investigated by XRD and TEM studies. The structural and morphological studies like FT-IR, and SEM had clearly revealed that both TiO₂ nanoparticles and nanoclay were successfully incorporated into the composites. The mechanical and thermal properties of the nanocomposites were determined using mechanical tests and TGA, respectively. The study discloses noteworthy changes in the observed properties of the prepared bio-nanocomposites with the amount of nanofillers. Furthermore, in comparison to the unfilled nanocomposites, nanoparticles filled ones were found to exhibit much better UV-resistance, flame retarding properties, and dimensional stability. The study reveals a strong interfacial interaction between the filler and the matrix within the prepared bio-nanocomposites.

**Section D: Study on the effect of ZnO and nanoclay on jute fabric reinforced soy flour bio-nanocomposites.**

In this part, synthesis of bio-nanocomposites *via* solution induced intercalation method by using SF, jute, glycerol, GA, ZNP and nanoclay are discussed and subsequently discussed their properties. The effect of ZNP alone and in combination with nanoclay on GA crosslinked jute fabric reinforced soy flour bio-nanocomposites were studied. The successful incorporation of ZNP and nanoclays were clearly revealed by FT-IR, SEM, XRD, and TEM investigation. The thermal and mechanical properties of the nanocomposites were determined using thermogravimetric analysis and mechanical tests, respectively. Significant differences were observed according to the amount of nanofillers used as reinforcement. Furthermore, in comparison to the unfilled nanocomposites, nanoparticles filled ones were found to exhibit

much better dimensional stability, UV-resistance, and flame retarding properties. Composites containing 5% ZNP and 3% nanoclay produced maximum improvement in several physicochemical properties. Thus, ZNP in combination with nanoclay can considerably improve the physical properties of natural resources based composites. The rate of degradation increased with the increase in concentration of nanoclay in the synthesized bio-nanocomposites as adjudicated by biodegradation study.

## Chapter 4. Results and Discussions: Jute based Starch nanocomposites

This chapter embodies the results of nanofillers into jute reinforced crosslinked starch bio-nanocomposites. This chapter has been subdivided into the following four sections.

### Section A: Study on the effect of crosslinker and nanoclay on jute fabric reinforced starch bio-nanocomposites.

Bio-nanocomposites were prepared by solution induced intercalation method using starch, jute, GA, nanoclay and glycerol. The concentration of glycerol was optimized. The synthesized composites were characterized by various physicochemical and spectrochemical techniques such as FT-IR, XRD, TEM, SEM, and TGA. FT-IR study indicated an interaction between the jute, starch and clay. SEM study reveals appreciable adhesion between starch and jute surface. The extent of exfoliation of clay was studied by XRD and TEM studies. The addition of glutaraldehyde and nanoclay was found to improve the thermal stability, flame retardancy, dimensional stability and mechanical strength of the prepared composite.

### Section B: Study on the effect of cellulose whisker and nanoclay on jute fabric reinforced starch bio-nanocomposites.

In this study, we had extracted CW from ordinary Whatman filter paper by acid hydrolysis. The synthesized CWs were characterized by XRD and FT-IR. The prepared CWs alone and in combination with nanoclay have been used as reinforcing agent for the preparation of bio-nanocomposites based on jute fabric and GA crosslinked starch. The formation of nanocomposites was confirmed by various physicochemical and spectroscopic techniques. The results of various analyses indicated a strong interfacial interactions between the filler and the matrix. The properties of nanoparticles filled starch/jute nanocomposites were compared with those of nanoparticles unfilled composites. Furthermore, the mechanical strength, thermal stability, flame retardancy and dimensional stability of the filled composite

were found to improve over those of the unfilled one, suggesting the processing of high performance nanocomposites.

**Section C: Study on the effect of $TiO_2$ and nanoclay on jute fabric reinforced starch bio-nanocomposites.**

Among many nanocomposite precursors, $TiO_2$ nanopowder is increasingly being investigated because it is non-toxic, chemically inert, low cost, corrosion resistant, and has a high refractive index, UV filtration capacity and high hardness. In this section, we discuss the effect of $TiO_2$ alone and in combination with nanoclay reinforced with jute fabric and GA crosslinked starch bio-nanocomposites. Solution-induced intercalation method was adopted for the successful fabrication of the nanocomposites. The structural and morphological studies like FT-IR, XRD, TEM, and SEM clearly revealed that both $TiO_2$ and nanoclay were successfully incorporated into composite. The thermal and mechanical properties of the nanocomposites were determined using TGA and mechanical tests, respectively. Significant differences were observed according to the amount of nanofillers used as reinforcement. Furthermore, in comparison to the unfilled nanocomposites, nanoparticles filled ones were found to exhibit much better UV-resistance, dimensional stability, and flame retarding properties. The study discloses a strong interfacial interaction between the filler and the matrix within the prepared nanocomposites.

**Section D: Study on the effect of ZnO and nanoclay on jute fabric reinforced starch bio-nanocomposites.**

In this section, ZNP and ZNP in combination with nanoclays are reported as reinforcing agents for the preparation of bio-nanocomposites based on GA crosslinked starch/jute fabric. A solution-induced intercalation method were used for the fruitful fabrication of the nanocomposites. Both ZNP and nanoclay were successfully incorporated into the composite as revealed by XRD, TEM, SEM, and FT-IR. The thermal and mechanical properties of the nanocomposites were studied using thermogravimetric analysis and mechanical tests, respectively. The study revealed significant changes in the observed properties of the synthesized composites fabricated with different amount of nanofillers. Interestingly, the flame retarding properties, UV-resistance, and dimensional stability of the nanoparticle filled composites were found to be much better than those of the unfilled one. The study exhibited an intimate bonding between the filler and the matrix in the synthesized

bio-nanocomposites. Therefore, such kind of nanofillers loaded jute fabric reinforced crosslinked starch composites are eco-friendly and can find applications in newer fields.

## Chapter 5.   Conclusion and Future Scope

This chapter outlines the concluding remarks, highlights of the findings followed by future scope of the present investigation.

# CONTENTS

# List of Abbreviations and Symbols

| | |
|---|---|
| ASTM | American Society for Testing and Materials |
| Å | Angstrom |
| BNC | Bacterial Nanocellulose |
| B3LYP | Becke Lee, Yang and Parr |
| CW | Cellulose Whisker |
| cm | Centimeter |
| CSF | Cross-linked soy flour |
| cc | Cubic centimeter |
| $T_D$ | Decomposition temperature at different weight loss (%) |
| ℃ | Degree centigrade |
| DFT | Density Functional Theory |
| $\theta$ | Diffraction angle |
| DRS | Diffuse Reflectance Spectroscopy |
| DMSO | Dimethyl sulfoxide |
| D-LFT | Direct long fibre thermoplastic moulding |
| d | Distance between two plane, |
| EDX | Energy Dispersive X-ray |
| FT-IR | Fourier Transform Infrared |
| g | Gram |
| h | Hour |
| $T_i$ | Initial decomposition temperature |
| J | Jute |
| K | Kelvin |
| kV | Kilovolt |
| LOI | Limiting oxygen index |
| LDPE | Low density polyethylene |
| GA | Glutaraldehyde |
| $T_m$ | Maximum pyrolysis temperature |
| MeV | Mega electron volt |
| MPa | Mega Pascal |

| | |
|---|---|
| MFC | Microfibrillated cellulose |
| $\mu$m | Micrometre |
| mg | Milligram |
| mL | Millilitre |
| mm | Millimetre |
| MSPI | Modified Soy Protein Isolate |
| MW | Molecular weight |
| MMT | Montmorillonite |
| NCC | Nanocrystalline cellulose |
| nm | Nanometre |
| NMR | Nuclear Magnetic Resonance |
| Pt | Platinum |
| EAA | Poly(ethylene-*co*-acrylic acid) |
| PLA | Poly(lactic acid) or polylactide |
| PMMA | Poly(methyl methacrylate) |
| PE | Polyethylene . |
| PN | Polymer nanocomposite |
| PP | Polypropylene |
| lbf | Pound force |
| $R^2$ | Regression value |
| RW | Residual Weight |
| SEM | Scanning Electron Microscopy |
| $SiO_2$ | Silicon dioxide |
| SF | Soy flour |
| SP | Soy protein |
| SPC | Soy protein concentrate |
| SPI | Soy protein isolate |
| TGA | Thermogravimetry Analysis |
| $TiO_2$ | Titanium dioxide |
| UV | Ultra Violet |
| UV-vis | Ultra Violet -visible |
| VARTM | vacuum assisted resin transfer moulding |
| $\lambda$ | Wave length, |

| | |
|---|---|
| XRD | X-Ray Diffraction |
| ZnO | Zinc oxide |
| ZNP | ZnO nanoparticles |

# List of Tables

# List of Figures and Schemes

## Schemes

# Chapter 1

## *Introduction*

## 1.1. General Aspects:

With the improvement of science and technology, the people of the modern civilized world are becoming more dependent on the advanced materials. In this regard, the chemist from all over the world has contributed a lot for the modernization of our society. One of such major gift-that chemist has ever bestowed to the human society is the "polymer" or "polymeric materials" without which the world have been in a totally different position [1-7]. However, as the environmental and health effects of chemicals or chemical processes have started considering, therefore, there has been an expanding search for new materials with high performance at affordable cost in recent years [8-13]. With growing environmental and health awareness, there has been a significant focus within the scientific, industrial, and environmental communities on the use of eco-friendly materials, and subsequently the terms such as "renewable", "recyclable", "sustainable", and "triggered bio-degradable" became buzzwords, to the scientific, industry and environmental community [14-20]. The development or selection of a material to meet the desired structural and design requirements calls for a compromise between conflicting objectives. This can be overcome by resorting to multi – objective optimization in material design and selection [21-26].

The development of sustainable materials has not only been a great encouraging factor for materials scientists, but also an important provider of opportunities to improve the living standard of people around the globe. This can also provide a potential for economic improvement based on these materials even though major thrust for their use has been driven by the needs of the industrialized countries [27-31]. For example, natural fibres such as jute, sisal, hemp, pineapple, etc., whose extraction is an important process that determines the properties of fibres, can generate rural jobs since those fibres have established their potential as reinforcing fillers in many polymers, and products based on these have found increasing use on a commercial scale in recent years. Another example for the generation of jobs by agro-based materials is provided by the use of rice husk, which constitutes more than 10% of a world rice production. These examples underline not only the development of new materials, but also possible generation of additional employment through the collection, transportation and development of new materials. It is reported that increasing use of renewable materials would create or secure employment in rural areas, the distribution of which would be

The use of natural polymers was superseded in the 20$^{th}$ century as wide-range of synthetic polymers was developed based on raw materials from low cost petroleum [32, 33]. However, since 1990s, there is a simultaneous and growing interest in developing bio-based products and innovative process technologies that can reduce the dependence of fossil fuel and move to a sustainable materials basis. The main reasons for development of such material are stated below: [34]

(i) Growing awareness in declining the environmental impact of polymers or composites due to increased consciousness to eco-friendliness,

(ii) Dwindling petroleum resources, shrinking pressures for the dependence of petroleum products with increasing attention in exploiting the use of renewable materials; and

(iii) Accessibility of enriched information on the properties and morphologies of natural materials such as lignocellulosic fibres, through modern instruments at diverse levels, and hence better understanding of their structure-property relationships.

These factors have greatly increased the understanding and development of new materials termed as biocomposites.

Commodity polymer-based composite materials are now well established all over the world. Because of their high specific strength, modulus and long durability compared to conventional materials such as metals & alloys, these materials have found wide applications. However, the use of large volumes of polymer-based synthetic fibre composites in different sectors has led to disposal problems. Therefore, researchers have been looking for the reduction of such environmentally abusive materials, and triggering greater efforts to find materials based on natural resources in view of the latter's eco-friendly attributes. In parallel, researchers have also focussed their works on the processing of nanocomposites (materials with nanosized reinforcement) to enhance mechanical properties. Similar to traditional microcomposites, nanocomposites use a matrix where the nanosized reinforcement elements are dispersed. The reinforcement is currently considered as a nanoparticle when at least one of its dimensions is lower than 100 nm. This particular feature provides nanocomposites unique and outstanding properties never found in conventional composites. Bio-based nanocomposites are the next generation of materials for the future [35-41].

## 1.2. Bio-based Polymers:

Modern scenario of the polymer market is mostly occupied by synthetic polymers and most of these polymers are non-degradable. The non-degradable nature of polymer causes disturbance in the earth ecosystem. Besides this, the earth has finite resources in terms of fossil origin fuel. The escalating increase of price of petroleum based products and alternative disposal method are also a great concern. Hence, the use of fossil-based products is not sustainable. So, there is an urgent need to overcome the dependence on such conventional polymers by using bio-degradable polymers and composites. In order to produce fully renewable and biodegradable composites, both the polymeric matrix and the reinforcement must be derived from renewable natural resources such as agricultural and biological origin. Also, the use of natural polymers, which are normally biodegradable, can pave new direction in designing of newer greener composites and could widen the spectrum of applications in different sectors such as automobiles, furniture, packing and construction industrial parts.

## 1.2.1. Bio-based matrix:

"Bio" is a Greek word that means "life". Bio-based materials, therefore, refer to products that consist mainly of a substance, or substances, derived from living matter (biomass) and either occurs naturally or are synthesized. The term "bio-based materials" should not be confused with "biomaterials," which has another meaning and relates to biocompatible materials used in and adapted to medical applications, which include implantable medical devices, tissue engineering, and drug delivery systems [42]. The range of bio-based materials, from natural fibres to biopolymers, is making significant advances in petroleum-based materials industries [43]. Renewable resource-based chemicals and bio-based polymers, such as starch, 1, 3- propanediol, soy, polyol, polylactic acids, and so on, are gaining momentum in commercialization as supplements and possible replacements for petroleum based products. For decades, cellulosic polymers have played a key role in a wide range of applications, such as apparel, food, and varnishes etc. Since 1980s, an increasing number of starch polymers have been introduced, which have made them one of the most important groups of commercially available bio-based materials.

Bio-based materials, are commonly thought to be greener alternatives than their petroleum-based counterparts, which are nonbiodegradable, have potentially devastating effects on animal and ocean life, and for the most part, have an inherently

toxic life cycle from their production through their final disposal. Bio-based materials frequently are labelled as produced from ''renewable'' resources, although this term is used loosely because biomass production requires non-renewable inputs, which include fossil fuels, and ties up other finite resources such as land and water. The claim that bio-based materials are friendlier to the environment than their petroleum-based counterparts is being scrutinized closely [34].

### 1.2.1.1. Starch Polymers:

Starch is one of the most exciting and promising raw materials for the production of biodegradable products. It is the major polysaccharide reserve material of photosynthetic tissues and of many types of plant storage organs such as seeds and swollen stems. The primary crops used for its production consist of potatoes, corn, wheat and rice. In all of these sources, starch is produced in the form of granules, which vary in size and somewhat in composition based on the resources. Starch granule is composed of two main polysaccharides, amylose and amylopectin with some minor components such as lipids and proteins. Amylose is linear polymer of $(1\rightarrow 4)$-linked $\alpha$-D-glucopyranosyl units with some slight branches by $(1\rightarrow 6)$-$\alpha$-linkages (Figure 1.1). Amylose can have a molecular weight between $10^4$ and $10^6$ g mol$^{-1}$, with solubility in boiling water [44, 45].
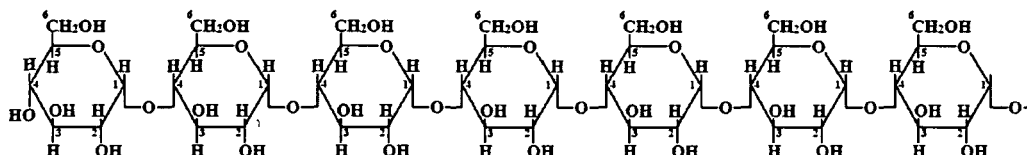


**Figure 1.1.** Structure of amylose.

Amylopectin is a highly branched molecule composed of chains of $\alpha$-D-glucopyranosyl residues linked together mainly by $(1\rightarrow 4)$-linkages but with $(1\rightarrow 6)$-linkages at the branched points. Amylopectin consists of hundreds of short chains of $(1\rightarrow 4)$-linked $\alpha$-D-glucopyranosyl interlinked by $(1\rightarrow 6)$-$\alpha$-linkages (Figure 1.2). It is an extremely large and highly branched molecule with a molecular weights ranging from $10^6$ to $10^8$ g mol$^{-1}$. Therefore, it is insoluble in boiling water, in body, both fractions are readily hydrolyzed at the acetal link by enzymes. Amylases attack $\alpha$-(1-4)-link of starch while the $\alpha$-(1-6)-link of amylopectin is by enzyme glucosidases.

*(Glucose α(1 - 4) - glucose)*
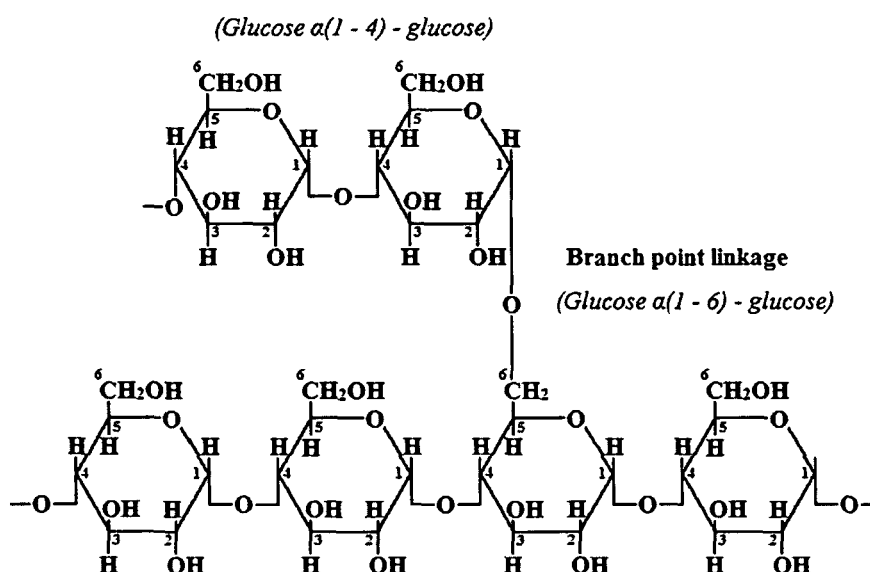


Figure 1.2. Structure of amylopectin.

The crystallinity of starch granules is attributed mainly to the amylopectin and not to amylose, which although linear, presents in a conformation that hinders its regular association with other chains [46, 47].

Starch has received significant interest during the past two decades as a biodegradable thermoplastic polymer. Starch offers an attractive and cheap alternative in developing degradable materials. Starch is not truly thermoplastic as most synthetic polymers. However, it can be melted and made to flow at high temperatures under pressure and shear. It has been widely used as a raw material in film production because of increasing prices and decreasing availability of conventional film-forming resins based on petroleum resources. Starch films possess low permeability and are thus potential materials for food packaging. Starch is also useful for making agricultural mulch films because it degrades into harmless products when placed in contact with soil microorganisms [48, 49].

By itself, starch is a poor alternative for any commodity plastic because, it is mostly water soluble, difficult to process, and brittle. Therefore, research on starch includes exploration of its water adsorptive capacity, the chemical modification of the molecule, its behaviour under agitation and high temperature, and its resistance to thermo mechanical shear. Although starch is a polymer, its stability under stress is not high. Above 150 °C, the glucoside links start to break, and after exceeding 250 °C the starch grain endothermally collapses. At low temperatures, a phenomenon known as

5

retrogradation is observed. This is a reorganization of the hydrogen bonds along with alignment of the molecular chains during cooling. In extreme cases below 10 °C, precipitation is observed. Thus, though starch can be dispersed into hot water and cast as films, the above phenomenon causes brittleness in the film [50].

Plasticised starch is essentially starch that has been modified by the addition of plasticisers to enable processing. Thermoplastic starch is plasticised to completely destroy the crystalline structure of starch to form an amorphous thermoplastic starch. Thermoplastic starch processing involves an irreversible order-disorder transition termed as gelatinisation. Starch gelatinisation is the disruption of molecular organization within the starch macromolecules and this process is affected by starch-water interactions. Most starch processing involves heating in the presence of water and some other additives; like sugar and salt to control the gelatinisation in the food industry, and glycerol as a plasticiser for biodegradable plastics applications. Most of the commercial researches on thermoplastic starches involve the use of modified starches and or blends with additives and other appropriate polymers for its application as biodegradable plastics [51]. The starch molecule has two important functional groups, the –OH group that is susceptible to substitution reactions and the C–O–C bond that is susceptible to chain breakage. The hydroxyl group of glucose has a nucleophilic character. To obtain various properties, starch can be modified through its –OH group. One example is the reaction with silane to improve its dispersion in polyethylene [52]. Crosslinking or bridging of the –OH groups changes the structure into a network subsequently increases the viscosity, reduces water retention and increases its resistance to thermo mechanical shear.

One of the approaches to modify this starch is by acetylation to from starch acetate. Acetylated starch do have advantages as a structural fibre or film-forming polymer as compared to native starch. The acetylation of starch is a well-known reaction and is relatively easy to synthesize. Starch acetate is considerably more hydrophobic than starch and has been shown to have better retention of tensile properties in aqueous environments. The degree of acetylation is easily controlled by trans esterification, allowing polymers to be produced with a range of hydrophobicities. Starch has been acetylated [with a high content (70%) of linear amylose] and its enzymatic degradation has been studied. Apart from acetylation and esterification, some other modification of starch such as carbonilation of starch with phenyl isocyanates, addition of inorganic esters to starch to produce phosphate or nitrate starch

esters, production of starch ethers, and hydroxypropylation of starches via propylene oxide modification has been performed. Generally all these modifications involve hydroxyl group substitution on the starch that will lower gelatinisation temperatures, reduce retrodegradation and improve flexibility of final product [46].

Starch has been used for many years as an additive to plastic for various purposes. Starch was added as a filler [53] to various resin systems to make films that were impermeable to water but permeable to water vapour. The use of starch as a biodegradable filler in LDPE was reported [54]. A starch-filled polyethylene film was prepared which became porous after the extraction of the starch. This porous film could be readily invaded by microorganisms and rapidly saturated with oxygen, thereby increasing polymer degradation by biological and oxidative pathways [55]. Otey *et al.* in a study on starch-based films, found that a starch– polyvinyl alcohol film could be coated with a thin layer of water-resistant polymer to form a degradable agricultural mulching film [51]. Starch-based polyethylene films were formulated and containing up to 40% starch, urea, ammonia and various portions of low density polyethylene (LDPE) and poly(ethylene-*co*-acrylic acid) (EAA). The EAA acted as a compatibilizer, forming a complex between the starch and the PE in the presence of ammonia. The resulting blend could be cast or blown into films, and had physical properties approaching to those of LDPE [56, 57].

Additionally, crosslinking of starch may be induced by the addition of organic/inorganic esters, hydroxyethers, aldehydes and irradiation. Kulicke *et al.* examined solution phase crosslinking of starch with epichlorohydrin and trisodium trimetaphosphate [58]. Jane *et al* examined the crosslinking of starch/zein cast films for improving water resistance [59]. The possibility of chemically combining starch or starch-derived products with commercial resins in such a manner that the starch would serve as both filler and a crosslinking agent may provide a possible approach for incorporating starch into plastics.

Commercial starch polymer based products are provided in Table 1.1 given below:

**Table 1.1.** Starch polymer based products and suppliers [46, 60].

| Base Polymer | Source Type | Advantages | Disadvantages | Potential Applications | Manufacturer (Product name) |
|---|---|---|---|---|---|
| Starch | Renewable | Low cost, Fast bio-degradation | Poor mechanical properties, Hydrophilicity | Foams, Films and bags, Moulded items, Starch-based composite | Novament (Mater-bi™), Biotec (Bioplast®, Bioflex®, Biopur®), National Starch (ECO-FOAM), Buna Sow Leuna (Sconacell), Starch Tech (ST1, ST2, ST3), Novon (Poly-NOVON®) |

One of the first starch based products was developed probably by the National Starch in the brand name ECO-FOAM™ and used as packaging material. ECO-FOAM™ materials are derived from maize or tapioca starch and include modified starches. This relatively short-term, protected-environment packaging use is ideal for thermoplastic starch polymers. National Starch now has additional thermoplastic starch materials, blends and speciality hydrophobic thermoplastic starches for a range of applications including injection moulded toys, extruded sheet and blown film applications [61]. Novament has been developing thermoplastic starch based polymers since 1990. Mater-Bi™ polymers are based on starch-blend technologies and product applications include biodegradable mulch films and bags, thermoformed packaging products, injection moulded items, personal hygiene products and packaging foam [62].

Similarlly, Biotech GmbH produces Bioplast™ based on starch for a wide range of applications including accessories for flower arrangements, bags, boxes, cups, cutlery, edge protectors, golf tees, horticultural films, mantling for candles, nets, packaging films, packaging materials for mailing, planters, planting pots, sacks, shopping bags, straws, strings, tableware, tapes, technical films, trays and wrap films [63]. Recently Plantic Technologies Ltd produced soluble Plantic™ thermoformed trays for confectionery packaging [46].

### 1.2.1.2. Soy Protein (SP):

Proteins are abundant in nature and widely available in various forms in plants (soy, corn, whey protein, and wheat gluten) and in animals (collagen, gelatin). SP has been used to develop bioplastics for various applications [64]. Among all those proteins, soy protein is one of the less expensive bio-polymers abundant worldwide. It was first introduced by Henry Ford in automobile manufacturing as alternating source for plastics and fibres [65].

**Table 1.2.** Typical composition of soy protein preparation.

| | Component (%) | | | | |
|---|---|---|---|---|---|
| | Protein | Fat | Fibre | Ash | Carbohydrates |
| Soy flours | 56 | 1.0 | 3.5 | 6.0 | 33.5 |
| Concentrates | 72 | 1.0 | 4.5 | 5.0 | 17.5 |
| Isolates | 96 | 0.1 | 0.1 | 3.5 | 0.3 |

Its purification process is benign and environment friendly. This protein can also be used as resin due to its ability to form ductile and viscous polymers. Soy protein is generally available in four different forms as soy protein isolate (SPI), soy protein concentrate (SPC), soy flour (SF), and soy meal. Chemically, SPI contains 90% protein and 4% carbohydrates, SPC contains 70% protein and 18% carbohydrates, SF, which requires less purification, contains about 55% protein and 32% carbohydrate and finally soy meal has 40% protein. Soy protein is globular, reactive and often water soluble, as compared to helical or planar, non-reactive and water resistant synthetic polymers [66, 67]. The typical compositions of these different sources are given in the Table 1.2.

Soy protein isolate and soy concentrate are most widely used in design and engineering of biodegradable plastics. This protein has many side groups like $-NH_2$ and

–OH, in which crosslinking reactions are easy to perform. Generally soy proteins are categorised on the basis of their sedimentation rate in fractional ultracentrifugation. Approximately 90% of the proteins in soybeans are globulins, and exist as dehydrated storage proteins. The major components are classified according to their sedimentation properties and are listed in Table 1.3. Based on Svedberg numbers (S), soy protein has mainly four fractions that include 2S, 7S, 11S, and 15S [68]. The main constituents of soy protein, the 7S fraction, is also called conglycinin and it comprises of many important enzymes and storage proteins. The 7S fraction is about 30% of the total soy protein by weight. The 11S fraction comprises about 52% of the total soy protein and is usually called glycinin [69]. The other two minor fractions are present as 2S (8%) and 15S (5%).

**Table 1.3.** Approximate distribution of the major components of soy proteins.

| Fraction | Content | Principle components |
| --- | --- | --- |
| 2S | 8 | Trypsin inhibitor, Cytochrome |
| 7S | 35 | Lipoxygenase, Amylase, Globulins |
| 11S | 52 | Globulins |
| 15S | 5 | Polymers |

It can be seen that storage proteins, 7S (conglycinin) and 11S (glycinin) are the principal components of soy protein. 7S has a quaternary structure and is highly heterogeneous according to Kineslla. Its principal component is beta-conglycinin, a sugar containing globulin. The fraction also comprises of enzymes (beta-amylase and lipoxygenase) and hemagglutinins. 11S fraction consists of glycinin, the principal protein of soybeans. 11S has also a quaternary structure and is composed of three acidic and three basic subunits with isoelectric points between pH 4.7–5.4 and 8.0–8.5, respectively. The polypeptides in native glycinin are tightly folded and stabilized via intermolecular disulphide bonds. The ability of soy proteins to undergo association–dissociation reactions under known conditions is related to their functional properties and particularly to their texturization. The major amino acid contents of soy protein are given in Table 1.4. It can be seen that soy protein consists mainly of the acidic amino acids (aspartic and glutamic acids) and their corresponding amides (asparagine and glutamine), non-polar amino acids (alanine, valine and leucine), basic amino acids (lysine and arginine), uncharged polar amino acid (glycine) and approximately 1% of

cystine. High proportions of glutamic and aspartic acid are found in soy proteins making it more hydrophilic than any other proteins. The sulfhydryl groups and disulfide bonds of 7S globulin are zero and two per molecule, respectively. In contrast, 11S globulin has two sulfhydryl groups and 20 disulfide bonds per molecule. The presence of various polar groups and reactive amino acids such as cystine, arginine, lysine, and hystidine in the structure of soy protein enable them for convenient chemical and physical modifications, thereby improving the tensile and .thermal properties of the biopolymer [70].

**Table 1.4.** Amino acid contents of some protein sources used for bioplastics.

| Amino acid | Amino acid content mol-% |
|---|---|
| Non-polar | |
| Valine | 5.00 |
| Leucine | 8.10 |
| Isoleucine | 4.80 |
| Phenylalanine | 5.20 |
| Methionine | 1.30 |
| Tryptophan | 1.30 |
| Alanine | 4.20 |
| Proline | 5.10 |
| Cystine | 1.30 |
| Glycine | 4.10 |
| Polar | |
| Serine | 5.20 |
| Threonine | 3.80 |
| Tyrosine | 3.80 |
| Acid residues | |
| Glutamic acid | 19.00 |
| Aspartic acid | 11.50 |
| Basic residues | |
| Lysine | 6.20 |
| Arginine | 7.50 |
| Histidine | 2.60 |

## 1.2.2. Reinforcing Biofibres:

In 1908, cellulose fibre reinforced phenolics composites were made and later it was extended to urea and melamine. In 1940, fibre reinforced composites received the commodity status with glass fibre in unsaturated polyesters. Composites are finding use in different fields ranging from guitars, tennis racquets, cars, microlight aircrafts and electronic components to artificial joints. Because of growing environmental awareness, the use of traditional composites, usually made of glass, carbon or aramid fibres being reinforced with epoxy, unsaturated polyester resins, polyurethanes, or phenolics, are considered unfavourably. The most significant disadvantage of traditional composite materials is the problem of suitable disposal after the end of life time. In the present polymer technology, it is essential that every material should exclusively be adapted to the environment. New fibre reinforced materials called biocomposites were created by implanting natural reinforcing fibres, e.g. jute, flax, hemp, ramie, etc. into bio based polymer matrix derived from virgin derivatives of cellulose, starch, lactic acid, etc [60, 71-74]. This is a challenging field of research with unlimited future prospects. The researches in this area are being pursued with great interest to develop newer bio composites.

Over the last few decenniums biofibre composites have been undergoing a notable transformation. These materials have become more and more satisfactory as new compositions and improvements have been intensively researched, developed and subsequently applied. The depletion of fossil fuel made biocomposites pointedly important and biocomposites have become engineering materials with a very diverse range of properties. The growth of natural fibre-thermoplastic composites, products that are progressively used in building materials and automotive interior parts, has been well recognized. These products have a number of key advantages in comparison with synthetic fibre-reinforced composites which includes low weight, low cost, lack of abrasiveness during processing, and the wide availability of the reinforcing fibres (wood or agricultural fibre) from renewable resources. This century could be called the cellulosic century, because more and more renewable plant resources are being discovered. It has been generally stated that natural fibres are renewable and sustainable, but they are in fact, neither. The living plants are renewable and sustainable from which the natural fibres are taken, but not the fibres themselves [75-80].

The plants, from which the natural fibres produce, are classified as primary and secondary depending on their utilization. Primary plants are those grown for their fibre

content while secondary plants are plants in which the fibres are produced as a by-product. Jute, hemp, kenaf, and sisal are examples of primary plants where as pineapple, oil palm and coir are the examples of secondary plants. Table 1.5 shows the main fibres used commercially in composites, which are now produced throughout the world [81]. There are six elementary types of natural fibres. The fibre classifications are shown in Table 1.6. The natural fibres are lignocellulosic in nature which is generally the most ample renewable biomaterial of photosynthesis on earth. In terms of mass units, the net primary production of natural fibre per year is estimated to be $2 \times 10^{11}$ tons as compared to $1.5 \times 10^8$ tons for synthetic polymers [82]. Lignocellulosic materials are widely distributed in the biosphere in the form of plants, trees (wood), and crops. Cellulose, in its several forms, constitutes approximately half of all polymers utilized in the industry worldwide.

**Table 1.5.** Commercially major fibre sources.

| Fibre source | World production ($10^3$ ton) | Fibre source | World production ($10^3$ ton) |
|---|---|---|---|
| Bamboo | 30,000 | Coir | 100 |
| Jute | 2300 | Ramie | 100 |
| Kenaf | 970 | Abaca | 70 |
| Flax | 830 | Grass | 700 |
| Sisal | 378 | Hemp | 214 |
| Sugar cane bagasse | 75,000 | | |

**Table 1.6.** Different types of fibre and their example.

| Fibre Type | Example |
|---|---|
| bast fibres | jute, flax, hemp, ramie and kenaf |
| leaf fibres | abaca, sisal and pineapple |
| seed fibres | coir, cotton and kapok |
| core fibres | kenaf, hemp and jute |
| grass and reed fibres | wheat, corn and rice |
| all other types | wood and roots |

## 1.2.2.1. Jute fibre:

Jute (*Corchorus capsularis L.*) is an important tropical crop and grows in some of Asian countries like India, Bangladesh, China, Thailand, Myanmar, Nepal and Indonesia. It occupies the second place in terms of world production levels of cellulosic fibres. Jute, a rainy season crop, grows best in warm and humid climates with temperature between 24 °C to 37 °C. India, China, and Bangladesh are the main producers of jute. To grow jute, farmers scatter the seeds on cultivated soil. About four months after planting, harvesting begins. The plants are usually harvested after they bloom, but before the blossoms go to seed. Jute plants are thinned out when they are about 6 inches (15 centimetres) tall. Jute is graded or rated according to its colour, strength, and fibre length. There are two types of Jute fibre: (a) White Jute (*Corchorus capsularis*) and (b) Tossa Jute (*Corchorus olitorius*). The fibres are off-white to brown and 3 to 15 feet (0.9 to 4.5 meters) long. Jute is pressed into bales for shipment to manufacturers. Jute grows in alluvial soils and can survive in heavy flooding. It will only grow in areas with high temperatures, sand or loam soils, and having annual rainfall over 1,000 millimetres. Large-scale jute cultivation is virtually confined to northern and eastern Bengal, mostly in the floodplains of the Ganges and Brahmaputra Rivers. More than 97 % of the world's jute is produced in Asia, including 65 % in India and 28 % in Bangladesh. Jute has played a vital role in the socioeconomic development in some of these countries [83]. Jute and its products have played an important role in this country's work force. It is one of the inexpensive lignocellulosic fibres and is currently the bast fibre with the highest production volume.

### 1.2.2.1.1. Chemical constituents and structural aspects of Lignocellulosic fibre:

The major constituents of lignocellulosic fibres are cellulose, hemicellulose and lignin. The amount of cellulose, in the bio-fibres can vary depending on the species and the age of the plant or species. Cellulose is better described as a high molecular weight homopolymer of $\beta$-1,4-linked anhydro-D-glucose [84] units in which every unit is corkscrewed 180° with respect to its neighbours, and the repeat segment is frequently taken to be a dimer of glucose, known as cellobiose (Figure 1.3) [85]. It contains alcoholic hydroxyl groups. These hydroxyl groups form intramolecular hydrogen bonds inside the macromolecule itself and among other cellulose macromolecules as well as with hydroxyl groups from the air. Therefore, all of the natural fibres are hydrophilic in nature [86].

14
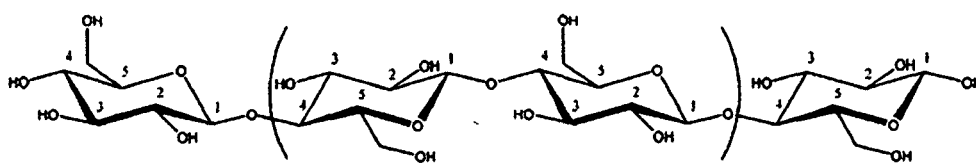
**Figure 1.3:** Structure of cellobiose.

Even though the chemical assembly of cellulose from different natural fibres is the same, the degree of polymerization shows a discrepancy. The mechanical properties of a fibre are significantly related to degree of polymerization. Among various natural fibres "Bast fibres" generally show the highest degree of polymerization. Approximately, the degree of polymerization for bast fibre is around 10000 [87].

Lignin is a phenolic compound, commonly resistant to microbial degradation, but the pre-treatment of fibre renders it susceptible to the cellulose enzyme [88, 89]. The actual chemical nature of the primary component of biofibre, the lignin, still remains vague [90-91]. No method has so far been available by which it is possible to isolate the lignin in the native state from the fibre. Hence the exact structural formula of lignin in natural fibre has yet not been established although most of the functional groups and units which make up the lignin molecule have been identified. It is highly unsaturated or aromatic in nature due to the high carbon and low hydrogen content. It is characterized by its related hydroxyl and methoxy groups. Ethylenic and sulfur-containing groups have also been found in lignin [92]. The chemical environment of lignin in lignocellulosic materials has been a challenging subject of research [93, 94]. Polysaccharides such as cellulose and hemicellulose are laid down first during synthesis of plant cell walls and lignin fills the spaces between the polysaccharide fibres, cementing them together. Thus it works as a structural support material in plants. This lignification process causes hardening of cell walls, and the carbohydrate is protected from chemical and physical damage. The topology of lignin from different sources may be different but has the same basic composition. Lignin is believed to be linked with the carbohydrate moiety though the exact nature of linkages in biofibre is not well known [95]. One of the linkages is alkali sensitive and formed by an ester-like combination between lignin hydroxyls and carboxyls of hemicellulose uronic acid. The other ether-type linkage occurs through the lignin hydroxyls combining with the hydroxyls of cellulose. The lignin, being poly functional, exists in combination with more than one neighbouring chain molecule of cellulose and/or hemicellulose, making a crosslinked structure. The lignocellulosic material possesses many active functional

15

groups [96] like primary and secondary hydroxyls, carbonyls, carboxyls (esters), carbon-carbon, ether, and acetal linkages. Like all the lignocellulosic fibre, the physical and chemical properties of jute fibre is also depend on the three chemical components viz. cellulose, hemicellulose and lignin. The chemical composition and structural parameters of jute fibres are represented in Table 1.7.

**Table 1.7.** Chemical composition and structural parameters of jute [86, 91, 95, 96].

| Chemical composition | wt. (%) | Chemical composition | wt. (%) |
|---|---|---|---|
| Cellulose | 61-71.5 | Pectin | 0.2 |
| Lignin | 12-13 | Wax | 0.5 |
| Hemicellulose | 13.6-20.4 | Moisture content | 12.6 |

*1.2.2.1.2. Properties of jute:*

The lignocellulosic fibres reveal substantial deviation in diameter along with the length of individual fibres. The qualities and properties of lignocellulosic fibres generally depend on features like size, maturity, as well as processing methods implemented for the extraction of fibres. The modulus of fibre reduces with proliferation in diameter. The internal structure and chemical composition of fibres are responsible for the properties such as density, electrical resistivity, ultimate tensile strength, initial modulus, etc. The strength and stiffness of fibre is generally correlated with the angle between axis and fibril of the fibre, *i.e.*, the smaller this angle, the higher the mechanical properties. The chemical constituents and complex chemical structure of natural fibres also affect the properties significantly. Because of the very complex structure of lignocellulosic fibres, it is not possible to correlate the fibre strength exactly with cellulose content and microfibrillar angle. However, individual fibre properties can vary extensively depending on the source, separating technique, age, moisture content, speed of testing, etc. The lignin content of the fibres influences its structure [87], properties [75, 87, 95-106] and morphology [107]. The waxy substances of natural fibres generally influence the fibre's wet ability and adhesion characteristics [108, 109].

Jute is 100% bio-degradable and recyclable and thus environmental friendly. It has high tensile strength, low extensibility, and ensures better breathability of fabrics. Therefore, jute is very suitable in agricultural commodity bulk packaging. It helps to make best quality industrial yarn, fabric, net, and sacks. It is one of the most versatile

natural fibre that has been used for packaging, textiles, non-textile, construction, and agricultural sectors. Bulking of yarn results in a reduced breaking tenacity and hence an increased breaking extensibility when blended as a ternary blend. Unlike the other fibre *e.g.* hemp, jute is not a form of *Cannabis*. Jute stem has very high volume of cellulose and hence it also can save the forest and meet cellulose and wood requirement of the world. The best varieties of Jute are *Bangla Tosha - Corchorus olitorius (Golden shine)* and *Bangla White - Corchorus capsularis (Whitish Shine)*. Raw Jute and jute goods are interpreted as Burlap, Industrial Hemp, and Kenaf in some parts of the world. The best source of Jute in the world is the Bengal Delta Plain, which is occupied by Bangladesh and India [110]. Image of jute crops grow in India is shown below (Figure 1.4):



**Figure 1.4.** Image of jute crops.

*The physical properties of jute are given below:*

➤ The cells of jute fibre vary from 0.05-0.19 inch in length and $20\text{-}22\mu m$ in thickness.

➤ The Aspect Ratio (L/D) (mm) is about 152-365.

➤ Externally the fibre is smooth and glossy.

➤ It has specific gravity of 1.29. It is a very good insulator of heat and electricity.

➤ It is highly hygroscopic fibre. Water absorption by jute takes place in two phases, i. e., molecular phase and capillary phase.

➤ The tenacity of jute varies from 3.5-4.5 (g/denier) at 4 cm test length. The tenacity may be as high as 6-7 g/denier.

➤ Its breaking elongation under normal atmospheric condition is 1-1.2%.

*The chemical properties of jute are:*

➤ In chemical composition, jute is different from linen and cotton. It is composed of a modified form of cellulose called lignocellulose (*bastose*).

➤ It develops yellow colour by iodine and sulphuric acid.

➤ It is more sensitive to the action of chemicals, than cotton or linen. Therefore, it cannot be bleached on treatment with alkalis. Bleaching powder weakens, and breaks down the fibre significantly.

➤ The use of sodium silicate, soda ash, or sodium hydroxide is not recommended for treatment of jute. Lime water makes the fibre brittle. Ammonia provides a harsh feel and decreases its lustre.

### *1.2.2.1.3. Cost aspects, availability & sustainable development:*

The world's supply of petroleum resources is being dwindling; the demand for sustainable and renewable raw materials is on high. So the use of available natural fibres has become an unavoidable task for scientists and industries. In order to confirm a reasonable profit to the farmers, non-traditional outlets have to be explored for natural fibres. One of such promising way is the natural fibre reinforced polymer composites. The price for lignocellulosic fibres which are viable for different applications differs a lot depending on the changed economy of the countries where such fibres are widely available [91]. It is one of the cheapest natural fibres in the world. In recent years, prices of natural fibres were not stable, especially for flax fibres [101], which is about 30% more expensive than glass fibres. For these economic reasons, a substitution of glass fibres by natural fibres seems not to be easily realized. However, lignocellulosic fibres offer several advantages; the most fascinating aspect about natural fibres is their positive environmental impact. They also present safer handling and working conditions compared to synthetic reinforcements. The worldwide availability is an additional factor.

### 1.2.2.2. Surface treatments:

The fabrication of polymer composites containing lignocellulosic fibres will often result in fibres physically spread in the polymeric environment. However in majority of cases, poor adhesion and subsequently insufficient mechanical properties result. Hence, surface treatment of the lignocellulosic fibres is playing a dynamic role.

Generally, surface treatment of lignocellulosic fibres is not mandatory to develop the bonding for the synthesis of biodegradable composites, in view of the analogous chemical scenery of both the biofibre and biopolymer matrix, which have a hydrophilic environment, unlike the situation with commodity polymers, which have an affinity to be hydrophobic. However, to improve many specific aspects of biodegradable composites, such as providing superior adhesion and diminished moisture sensitivity, surface treatment can be useful. Although better adhesion between the bio polymer matrix and lignocellulosic fibres is contributed by the similar polarities of the two materials, these results in an increase in water absorption of the composite. Hence, these fibres need appropriate surface treatments.

Different surface treatment methods namely chemical, physical, or combination of physical–chemical and physical–mechanical are employed. These modification methods are different for different types of fibres [86]. Dewaxing and alkali treatments are generally done for surface modification of jute fabrics. Jute is first treated with 2% liquid detergent at 70 °C, followed by washing with distilled water and finally dried in oven. The washed fabrics are then dewaxed by treatment with a mixture of alcohol and benzene (1:2) for 72 h at 50 °C, washed with distilled water and finally dried. The fabrics were then treated with 5% ($^w/_v$) NaOH solution for 30 min at room temperature, and washed with distilled water for several times to leach out the absorbed alkali. The fabrics were then kept immersed in distilled water for overnight and washed repeatedly to avoid the presence of any traces amount of alkali. The alkali treated fabrics were dried in an oven and stored at ambient temperature in a desiccator [111]. This treatment has helped to improve its interaction with the matrix materials, and increase adhesion of fibres with the matrix through surface roughness of fibre, leading to increased strength or other properties of composites through higher fibre incorporation and possibly providing greater durability of the composites.

A variety of moulding methods can be used according to the end-item design requirements. The principal factors impacting the methodology are the nature of the chosen matrix and reinforcement materials. Another important factor is the gross quantity of material to be produced. Large quantities can be used to justify high capital expenditures for rapid and automated manufacturing technology. Small production quantities are accommodated with lower capital expenditures but higher labour and tooling costs at a correspondingly slower rate. Based on the type of resins, the fabrication process may be of two types. The processes used for thermosetting resins

are: compression moulding, hand lay up, resin transfer moulding, vacuum assisted resin transfer moulding (VARTM), pultrusion etc. The processes for thermoplastic resins include injection moulding, extrusion moulding, needle punched, direct long fibre thermoplastic moulding (D-LFT) etc.

### 1.2.2.3. Jute reinforced Bio-composites:

Jute is one of the most common bast fibres having high tensile modulus and low elongation at break. If the low density (1.45 g/cm$^3$) of jute fibre is taken into consideration, then its specific stiffness and strength are similar to the respective quantities of glass fibre [112-114]. The specific modulus of jute fibre is better than glass fibre, and on a modulus per cost basis, jute is far superior. There are many reports that use jute as reinforcing agent for the synthesis of biodegradable composite. Mitra et al. [115] have reported the studies on jute-reinforced composites, their limitations and some solutions through chemical modifications of fibres. Flexural strength, flexural modulus and the dynamic strength of chemically modified jute-poly (propylene) composites have been found to increase by 40%, 90% and 40% respectively compared to unmodified jute- poly (propylene) composites [116] due to the chemical modification of jute with maleic anhydride grafted polypropylene. The effect of different additives on performance of biodegradable jute fabric-Biopol composites has been reported [117]. Biopol biodegradable polyester is a thermoplastic which has gained industrial consideration since it has a tensile strength comparable to that of isotactic poly (propylene) and is fully biodegradable. In absence of any additive, both tensile strength and bending strength of composites are found to increase around 50% whereas elongation at break reduced only 1% as compared to pure Biopol sheet. In order to study the effects of additives, the jute fabrics were soaked with several additive solutions of different concentrations. During such treatments dicumyl peroxide was used as the initiator. The effects of various surface modifications of jute on performance of biodegradable jute-Biopol composites as prepared by hot-press technique have been reported by Mohanty et al. [111, 118]. The surface modification of jute, involving dewaxing, alkali treatment, cyanoethylation and grafting are made with the aim to improve the hydrophobicity of the fibre in order to obtain decent fibre-matrix adhesion in the resulting composites. Differently chemically modified jute yarn-Biopol composites [107] showed maximum enhancement of mechanical properties like tensile strength, bending strength, impact strength and bending-modulus by 194%, 79%, 166%

20

and 162% respectively in comparison to pure Biopol. With 10 and 25% acrylonitrile grafted yarns, the tensile strength of composites was enhanced by 102 and 84 % in comparison to pure Biopol. Thus with the increase of grafting percent in yarn, the mechanical properties of the composite were found to decline. The composites made from alkali treated yarns produced better mechanical properties than dewaxed and grafted yarns. Orientation of jute yarn played an important role on the properties. The enhancement of mechanical properties of composites were noticed only when the properties of composites were measured along the yarn wrapping direction. Unlike jute yarn, the enhancement of mechanical properties of jute fabric-Biopol composites did not show any variation with the direction of measurement of properties [119]. An enhancement in more than 50% tensile strength, 30% bending strength and 90% impact strength of resulting composites as compared to pure Biopol sheets was observed under the experimental conditions used. Scanning electron microscopy also showed that the surface modifications improved the fibre matrix adhesion. The improvement in adhesion may be attributed to the formation of rough surface due to the removal of natural and artificial impurities from the surface of jute by the treatment with alkali [120]. In addition, alkali treatment leads to fibre fibrillation, *i.e.*, breaking down the fibre bundle of fabrics into smaller fibres which improves the effective surface area available for contact with matrix polymer. Degradation studies showed that after 150 days of compost burial more than 50% weight loss of the jute/Biopol composites occurred.

Sarkar *et al.* and other researchers have broadly investigated the properties of alkali treated jute fibre reinforced with vinyl ester resin [121, 122]. In their studies, they compared the mechanical, thermal, dynamic, and impact fatigue behaviour of treated composites to those of untreated jute fibre–vinyl ester composites. Longer alkali treatment removed the hemicelluloses and improved the crystallinity, enabling better fibre dispersion. The dynamic, mechanical, thermal and impact properties were superior owing to the alkali treatment. The effects of hybridization [123] on the tensile properties of jute–cotton woven fabric reinforced polyester composites were investigated as functions of the fibre content, orientation and roving texture. It was observed that tensile properties along the direction of jute roving alignment (transverse to cotton roving alignment) increased steadily with fibre content up to 50% and then showed a decreasing trend. The tensile strength of composites with 50% fibre content parallel to the jute roving is about 220% higher than pure polyester resin. Jute fibre

reinforced PP composites were evaluated in terms of the effect of matrix modification [111], the influence of gamma radiation [124], the effect of interfacial adhesion on creep and dynamic mechanical behaviour [125], the influence of silane coupling agent [126], and the effect of natural rubber [127]. The properties of jute/plastic composites were studied, including the thermal stability, crystallinity, modification, trans-esterification, weathering, durability, fibre orientation on frictional and wear behaviour, eco-design of automotive components, and alkylation [128-131]. Polyester resin was used as matrix for jute fibre reinforced composites and the relationship between water absorption and dielectric behaviour [132], impact damage characterization [133], weathering and thermal behaviour, and effect of silane treatment [134] were examined. Behera *et al.* [135] has developed jute reinforced soy milk based composites using non-woven and woven jute fabrics. They have studied and reported the mechanical properties, viz., tensile strength, tensile and flexural modulus, flexural strength and elongation at break. Composites having 60 wt % jute fabric possessed the best mechanical properties. Hydrophilicity of the composites was assessed by the measurement of contact angle and water absorption after immersing in water at ambient temperature as well as in boiling condition. Biodegradability of the composites was evaluated in compost soil burial condition. Fourier transform infra-red and optical microscope analyses of the buried samples confirmed the degradation of the composites.

## 1.3. Nanomaterials:

Nanomaterials are such a stuff which has at least one dimension in nanometre scale *i.e.* 1 to 100 nm. Nanomaterials can be classified into two categories viz. nanostructured material and nanophase/nanoparticle materials. Nanostructured materials usually refer to condensed bulk materials that are made of grains (agglomerates), with nanometric size range. The latter are generally the dispersive nanoparticles. Nanotechnology is the study and control of nanomaterial which also deals with the design, fabrication and application of nanostructures. Nanomaterials, a new branch of materials research, are attracting a great deal of attraction because of their potential applications in areas such as optics, electronics, magnetic data storage, catalysis and polymer nanocomposites (PN).

Incorporation of inorganic/organic nanoparticles as additives into polymer systems has resulted in PN displaying multifunctional, high performance polymer

characteristics beyond what conventional filled polymeric materials acquire. Multifunctional features attributable to PN consist of improved mechanical properties, thermal properties and / or flame retardency, moisture resistance, chemical resistance, decreased permeability, and charge dissipation. Through control/alteration of the nanoscale additives, one can maximize the property enhancements of selected polymers to meet or exceed the needs. Uniform dispersion of these nanoscale materials produces super interfacial area per volume between the nanoparticle and the polymer. There are different types of commercially available nanoparticles such as montmorillonite organoclays, carbon nanofibres, carbon nanotubes, nanosilica, nanotitanium dioxide, nano ZnO and others that can be incorporated into the polymer matrix to form PN [136].

The term "nano" is derived from the Greek word *nanos* meaning "dwarf", though in nanoscience and nanotechnology, it is used to indicate the size of the used material ($10^{-9}$ metre). PN are polymers (thermoplastics, thermosets or elastomers) that have been reinforced with small quantities of nano-sized particles having high aspect ratios ($l/h > 300$) [137]. Thus, one component of nanocomposite has at least one dimension (length or width or thickness) in the nanometre range. The advantages of nanocomposites over macro composites include reduced filler amount and better properties than obtained for the conventional composites. Different types of thermoplastic and thermosetting polymer nanocomposites, *viz.* clay/polymer nanocomposites, carbon nanotube/polymer nanocomposites, metal/polymer nanocomposites (metals like Au, Ag, Cu, Cd, Zn, Fe, etc. and their oxides, sulphides, etc.) are good demonstration of nanotechnology. The main significance of polymer nanocomposites are:

> ➤ Superior physical properties; modulus, dimensional stability, etc.

> ➤ Improved chemical resistance, weatherability and biodegradation

> ➤ Better barrier properties; reduced gas permeability to oxygen and carbon dioxide

> ➤ Enhanced flame retardance and slow smoke emission

> ➤ Improved optical clarity over that of conventional filler

> ➤ Increased heat distortion temperature

Nanotechnology is one of the most popular regions for present research and development in basically all technical disciplines. This obviously includes polymer science and technology and even in this field the investigations cover a broad range of

topics. The areas include bio-polymer-based materials, nanoelectronics, miniemulsion particles, nanoparticle drug delivery, fuel cell electrode polymer bound catalysts, electrospun nanofibres, imprint lithography, polymer blends layer-by-layer self-assembled polymer films, and nanocomposites. Even in the field of nanocomposites, many diverse topics exist including composite reinforcement, barrier properties, flame resistance, electro-optical properties, cosmetic applications, bactericidal properties etc. There are different types of commercially available nanofillers that can be incorporated into the polymer matrix to form polymer nanocomposites. Depending on the application, the researcher must determine the type of nanoparticle needed to provide the desired effect. The commonly used nanoparticles are:

## 1.3.1. Clay

Nanoclay is the most widely investigated nanoparticle in a variety of different polymer matrices for a spectrum of applications. The origin of natural clay *i.e.* bentonite is most commonly formed by the in-situ alteration of volcanic ash. Bentonite contains montmorillonite but also can contain glass, mixed layer clays, illite, kaolinite, quartz, zeolite, and carbonates. The expanding clays are phyllosilicates, smectite, and montmorillonite, and the nonexpanding clays are talc, kaolin, and mica. Clay soil has particles size of less than 2 μm. Silica is the dominant constituent of the montmorillonite clays, with alumina being essential. The chemical structure of montmorillonite is illustrated in Figure 1.5, showing its structure consisting of the tetrahedral silicate layer and the octahedral alumina layer. The tetrahedral silicate layer consists of $SiO_4$ groups linked together to form a hexagonal network of the repeating units of composition $Si_4O_{10}$. The alumina layer consists of two sheets of closely packed oxygens or hydroxyls, between which octahedrally coordinated aluminium atoms are imbedded in such a position that they are equidistant from six oxygens or hydroxyls. The two tetrahedral layers sandwich the octahedral layer, sharing their apex oxygens with the latter. The layer thickness is around 1 nm and the lateral dimensions of these layers may vary from 300 Å to several microns and even larger depending on the particular silicate. These layers organize themselves to form stacks with a regular van der Waals gap in between them called the interlayer or the gallery. The chemical formula of montmorillonite clay is $Na_{1/3}(Al_{5/3}Mg_{1/3})\ Si_4O_{10}(OH)_2$. In its natural state $Na^+$ cation resides on the montmorillonite clay surface [136, 139].
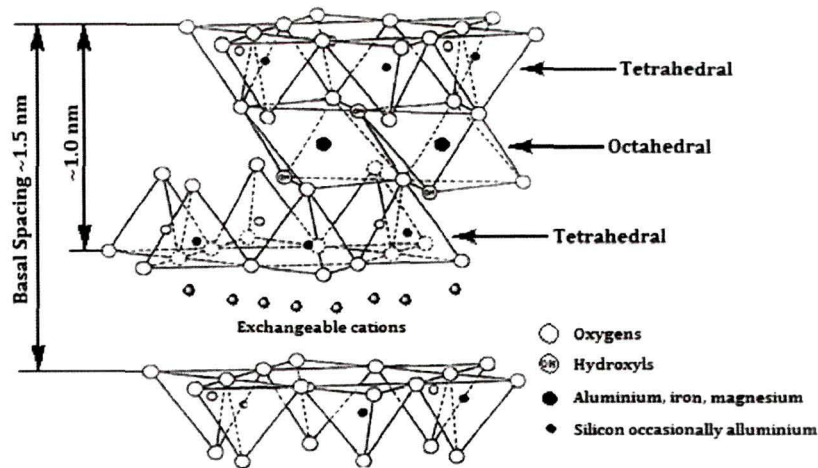
**Figure 1.5.** Chemical structure of montmorillonite nanoclay.

The dispersion of clay tactoids in a polymer matrix can result in the formation of three types of composites, as shown in Figure 1.6.
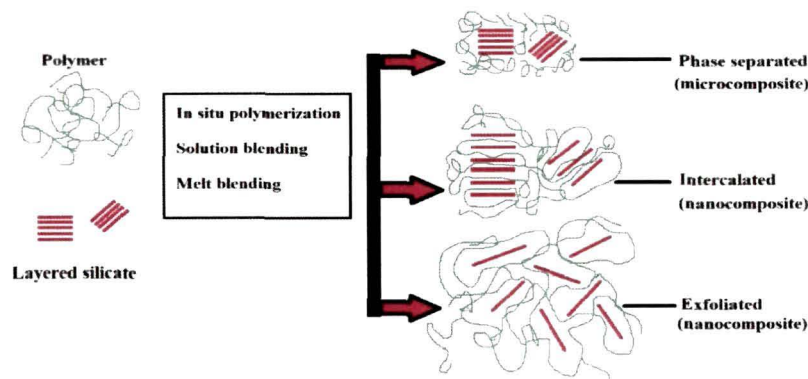


**Figure 1.6.** Schematic structure of polymer/clay nanocomposites.

*(i) Phase separated (microcomposite) structure:* It is a conventional composite that contains clay tactoids dispersed simply as a segregated phase, resulting in poor mechanical properties of the composite.

*(ii) Intercalated structures:* The second type is intercalated polymer-clay nanocomposite, which is formed by the infiltration of one or more molecular layers of polymer into the clay host galleries.

*(iii) Exfoliated structures:* In this case, the host clay layers have lost their registry and are well separated into single layers within a continuous polymer matrix. The exfoliated polymer-clay nanocomposites, characterized by low clay content, a monolithic

structure, and a separation between clay layers that depends on the polymer content of the composite.

Exfoliation is particularly desirable for improving specific properties that are affected by the degree of dispersion and resulting in interfacial area between polymer and clay nanolayers. Exfoliated nanocomposites usually provide the best properties enhancement due to the large aspect ratio and surface area of the clay.

## 1.3.2. Zinc oxide (ZnO)

ZnO a wide, direct band gap (3.37eV, 298K) semiconductor with extonic Bohr radius of 1.8 nm has been intensively studied in the past decade [140]. Its excitation binding energy is about 60 MeV, which is much larger than other band gap semiconductors [141]. Because of the high UV–protection property in the range of wave-length 240-380 nm and low refractive index (n=1.9), ZnO is considerd as an ideal UV protector and usually added into cosmetics for ultra-violet protection [142-145]. So far, various nanostructures of ZnO, such as nanowires, nanorods, nanobelts, nanotubes, and nanocables have been fabricated by means of various methods, including vapour phase transport, metal organic vapour phase epitaxy, aqueous thermal deposition and electrochemical deposition. Inorganic UV absorbers are used widely owing to their higher chemical stability, thermal stability, nontoxicity, and non-irritant compared with organic absorbers. Besides, it is very interesting multifunctional material for its applications in solar cells, sensors, displays, gas sensors, varistors, piezo-electric devices, electro-acoustic transducers, photodiodes and UV light emitting devices [146]. However, ZnO nanoparticles, like other nanoparticles, possess high surface energy, which may result in the agglomeration of particles when ZnO nanoparticles are dispersed in organic solvent and matrices.

In polymer composite, nano ZnO is widely used as photostabilizer. Besides UV stabilizing effect, ZnO nanopowder can also improve thermal stability of polymer. In recent years, most of the researchers have examined the role of ZnO nanoparticles in exterior coatings to improve photostability [147], as a component of UV coatings for nanocomposites or modelling UV permeability of nano-ZnO filled coatings [148, 149]. Laachachi and co-workers have reported the increased thermal properties of PMMA by incorporation of ZnO and organo-montmorillonite [150].

### 1.3.3. Titanium dioxide (TiO₂)

Titanium dioxide adopts at least eight (8) structures. Besides its four polymorphs found in nature (*i.e.* rutile, anatase, brookite, $TiO_2$ (B)), additional high-pressure forms have been synthesized: $TiO_2$ (II) with the $\alpha$-$PbO_2$ structure, $TiO_2$ (H) with hollandite, baddelleyite with $ZrO_2$, Cotunnite with $PdCl_2$ [151]. The anatase phase of $TiO_2$ has long been considered as the most photoactive of these four phases [152-156]. $TiO_2$ has received a great attention due to its strong oxidizing power of the photo-generated holes, chemical inertness, non-toxicity, low cost, high refractive index and other advantageous surface properties. $TiO_2$ was first industrially introduced to replace toxic lead oxides as a white paint pigment in 1900's. It is used as a white pigment in paints, plastics, paper and cosmetic products which represent the major end-use sectors of $TiO_2$. $TiO_2$ has also been used for photo-assisted degradation of organic compounds and reduction of inorganic compounds. As a semiconductor oxide, a wide-band gap $TiO_2$ is easy to be irradiated by sunlight (especially UV light) to create the excited electron–hole pairs which could separate and the resulting charge carriers might migrate to the surface where they react with adsorbed water and oxygen to produce radical species. These radicals attack any adsorbed organic or even micro-organic molecules, resulting in complete or selective decomposition; or transformation of inorganic molecules into their oxidized and/or reduced states. Furthermore, due to presence of wide band gap of ~3.2 eV, $TiO_2$ can be used as semiconductor devices. Its other applications are studied for antifouling, antimicrobial, deodorizing and photovoltaic effects.

$TiO_2$ is regarded as the best photocatalyst for the decomposition of many organic pollutants in water and air [157]. It can be used in various processes such as the odour elimination from drinking water, the degradation of oil spills in surface water systems and the degradation of harmful organic contaminants like herbicides, pesticides and refractive dyes [158-160]. Nanosized $TiO_2$ powder has a large specific surface area, and good photo catalytic activities since reactions take place on the $TiO_2$ surface.

### 1.3.4. Cellulose and cellulose derivatives:

Cellulose is one of the most fascinating organic resources, an almost inexhaustible raw material, and a key source of sustainable materials on an industrial scale in the biosphere. Natural cellulose based materials (cotton, wood, linen, hemp, etc.) have been used by our society as engineering materials for millennia and their use

continues today as verified by the extent of the world wide industries in building materials, paper, textiles, etc. Generally, cellulose is a fibrous, tough, water-insoluble natural polymer that plays a vital role in maintaining the structure of plant cell walls. It was first discovered and isolated by Anselme Payen [161] in 1838, and since then, numerous physical and chemical prospects of cellulose have been extensively studied. Cellulose has been used for about 150 years for wide spectrum of products and materials in daily life. Many polymer researchers are with the opinion that polymer chemistry had its origins with the characterization of cellulose. Cellulose differs in some respects from other polysaccharides produced by plants, the molecular chain being very long and consisting of one repeating unit. Cellulose can be characterized as a high molecular weight homopolymer of $\beta$-1,4-linked anhydro-D-glucose units in which every unit is corkscrewed 180° with respect to its neighbours, and the repeat segment is frequently taken to be a dimer of glucose, known as cellobiose.

Naturally, it occurs in a crystalline state. From the cell walls, cellulose is isolated in microfibrils by chemical extraction. In all forms, cellulose is a very highly crystalline, and high molecular weight polymer. Because of its infusibility and insolubility, cellulose has driven the step-by-step creation of novel types of materials. Breakthrough were the development of cellulose esters and cellulose ethers as well as of cellulose regenerates and the discovery of the polymeric state of molecules. The very first thermoplastic polymeric material of cellulose was manufactured by Hyatt Manufacturing Company in 1870 to make celluloid in which they had reacted cellulose with nitric acid to form cellulose nitrate. The chemical modification of cellulose on an industrial scale led to a broad range of products based on cellulose from wood. The first example was the fabrication of regenerated cellulose filaments by spinning a solution of cellulose in a mixture of copper hydroxide and aqueous ammonia [85].

Natural cellulose has earned in the materials society a tremendous level of awareness that does not emerge to be yielding. The cellulose biopolymer imprimatur such interest not only because of their unsurpassed quintessential physical and chemical properties but also because of their inherent renewability and sustainability in addition to their abundance. They have been the subject of a wide array of research efforts as reinforcing agents in nanocomposites due to their availability, low cost, renewability, light weight, nanoscale dimension, unique morphology and most importantly they have low environmental, animal/human health and safety risks. Currently, the isolation, characterization, and search for applications of novel forms of cellulose, variously

termed crystallites, nanocrystals, whiskers, nanofibrils, and nanofibres, is generating much activity. Novel methods for their production range that begins at the highest conceptual level and works down to the details methods involving enzymatic/ chemical/physical methodologies for their isolation from wood and forest/agricultural residues to the bottom-up production of cellulose nanofibrils from glucose by bacteria [38, 162]. Some fungi can secrete enzymes that catalyze oxidation reactions of either cellulose itself or the lower molecular weight oligomers produced from the enzymatic hydrolysis of cellulose. Of these, the peroxidases can provide hydrogen peroxide for free radical attack on the $C_2$–$C_3$ positions of cellulose to form 'aldehyde' cellulose, which is very reactive and can hydrolyze to form lower molecular weight fragments while other oxidative enzymes can oxidize glucose and related oligomers to glucuronic acids. Such isolated cellulosic materials with one dimension in the nanometre range are referred to generically as nanocelluloses [163]. These nanocelluloses provide important cellulose properties—such as hydrophilicity, wide spectrum of chemical-modification capacity, and the formation of versatile semi crystalline fibre with very large aspect ratio which is the specific features of nanoscale materials. On the basis of their dimensions, functions, and preparation methods, which in turn depend mainly on the cellulosic source and on the processing conditions, nanocelluloses may be classified in three main subcategories.

*(i) Microfibrillated cellulose (MFC):* MFC is normally produced from highly purified wood fibre (WF) and plant fibre (PF) pulps by high pressure homogenization according to the procedures developed at ITT Rayonnier [164]. Pulp is produced by using a mixture of sodium hydroxide and sodium sulphide and thus so-called kraft pulp (almost pure cellulose fibres) is obtained. Pulping with salts of sulfurous acid leads to cellulose named sulphite pulp (which contains more by-products in the cellulose fibres). MFC particles are considered to comprise of several elementary fibrils. Each one of them consisting of 36 cellulose chains has a high aspect ratio or ~10-100 nm wide and 0.5-10 μm in length. MFCs are ~100% cellulose, and contain both amorphous and crystalline regions. In food and cosmetic industries, MFCs have been used as a thickening agent [165].

*(ii) Nanocrystalline cellulose (NCC):* NCC is the term frequently used for the cellulose nanocrystals or cellulose whiskers prepared from natural cellulose by acid hydrolysis. NCC is the enlightened crystalline segments of elementary nanofibrils after the amorphous segments have been removed via the treatment with strong acids at eminent

temperature. The nanocrystals formed from wood pulp are shorter and thinner than the MFC. NCCs have a high aspect ratio (3–5 nm wide, 50–500 nm in length), are ~100% cellulose, and are highly crystalline (54–88%). Most likely, from the result of acid hydrolysis process, the end of the cellulose nanocrystals are narrowed due to which they look like whiskers. This hierarchical structure of natural fibres, based on their elementary nanofibrilar components, leads to the unique strength and high-performance properties of different species of plants. The mechanical properties of cellulose can be characterized by its properties in both the ordered (so-called crystalline) and disordered (so-called amorphous) regions of the molecule. The chain molecules in the disordered regions contribute to the flexibility and the plasticity of the bulk material, while those in the ordered regions contribute to the elasticity of the material. As they are almost defects free, the modulus of cellulosic nanocrystals is close to the theoretical limit for cellulose. It is potentially stronger than steel and similar to Kevlar [166, 167].

*(iii) Bacterial Nanocellulose (BNC):* BNCs are also known as bacterial cellulose, microbial cellulose, or biocellulose. BNCs are microfibrils concealed by aerobic bacteria, such as acetic acid bacteria of the genus Gluconacetobacter, as a pure component of their biofilms. The resulting microfibrils are microns in length, have a large aspect ratio with morphology depending on the specific bacteria and culturing conditions. These bacteria are wide-spread in nature where the fermentation of sugars and plant carbohydrates takes place. In contrast to other forms of cellulose *i. e.* MFC and NCC, materials isolated from cellulose sources, BNC is formed as a polymer and nano material by biotechnological assembly processes from low-molecular weight carbon sources, such as d-glucose. The bacteria are cultivated in common aqueous nutrient media, and the BNC is excreted as exopolysaccharide at the interface to the air. The resulting form-stable BNC hydrogel is composed of a nanofibre network (fibre diameter: 20–100 nm) enclosing up to 99% water. This BNC is proved to be very pure cellulose with a high weight-average molecular weight (MW), high crystallinity, and good mechanical stability. The bio-fabrication approach opens up the exciting option to produce cellulose by fermentation in the sense of white biotechnology and to control the shape of the formed cellulose bodies as well as the structure of the nanofibre network during biosynthesis. The resulting unique features of BNC lead to new properties, functionalities, and applications of cellulose materials [168-175].

## 1.4. Different additives for jute based bionanocomposites:

The chemicals or substrate or materials, which are necessary to incorporate into the virgin polymers to obtain the desired level of properties for their different applications are known as additives for polymers. All the chemicals or materials cannot be an additive for polymers. They should fulfil some criteria to act as an additive for polymers. They should be efficient in their function, *i.e.* the purpose for which they are being incorporated into the polymer, and should efficiently work for that. They should be stable under processing as well as service conditions. The additive should not degrade or decompose or alter its nature during processing and under service conditions. They should not bleed or bloom. They should be non-toxic and should not impart any taste, odour or colour to the polymer matrix. The additives should be inert other than their own functions. They should be available in sufficient quantity as required and should have low cost. The physical state of additive may be solid, liquid or even gaseous. The semi-liquid like rubbery and gel are also used in some cases. However, gaseous additives are only used in case of foam products.

### 1.4.1. Crosslinking agent

Crosslinking agents are additives used to enhance crosslinking or bonding between polymer chains, so that the resultant polymer mainly exists in a 3D network form in biopolymers, which could increase reaction rate and significantly improve the dimensional stability, mechanical properties, wear resistance, impact strength of polymer nanocomposites. These are used in small quantities to provide a stable bond between two otherwise nonbonding and incompatible surfaces [176]. They play remarkable role in improving the affinity, compatibility, and adhesion between fibres and polymers in composite. Among the many available crosslinking agents, glutaraldehyde has undoubtedly establish the extensive application in various fields such as leather tanning industry, enzyme technology, chemical sterilization, and biomedical and pharmaceutical sciences. Glutaraldehyde, a linear, 5-carbon dialdehyde, is a clear, colourless to pale straw-coloured, pungent oily liquid that is soluble in all proportions in water and alcohol, as well as in organic solvents. It is mainly available as acidic aqueous solutions (pH 3.0–4.0), ranging in concentration from less than 2% to 70% (w/v). Glutaraldehyde has had great success because of its commercial availability and low cost in addition to its high reactivity. It reacts rapidly with amine groups at around neutral pH and is more efficient than other aldehydes in

31

generating thermally and chemically stable crosslinks [177]. The simple structure of glutaraldehyde is not indicative of the complexity of its behaviour in aqueous solution and its reactivity. Knowledge of the structure and mechanism of crosslinking reagents is important for their use. However, the structure of glutaraldehyde in aqueous solution has been the subject of more debate than any of the other crosslinking reagents. In fact, glutaraldehyde structure in aqueous solution is not limited to the monomeric form (Figure 1.7, structure I). Figure 1.7 gives an overview of the possible molecular forms of glutaraldehyde in aqueous solution [178].
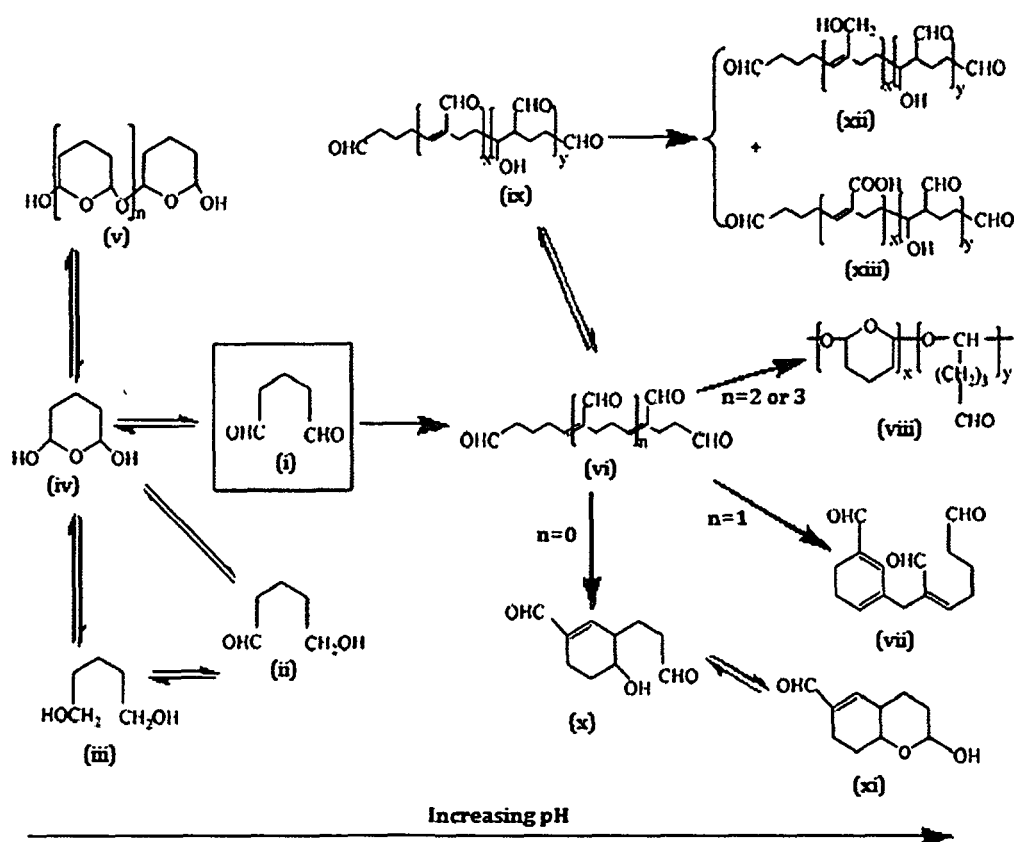


**Figure 1.7.** Possible forms of glutaraldehyde in aqueous solution.

## 1.4.2. Plasticizer

A great devotion has been made to thermoplastic SP and starch because thermo-mechanical processing technique is an easy and effective way to prepare complete biodegradable materials [179]. However, both soy protein and starch are very brittle, weak and difficult to process into useful films. In a state to improve the processing assets of soy protein and starch, plasticizers have to be added into the matrix to

overcome the brittleness of pure biopolymers. Plasticizer has the ability to reduce internal hydrogen bonding between macromolecule chains as well as to increase the molecular spacing of them [180]. The most effective plasticizers will resemble most closely in the structures of the polymers they plasticize. The best plasticizers for soy protein and starch are compounds containing hydroxyl groups, such as glycerol [181]. Glycerol is a simple naturally occurring polyols. It is an odorless, colorless, viscous liquid, and generally considered as non-toxic. It is widely used in pharmaceuticals. It contains three hydroxyl groups which are accountable for its solubility in water and hygroscopic nature. The chemical structure of glycerol is depicted in Figure 1.8.
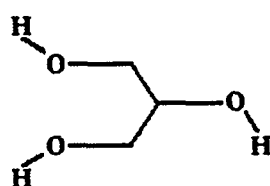


**Figure 1.8.** Chemical structure of glycerol.

**1.5. Review of Literature:**

Mohanty *et al.* [111, 182] has developed the chemical surface modification of jute fabrics to improve the interfacial properties. The modification involves bleaching, dewaxing and alkali treatment. The mechanical properties of composites like tensile and bending strengths have increased as a result of surface modification. Wang *et al.* [183] has developed a new technique including chemical (room temperature alkaline, acid steam and $80^{\circ}$ c alkaline) and physical (high pressure steam) for treatment of natural fibres. They have used scanning electron microscopy (SEM) to study the effects of chemical and physical treatments on the morphological development of jute fibres from micro-to- nano-scale. The thermal stability of the jute fibres has been found to enhance after treatment. Khanam and co-workers [184] has carried out fibre surface treatment to produce good interface between the fibre and the matrix to improve the mechanical properties. They have reported that the untreated sisal fibre shows lower tensile, flexural properties than the treated one. The sisal fibre reinforced composites are resistant to all chemicals except carbon tetrachloride.

Chabba *et al.* [185] have prepared environment-friendly, fully biodegradable, 'green' composites using glutaraldehyde (GA) modified soy protein concentrate (MSPC-G) and flax fabric. The polymer has been cross-linked with GA to increase its

tensile properties and to improve its process ability. Fracture stress, young modulus and moisture resistance have been found to improve in glutaraldehyde modified MSPC-flax fabric composite compared to glutaraldehyde modified SPC-flax fibre composite. Chabba and Netravali [186] have blended the cross-linked soy protein concentrate (SPC) with poly (vinyl alcohol) for improving its toughness and thermal properties. Chabba *et al.* [66] has also prepared green composites based on plant based fibres and resins. They have modified deffated soy flour by cross-linking with glutaraldehyde and the composites using cross-linked soy flour (CSF) and flax yarn. They have studied the effect of glycerol on mechanical properties of the soy flour composite. CSF polymer has shown improved tensile properties and thermal stability, compared to unmodified SF resin. Lodha and Netravali [187] have investigated the effect of stearic acid on tensile and thermal properties of ramie fibre-reinforced soy protein isolate (SPI) resin green composites. It is observed that part of the stearic acid crystallized in SPI resin and the crystallizability is affected by the addition of glycerol as a plasticizer. The fabricated green composites are found to have enormous potential for certain indoor applications. SEM photomicrographs of some of the fractured tensile surfaces of the ramie/SPI and ramie/modified soy protein isolate (MSPI) composites do not show any resin whereas a few other fibres clearly show resin sticking to the surface. The presence of resin on some fibre surfaces for the SPI and MSPI resins clearly indicates good interfacial interaction between the fibre and the resins.

Khondker *et al.* [188] has fabricated long fibre reinforced unidirectional thermoplastic composites using jute yarns (both untreated and treated). They have used two types of polymeric materials (biodegradable poly (lactic) acid and non-biodegradable homo-polypropylene) as matrix. The jute/PP composites, specimens with only 20% of jute fibre content have shown remarkable improvement in tensile and bending properties when compared to those of the virgin PP specimens. Park *et al.* [189] has fabricated the composite using cellulose acetate powder, eco-friendly triethyl citrate plasticizer and organically modified clay. The tensile strength and modulus of cellulosic plastic reinforced with organoclays are improved by decreasing the plasticizer content. The heat deflection temperature is improved and the water vapour permeability is reduced. But the impact strength is decreased. Nam *et al.* [190] has used ramie fibres to reinforce SPC and obtained composites with excellent mechanical properties. Kumar and Zhang [191] have aligned the ramie fibres in vertical, horizontal as well as both vertical and horizontal to enhance the strength of soy protein composite.

The materials in which ramie fibres are aligned vertically, exhibit the highest water resistance and mechanical properties compared to either horizontal or vertical one. They have coated the soy protein isolate with 2,2-diphenyl-2-hydroxyethanoic acid to get the arylated soy protein in order to further improve the water resistance property of the composite. This work provides a novel idea to improve the water resistance and modulus by reinforcing the protein matrix with natural fibres.

Goda *et al.* [192] has explored the effect of mercerization on tensile properties of ramie fibres. They have treated the ramie fibre with 15% NaOH solution. The results show that tensile strength of the treated ramie fibre has increased by 4–18% than that of the untreated ramie fibre. They also have found that fracture strain of the treated ramie fibre drastically increases. Kim and Netravali [193] have used modified soy flour (MSF) and ramie fibre to prepare biodegradable, green composites. They have modified defatted soy flour by a lab-scale filtration system to improve its mechanical, interfacial and thermal properties through increasing the protein content. Tensile stress and Young's modulus of MSF resins are 35.5 and 1411.7 MPa, respectively, which is significantly higher than those (12.7 and 379.3 MPa) of SF resins. Interfacial shear strength of single ramie fibres with MSF resins ranges from 8.8 to 15.2 MPa, which were about 40-50% higher than those obtained with SF resins. Nanocomposites, with nanoparticles dispersed, have been studied extensively due to their capability to improve mechanical, physical, thermal and barrier properties with very low nanoparticles loading of 1-5 wt% [194-198]. Huang and Netravali [199] have used phytagel and nano-clay particles to improve the mechanical, thermal and moisture resistance of soy protein concentrate (SPC) resin. The Phytagel-modified SPC resin (PH-SPC) has shown improved tensile strength, modulus, moisture resistance, and thermal stability as compared to the unmodified SPC resin. The incorporation of 40% Phytagel and 20% glycerol led to an overall 340% increase in the tensile strength (over 50 MPa) and approximately 360% increase in the Young's modulus (over 710 MPa) of the SPC resin. Nano-clay has been uniformly dispersed into PH-SPC resin to further improve the properties.

Pandey and Singh [200] have studied the effect of plasticizer on the nanocomposites of starch and reported that the mechanical properties are improved for the composites where plasticizer has been added after mixing of clay in the starch matrix. Darder et al. [201] has worked in the intercalation of the cationic biopolymer chitosan in $Na^+$- montmorillonite and reported that the chitosan layer is first adsorbed

through a cationic exchange procedure and the second layer is adsorbed in the acetate salt form. He has used this material in the development of bulk modified electrodes exhibiting numerous advantages as easy surface renewal, ruggedness, and long-time stability. He has applied the resulting sensors in the potentiometric determination of several anions and has found that the sensor showed high selectivity towards the monovalent anions. Biodegradable starch based materials has been prepared by Averous *et al.* [202] from wheat starch, polyesteramide and glycerol by melt blending. They have noticed that the polyester amide blended thermoplastic starch overcomes the weakness of pure thermoplastic starch like low mechanical properties, high moisture sensitivity and high shrinkage in injection. Viville *et al.* [203] has grafted polymer chains onto clay nano platelets by coordination-insertion polymerization of $\xi$-caprolactone in toluene with montmorillonite type clay. The work highlights the possibility of producing organic-inorganic nanohybrids, where the nanoscale components are linked to each other through electrostatic interactions.

Cao *et al.* [204] has prepared nanocomposites from polycaprolactone-based waterborne polyurethane and a suspension of cellulose nanocrystals. The cellulose nanocrystals are obtained by acid hydrolysis of flax fibre. The prepared composites show significant increase in Young's modulus and tensile strength with increasing filler content. Chen and Evans [205] have prepared nanocomposites of glycerol plasticized starch with untreated montmorillonite and hectorite. The nanocomposites prepared by them have shown an increase in modulus for a given volume fraction of clay. Jute fabric reinforced starch/polyvinyl alcohol/clay composites have been prepared by Ray *et al.* [206]. They have found that the composites having higher amount starch show superior mechanical properties than the others. Jong *et al.* [207] has blended soy protein concentrate with styrene-butadiene latex to form elastomer composites. This elastomer has shown an increase in the shear elastic modulus in a small strain region and also improved the recovery behaviour. Thomas *et al.* [208] has reviewed and evaluated various properties of starch/clay/glycerol nanocomposites. The sequence of addition of starch, glycerol and clay has a significant effect on the properties of composites. MMT modified with octadecylammonium chloride has been used as organoclays for nanocomposites preparation. Poly (hydroxyl butyrate)/layered silicate nanocomposites have been successfully prepared by Maiti and co-workers [209]. The nanocomposites exhibit a higher storage modulus, better biodegradation behaviour as compared to the neat Poly (hydroxyl butyrate).

## 1.6. Application & Market:

Unlike many biopolymer products being developed and marketed, very few biodegradable composites have been developed, with most of their technologies still in the research and development stages. This is despite the fact that the environmentally friendly composites, where biodegradability is important, provide designers new alternatives to meet challenging requirements. These include aquatic and terrestrial environments, municipal solid waste management and compostable packaging, while those for automobiles include parcel shelves, door panels, instrument panels, armrests, headrests and seat shells. Accordingly, a wide range of biodegradable products have been produced using LC fibres and biopolymers for different applications, ranging from automotive vehicles including trucks, construction (hurricane resistant housing and structures, especially in the USA) and insulation panels, to special textiles (geotextiles and nonwoven textiles) [210]. The hurricane resistant housing, structures and a variety of products developed using soy oil with LC fibres could be the predecessor for diverse range of applications for the biodegradable composites. Other identified uses for these materials include bathtubs, archery bows, golf clubs and boat hulls. This is further underlined with the estimated global market of about 900,000 metric tons of wood plastics and natural fibre composites as per Steven Van Kourteren, Consultant, Principia Partners [211]. Hence the market for biodegradable composites can be expected to grow in near future. This is based on continued technical innovations, identification of new applications, persistent political and environmental pressures, and investments mostly by governments in new methods for fibre harvesting and processing of natural fibres [212, 213].

## 1.7. Objectives and plan of work:

Biopolymer based materials immobilized with nanoparticles have recently dominated over the traditionally available petroleum based polymer materials. Due to their outstanding mechanical properties and biodegradability, bio based polymer nanocomposites are now a days considered to be promising future material. These materials have the potential to overcome the disadvantages possesses by material commercially obtained from petrochemical supply chain. Moreover, the use of bio based polymer nanocomposites plays a vital role in sustainable development so called the development of newer methods for production of environmentally benign 'greener products'.

Among the various biodegradable polymers, two of the most studied and promising polymers are starch and soy flour (SF). They are natural and renewable biodegradable polymers which are produced by many plants as a source of stored energy. The presence of various polar and reactive groups in the structure of starch and soy flour augment them to crosslink with some crosslinking agent such as glutaraldehyde, thereby improving the mechanical and thermal properties. However, the potentiality of such material has been less explored in synthesizing bio based composites. Besides having various advantages, SF based material too exhibits certain disadvantages. For example soy protein based plastics have poor flexibility and water resistance. Although several plasticizers like glycerol, polyethylene glycol, sorbitol etc, have been used to improvise the flexibility of SF but found to provide less mechanical strength and high water sensitivity. In this respect, biofibres evolved to be one of the promising materials in improving the mechanical strength of such material. The salient features of natural fibres over the conventional counterparts include comparatively low cost, low weight, high specific modulus, less hazards, copious and renewable resources. The applications of natural fibres in the sectors such as automobiles, furniture, packing and construction industries sectors are now of highly demanding. Currently, kenaf, bamboo and palm-tree fibres are used as reinforcing agent at micro and macro levels to improve the thermal and mechanical properties of natural biodegradable polymers. Similarly, palm tree and kenaf natural fibres are used as reinforcing agents for the development of self-bonded polymer bio-composite. Besides the above mentioned natural fibres, jute fibre is one which can be used as reinforcing agent and can be used for fabrication of polymer composite. Jute, mainly comprising of cellulose and lignin, is an extensively demanding materials in cloth and other such industries. The most attractive features of such fibre are that they are cheap, widely available and most importantly can be modified to a cost – effective and environmental friendly green products with improvised physical properties like thermal, mechanical etc. The combination of bio-polymer and jute fibre crosslinked with glutaraldehyde can lead to a bio based polymer composites and their properties can be improved by dispersing the nanofillers into their matrix.

Nano technology deals with the material in sub-micron level. It has been successfully applied in many fields. Nano structured material will have substantially different properties from a larger dimensional material (conventional composite) of same composition. Nano materials can provide reinforcing efficiency because of their

high aspect ratio. The properties of nanocomposites are greatly influenced by the size scale of its component phases and degree of mixing between the two phases. Without proper dispersion the nano materials will not offer improved mechanical properties over that of conventional composites. Among the various nanofillers, clay, ZnO, $TiO_2$ and cellulose whisker are extensively used for modification of conventional polymer composite. The immobilization of nanoparticles results in high interfacial area between the matrix and the filler. This in turn assists the polymer nanocomposites to show high thermo – mechanical performance.

Keeping in mind the advantages of bio based polymer and increasing demand of a greener products, it is proposed to develop a bio based polymer nanocomposites comprising of soy flour/starch, jute, glutaraldehyde, and clay/ZnO/$TiO_2$/cellulose whisker either alone or in combination for improved thermo – mechanical properties. Efforts will be made to develop a treatment/process which can confer properties like fire retardation, UV resistance etc. all at the same time.

***The plan of work has been segregated as follows:-***

The plan of research is divided into different parts. Following the standard procedure mentioned in the literature the main approaches will be done as given below:

✓ Surface modification of the jute fabric.

✓ Preparation of bio-nanocomposites employing natural polymers (like soy flour and starch), jute fabric, plasticizer, clay, cross linking agent and other additives (like $TiO_2$, ZnO, Cellulose whisker etc.).

✓ Dispersion of clay and other additives in deionised water using magnetic stirrer, mechanical stirrer and ultra sonicator. Mixing of the slurry containing clay and other additives into dispersed soy flour/starch etc. for preparation of polymeric slurry. Impregnation of jute fabric with polymeric slurry followed by drying.

✓ Characterization the composites using FT-IR, tensile tester, thermogravimetric analyser (TGA), X-ray diffractometer (XRD), scanning electron microscope (SEM), transmission electron microscope (TEM) etc. Evaluation of properties in terms of moisture absorption, dimensional stability, etc.

✓ Study of the biodegradability of the nanocomposites.

**References**

[1] Satyanarayana, K.G., Ramos, L.P., & Wypych,F. In *Biotechnology in energy management*, APH Publishing Corporation, New Delhi, 2005.

[2] Uddin, M.K., et al. *Polym. Degrad. Stab.* **55**(1), 1--7, 1997.

[3] Wollerdorfer, M., & Bader,H. *Ind. Crops Prod.* **8**(2), 105--112, 1998.

[4] Luo,S., & Netravali, A.N. *J. Appl. Polym. Sci.* **73**(6), 1059--1067, 1999.

[5] Lankey, R.L., & Anastas, P.T. *Advancing Sustainability through Green Chemistry and Engineering*, American Chemical Society, Washington, DC, 2002.

[6] Mohanty, A.K., et al. *J. Polym. Environ.* **10**(1-2), 19--26, 2002.

[7] Mohanty, A.K. *J. Adhes. Sci. Technol.* **16**(8), 999--1015, 2002.

[8] Coates, G.W., & Hillmyer, M.A. *Macromolecules* **42**(21), 7987--7989, 2009.

[9] Ryberg, Y.Z.Z. *Biomacromolecules* **12**(4), 1355--1362, 2011.

[10] DeWit, M.A., & Gillies, E.R. *J. Am. Chem. Soc.* **131**(51), 18327--18334, 2009.

[11] Hartman, J., et al. *J. Appl. Polym. Sci.* **100**(4), 2985--2991, 2006.

[12] Tian, H., et al. *Prog. Polym. Sci.* **37**(2), 237--280, 2012.

[13] Odelius, K. *J. Appl. Polym. Sci.* **127**(1), 27--33, 2013.

[14] Muggli, D.S., et al. *Macromolecules* **31**(13), 4120--4125, 1998.

[15] Metters, A.T. *Polymer* **41**(11), 3993--4004, 2000.

[16] Ray, S.S., et al. *Nano Lett.* **2**(10), 1093--1096, 2002.

[17] Nam, J.Y., et al. *Macromolecules* **36**(19), 7126--7131, 2003.

[18] Tang, X., & Alavi, S. *J. Agric. Food Chem.* **60**(8), 1954--1962, 2012.

[19] Lim, S.T., et al. *Chem. Mater.* **14**(4), 1839--1844, 2002.

[20] Dash, B.N., et al. *J. Reinf. Plast. Compos.* **21**(6-15), 1493--503, 2002.

[21] Mishra, S., et al. *J. Reinf. Plast. Compos.* **21**(1), 55--70, 2002.

[22] Wang, A.N., & Chabba, S. *Mater. Today* **6**(2), 22--29, 2003.

[23] Wambua, P., et al. *Compos. Sci. Technol.* **63**(9), 1259--1264, 2003.

[24] Plackett, D., et al. *Compos. Sci. Technol.* **63**(9), 1287--96, 2003.

[25] Mohanty, A.K., et al. *Composites A* **35**(4), 363--370, 2004.

[26] Geeta, M., et al. *J. Polym. Environ.* **13**(2), 169--175, 2005.

[27] Liu, W., et al. *Polymer* **46**(8), 2710--2721, 2005.

[28] Liu, W., et al. *Ind. Eng. Chem. Res.* **44**(18), 7105--7112, 2005.

[29] Bhardwaj, R., et al. *Biomacromolecules* **7**(6), 2044--2051, 2006.

[30] Maya, J.J., & Thomas, S. *Carbohydr. Polym.* **71**(3), 343--364, 2008.

[31] Williams, C.K., & Hillmayer, M. A. *Polym. Rev.* **48**(1), 1--10, 2008.

[32] Cheng, M., et al. *J. Am. Chem. Soc.* **121**(49), 11583--11584, 1999.

[33] Amass, W., et al. *Polym. Int.* **47**(2), 89--144, 1998.

[34] Satyanarayana, K.G., et al. *Prog. Polym. Sci.* **34**(9), 982--1021, 2009.

[35] Faruka, O., et al. *Prog. Polym. Sci.* **37**(11), 1552--1596, 2012.

[36] Summerscales, J., et al. *Composites Part A* **41**(10), 1329--1335, 2010.

[37] Witt, U., et al. *Angew. Chem. Int. Ed.* **38**(10), 1438--1442, 1999.

[38] Klemm, D., et al. *Angew. Chem. Int. Ed.* **50**(4), 5438--5466, 2011.

[39] Maiti, P., et al. *Biomacromolecules* **8**(11), 3393--3400, 2007.

[40] Richard, T.L. *Science* **329**(5993), 793--796, 2010.

[41] Blanch, H.W., et al. *ACS Chem. Biol.* **3**(1), 17--20, 2008.

[42] Lakshmi, S.N., & Laurencin, C. T. *Prog. Polym. Sci.* **32**(8-99), 762--798, 2007.

[43] Carole, T.M., et al. *Appl. Biochem. Biotechnol.* **115**(1-3), 871--885, 2004.

[44] Buléon, A., et al. *Int. J. Biol. Macromol.* **23**(2), 85--112, 1998.

[45] Roger, P., et al. *J. Cereal Sci.* **24**(3), 247--262, 1996.

[46] Halley, P.J. Thermoplastic starch biodegradable polymers, in *Biodegradable Polymers for Industrial Applications*. R. Smith, Ed.; CRC Press, Washington, DC, 2005; Vol 1; p 140.

[47] Thomson, D.B. *Carbohydr. Polym.* **43**(3), 223--239, 2000.

[48] Dufresne, A., & Vignon, M. R. *Macromolecules* **31**(8), 2693--2696, 1998.

[49] Otey, F.H., et al. *Ind. Eng. Chem. Prod. Res. Dev.* **16**(4), 305--308, 1977.

[50] Chandra, R., & Rustogi, R. *Prog. Polym. Sci.* **23**(7), 1273--1335, 1998.

[51] Otey, F., et al. *Ind. Eng. Chem. Prod. Res. Dev.* **13**(1-2), 90--95, 1974.

[52] Huang, J.C., et al. *Adv. Polym. Technol.* **10**(1), 23--30, 1990.

[53] Shulman J., & Howarth, J.T. *Waterproof plastic films of increased water vapour permeability and method of making them.* **U.S. Patent No. 3137664**, June 16, 1964.

[54] Griffin, G.J.L. *Am. Chem. Soc. Div. Org. Coat. Plast. Chem.* **33**(2), 88--96, 1973.

[55] Deanin, R.D., & Schott, N.R. (eds.). *Advances in Chemistry Series, 134*, American Chemical Society, Washington, DC, 1974.

[56] Otey, F.H. & Doane, W.M.A. Starch based degradable plastic film, in Society of the Plastic Industry. Washington, DC, 1987, p. 39-40.

[57] Otey, F.H., et al. *Ind. Eng. Chem. Prod. Res. Dev.* **19**(4), 592--595, 1980.

[58] Kulicke, W.M., et al. *Starch*, **41**(4), 140--146, 1989.

[59] Fishman, M., Friedman, R., & Huang, S.J. (eds.). *Polymers from Agricultural Co-products*; American Chemical Society, Washington, DC, 1993.

[60] Mohanty, A.K., et al. *Macromol. Mater. Eng.* **276/277**(1), 1--24, 2004.

[61] *http://www.eco-foam.com/loosefill.asp* (07-07-2014)

Bailey, D.H. & Rudolph, D. An Ergodic proof that rational times normal is normal. http://crd.lbl.gov/~dhbailey/dhbpapers/tarxnormal.pdf, 2002.

[62] *http://www.novament.com* (07-07-2014)

[63] *http://www.biotech.de/engl/index_engl.htm* (07-07-2014)

[64] Pommet, M., et al. *Polymer* **44**(1), 115--122, 2003.

[65] Erickson, D.R. (ed.). Industrial Uses for Soybeans, in *Practical Handbook of Soybean Processing and Utilization*, AOCS Press: Champaign, IL, 1995.

[66] Chabba, S., et al. *Green. Chem.* **7**(8), 576--581, 2005.

[67] Reddy, M., et al. *J. Biobased Mater. Bioenergy* **4**(4), 298--316, 2010.

[68] Khorshid, N., et al. *J. Food Eng.* **79**(4), 1214--1220, 2007.

[69] Kumar, R., et al. *J. Biobased Mater. Bioenergy* **2**(1), 1--24, 2008.

[70] Kinsella, J.E. *J. Am. Oil Chem. Soc.* **56**(2), 242--258, 1979.

[71] Shinoja, S. *Ind. Crops Prod.* **33**(1), 7--22, 2011.

[72] Venkateshwaran, N., & Elayaperumal, A. *J. Reinf. Plast. Compos.* **29**(15), 2387--2396, 2010.

[73] Hassan, A., et al. *Polym. Compos.* **31**(12), 2079--2101, 2010.

[74] Franck, R.R. (ed.). *Bast and Other Plant Fibres*. CRC Press: Boca Raton, FL; 2005.

[75] Bledzki, A.K., & Gassan, J. *Prog. Polym. Sci.* **24**(2), 221--274, 1999.

[76] Bledzki, A.K., et al. *Rapra Rev. Rep.* **13**(8), 1--144, 2002.

[77] Baillie, C. (ed.). *Green Composites: Polymer Composites and the Environment*. Woodhead Publishing Limited: Cambridge, 2004.

[78] Mohanty, A.K., Misra, M., & Drzal, L. T. (eds.). *Natural Fibres, Biopolymers, and Biocomposites*. Taylor & Francis Group: Boca Raton, Florida, 2005.

[79] Pickering K. (ed.). *Properties and Performance of Natural-Fibre Composites*. Woodhead Publishing Limited, Cambridge, 2008.

[80] Thomas, S., & Pothan, L.A. (eds.). *Natural Fibre Reinforced Polymer Composites: From Macro to Nanoscale*. Old City Publishing, Philadelphia, 2009.

[81] Staiger, M.P., & Tucker, N. Natural-fibre composites in structural applications, in *Properties and Performance of Natural-Fibre Composites*, K. Pickering, ed., Woodhead Publishing Limited, Cambridge, 2008, 269—300.

[82] Hon, D.N.S. *Polym. News* **13**(1), 34--140, 1988.

[83] Wang, W-M., et al. *Fibers Polym.* **10**(4), 776--780, 2009.

[84] Li, H., et al. *Polym. Compos.* **8**(3), 199--202, 1987.

[85] Habibi, Y., et al. *Chem. Rev.* **110**(6), 3479--3500, 2010.

[86] Bledzki, A.K., et al. *J. Appl. Polym. Sci.* **59**(9), 1329--1336, 1996.

[87] Lewin, L.M., & Pearce, E. M. *Handbook of Fibre Science and Technology Volume IV Fiber Chemistry*, Marcel Dekker, New York, 1985.

[88] David, C., & Fornasier, R. *Macromolecules* **19**(3), 552--557, 1986.

[89] Paillet, M., & Peguy, A. *J. Appl. Polym. Sci.* **40**(3-4), 427--433, 1990.

[90] Mohanty, A.K., & Misra, M. *Polym. Plast. Technol. Eng.* **34**(5), 729--792, 1995.

[91] Mohanty, A.K., *J. Macromol. Sci., Part C: Polym. Rev.* **27**(3-4), 593--639, 1987.

[92] Hon, D.N-S. *Polym. News* **17**, 102--107, 1992.

[93] Crawford, R.L. *Lignin Biodegradation and Transformation*, Wiley, New York, 1981.

[94] Kirk, T.K., Higuchi, T., & Chang, H. M. *Lignin Biodegradation: Microbiology, Chemistry and Potential Applications*, CRS Press, Boca Raton, Florida, 1980.

[95] Ugbolue,S.C.O. *Text. Prog.* **20**(1), 1--43, 1990.

[96] Kucharyov, M.S. *Tekst. Prom.* **8–9**, 23--25, 1993.

[97] Wuppertal, E.W. *Die Textilen Rohstoffe (Natur und Chemiefasern)*, Dr. Spohr-Verlag/Deutscher Fachverlag, Frankfurt, 1981.

[98] Rowell, R.M., Schultz, T.P. & Narayan, R. (eds.). *Emerging Technologies for Materials and Chemicals from Biomass*, American Chemical Society, Washington, DC, 1992.

[99] Varma, D.S., et al. *Text. Res. Inst.* **54**(12), 821--832, 1984.

[100] Mukherjee, P.S., & Satyanarayana, K. G. *J. Mater. Sci.* **21**(5), 51--56, 1986.

[101] Cheremisinoff, N.P. (ed.) *Handbook of Engineering Polymeric Materials*, Marcel Dekker, Inc, New Jersey, 1997.

[102] Varma, D.S., et al. *Thermochim. Acta* **108**(1), 199--210, 1986.

[103] Chand, N. & Rohatgi, P.K. *Natural Fibres and Composites*, Periodical Experts Agency, Delhi, India, 1994.

[104] Zeronian, S.H. *J. Appl. Polym. Sci.* **47**(2), 445--461, 1991.

[105] Saechtling, H. *International Plastics Handbook: for the Technologist, Engineer, and User;* 2nd ed., Hanser, Munich, 1987.

[106] Barkakaty, B.C. *J. Appl. Polym. Sci.* **20**(11), 2921--2940, 1976.

[107] Bisanda, E.T.N., & Ansell, M.P. *Compos. Sci. Technol.* **41**(2), 165--178, 1991.

[108] Zeronian, S.H., et al. *Text. Res. Inst.* **60**(3), 179–183, 1990.

[109] Safonov, V.V. *Treatment of Textile Materials*, Legprombitizdat, Moscow, 1991.

[110]     http://textilelearner.blogspot.com/2012/03/features-oa-jute-fiber-properties-of.html#ixzz2qwXyya5u (07-08-2014)

[111] Mohanty, A.K., et al. *Compos. Sci. Technol.* **60**(7), 1115--1124, 2000.

[112] Albertsson, A-C., & Karlsson, S. *J. Macromol. Sci. A* **33**(10), 1565--1570, 1996.

[113] Rao, P.J., & Ansell, M.P. *J. Mater. Sci.* **20**(11), 4015--4020, 1985.

[114] Karmaker, A.C., & Youngquist, J. *J. Appl. Polym. Sci.* **62**(8), 1147--1151, 1996.

[115] Mitra, B.C., et al. *J. Appl. Polym. Sci.* **67**(6), 1093--1100, 1998.

[116] Gassan, J., & Bledzki, A.K. *Composites Part A* **28**(12), 1001--1005, 1997.

[117] Khan, M.A., et al. *Polym. Plast. Technol. Eng.* **38**(1), 99--112, 1999.

[118] Mohanty, A.K., et al. *J. Mater. Sci.* **35**(10), 2589--2595, 2000.

[119] Ray, D., et al. *Compos. Sci. Technol.* **62**(7-8), 911--917, 2002.

[120] Ray, D., et al. *Composites Part A* **33**(2), 233--241, 2002.

[121] Sarkar, B.K., & Ray, D. *Compos. Sci.Technol.* **64**(13-14), 2213--2219, 2004.

[122] Doan, T.T.L., et al. *Compos. Sci.Technol.* **66**(7-8), 952--963, 2006.

[123] Haydaruzzaman, et al. *Radiat. Phys. Chem.* **78**(11), 986--993, 2009.

[124] Acha, B.A., et al. *Composites Part A* **38**(6), 1507--1516, 2007.

[125] Wang, X., et al. *J. Vinyl Add. Tech.* **16**(3), 183--188, 2010.

[126] Hong, C.K., et al. *J. Ind. Eng. Chem.* **14**(1), 71--76, 2008.

[127] Sarkar, S., & Adhikari, B. *Polym. Compos.* **22**(4), 518--527, 2001.

[128] Samal, R.K., et al. *J. App. Polym. Sci.* **79**(4), 575--581, 2001.

[129] Dwivedi, U.K., & Chand, N. *Appl. Compos. Mater.* **16**(2), 93--100, 2009.

[130] Mir, A., et al. *J. Reinf. Plas. Compos.* **29**(11), 1669--1680, 2010.

[131] Fraga, A.N., et al. *Polym. Test.* **25**(2), 181--187, 2006.

[132] Sabeel, A.K., et al. *Mater. Des.* **28**(8), 2287--2294, 2007.

[133] Dash, B.N., et al. *J. App. Polym. Sci.* **78**(9), 1671--1679, 2000.

[134] Sever, K., et al. *J. Compos. Mater.* **44**(15), 1913--1924, 2010.

[135] Behera, A.K., et al. *Carbohydr. Polym.* **88**(1), 329--335, 2012.

[136] Koo, J.H., (ed.). *Polymer Nanocomposites: Processing, Characterization, and Applications;* McGraw-Hill, New York, 2006.

[137] Paul, D.R., & Robeson, L.M. *Polymer* **49**(15), 3187--3204, 2008.

[138] http://braungroup.beckman.illinois.edu/IanBlitz.html (20-08-2014)

[139] Theng, B.K.G. *The Chemistry of Clay-Organic Reactions*, John Wiley & Sons, New York, 1974.

[140] Fereshten, Z., Loghman-Estarki, M.R., Razavi, R.S. Taheran, M. *Mater. Sci. Semicond. Process.* **16**(2) 547--553, 2013.

[141] Chen, X.L., et al. *J. Appl. Polym. Sci.* **105**(3), 1490--1495, 2007.

[142] Hayashi, S., et al. *J. Photochem. Photobio. B*, **64**(1), 27--35, 2001.

[143] Yadav, A., et al. *Bull. Mater. Sci.*, **29**(6), 641--645, 2006.

[144] Vigneshwaran, N., et al. *Nanotechnology* **17**(20), 5087--5095, 2006.

[145] Katangur, P., et al. *Polym. Degrad. Stab.* **91**(10), 2437--2442, 2006.

[146] Tang, Z.K., et al. *Appl. Phys. Lett.* **72**(25), 3270--3272, 1998.

[147] Hegedus, C., et al. *JCT Coatings Tech.* **5**(4), 42--53, 2008.

[148] Lei, H., et al. *J. Coat. Technol. Res.* **7**(1), 91--97, 2010.

[149] Lowry, M. S., et al. *J. Coat. Technol. Res.* **5**(2), 233--239, 2008.

[150] Laachachi, et al. *Polym. Degrad. Stab.* **94**(4), 670--678, 2009.

[151] Banfield, J.F., & Navrotsky, A. *Nanoparticles and the Environment*, Mineralogical Society of America, Washington, DC, 2001

[152] Yang, D., et al. *J. Phys. Chem. C* **111**(2), 999--1004, 2006.

[153] Yang, D., et al. *J. Am. Chem. Soc.* **131**(49), 17885--17893, 2009.

[154] Yang D, et al. *Adv. Mater.* **20**(14), 2777--2781, 2008.

[155] Yang, H., & Deng, Y. *J. Colloid Interface Sci.* **325**(2), 588--593, 2008.

[156] Kibanova, D., et al. *Appl. Clay Sci.* **42**(3–4), 563--568, 2009.

[157] Hoffmann, M.R., et al. *Chem. Rev.* **95**(1), 69--96, 1995.

[158] Nishimoto, S.I., et al. *J. Chem. Soc., Faraday Trans.* **81**(1), 61--68, 1985.

[159] Fujishima, A., et al. *J. Photochem.Photobio.* **1**(1), 1--21, 2000.

[160] Martínez-Ortiz, M.J., et al. *Mesopor. Mater.* **58**(2), 73--80, 2003.

[161] Payen, A. *Compt. Rend.* **7**, 1052--1056, 1838.

[162] Dufresne, A. Nanocellulose: Potential reinforcement in Composites, in *Natural Polymers: Volume 2: Nanocomposites,* M.J. John, & S. Thomas, eds., RSC Publication, London, 2012, 1—32.

[163] Herrick, F. W., et al. *J. Appl. Polym. Sci. Appl. Polym. Symp.* **37**(3), 797--813, 1989.

[164] Henriksson, M. et al. *Biomacromolecules* **9**(6), 1579--1585, 2008.

[165] Beck-Candanedo, S., et al. *Biomacromolecules* **6**(2), 1048--1054, 2005.

[166] Turbak, A. F. et al. *J. Appl. Polym. Sci. Appl. Polym. Symp.* **37**(3), 815--827, 1989.

[167] de Rodriguez, N. L. G., et al. *Cellulose* **13**(3), 261--270, 2006.

[168] Bai, W., et al. *Cellulose* **16**(3), 455--465, 2009.

[169] Moon, R. J., et al. *Chem. Soc. Rev.* **40**(11), 3941--3994, 2011.

[170] Tokoh, C., et al. *Cellulose* **5**(4), 249--261, 1998.

[171] Klemm, D., et al. *Prog. Polym. Sci.* **26**(9), 1561--1603, 2001.

[172] Yamanaka, S., et al. *J. Mater. Sci.* **24**(9), 3141--3145, 1989.

[173] Vandamme, E. J., et al. *Polym. Degrad. Stab.* **59**(1), 93--99, 1998.

[174] Sakairi, N., et al. *Carbohydr. Polym.* **35**(3-4), 233--237, 1998.

[175] Guhados, G., et al. *Langmuir* **21**(14), 6642--6646, 2005.

[176] Chen, M., et al. *Adv. Polym. Technol.* **14**(2), 97--109, 1995.

[177] Okuda, K., et al. *J. Ferment. Bioeng.* **71**(2), 100--105, 1991.

[178] Migneault, I., et al. *BioTechniques* **37**(5), 790--802, 2004.

[179] Park, S. K., et al. *J. Agric. Food Chem.* **48**(7), 3027--3031, 2000.

[180] Wu, Q., & Zhang, L., *Ind. Eng. Chem. Res.* **40**(8), 1879--1883, 2001.

[181] Song, F., et al. *Biomacromolecules* **12**(10), 3369--3380, 2011.

[182] Mohanty, A. K., et al. *Composites Part A* **31**(2), 143--150, 2000.

[183] Wang, H., et al. *Fibres Polym.* **10**(4), 442--445, 2009.

[184] Khanam, P. N., et al. *J. Polym. Environ.* **19**(1) ,115--119, 2011.

[185] Chabba, S., & Netravali, A. N. *J. Mater. Sci.* **40**(23), 6263--6273, 2005.

[186] Chabba, S., & Netravali, A. N. *J. Mater. Sci.* **40**(23), 6275--6282, 2005.

[187] Lodha, P., & Netravali, A. N. *Compos. Sci. Technol.* **65**(7-8), 1211--1225, 2005.

[188] Khondker, O.A., et al. *Composites Part A* **37**(12), 2274--2284, 2006.

[189] Park, H., et al. *Biomacromolecules* **5**(6), 2281--2288, 2004.

[190] Nam, S., & Netravali, A. N., *Fibres Polym.* **7**(4), 372--379, 2006.

[191] Kumar, R., & Zhang, L. *Compos. Sci. Technol.* **69**(5), 555--560, 2009.

[192] Goda, K., *Composites Part A* **37**(12), 2231--2220, 2006.

[193] Kim, J. T., & Netravali, A. N. *J. Agric. Food Chem.* **58**(9), 5400--5407, 2010.

[194] Pegoretti, A., et al. *Polymer* **45**(8), 2751--2759, 2004.

[195] Lee, K. M., & Han, C. D. *Macromolecules* **36**(3), 804--815, 2003.

[196] Chang, J. H., et al. *Polymer* **43**(10), 2969--2974, 2002.

[197] Ma, J., et al. *Macromol. Rapid Commun.* **25**(19), 1692--1696, 2004.

[198] Fornes, T. D., & Paul, D. R. *Macromolecules* **37**(20), 7698--7709, 2004.

[199] Huang, X., & Netravali, A. N. *Biomacromolecules* 7(10), 2783--2789, 2006.

[200] Pandey, J. K., & Singh, R. P. *Starch/Stärke* 57(1), 8--15, 2005.

[201] Darder, M., et al. *Chem. Mater.* 15(20), 3774--3780, 2003.

[202] Averous, L., et al. *J. Appl. Polym. Sci.* 76(5), 1117--1128, 2000.

[203] Viville, P., *J. Am. Chem. Soc.* 126(29), 9007--9012, 2004.

[204] Cao, X., et al. *Biomacromolecules* 8(3), 899--904, 2007.

[205] Chen, B., & Evans, J. R. G. *Carbohydr. Polym.* 61(4), 455--463, 2005.

[206] Ray, D., et al. *Macromol. Mater. Eng.* 292(10-11), 1075--1084, 2007.

[207] Jong, L. *Composites Part A* 37(3), 438--446, 2006.

[208] John, M. J., & Thomas, S. *Carbohydr. Polym.* 71(3), 343--364, 2008.

[209] Ray, S. S., et al. *Macromolecules* 35(8), 3104--3110, 2002.

[210] Craig, M.C. & Daniel, F.C. Natural fibres, in *Functional fillers for plastics*, M. Xanthos, ed. Weinheim: Wiley-VCH, Verlag, 2005, 195—206.

[211] Marikarian, J. *Plast. Addit. Compd.* 10(1), 20--25, 2008.

[212] O'Donnell, A., et al. *Compos. Sci. Technol.* 64(9), 1135--1145, 2004.

[213] Dweib, M. A., et al. *Compos. Struct.* 63(2), 147--157, 2004.
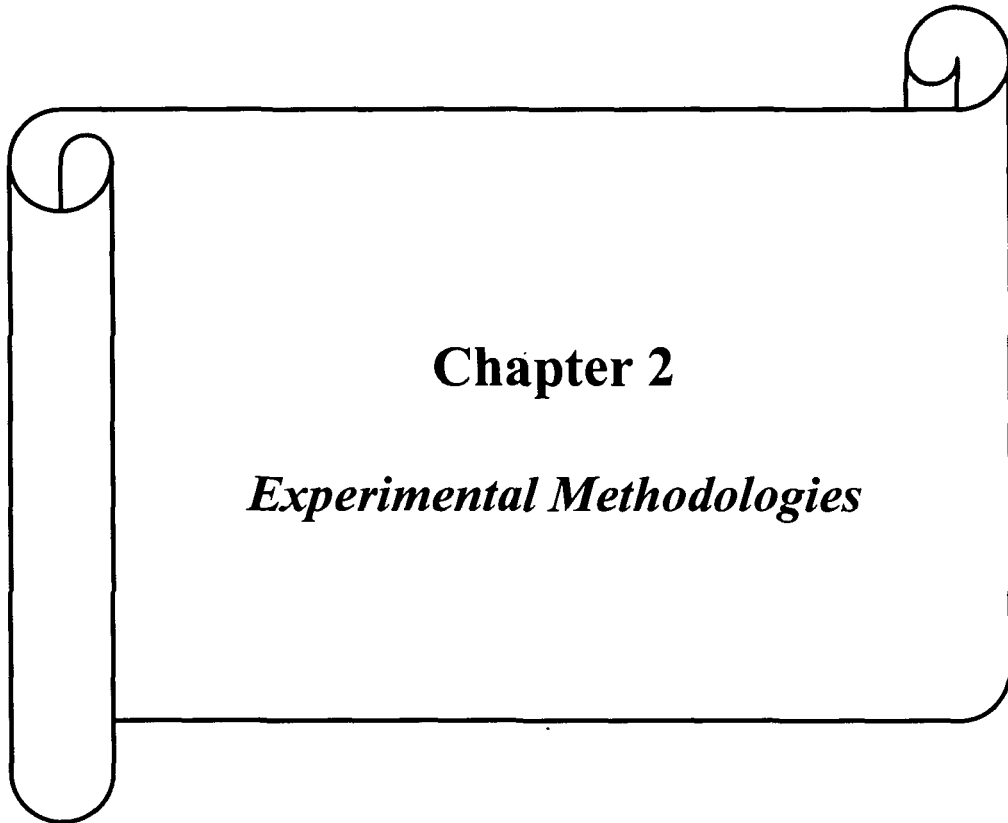
# Chapter 2

## *Experimental Methodologies*

This chapter deals with the materials, methodologies and characterization techniques employed for the synthesis of various virgin polymers, nanoparticles and nanoparticle incorporated nanocomposites. The various physicochemical and spectrochemical techniques *viz.* Scanning Electron Microscope (SEM), Energy-Dispersive X-ray (EDX), X-ray Diffraction (XRD), Thermo Gravimetric Analysis (TGA), Fourier Transform Infrared (FT-IR) spectroscopy, and UV-Visible/ Diffuse Reflectance Spectroscopy (UV-vis/DRS) were used for the characterization of the fabricated composites.

## 2.1. Materials Used

**Table 2.1.** The chemicals used in this study along with the manufacturers are listed below.

| Chemicals | Suppliers |
| --- | --- |
| i) Jute (*Corchorus capsularis* L.) | Local market (Tezpur), India |
| ii) Soy flour (SF) | Raja Soya (Tezpur), India |
| iii) Starch | E-Merck, India |
| iv) Glutaraldehyde (GA) 25 % (w/v) | do |
| v) Benzene | do |
| vi) Glycerol | do |
| vii) NaOH pellets | do |
| viii) $H_2SO_4$ | RANKEM, India |
| ix) Dimethyl sulfoxide (DMSO) | do |
| x) Whatman filter paper (No. 1) | GE Healthcare, U.K. |
| xi) Montmorillonite K-10 clay | Sigma-Aldrich, USA |
| xii) Zinc oxide (ZnO) | do |
| xiii) Titanium dioxide (TiO$_2$) | do |
| xiv) Liquid detergent, Rankleen | RANKEM, India |
| xv) Rectified spirit B.P. | Bengal Chemicals & Pharmaceuticals ltd. |

Besides these, other reagents used for the study were of analytical grade (AR).

## 2.2. Experimental Methods

### 2.2.1. Surface Modification of Jute

Jute fabrics were first treated with 2% liquid detergent at 70 °C for 1 h, washed with distilled water, and finally dried in a vacuum oven at 70 °C until reaching constant weight. The washed fabrics were dewaxed by treatment with a mixture of alcohol and

benzene (1:2) for 72 h at 50 °C. The dewaxed fabrics were again washed with distilled water and subsequently dried till constant weight achieved. The fabrics were then treated with 5% (w/v) NaOH solution for 30 min at 30 °C and washed with distilled water several times to leach out the adsorbed alkali. The fabrics were finally kept immersed in distilled water overnight and washed repeatedly to remove any trace amount of alkali. The alkali-treated fabrics were dried in a vacuum oven at 50 °C to constant weight and stored at ambient temperature in a desiccator.

## 2.2.2. Preparation of Cellulose Whiskers (CWs)

CWs were obtained by acid hydrolysis of commercial filter paper (15 g, Whatman No. 1, GE Healthcare, Chalfont St. Giles, Buckinghamshire, U.K.). The Whatman cellulose filter paper was processed through a test sieve (Scientific Engineering Corporation, New Delhi, India) equipped with a 100-mesh screen. The resulting cellulose powder was then transferred into a beaker containing 100 mL of 5 M NaOH solution. The mixture was stirred at 65 °C for 2 h. The resultant slurry was then filtered, thoroughly washed with distilled water until the wash water was of neutral pH to avoid any trace amount of alkali, and finally air-dried. To the air dried sample was added 100 mL of DMSO, and the slurry was then kept in a water bath at 65 °C for an additional 2 h. The slurry was filtered, washed with 500 mL of distilled water, and air-dried.
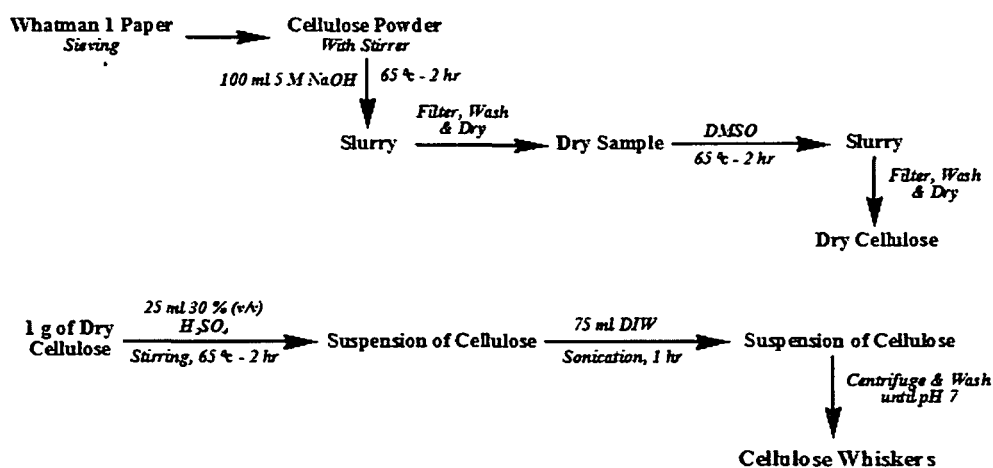


**Scheme 2.1.** Represents the preparation procedure of Cellulose Whiskers.

Then, 1 g of the obtained cellulose was dispersed in 25 mL of 30% (v/v) $H_2SO_4$ in a three-necked (250 mL) round bottom flask equipped with a mechanical stirrer and

a thermometer. The flask was then placed in a water bath, and its contents were stirred vigorously for 4 h while the temperature was maintained at 65 °C. The suspension was then diluted with 75 mL of distilled water and sonicated for 1 h. The dispersion was centrifuged at nearly 8000 rpm for 30 min and washed with distilled water until the pH of the supernatant liquid was nearly 7. The residues (cellulose whiskers) separated after high-speed centrifugation was collected and freeze-dried. These cellulose whiskers were further used for the preparation of the composites.

### 2.2.3. Preparation of the Slurry

*2.2.3.1. Preparation of crosslinked jute-SF composite reinforced with nanoclay*

Bio-composites were synthesized from suitable resin prepared by using SF powder which was first mixed thoroughly with deionized water at 1:10 ratio (w/w) and stirred continuously. Then glycerol was added as a plasticizer. SF was found to be brittle, weak and difficult to process into useful films in absence of plasticizer. The slurry containing SF and glycerol was transferred to a 500 ml round bottom flask and stirred with a mechanical stirrer for 4 h maintaining the temperature at 55±5 °C. The temperature of the slurry was then brought down to 35±5 °C. After that glutaraldehyde (GA) was added and stirred for another 5 min at that temperature. The amount of GA was varied from 30 - 70% (w/w of SF). This stage is referred to as pre-cured resin. In order to prepare clay filled resin, desired amount of clay {1 - 5 % (w/w) of SF} was first taken in a beaker containing water, stirred for 6 h using magnetic stirrer followed by sonication for 30 min under 0.5 cycle and a wave amplitude of 140 μm using a sonicator (model Heilscher UP200S, Germany) and finally added to the pre-cured resin.

*2.2.3.2. Preparation of crosslinked jute-SF composite reinforced with CW and nanoclay*

SF powders were first mixed thoroughly with deionized water (1:10, w/w) at room temperature for 1 h to obtain a suitable resin for the fabrication of "bio-composites". 5% glycerol (w/w with respect to dry SF) was added as a plasticizer. The slurry containing SF and glycerol was transferred to a 500 mL round-bottom flask and stirred with a mechanical stirrer while the temperature was maintained in the range of 55 - 60 °C for 4 h. The slurry was then cooled to 35 °C. The resultant mixture was stirred for an additional 5 min at that temperature with subsequent addition of GA. To prepare CW-filled resin, the desired amount of CWs (1-5% w/w with respect to dry SF) was first placed in a beaker containing water, stirred for 8 h using a mechanical stirrer,

sonicated for 30 min under 0.5 cycle and a wave amplitude of 140 $\mu$m, and finally added to the pre-cured resin. Similarly, for the CW and nanoclay filled resin, 5% CWs (w/w with respect to dry SF) and nanoclay (1 - 5% w/w with respect to dry SF) were first placed in a beaker containing water. Then, the mixture was stirred for 8 h using a mechanical stirrer, after which it was sonicated for 30 min. The mixture was then poured into the pre-cured resin system, and the whole resin mixture was stirred for an additional 1 h with a high-speed mechanical stirrer and then sonicated for 30 min so that the CWs and nanoclay particles were well-dispersed inside the resin matrix.

*2.2.3.3. Preparation of crosslinked jute-SF composite reinforced with TiO2 and nanoclay*

SF powders were first carefully mixed with deionized water in 1:10 ratio (w/w) at room temperature for 1 h to obtain a suitable resin for fabrication of "bio-composites". 5 % glycerol (w/w of dry SF) was added as a plasticizer. The slurry containing SF and glycerol was transferred to a 500 mL round bottom flask and stirred with a mechanical stirrer maintaining the temperature in the range 55–60 °C for 4 h. The temperature of the slurry was then cooled to 35 °C. The resultant mixer was further stirred for another 5 min at the same temperature with subsequent addition of GA. In order to prepare TiO2 filled resin, desired amount of TiO2 (1 – 5 % w/w of dry SF) was first taken in a beaker containing water, stirred for 8 h using mechanical stirrer followed by sonication for 30 min under 0.5 cycle and a wave amplitude of 140 $\mu$m, and finally added to the slurry containing SF and glycerol. Similarly, for the TiO2 and nanoclay filled resin, 5% TiO2 (w/w of dry SF) and nanoclay (1-5 % w/w of dry SF) were first taken in a beaker containing water. Then the mixture was stirred for 8 h using a mechanical stirrer and sonicated for 30 min. The mixture was then poured in the pre-cured resin system. Subsequently the whole resin mixture was stirred for another 1 h with the help of high speed mechanical stirrer followed by sonication for 30 min so that the TiO2 and nanoclay particles were well dispersed inside the resin matrix.

*2.2.3.4. Preparation of crosslinked jute-SF composite reinforced with ZnO and nanoclay*

SF powders were first carefully mixed with deionized water in 1:10 ratio (w/w) at room temperature for 1 h to obtain a suitable resin for fabrication of "bio-composites". 5 % glycerol (w/w of dry SF) was added as a plasticizer. The slurry containing SF and glycerol was transferred to a 500 mL round bottom flask and stirred with a mechanical stirrer maintaining the temperature in the range 55–60 °C for 4 h.

The temperature of the slurry was then cooled to 35 °C. The resultant mixer was further stirred for another 5 min at the same temperature with subsequent addition of GA. In order to prepare ZnO filled resin, desired amount of ZnO (1 – 5 % w/w of dry SF) was first taken in a beaker containing water, stirred for 8 h using mechanical stirrer followed by sonication for 30 min under 0.5 cycle and a wave amplitude of 140 $\mu$m, and finally added to the slurry containing SF and glycerol. Similarly, for the ZnO and nanoclay filled resin, 5% ZnO (w/w of dry SF) and nanoclay (1-5 % w/w of dry SF) were first taken in a beaker containing water. Then the mixture was stirred for 8 h using a mechanical stirrer and sonicated for 30 min. The mixture was then poured in the pre-cured resin system. Subsequently the whole resin mixture was stirred for another 1 h with the help of high speed mechanical stirrer followed by sonication for 30 min so that the ZnO and nanoclay particles were well dispersed inside the resin matrix.

### 2.2.3.5. Preparation of crosslinked jute-starch composite reinforced with nanoclay

To process starch powder into a suitable resin for fabricating "bio-composites", it was mixed thoroughly with deionized water at 1:10 ratio (w/w) and stirred continuously. Starch was found to be very brittle, weak and difficult to process into useful films in absence of plasticizer. Therefore, glycerol was added as a plasticizer. The optimum amount of glycerol required to process starch into useful film was 5% (w/w of dry starch). The slurry containing starch and glycerol (5 %, w/w) was transferred to a 500 mL round bottom flask and stirred with a mechanical stirrer maintaining the temperature in the range 55-60 °C for 4 h. The temperature of the slurry was then cooled to 35 °C. To this, GA was added and stirred for another 5 min at that temperature. The amount of GA was varied from 30 - 70% (w/w of dry starch). This stage is referred to as pre-cured resin. In order to prepare clay filled resin, desired amount of clay (1 – 5 % w/w of dry starch) was first taken in a beaker containing water, stirred for 6 h using mechanical stirrer followed by sonication for 30 min under 0.5 cycle and a wave amplitude of 140 $\mu$m, and finally added to the pre-cured resin.

### 2.2.3.6. Preparation of crosslinked jute-starch composite reinforced with cellulose whisker and nanoclay

Starch powders are first mixed thoroughly with deionized water at 1:10 ratio (w/w) at room temperature for 1 h to obtain a suitable resin for fabrication of "bio-composites". 5 % of glycerol (w/w of dry Starch) is added as a plasticizer. The slurry containing starch and glycerol is transferred to a 500 mL round bottom flask and stirred with a mechanical stirrer maintaining the temperature in the range 55-60 °C for 4 h.

The temperature of the slurry is then cooled to 35 °C. The resultant mixer is further stirred for another 5 min at that temperature with subsequent addition of 50 % GA (w/w of dry Starch). In order to prepare CWs filled resin, desired amount of CWs (1 – 5 % w/w of dry Starch) is first taken in a beaker containing water, stirred for 8 h using mechanical stirrer followed by sonication for 30 min under 0.5 cycle and a wave amplitude of 140 $\mu$m, and finally added to the pre-cured resin. A similar procedure is followed for synthesizing the CWs and nanoclay filled resin. The mixture is then poured in the pre-cured resin system. After adding to the pre-cured resin system, the whole resin mixture is stirred for another 1 h with the help of high speed mechanical stirrer followed by sonication for 30 min so that the CWs and nanoclay particles are well dispersed inside the resin matrix. The temperature of the slurry is then cooled to 35 °C and finally this mixer is stirred for another 5 min at that temperature with subsequent addition of 50 % GA (w/w of dry Starch).

### 2.2.3.7. Preparation of crosslinked jute-starch composite reinforced with TiO₂ and nanoclay

*2.2.3.7. Preparation of crosslinked jute-starch composite reinforced with $TiO_2$ and nanoclay*

Starch powders are first mixed thoroughly with deionized water at 1:10 ratio (w/w) at room temperature for 1 h to obtain a suitable resin for fabrication of composites. 5 % glycerol (w/w of dry Starch) is added as a plasticizer. The slurry containing starch and glycerol is transferred to a 500 mL round bottom flask and stirred with a mechanical stirrer maintaining the temperature in the range 55–60 °C for 4 h and subsequently cooled to 35 °C. The resultant mixture is further stirred for another 5 min at that temperature with subsequent addition of GA. In order to prepare $TiO_2$ filled resin, desired amount of $TiO_2$ (1 – 5 % w/w of dry Starch) is first taken in a beaker containing water, stirred for 8 h using mechanical stirrer followed by sonication for 30 min under 0.5 cycle and a wave amplitude of 140 $\mu$m, and finally added to the slurry containing starch and glycerol. Similarly, for the $TiO_2$ and nanoclay filled resin, desired amount of $TiO_2$ (5% w/w of dry Starch) and nanoclay (1-5 % w/w of dry Starch) is first taken in a beaker containing water. Then the mixture is stirred for 8 h using a mechanical stirrer and sonicated for 30 min. The mixture is then poured in the pre-cured resin system. After adding to the pre-cured resin system, the whole resin mixture is stirred for another 1 h with the help of high speed mechanical stirrer followed by sonication for 30 min so that the $TiO_2$ and nanoclay particles are well dispersed inside the resin matrix.

*2.2.3.8. Preparation of crosslinked jute-starch composite reinforced with ZnO and nanoclay*

Starch powders are first mixed thoroughly with deionized water at 1:10 ratio (w/w) at room temperature for 1 h to obtain a suitable resin for fabrication of composites. 5 % glycerol (w/w of dry Starch) is added as a plasticizer. The slurry containing starch and glycerol is transferred to a 500 mL round bottom flask and stirred with a mechanical stirrer maintaining the temperature in the range 55–60 °C for 4 h and subsequently cooled to 35 °C. The resultant mixture is further stirred for another 5 min at that temperature with subsequent addition of GA. In order to prepare ZnO filled resin, desired amount of ZnO (1 – 5 % w/w of dry Starch) is first taken in a beaker containing water, stirred for 8 h using mechanical stirrer followed by sonication for 30 min under 0.5 cycle and a wave amplitude of 140 $\mu$m and finally added to the slurry containing starch and glycerol. Similarly, for the ZnO and nanoclay filled resin, desired amount of ZnO (5% w/w of dry Starch) and nanoclay (1-5 % w/w of dry Starch) is first taken in a beaker containing water. Then the mixture is stirred for 8 h using a mechanical stirrer and sonicated for 30 min. The mixture is then poured in the pre-cured resin system. After adding to the pre-cured resin system, the whole resin mixture is stirred for another 1 h with the help of high speed mechanical stirrer followed by sonication for 30 min so that the ZnO and nanoclay particles are well dispersed inside the resin matrix.

### 2.2.4. Impregnation of jute fabrics & fabrication of composites

The prepared pre-cured resin (filled with nanoclay/CW/$TiO_2$/ZnO/CW-nanoclay/$TiO_2$-nanoclay/ZnO-nanoclay) was first poured in a bowl, and then surface modified jute fabric was dipped into the pre-cured resin slurry. The resultant mixture was kept for 24 h at 25 °C. The impregnated jute fabrics were placed in a Teflon coated glass plate and dried over a heating plate at 30-40 °C for 12 h. The weight of jute fabrics before impregnation was recorded as $W_1$.

Composite laminates were prepared by the method of film stacking. Layers of impregnated jute fabric were placed on one another on 15 levels in a metal mould of thickness 3 mm. The laminates were then compression moulded in a compression moulding press (Santec, New Delhi) at 80 °C under a pressure of 100 MPa. The laminates were 3 mm in thickness. The final weight of the composite was recorded as $W_2$. The calculations were performed according to the following equations:

$$Percentage\ of\ Jute\ in\ the\ Composite\ = \left(\frac{W_1}{W_2}\right) \times 100 \tag{i}$$

$$Percentage\ of\ Resin\ in\ the\ Composite\ = \left\{\frac{(W_2 - W_1)}{W_2}\right\} \times 100 \tag{ii}$$

Where, $W_1$ = Weight of jute fabrics before impregnation

$W_2$ = Weight of the final composite.
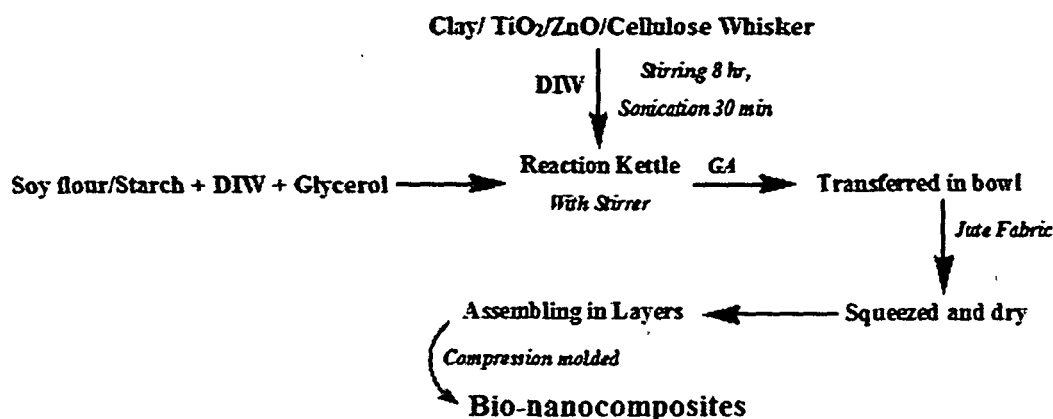


**Scheme 2.2.** Fabrication of bio-nanocomposites employing various nanoparticles.

### 2.2.5. Bacterial Media

The preparation of mineral salt medium for bacterial growth was carried out according to the following composition: 4.75 g of $KH_2PO_4$, 2.0 g of $(NH_4)_2SO_4$, 2.0 g of $Na_2HPO_4$, 1.2 g of $MgSO_4 \cdot 7H_2O$, 100 mg of $CuSO_4 \cdot 7H_2O$, 100 mg of $MnSO_4 \cdot 5H_2O$, 70 mg of $ZnSO_4 \cdot 7H_2O$, 10 mg of $MoO_3$, 10 mg of $H_3BO_3 \cdot 5H_2O$, 1 mg of $FeSO_4 \cdot 7H_2O$, and 0.5 mg of $CaCl_2 \cdot 2H_2O$ dissolved in 1000 mL of demineralized water. 3 mL of this liquid culture medium was then transferred into a 50 mL conical test tube and it was sterilized by autoclave at 121 °C and 15 $lb_f$ pressure for 15 min [1]. The autoclaved media were then allowed to cool to room temperature and composite samples were added into the media under sterile condition inside a laminar air flow hood. Media which contained S/J/GA50 composites were cultured as negative control. The S/J composites were exposed to fungal colonization and degradation for 90 days.

### 2.2.6. Bacterial Strains

For degradation of bio-polymer composite, microbial strains were isolated from garden soil containing biomass by enrichment of minimal salt medium using 2 % cellulose [2]. The strain showing highest growth was selected for checking the rate of

biodegradation of the composites. Bacterial cultures were centrifuged at 6000 rpm for 15 min at room temperature and the pellets were washed with sterilized 0.85 % NaCl solution and re-suspended in mineral salt medium. An amount of the culture medium containing approximately $1 \times 10^8$ $ml^{-1}$ microbes were inoculated to the test tube containing medium for each test. The composite samples were cut in small blocks (5 mm × 20 mm × 40 mm) and were sterilized with 70 % alcohol and exposed to UV for 30 minutes in each side of the composite block. The blocks were immersed in sterilized minimal salt medium in test tubes under sterile condition inside a laminar air hood. Media containing no wood composite were also cultured as negative control. The samples were incubated in a shaker incubator at 37 °C with 20 revolutions per minutes for 90 days for degradation study. The samples were collected for spectrophotometric observation at 600 nm against blank culture media on monthly basis under sterile condition.

## 2.3. Methods of Characterization

### 2.3.1. X-ray diffractometry (XRD)

Powder X-ray diffraction (XRD) patterns were recorded on a Rigaku X-ray diffractometer (Miniflex, UK) using Cu K$\alpha$ ($\lambda$= 0.154 nm). XRD patterns were recorded in the $2\theta$ ranging from 2° to 70° at a scanning rate of 2° $min^{-1}$. The interlayer spacing for clay was calculated according to Bragg's law,

$$n\lambda = 2d\ sin\theta \hspace{4cm} \text{(iii)}$$

where, n = order of reflection (n=1, for first order; n=2, for second order reflection),

$\lambda$ = wave length, d = distance between two plane, $\theta$ = diffraction angle.

### 2.3.2. Transmission electron microscope (TEM)

The samples were prepared by following the method of Devi *et al* [3]. The samples were embedded with epoxy resin. Ultrathin sections (approximately 100 nm thick) of the transverse film surfaces had been sectioned using an ultramicrotome fitted with a diamond knife. The sections were then stained with 1 wt % uranyl acetate for sufficient contrast. After staining, the sections were mounted on grids and examined with a High Resolution Transmission Electron Microscope (HRTEM) (JEOL, JEM 2100) at an accelerating voltage of 200 kV.

## 2.3.3. Scanning electron microscopy (SEM)

The surface morphology of some of the prepared samples was studied by scanning electron microscopy (SEM) before it was subjected to mechanical test. The morphology of the fracture surface of the samples obtained from flexural test was also studied by SEM. All the samples were coated with Pt for analysis. SEM analysis was performed by using a JEOL scanning electron microscope (model JSM-6390LV) at an accelerating voltage of 15 kV.

The presence of the nanoparticles in the synthesized composites was identified through energy-dispersive X-ray analysis of the samples at the same time when the scanning was performed.

For biodegradation study, sample preparation was done according to Gu *et al.* [4], and Lomeli-Ramirez *et al.* [5] with some modifications. Samples were prepared by cutting small pieces from randomly chosen part of the processed specimen with the help of sharp surgical blade. The samples were treated with 3 % glutaraldehyde, dehydrated with ethanol as gradient and fixed with 1 % osmium tetroxide. Treated samples were mounted on aluminum stubs and coated with gold and observed by SEM (JEOL JSM–390 LV) at an accelerated voltage of 5–15 kV.

## 2.3.4. Fourier-transform infrared spectroscopy (FT-IR)

FT-IR spectra were recorded in FT-IR (Impact-410, Nicolet, USA) spectrophotometer using KBr pellet. Small quantities of finely powdered samples were thoroughly grounded with exhaustively dried KBr and subsequently pellets were prepared by compression under vacuum. FT-IR spectra were recorded in the range of 4000-400 cm$^{-1}$.

## 2.3.5. Ultra Violet visible/ Diffuse Reflectance Spectroscopy (UV-vis/DRS)

The electronic absorption spectra were recorded using a Shimadzu Corporation /UV2450, Japan spectrophotometer with a diffuse reflectance attachment equipped with an integrating sphere of 60 mm inner diameter. Monochromatic light was used in the whole spectral region in order to minimize the effect of fluorescence. For recording the spectra of the synthesized bio-nanocomposites, the powdered samples were placed in a black absorbing hole (10 mm, in diameter, and 3 mm deep) of a sample holder, and the surface was smoothed.

## 2.3.6. Nuclear magnetic resonance (NMR) spectrophotometer

The $^{13}$C solid state Nuclear Magnetic Resonance (NMR) study of the synthesized composite was performed by using BRUKER DSX-300 solid state NMR spectrometer.

## 2.3.7. Thermal property

Thermal properties of SF, starch, jute, nanoparticles and the synthesized Nano composite samples were evaluated by employing thermo gravimetric analyzer (TGA) *(model TGA 50, Shimadzu) under the nitrogen flow rate of 30 mL min$^{-1}$ at the heating rate of 10 °C min$^{-1}$* from 30 °C to 600 °C. The sample weight is maintained 5 mg and each set is recorded thrice to check the consistency of the observation.

## 2.3.8. Mechanical property

The tensile and flexural tests for the prepared composites loaded with different percentage of clay alone or with other nanoparticles were carried out using Universal Testing Machine-HOUNSEFIELD, England (model H100K-S) at a crosshead speed of 2 mm min$^{-1}$ at room temperature according to ASTM D-638 and D-790 respectively. Ten samples of each category were tested and their average values were reported.

## 2.3.9. UV Resistance

The UV degradation study of the composite samples were carried out using a UV chamber (Model S.L.W, voltage, 230 V, power, 1000 W; Advanced Research Co., India) employing a mercury arc lamp system that produces a collimated and highly uniform UV flux in the 254–365 nm range. Specimen's dimensions of (25 × 25 × 3) mm$^3$ were exposed in the UV chamber at room temperature and characterized at definite time intervals. The exposure period was varied from 0 to 60 days. The weight loss was measured using an analytical balance and was calculated as follows [6]:

$$\% \, Weight \, loss = \left\{ {}^{(W_t - W_0)}\!/_{W_0} \right\} \times 100 \qquad \text{(iv)}$$

Where, '$W_t$' is the specimen weight at time t, and '$W_0$' is the specimen weight before UV exposure. The chemical degradation of the samples was studied by FT-IR analysis. The relative intensity of the carbonyl (C=O) stretching peaks at 1650 cm$^{-1}$ corresponding to starch of the composite is measured. The net peak heights were determined by subtracting the height of the baseline directly from the total peak height.

The same baseline was taken for each peak before and after exposure to UV radiation [7]. The S/J composites degradation was studied by carbonyl index which was calculated by the following equation:

$$carbonyl\ index\ =\ {^{I_c}/_{I_R}}\ \times 100 \tag{v}$$

Where '$I_C$' is the intensity of the carbonyl absorption band (1650–1750 cm$^{-1}$) and '$I_R$' is the intensity of the reference band (2900–2950 cm$^{-1}$). This peak was chosen as reference due to its least change during irradiation. Mechanical properties were also studied after UV exposure.

### 2.3.10. Dimensional stability

The prepared composites were cut into blocks of 3 mm × 10 mm × 25 mm (radial × tangential × longitudinal) for dimensional stability test. Then samples were kept at room temperature and 30 % relative humidity. The samples were then placed in a humidity chamber for 72 h at room temperature maintaining relative humidity of 65%. The specimens were taken out from the humidity chamber after stipulated time period and volumes were measured with the help of slide calipers. The percentage of swelling in water vapour was calculated as per formula given below:

$$\%\ Swelling\ =\ \left\{ {^{(V_t\ -\ V_0)}/_{V_0}} \right\} \times 100 \tag{vi}$$

Where, '$V_t$' is volume of the sample after "t" time and '$V_0$' is initial volume of composite sample before water vapour adsorption.

### 2.3.11. Limiting oxygen index (LOI)

LOI is defined as the minimum concentration of oxygen, expressed as percent volume, in a flowing mixture of oxygen and nitrogen that will support flaming combustion of a material initially at room temperature. The specimens were cut into 100 mm × 6 mm × 3 mm (longitudinal × tangential × radial) according to ASTM-D 2863 and placed vertically in the flammability tester (S.C. Dey Co., Kolkata). The total volume of the gas mixture ($N_2$ + $O_2$) was kept fixed at 18 cc. The volume of nitrogen gas and that of oxygen gas were kept initially at a maximum and minimum level, respectively. Thereafter, the volume of nitrogen gas was decreased and that of oxygen gas is increased gradually. However, the total volume of gas mixture was kept fixed at 18 cc during the experiment. The ratio of nitrogen and oxygen at which the sample continued to burn for at least 30 s was recorded. LOI is calculated as:

$$LOI = \left\{ \frac{Volume\ of\ O_2}{Volume\ of\ (O_2 + N_2)} \right\} \times 100 \qquad \text{(vii)}$$

### 2.3.12. Biodegradation study

The microbial degradation was studied spectrophotometrically by using a UV visible spectrophotometer (Shimadzu Corporation UV2450 spectrophotometer, Kyoto, Japan) at 600 nm against blank culture media under sterile condition.

### References

[1]. Deka, B. K., et al. *Ind. Eng. Chem. Res.* **51**(37), 11881--11891, 2012.

[2]. di Franco, C.R., et al. *Polym. Degrad. Stab.* **86**(1), 95--103, 2004.

[3] Devi, R. R., & Maji, T.K. *Ind. Eng. Chem. Res.* **51**(10), 3870--3880, 2012.

[4] Gu, J.D., et al. *Int. Biodeterior. Biodegrad.* **41**(2), 101--109, 1998.

[5] Lomeli-Ramirez, M.G., et al. *Int. Biodeterior. Biodegrad.* **63**(8), 1030--1035, 2009.

[6] Fa, W., et al. *J Appl. Polym. Sci.* **118**(1), 378--384, 2010.

[7] Stark, N. M., & Matuana, L. M. *Polym. Degrad. Stab.* **86**(1), 1--9, 2004.

# Chapter 3

*Results & Discussion: Jute based Soy flour nanocomposites*

*Section A*: **Study on the effect of crosslinker and Nanoclay on jute fabric reinforced Soy flour bio-nanocomposites**

Conventional polymers which are obtained from petrochemicals are non-renewable and environment unfavourable [1, 2]. The environmental impact of polymeric waste is increasing global concern, and besides alternative disposal methods are limited. Moreover, the use of natural fibres to reinforce thermoplastics as an alternative to synthetic or glass fibres has been and continues to be the subject of research and development [3, 4]. The fibre reinforcement of biopolymers such as Poly(lactic acid) (PLA) can produce composites with suitable mechanical properties for light weight construction materials. Soy protein is one of the less expensive bio-polymers abundant worldwide. Its purification process is benign and environment friendly. This protein can also be used as resin due to its ability to form ductile and viscous polymers. Jute, a kind of natural fibre, is widely available and can be used for making composites. Surface modification like dewaxing and mercerization of jute fabrics are essential prior to their use for composite preparation.

In this part of work, we have studied the impact of nanoclay on the various properties of the composite formed by a mixture of jute fabric, soy flour, nanoclay and glutaraldehyde. Furthermore, the effect of glutaraldehyde on different properties of the composite has also been studied.

## 3.1. RESULTS & DISCUSSION

We have prepared the samples as coded in Table 3.1.1. The wt (%) of the components viz. SF, glycerol and Jute were kept constant in all the samples where as the wt (%) of GA and nanoclay were varied. The wt (%) of the various components used for the synthesis of the composite are provided in Table 3.1.1.

**Table 3.1.1.** Composition of plasticized soy flour based composite.

| Sample | Soy Flour[a] | Glycerol | GA[b] (Wt. %) | Jute | Nanoclay |
|---|---|---|---|---|---|
| S/J | 100 | 5 | - | 75 | - |
| S/J/G30 | 100 | 5 | 30 (6) | 75 | - |
| S/J/G40 | 100 | 5 | 40 (8) | 75 | - |
| S/J/G50 | 100 | 5 | 50 (10) | 75 | - |
| S/J/G60 | 100 | 5 | 60 (12) | 75 | - |
| S/J/G70 | 100 | 5 | 70 (14) | 75 | - |
| S/J/G50/M1 | 100 | 5 | 50 | 75 | 1 |
| S/J/G50/M3 | 100 | 5 | 50 | 75 | 3 |
| S/J/G50/M5 | 100 | 5 | 50 | 75 | 5 |

[a] 20 g of soy flour is assumed to be 100.

[b] The percentage of GA with respect to Soy flour. The value in the parenthesis indicates the amount of GA in gram.

### 3.1.1. XRD study

Figure [3.1.1 (a-c)] represents the XRD pattern of pure clay, jute and SF, respectively. A broader peak at $2\theta = 19°$ was found to appear in SF diffractograms [5]. Figure 3.1.1d and 3.1.1e represents the XRD pattern of mixtures of S/J and S/J/G50, respectively. It has been seen from the XRD pattern that the mixing of the polymer components along with the crosslinker did not modify the crystallinity of either of the components. However, on incorporation of nanoclay in the synthesized composite (prepared by SF, Jute, GA and nanoclay), a change in the XRD pattern was observed. In the absence of nanoclay, the composite showed sharp peaks at $2\theta = 22°$ (002 plane of cellulose I) and 19° (101 plane of cellulose II) [6]. However, after its modification with nanoclay the intensity of the peak at $2\theta = 22°$ corresponding to 002 plan of cellulose I get diminished and concomitantly a new low intense peak at $2\theta = 7.5°$ was emerged. This indicated that the clay particles were partially exfoliated and dispersed into the composite. The lowering of intensity of the peak at $2\theta = 9°$ indicated the breakdown of the layered structure of nanoclay in the treated composite [7].
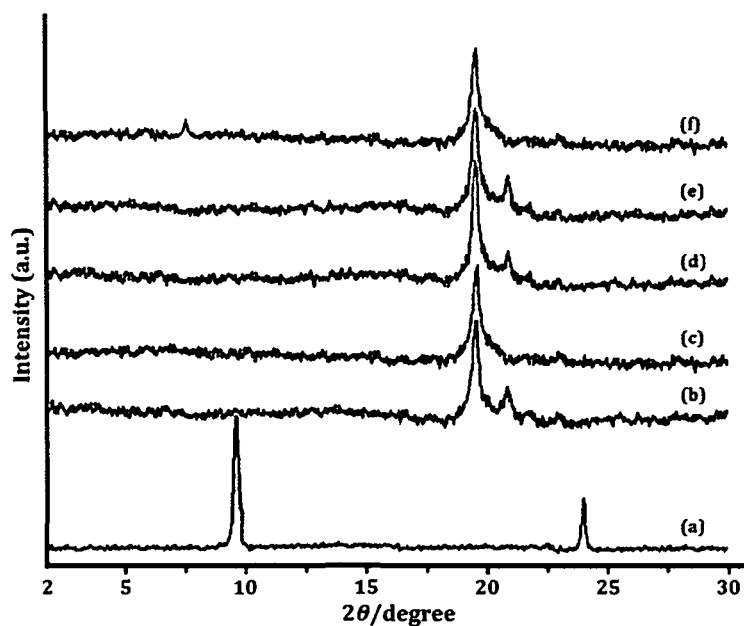
**Figure 3.1.1.** XRD patterns of (a) clay, (b) Jute, (c) soy flour, (d) S/J, (e) S/J/G50 and (f) S/J/G50/M5.

### 3.1.2. TEM study

TEM analysis was carried out to verify the extent of exfoliation of nanoclay particles in the prepared composites and is presented in Figure 3.1.2. Figure 3.1.2a represents the TEM micrographs without clay composite within 200 nm range whereas Figure 3.1.2b and 3.1.2c are taken within a range of 200 and 600 nm, respectively.
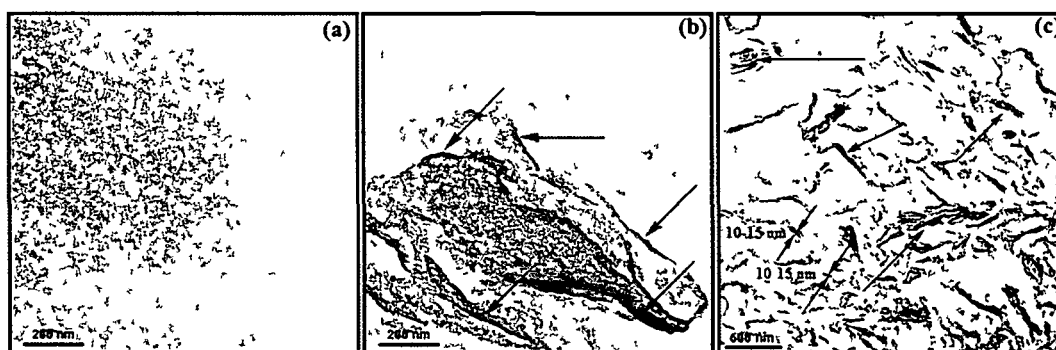


**Figure 3.1.2.** TEM micrographs of Soy flour/jute composite (a) without clay taken within 200 nm range and (b) and (c) with clay composite at 200 nm and 600 nm scale.

The dispersion of clay layers as dark lines (shown by arrow mark) was observed in both the images. A closer look at Figure 3.1.2b and c revealed the successful incorporation of nanoclay into the composite which was clearly evident in Figure 3.1.2b but not in Figure 3.1.2a. Moreover, Figure 3.1.2b and c inferred that the clay layers were

delaminated into thin lamellas by soy protein with a dimension of about 10~15 nm in thickness. This suggests that the nanoclay layers were dispersed and partially exfoliated into soy protein matrix. Similar type of delaminated structure of MMT was also reported in literature and had been considered as a successful intercalation of the nanocomposites [8, 9]. These transmission electron microscopic analyses are in accordance with the XRD findings. So, it can be concluded that jute reinforced soy flour clay nanocomposites with a delaminated structure could be prepared by solution induced intercalation method in neutral aqueous medium.

### 3.1.3. SEM study

The SEM micrograph of SF as shown in Figure 3.1.3a indicated that the particles were irregular compact disc shaped [10], whereas the SEM micrographs of the jute fibres were smooth and regular as observed from Figure 3.1.3b. Figure 3.1.3. (c & d) showed micrographs of composites without and with GA. From the micrographs, it was observed that composites with GA crosslinks showed better adhesion of the SF matrix onto the jute surface compared to the composites without GA. The surface of the composite having GA seemed to be less smooth compared to that of composite without GA. This was due to the less adherence of the resin to the fibre surface. On · addition of GA into the composite, less fibre was seen to protrude out of the composite (Figure 3.1.3e).

From Figure 3.1.3d, it was also found that the surface of glutaraldehyde crosslinked S/J composite was rough [11]. However, on addition of the clay nano particles, the brittleness along with the roughness of the composites was increased · [Figure 3.1.3. (f-i)]. This might be due to the fact that the clay particles reinforced the interaction between resin and jute surface through its hydroxyl groups which results in enhancement of adhesion and consequently less pull out of fibres from the fractured surface [12]. The brittleness and roughness of the composite surface was found to increase with the increase in concentration of nanoclay particles from (1-5) % (Figure 3.1.3f & 3.1.3h). The increase in roughness and· brittleness might be due to the adherence of either the soy flour or the soy flour/clay to the jute surface.
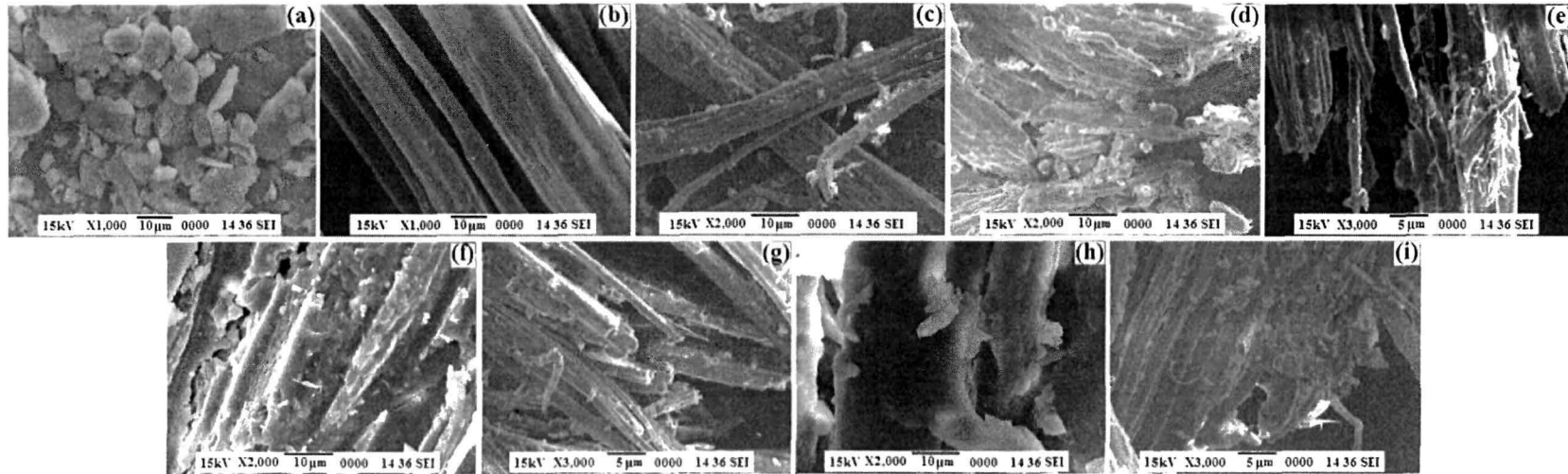
**Figure 3.1.3.** SEM micrographs of (a) soy flour, (b) jute, (c) S/J surface, (d) S/J/G50 surface, (e) S/J/G50 fracture surface, (f) S/J/G50/M1 surface, (g) S/J/G50/M1 fracture surface, (h) S/J/G50/M5 surface and (i) S/J/G50/M5 fracture surface.

### *3.1.4. FT-IR study*

FT-IR spectra for soy flour, jute, clay, S/J, S/J/G50 and S/J/G50/M are presented in Figure 3.1.4. The FT-IR spectra for all the samples except clay and jute showed the peaks in the region 3400 - 3000cm$^{-1}$ which could be attributed to the – OH and – NH stretching vibrations respectively. The spectrum of SF (Figure 3.1.4a) shows peaks in the region 1648, 1544 and 1248 cm$^{-1}$ for C = O stretching of amide – I, – NH bending of amide – II and C – N stretching of amide – III [13]. A peak was observed in the
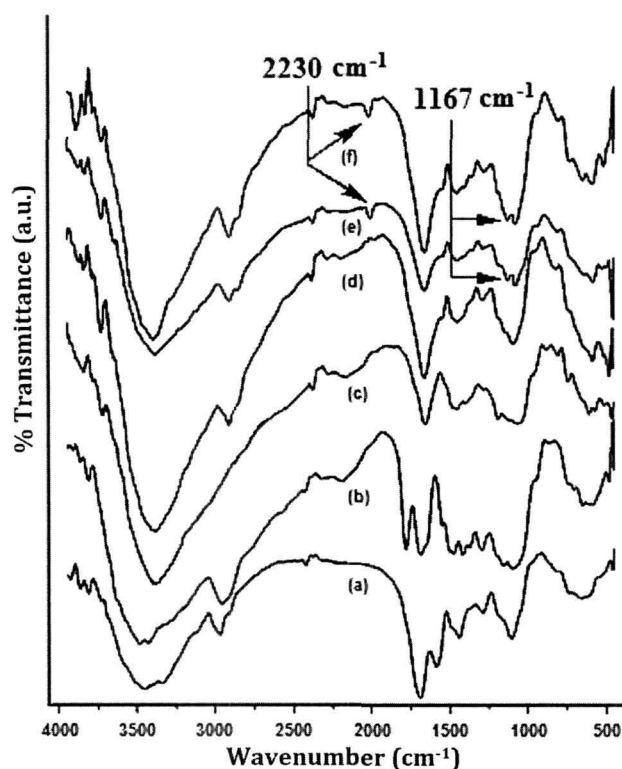


**Figure 3.1.4.** FT-IR spectra of (a) soy flour, (b) Jute, (c) clay, (d) S/J, (e) S/J/G and (f) S/J/G/M.

region 1738 cm$^{-1}$ in the jute spectrum which might be due to the C = O stretching vibration of ester groups of hemicelluloses. Similarly, the peaks appeared in the FT-IR spectrum of jute at 1640, 1254 and 1057-1116 cm$^{-1}$ were for C = O stretching, – C – O – C – bond in cellulose chain and C – O stretching [14]. The peak observed in the region 1619 cm$^{-1}$ is due to – OH bending vibration (Figure 3.1.4b). The peaks shown in the range 1030 – 460 cm$^{-1}$ were the characteristic peaks of oxide bonds of metals (M – O) like Si, Al, Mg etc. present in the nanoclay (Figure 3.1.4c).

66

Characteristics peaks of soy flour and jute is apparent in all the spectra of the prepared composite [Figure 3.1.4. (d-f)]. However, on addition of GA into the S/J composite (Figure 3.1.4e), the peak intensities in the region 3400-3000 cm$^{-1}$ assigned for – OH and – NH stretching vibrations were found to decrease. Further, two peaks corresponding to 2230 and 1167 cm$^{-1}$ assigned for –N–C=O and C–N stretching vibration were appeared [Figure 3.1.4. (e-f)]. This might be attributed to the interaction of – OH and – NH$_2$ groups present in jute and SF with the GA. It was reported in the literature that GA could exist in different form in the solution and could able to crosslink proteins, leading to formation of a broad range of conjugates [15]. The probable interaction of soy protein and jute with GA is discussed below. On addition of MMT, the peak intensity in the region 3400-3000 cm$^{-1}$ corresponding to – OH and – NH stretching vibration was reduced and sharpened. The peak intensities in the region 1030-460 cm$^{-1}$ and 1620 cm$^{-1}$ were also found to enhance. These results further confirmed the interaction of clay particles with GA and S/J composite [16].

### 3.1.5. Mechanical property study

The flexural properties of composites with varying percentage of glutaraldehyde and clay are shown in Figure 3.1.5. The values shown in the Figure 3.1.5 are the mean value of ten readings. It was observed that both the flexural modulus
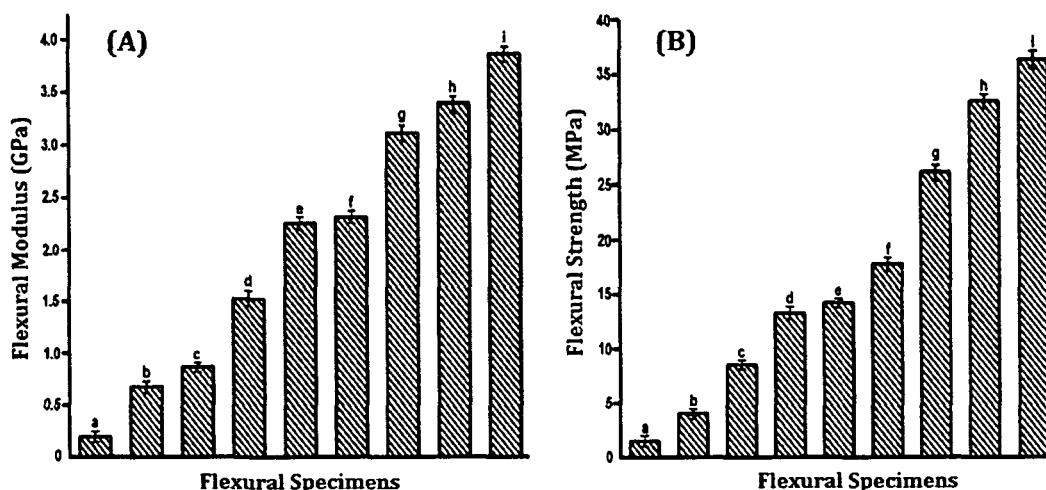


**Figure 3.1.5.** Mechanical properties of (a) S/J, (b) S/J/G30, (c) S/J/G40, (d) S/J/G50, (e) S/J/G60, (f) S/J/G70, (g) S/J/G50/M1, (h) S/J/G50/M3 and (i) S/J/G50/M5.

and strength increased with the increase in the concentration of glutaraldehyde. The increase in flexural values could be ascribed to the formation of crosslinking between

the polar groups of soy flour and jute by glutaraldehyde as shown in Figure 3.1.6. The crosslinking between soy protein and cellulose fibres was reported in the literature [17]. Although the mechanical properties of composites were found to increase with the concentration of GA, however, the increase in strength was significant up to 50%.
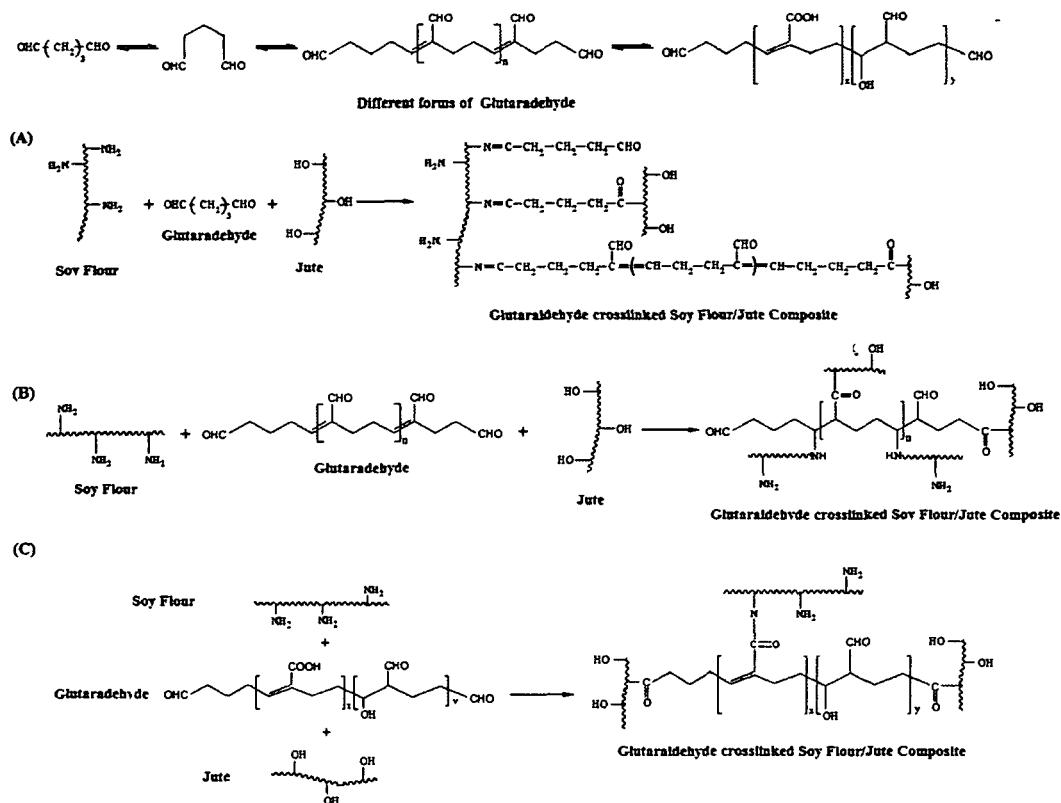


**Figure 3.1.6.** Schematic diagram of GA crosslinked soy flour/jute composite.

Beyond that we did not observe much improvement in the flexural properties, which probably be due to the saturation of crosslinking sites of SF and jute surface. Hence, considering the 50% concentration of the crosslinker as optimum, we modified the composite (S/J/G50/M1, S/J/G50/M3 and S/J/G50/M5) with different percentage of nanoclay ranging from 1-5%. The flexural properties of the samples viz. (S/J/G50/M1, S/J/G50/M3 and S/J/G50/M5 were found better compared to the clay untreated samples. The higher the percentage of clay, the higher was the flexural properties. The increase in flexural values was due to the restriction in the mobility of the intercalated polymer chains present inside the silicate layers of clay [18].

### 3.1.6. Thermal property study

The initial decomposition temperature $(T_i)$, maximum pyrolysis temperature $(T_m)$, decomposition temperature $(T_D)$ at different weight loss (%) and residual weight (RW) for soy flour, jute, S/J composites with or without crosslinker and nanoclay treated S/J composite are shown in Table 3.1.2. $T_i$ values of S/J composites were found to enhance with the increase in the percentage of crosslinker. $T_i$ values increased further

**Table 3.1.2.** Thermal properties of soy flour, jute and S/J glutaraldehyde and nanoclay composite.

| Sample Particulars | $T_i$ | $T_m^I$ | $T_m^{II}$ | Temperature of Decomposition at different weight loss (%) | | | | | RW % at 600 °C |
|---|---|---|---|---|---|---|---|---|---|
| | | | | 20 | 30 | 40 | 50 | 60 | |
| Soy Flour | 182 | 235 | 308 | 255 | 285 | 315 | 337 | 394 | 29 |
| Jute | 195 | | 368 | 326 | 347 | 360 | 364 | 368 | 7 |
| S/J | 168 | 221 | 309 | 250 | 280 | 302 | 325 | 378 | 26 |
| S/J/G30 | 187 | 230 | 313 | 254 | 282 | 310 | 326 | 363 | 27 |
| S/J/G50 | 191 | 234 | 317 | 261 | 285 | 312 | 329 | 356 | 28 |
| S/J/G70 | 230 | 326 | 378 | 286 | 290 | 321 | 332 | 344 | 30 |
| S/J/G50/M1 | 200 | 250 | 322 | 250 | 292 | 322 | 330 | 382 | 30 |
| S/J/G50/M5 | 214 | 252 | 325 | 268 | 300 | 327 | 364 | 427 | 31 |

$^I T_m$ value for 1$^{st}$ step; $^{II} T_m$ value for 2$^{nd}$ step.

due to incorporation of clay. $T_m$ value for jute apparent at 368 °C was due to the decomposition of cellulose [19]. In the case of soy flour, $T_m$ values for the first and second stages of pyrolysis were due to the dissociation of the quaternary structure of proteins and degradation of peptide bonds in the amino acid residues [20]. $T_m$ values for both the stages of pyrolysis were found to increase as the percentage of crosslinker were increased. Nanoclay incorporation further increased the values. $T_D$ values of the crosslinked S/J composite were higher than uncrosslinked S/J composite. The higher the crosslinker concentration, the higher the $T_D$ value. This might be due to the formation of crosslinking caused by the interaction between glutaraldehyde and

different polar groups such as amine, carboxyl and hydroxyl group present in soy flour and jute. The interaction is shown in Figure 3.1.6. The $T_D$ values were improved further when clay were added to it. The increase in thermal stability was attributed to the hindered diffusion of volatile decomposition products within the nanocomposites [21]. This might be also due to the physicochemical adsorption of the volatile degradation products on the silicates [22]. The silicates delayed the volatilisation of the products originated by carbon-carbon bond scission in the composite [23]. Clay treated composite showed a marginal increase in RW values over clay untreated composite. These results provide evidence that the thermal stability of the S/J composites increased on addition of crosslinker and nanoclay.

### 3.1.7. LOI study

The LOI values of the S/J composites with different percentage of crosslinker and clay are shown in the Table 3.1.3. From that table, it is observed that LOI value increased with the increase in crosslinker percentage. Since GA formed crosslinks between jute and soy flour and it increases with the increase in the concentration of glutaraldehyde. The network structure would restrict the accessibility of oxygen for the production of degradable components from the composites and hence LOI value would be higher. LOI values were further improved with increasing concentration of nanoclay and were found more than the nanoclay untreated composite. Jute fabrics primarily composed of plant materials cellulose and lignin which require a very low amount of oxygen for the production of flammable volatiles and propagation of flame and hence showed very low LOI value. The addition of the clay particles produced a silicate char on the surface of the composites which increased their flame resistance property [24]. The silicate rich surface had better barrier property to heat and oxygen transport due to which ignition of the composite delayed. The higher the percentage of clay, better was the resistance of flame propagation and hence higher the values of LOI.

**Table 3.1.3.** LOI and Flaming Characteristics of the prepared composites.

| Samples | LOI (%) | Flame description | Smoke & Fumes | Char |
|---|---|---|---|---|
| S/J | 29 (±1.0) | Candle like Flame | Small and black smoke | Little |
| S/J/G30 | 29 (±2.0) | Small localised flame | Small and black smoke | Little |
| S/J/G40 | 38 (±1.0) | Small localised flame | Small and black smoke | Little |
| S/J/G50 | 38 (±3.0) | Small localised flame | Small and black smoke | Little |
| S/J/G60 | 44 (±1.0) | Small localised flame | Small and black smoke | Little |
| S/J/G70 | 47 (±2.0) | Small localised flame | Small and black smoke | Little |
| S/J/G50/M1 | 50 (±2.0) | Small localised flame | Small and black smoke | Higher |
| S/J/G50/M3 | 56 (±1.0) | Small localised flame | Small and black smoke | Higher |
| S/J/G50/M5 | 56 (±1.0) | Small localised flame | Small and black smoke | Higher |

### 3.1.8. Correlation between Mechanical, Thermal and LOI study

From the above mechanical, thermal and LOI studies, it was found that all these properties were significantly improved on modification of the S/J composite with crosslinker, GA, as well as with nanoclay. The plot of Residual weight (%) at 600 °C *i.e.* the thermal properties against LOI values gave the regression value ($R^2$) to be 0.964, which indicated a good correlation between these two properties (Figure 3.1.7a). Furthermore, the co-efficient value in the equation shown in the plot was found to be positive indicating an increase in thermal properties with the increase in the LOI values or vice versa. Similarly, the plot of thermal vs. mechanical and LOI vs. mechanical also showed the $R^2$ value as 0.9017 and 0.9541 respectively and their respective equations also showed positive slope. According to regression analysis, a value of $R^2$ > 0.8 was considered to be significant [25]. From our analysis, the $R^2$ value was found

to be highly significant hence we can conclude that there was an intrinsic link between these three properties *e.g.* increases in the thermal property increased the mechanical as well as LOI values. Moreover, the improvement in all the properties (*e.g.* mechanical, thermal, LOI) might be due to the crosslinks formed between SF and Jute by GA as shown in Figure 3.1.6.
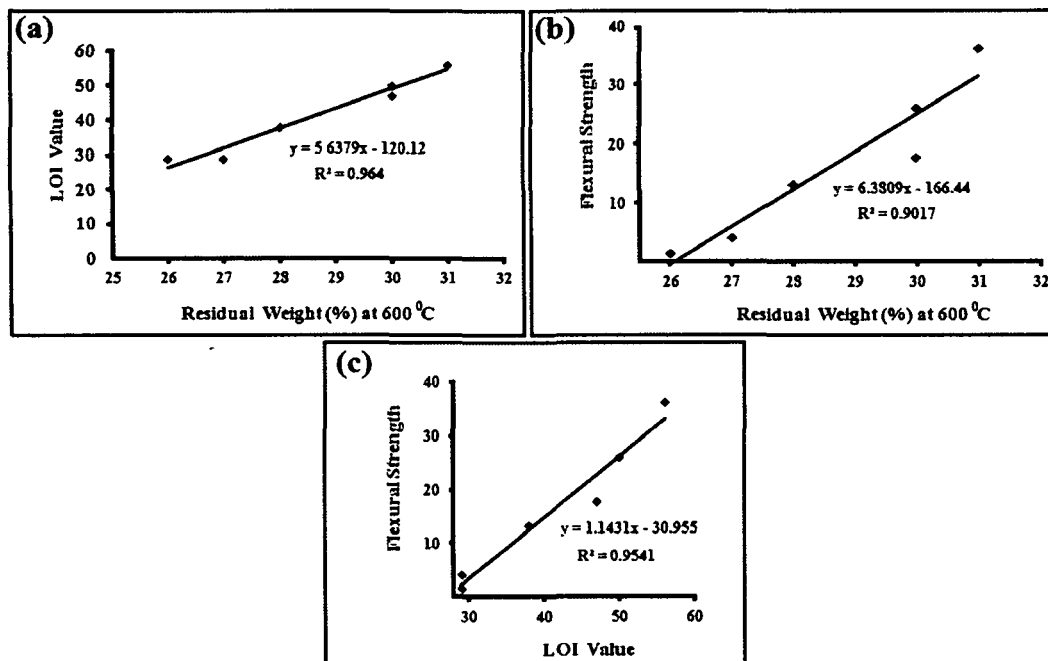


**Figure 3.1.7.** (a) Plot of Residual Weight (%) vs. LOI Value, (b) Plot of Residual Weight (%) vs. Flexural Strength and (c) Plot of LOI Value vs. Flexural Strength.

### *3.1.9. Dimensional stability test*

The effect of swelling in water vapour at room temperature and 65% relative humidity for the composite samples for different time periods is shown in Figure 3.1.8. From the Figure, it is found that the composites having higher percentage of GA showed less swelling than the composites containing lower percentage of glutaraldehyde. Composites containing higher percentage of glutaraldehyde swelled less due to higher crosslink densities and less availability of the polar groups [26]. Clay treated composites swelled less than those of clay untreated samples. The higher the amount of clay, the lower was the swelling. The silicate layer of clay provided a tortuous path which hindered the diffusivity of water through the composites [27].
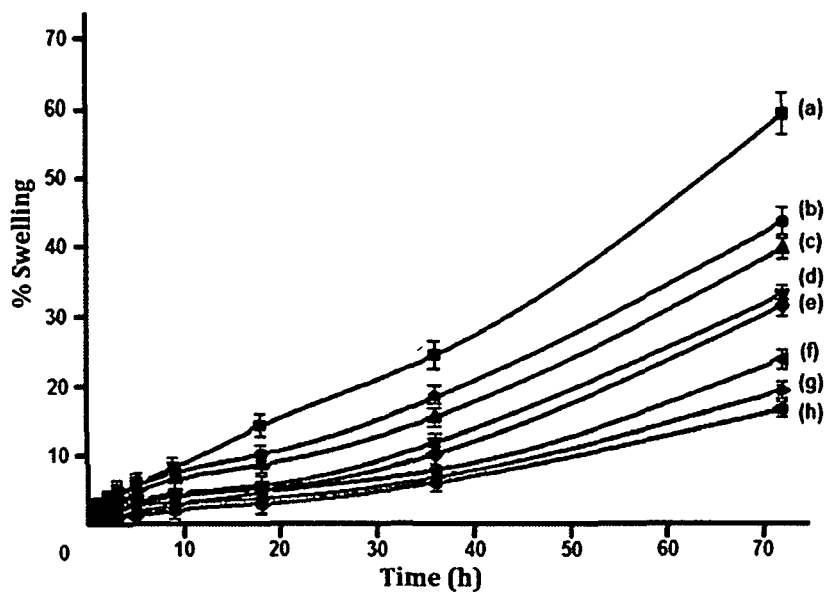
**Figure 3.1.8.** Swelling behaviour of (a) S/J, (b) S/J/G30, (c) S/J/G40, (d) S/J/G50, (e) S/J/G70, (f) S/J/G50/M1, (g) S/J/G50/M3 and (h) S/J/G50/M5.

***Section B*: Study on the effect of cellulose whisker and nanoclay on jute fabric reinforced soy flour bio-nanocomposites**

Biopolymer based materials immobilized with nanoparticles have recently dominated the traditionally available petroleum based polymer materials [28, 29]. Due to their outstanding mechanical properties and biodegradability, bio based polymer nanocomposites are now a days considered to be promising future material. These materials have the potential to overcome the disadvantages possesses by material commercially obtained from petrochemical supply chain. Moreover, the use of bio based polymer nanocomposites plays a vital role in sustainable development so called the development of newer methods for production of environmentally benign 'greener products' [30-34].

Keeping in mind the advantages of bio based polymer and increasing demand of a greener products, herein we report the preparation of bio based polymer nanocomposites comprising of soy flour, jute, glutaraldehyde, cellulose whiskers and nanoclay with high thermo – mechanical properties.

## 3.2. RESULTS & DISCUSSION

The codification and composition of the resulting nanocomposites (3 mm thick approximately) are reported in Table 3.2.1. The samples as coded in Table 3.2.1, has been prepared by keeping the weight (%) of the components viz. SF, glycerol, glutaraldehyde and jute fixed in all the samples where as the percentages (%) of CWs and nanoclay were varied.

**Table 3.2.1.** Codification and filler content of the nanocomposites based on Jute and crosslinked SF with CWs and nanoclay (wt %).

| Sample | Soy Flour (SF) | Glycerol | Glutaraldehyde (G) | Jute (J) | CWs (C) | Nanoclay (M) |
|---|---|---|---|---|---|---|
| SF/J/G50 | 100 | 5 | 50 | 75 | - | - |
| SF/J/G50/C1 | 100 | 5 | 50 | 75 | 1 | - |
| SF/J/G50/C3 | 100 | 5 | 50 | 75 | 3 | - |
| SF/J/G50/C5 | 100 | 5 | 50 | 75 | 5 | - |
| SF/J/G50/C5/M1 | 100 | 5 | 50 | 75 | 5 | 1 |
| SF/J/G50/C5/M3 | 100 | 5 | 50 | 75 | 5 | 3 |
| SF/J/G50/C5/M5 | 100 | 5 | 50 | 75 | 5 | 5 |

### *3.2.1. FT-IR study*

In order to confirm the formation of CWs on acid hydrolysis of cellulosic filter paper, FT-IR analysis was performed. The composition change of filter paper with that of the resultant CWs is shown in Figure 3.2.1. In the FT-IR-spectrum of the untreated filter paper (curve a) a strong broad band is observed at 3432 cm$^{-1}$ which is attributed to stretching of H-bonded hydroxyl groups [35]. The peak at 2902 cm$^{-1}$ is due to symmetric C–H vibrations [36]. An intense band at 1642 cm$^{-1}$ is assigned to the stretching vibration resulting from H–O–H intermolecular linkages. The bands at 1433 and 1328 cm$^{-1}$ in the spectrum are assigned to the symmetric $CH_2$ bending and wagging, the C–H bending occurs at 1369 cm$^{-1}$, 1255 cm$^{-1}$ [37, 38]. The two bands at 1162 cm$^{-1}$ and 898 cm$^{-1}$ corresponds to C-O-C stretching at the $\beta$-(1→4)-glycosidic linkages [39]. The in-plane ring of $\beta$-(1→4)-glycosidic linkages gives a shoulder at 1109 cm$^{-1}$. Strong peaks at 1054 cm$^{-1}$ indicates the C–O stretching at C-3 [40]. The vibrational frequencies of cellulose filter paper (as obtained from FT-IR spectra) were very similar before and after acid hydrolysis treatment. However, the intensity of some peaks was found to be different to some extent in the CWs spectrum (curve b). For CWs, the intensity of peaks at 898 cm$^{-1}$, 1109 cm$^{-1}$ and 1369 cm$^{-1}$ has been found to increase slightly, whereas the intensity of the peaks at 1255 cm$^{-1}$, 1328 cm$^{-1}$, 1642 cm$^{-1}$ and 2900 cm$^{-1}$ did not change during acid hydrolysis. This indicates that the acid hydrolysis affects the surface and amorphous zone of cellulose. In the spectra of untreated filter

paper and CWs, the band occurred at 710 cm$^{-1}$ and 755 cm$^{-1}$ are the characteristic absorption of cellulose I$_\alpha$ and I$_\beta$ [41].
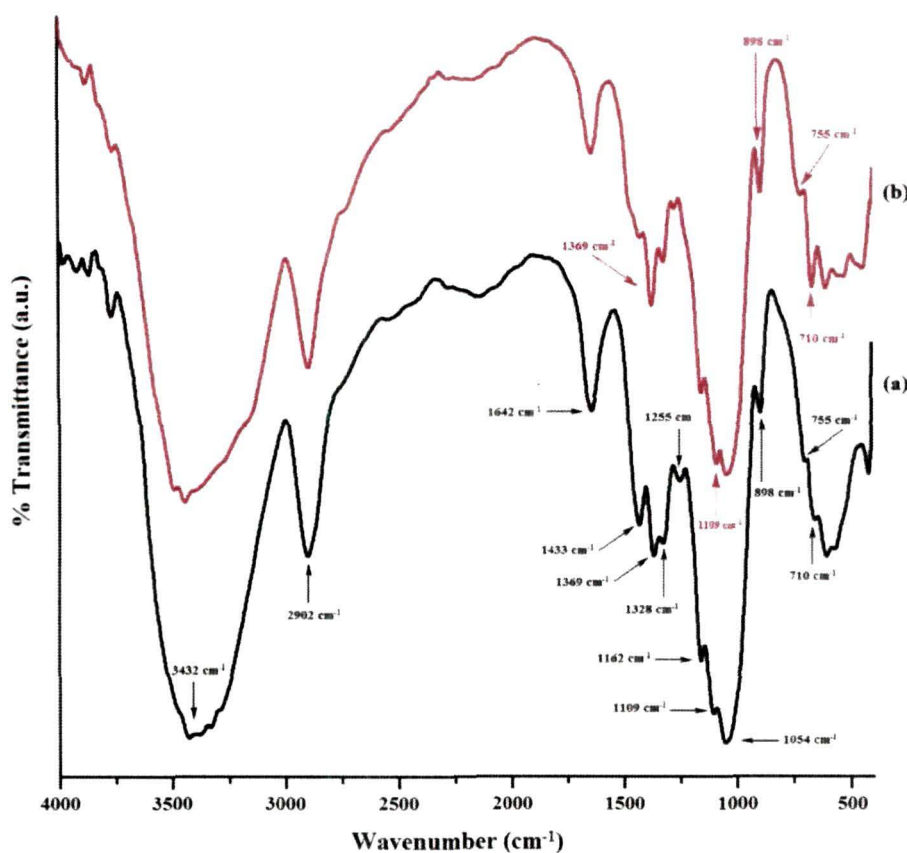


**Figure 3.2.1.** FT-IR spectra of (a) Filter paper and (b) Cellulose Whiskers.

The FT-IR spectrum for the composite SF/J/G50 (curve a), SF/J/G50/C1 (curve b), SF/J/G50/C5 (curve c), SF/J/G50/C5/M1 (curve d) and SF/J/G50/C5/M5 (curve e) are shown in Figure 3.2.2. The FT-IR spectra for all the samples show peaks in the region 3400-3000 cm$^{-1}$, that can be attributed to the –OH and –NH stretching vibrations, respectively. Characteristic peaks of SF at 1648, 1544 and 1248 cm$^{-1}$ for C=O stretching of amide–I, –NH bending of amide –II and C–N stretching of amide –III are present in all the spectrum. It is known that polypeptides and proteins of mainly $\alpha$-helical structure exhibit absorption bands near 1650 cm$^{-1}$ (amide I) and 1540 cm$^{-1}$ (amide II). The amide III band in the spectrum is due to the presence of glutamic acid of soy flour. Similarly, the peaks appeared in all the spectrum at 1254 and 1116-1057 cm$^{-1}$ are for –C–O–C– bond in cellulose chain and C–O stretching vibration, which are characteristic peaks for jute. The entire spectrum shows the peak around 900 cm$^{-1}$ due to the $\beta$-(1→4)-glycosidic linkages. The intensities of –OH and –NH stretching vibrations were found

to decrease with respect to unfilled composite. From the IR spectrum, it has been found that with the increase in CWs concentration the peak intensity decreases. This behaviour can be ascribed to the interaction between the free –OH and –NH group of jute and SF with –OH group of CWs. Upon the addition of nanoclay, the peaks in the 3400-3000 cm$^{-1}$ range corresponding to –OH and –NH stretching vibrations were reduced in intensity and sharpened. The peak intensities in the ranges of 1030-460 cm$^{-1}$ and 1620 cm$^{-1}$ were also found to be enhanced. These results confirm the interaction of clay particles with GA and SF/J composite [16].
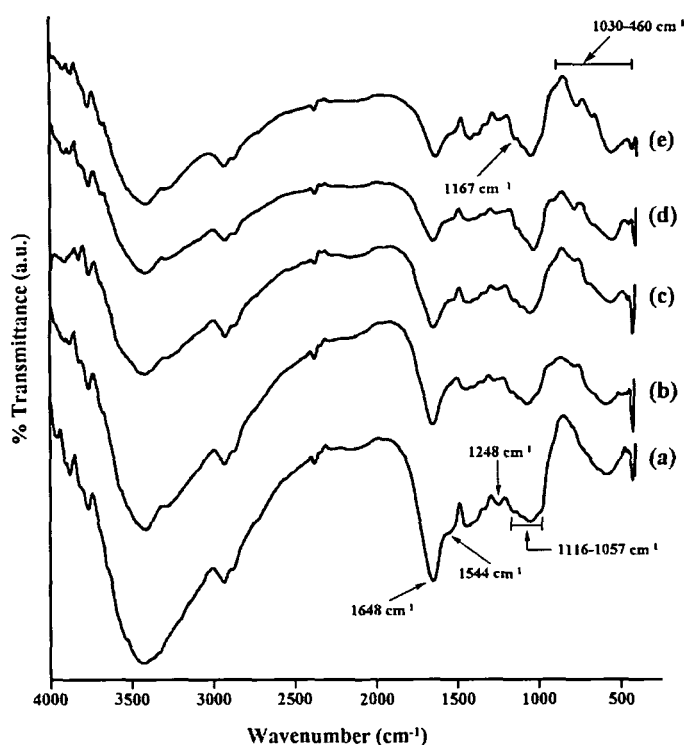


**Figure 3.2.2.** FT-IR spectra of (a) SF/J/G50, (b) SF/J/G50/C1, (c) SF/J/G50/C5, (d) SF/J/G50/C5/M1 and (e) SF/J/G50/C5/M5.

Glutaraldehyde can exist in different form in solution and can crosslink proteins, leading to the formation of a broad range of conjugates. In the FT-IR spectrum of all composites two common bands were observed at 1648 and 1167 cm$^{-1}$. The presence of these two peaks corresponding to –N–C=O and C–N stretching vibration, respectively, indicates the interaction of the aldehydic (–CHO) group of GA with –OH and –NH₂ groups present in jute and SF, respectively. A plausible mechanism for the formation of –N–C=O and C–N linkage is represented schematically in scheme 3.2.1.
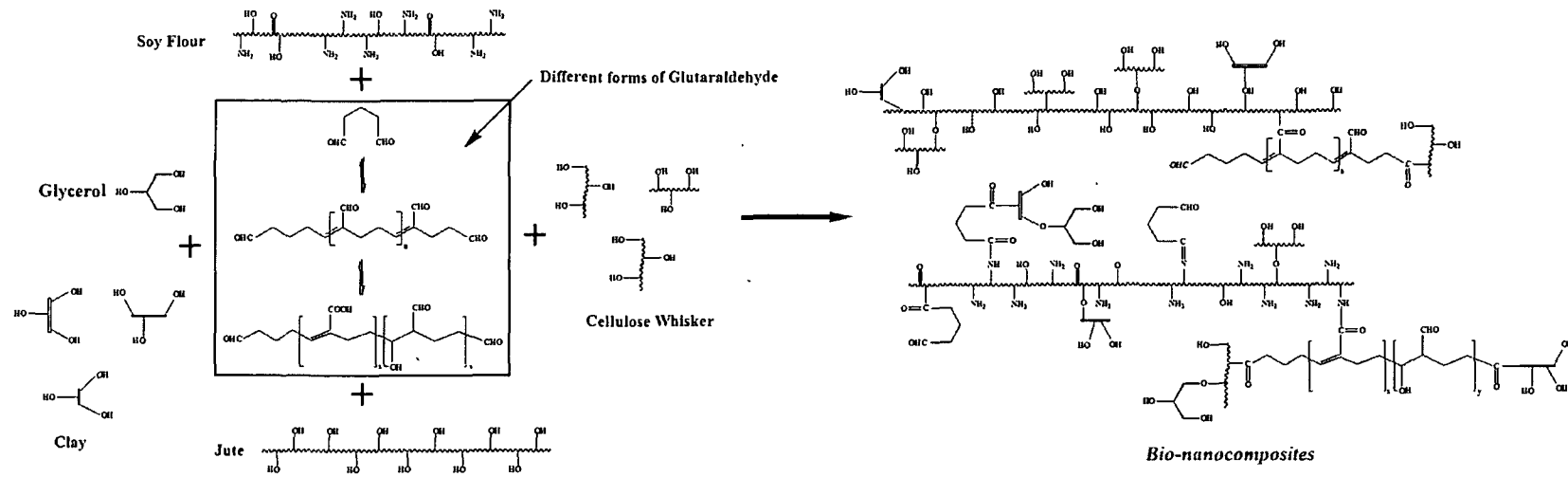
**Scheme 3.2.1.** Probable interaction of Glutaraldehyde with SF, Jute, cellulose whiskers and nanoclay.

To further confirm the possibility of C–N linkages between SF and GA we performed DFT calculation at B3LYP/6-31G level of method using Gaussian 03 programme [42]. In these calculations, we considered a small unit of the GA consisting of 12 C-atoms including aldehydic (CHO) and hydroxyl (OH) functional groups and a small unit of SF including a $NH_2$ group at the terminal position. The optimized geometry of the cross linked product formed by C–N linkage is shown in Figure 3.2.3.
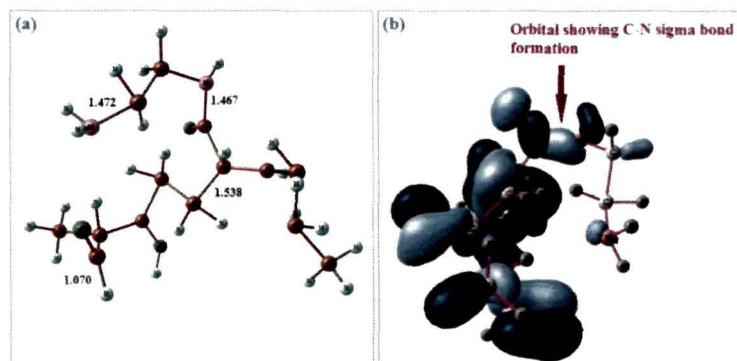


**Figure 3.2.3.** The optimized geometry of the cross linked product formed by C-N linkage is shown.

In the optimized geometry C–H, C–O, C–N, O–H, N–H and C-C bond length were found to be 1.071, 1.258, 1.467, 0.959, 0.999 and 1.540 Å, respectively. These bond lengths are within the ranges of those obtained experimentally and from theoretical calculation [43]. It can be observed from the Figure 3.2.3 that C–O bond in N–C=O linkage is slightly longer than that of the free carbonyl moiety. Similarly, the N–H bond distance of the amide moiety slightly get compressed after formation of N–C=O linkage by release of $H_2O$ molecule. The elongation and compression of the C–O and N–H bond, respectively can be attributed to a kind of $p\pi \rightarrow p\pi$ back bonding from filled $\pi$ orbital of N to vacant $\pi$ orbital of C=O. It can also be observed from the Figure 3.2.3 that the $\angle$NCO bond angle is 118.5°. This indicates N–C=O linkage does not orient in a linear fashion rather is twisted from the molecular plane. Natural bond orbital (NBO) analysis further shows a sufficient amount of overlapping between carbon and nitrogen atoms, leading to the formation of C–N $\sigma$ bond.

A comparison of the IR-frequencies obtained from theoretical calculation with those obtained from experimental shows almost similar results (Figure 3.2.4). The corresponding vibrational frequencies at 1162 and 1658 cm$^{-1}$ indicating the formation C–N linkage were predicted both theoretically and experimentally. A comparison of

the observed vibrational frequencies to the calculated values provided a clear indication of the possibility of a strong interaction between the carbonyl group of GA and amide group of SF.
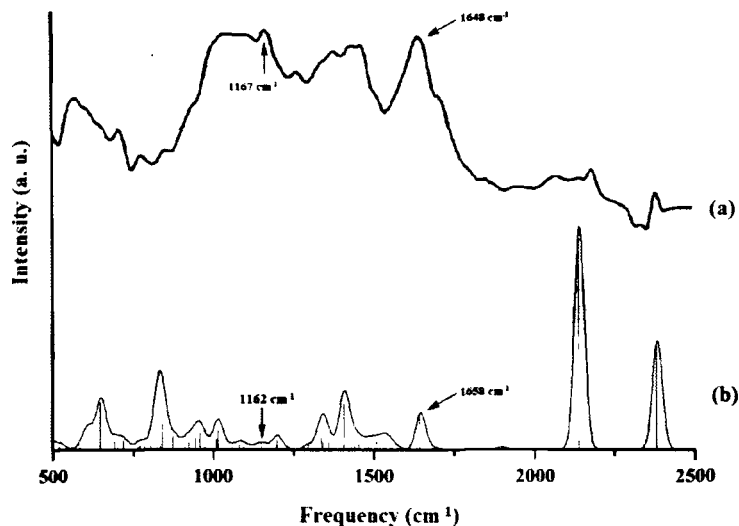


**Figure 3.2.4.** A Comparative study of (a) Experimental and (b) Theoretical IR frequency.

### 3.2.2. $^{13}C$ solid state NMR study

From the FT-IR spectroscopy, it is evident that the components are linked via N–C=O linkage.  In order to have more significant evidence for the proposed mechanism, we performed $^{13}C$ NMR analysis of GA and the composites SF/J/G50, SF/J/G50/C5 and SF/J/G50/C5/M5. The $^{13}C$ NMR spectroscopy of GA (Figure 3.2.5) showed characteristic chemical shift values above at 186 ppm which is due to the carbon atom of the carboxyl group.  The chemical shift values at 207 and 215 correspond to the carbon atom of the free aldehydic moiety of the glutaraldehyde. After GA had been treated with SF, the intensity of the signal at $\delta$= 215 ppm greatly diminished, indicating the most of the free aldehydic group has participated in the formation of C–N linkage with the free amino group of SF {(–CHO + NH$_2$ → –C=N–), Scheme 3.2.1}. Moreover, a new signal appears at $\delta$= 48.79 corresponding to C–N linkage. This provides clear evidence that the SF and GA form a composite which are linked via the formation of C–N bond, resulting from the aldehydic group (–CHO) and (–NH$_2$) group of SF [44].

The composite of GA and SF was then treated with jute fibre. To confirm the presence of jute and its combination with GA and SF composite we performed solid

state $^{13}$C NMR spectroscopy of the resultant composite. The $^{13}$C NMR spectrum of the composite showed chemical shift values at $\delta$= 24-42, 55-65, 134, 173 and 214 ppm which corresponds to aliphatic –C–, C–N linkage, >C=C, –NC=O and –CHO. More prominently, a doublet appears at $\delta$=74.89 and 72.49 ppm, corresponding to –C–O bond formation [16]. This indicated that the –OH group of jute fibre linked to the free –CHO and –NH$_2$ group of SF and GA composite through C–O and –C–N bond formation. To the composite of SF + GA and jute, we added cellulose whiskers. The cellulose whisker also contain –OH group. Hence, we observed almost a similar pattern of $^{13}$C NMR spectrum. However, there was a slight shift in the chemical shift value that might be due to the covalent interaction of the cellulose whisker with the free functional group of the SF + GA + jute composite. The shifting of the chemical shift values and the presence of the chemical shift values corresponding C–O and C–N further confirms the presence of the cellulose whisker and their linkage to the composite. Finally, to improve the thermal and mechanical properties of these composites, we also added nanoclay. Clay particles are basically layered structures in which the octahedral and tetrahedral sheets are linked through exchangeable cations or –OH group. Upon addition of clay particles, some sort of interaction occurs between the clay particles and the synthesized composites. From the $^{13}$C NMR spectrum of the clay-added composite, it is evident that, except for a decrease of the peak intensity and a very slight change in the chemical shift, no significant change occurs. This fact provides strong evidence that the addition of the clay does not cause any structural modification of the composite. Rather, it is possible that some amount of the composite might remain in the interlayer spacing of the clay. Thus, from the $^{13}$C NMR spectrum, it is truly evident that bio-composites were formed through C–N, N–C=O, C–O linkages. The addition of the clay nanoparticles did not cause any structural modification, and these might be taken as strong evidence for our proposed mechanism.
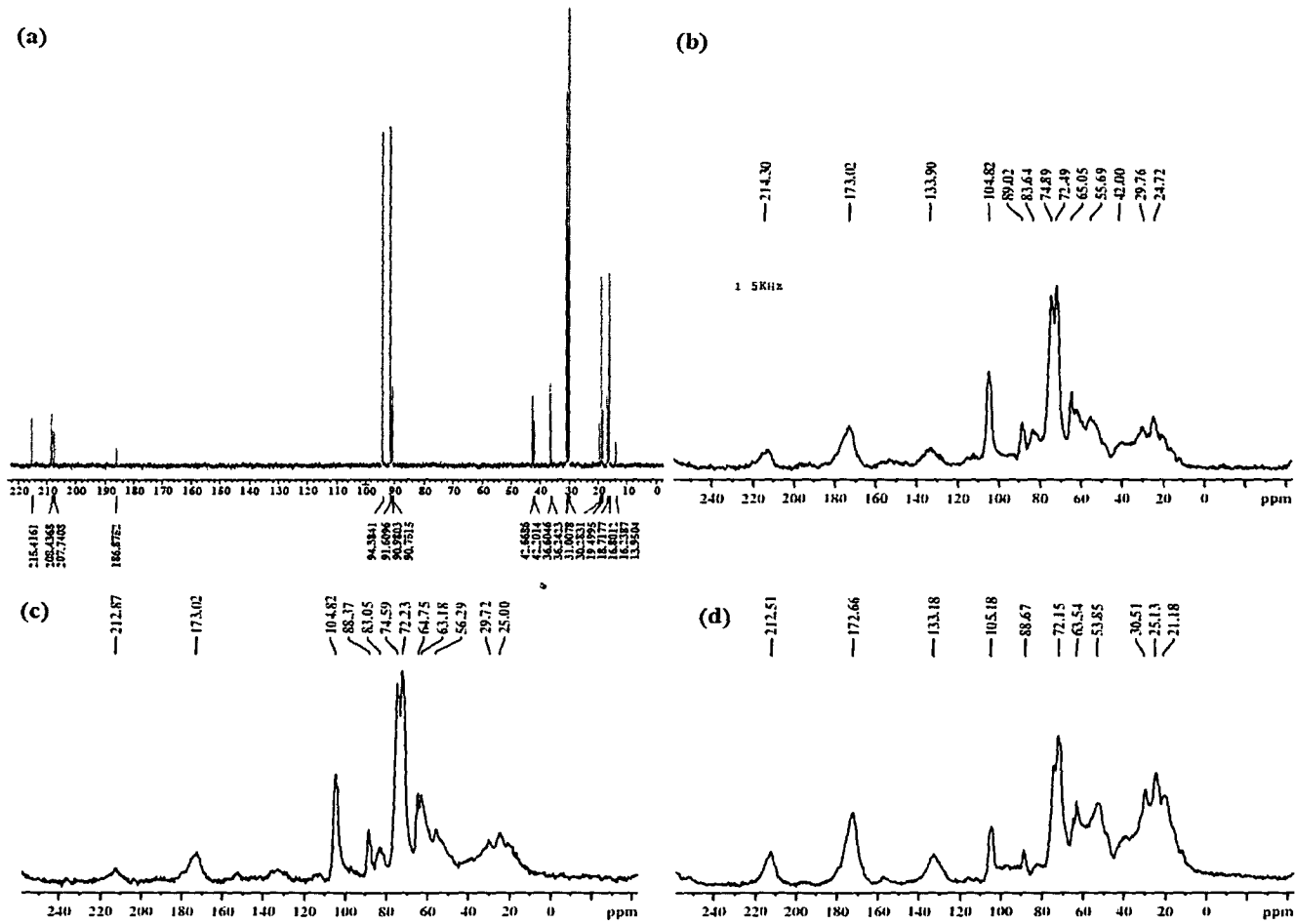
**Figure 3.1.3.** SEM micrographs of (a) soy flour, (b) jute, (c) S/J surface, (d) S/J/G50 surface, (e) S/J/G50 fracture surface, (f) S/J/G50/M1 surface, (g) S/J/G50/M1 fracture surface, (h) S/J/G50/M5 surface and (i) S/J/G50/M5 fracture surface.

### 3.2.3. UV-Visible spectroscopy study

The UV-visible spectra of SF, GA and a mixture of SF and GA are shown in Figure 3.2.6. The UV-visible spectrum of SF shows three absorbance peaks at 217, 265 and 330 nm. The peak at 217 nm is due to the $\pi \rightarrow \pi^*$ transition originated from $RCONH_2$ linkages. The two weak intense band at 265 and 330 nm are due to $n \rightarrow \pi^*$ transition of the $C=O$ group. In case of GA, two absorbance peaks are observed at 233 and 280 nm are due to $\pi \rightarrow \pi^*$ and $n \rightarrow \pi^*$ transition of the –CHO group. In the mixture of SF + GA, three bands are observed. These bands are different from those of pure SF and GA. The first peak at 214 nm is again because of the $\pi \rightarrow \pi^*$ transition of the –CHO group. The peak at 276 nm is because of the $n \rightarrow \pi^*$. This indicates that, upon mixing of SF and GA, the two electronic transitions are blue-shifted and their intensities are diminished. This might be because of the participation of the –CHO group of GA in the formation of –CN linkage with the $RCONH_2$ group of SF. The presence of a weak band at 227 nm in the mixture of SF and GA is because of the $\pi \rightarrow \pi^*$ of the –CN group, which further reveals the formation of –CN linkage in between SF and GA.

Diffuse reflectance spectra of the SF/J/GA50, SF/J/GA/C5 and SF/J/GA/C5/M5 composites are shown in Figure 3.2.6 and their peak assignments are listed in Table 3.2.2. The patterns of the UV-visible spectra of the composites are more or less similar. In all of the spectra, we observe basically two electronic transitions due to $\pi \rightarrow \pi^*$ and $n \rightarrow \pi^*$ appearing at different wavelengths. The peak appearing nearly at ~ 215 nm indicates the presence of $RCONH_2$ group in all the synthesized composite. The peaks nearly at ~ 272 nm indicates the presence of unreacted –CHO functional group. More interestingly, in all of the composite we observe peaks above 320 and 350 nm and this provides further strong evidence that, because of an increase in the conjugation of the synthesized composite, a bathochromic (red) shifts of the $\pi \rightarrow \pi^*$ and $n \rightarrow \pi^*$ transitions occurs [16]. Furthermore, the clay added nanocomposites give a similar electronic transition, in addition to a greater bathochromic shifts of the $n \rightarrow \pi^*$ transition to the 446 nm region. This also indicates the participation of clay nanoparticles in the conjugated system. Hence, as shown in the plausible mechanism (scheme 3.2.1), it can be said that the bio-nanocomposites comprising SF, jute, GA, CW and nanoclay are crosslinked by –N–C=O and –CN linkages, among others.
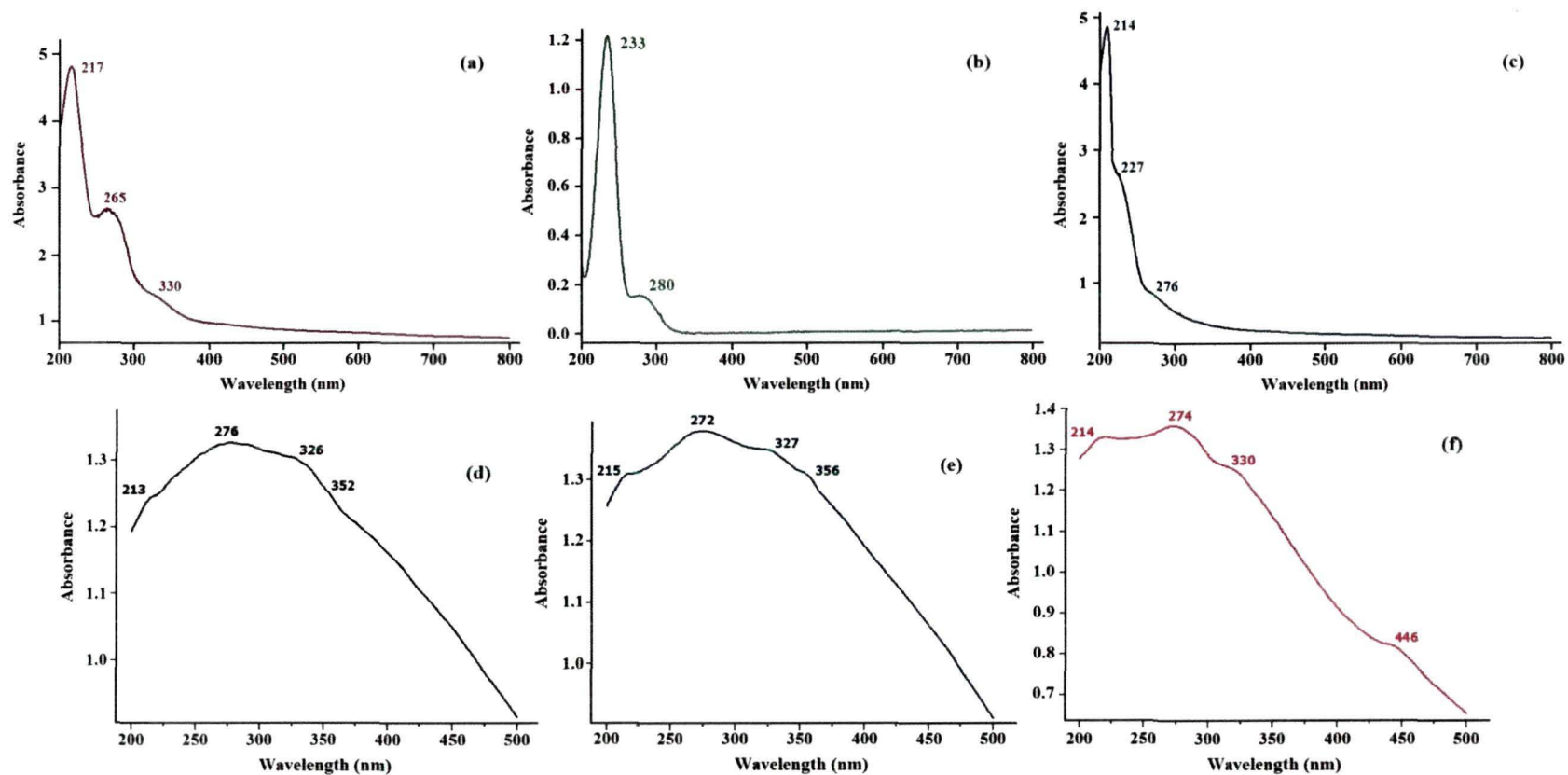
**Figure 3.2.6**. UV-Vis. and DR spectra of (a) SF, (b) GA, (c) SF/GA50, (d) SF/GA50/J, (e) SF/J/GA50/C5 and (f) SF/J/GA50/C5/M5.

**Table 3.2.2.** UV-Vis/DRS Spectra Data ($\lambda_{max}$ in nm) for the neat SF, GA and their Composites.

| Sample | Electronic Transition | |
| --- | --- | --- |
| | $\pi \rightarrow \pi^*$ | $n \rightarrow \pi^*$ |
| SF | 217 | 265, 330 |
| GA | 233 | 280 |
| SF/GA50 | 214, 227 | 276 |
| SF/J/GA50 | 213 | 276, 326, 352 |
| SF/J/GA50/C5 | 215 | 272, 327, 356 |
| SF/J/GA50/C5/M5 | 214 | 274, 330, 446 |

## 3.2.4. XRD study

As an indirect but non-invasive technique, XRD analysis is capable of providing detailed information regarding crystal structure of CWs and the synthesized composites. Figure 3.2.7 represent the diffractograms of (a) grinded filter paper and (b) prepared CWs. The diffraction profiles were obtained with peak maxima at $2\theta$ angles of 15.3°, 17.1°, 23° and 34.8° corresponding to the (1-10), (110), (002), and (004) crystallographic planes, respectively. The values are compared with those reported in
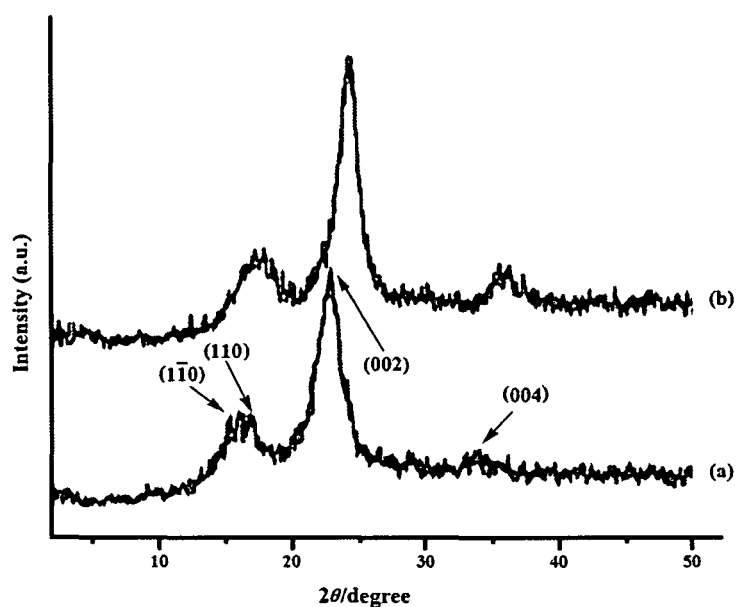


**Figure 3.2.7.** XRD pattern of (a) Whatman 1 Filter paper and (b) Cellulose Whiskers.

the literature, confirming that the extracted CWs were typical of cellulose –I [45]. The peak for the (002) plane ($2\theta$ = 23°) in the intensity profiles of the treated cellulose is much sharper than that of the untreated sample. The intensity of the peak for the (110) plane ($2\theta$ = 17.1°) in the case of CWs is greater than that in the case of the filter paper one [46]. It has been noticed in the diffractograms that peaks for treated cellulose is slightly shifted towards higher $2\theta$ value, indicating a decrease in the $d$-spacing of the CWs. On the other hand, the crystallinity is increased, as the peak intensity of the CWs is greater than that of untreated filter paper.

Further, X-ray diffraction was used to detect the incorporation of CWs and nanoclay into the jute based crosslinked SF composites prepared by solution induced intercalation method. Figure 3.2.8 shows the XRD patterns of SF, jute, nano clay, and
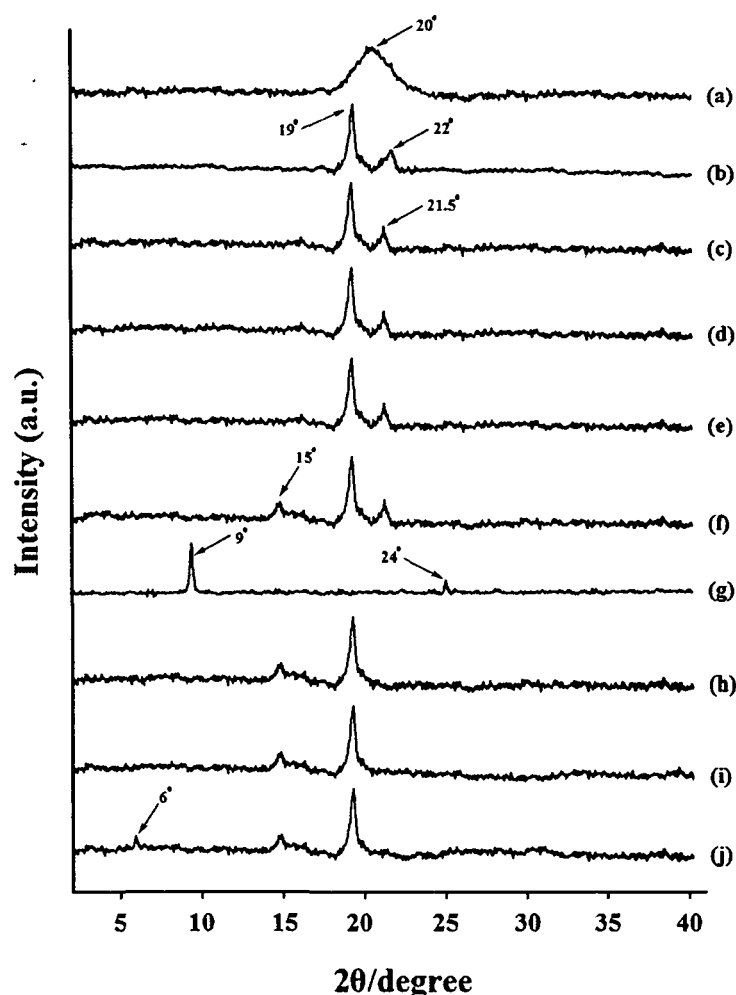


**Figure 3.2.8.** XRD pattern of (a) Soy Flour, (b) Jute, (c) SF/J/G50, (d) SF/J/G50/C1, (e) SF/J/G50/C3, (f) SF/J/G50/C5, (g) Nanoclay, (h) SF/J/G50/C5/M1, (i) SF/J/G50/C5/M3 and (j) SF/J/G50/C5/M5.

SF/J/G50 composites with or without CWs and nanoclay. Curve (a) represents the diffractograms of SF. A broader hump representing the amorphous nature of SF is observed at $2\theta = 20°$ [5]. Jute shows (curve b) peaks at $2\theta = 22°$ (002 plane of cellulose I) and $19°$ (101 plane of cellulose II) [6]. The peak due to 002 plane of cellulose I is found to shift marginally towards lower angle in jute reinforced crosslinked SF composites (curve c). The position of the peaks remains unchanged irrespective of the variation of CWs in the composite {Figure 3.2.8 (d & e)}. This reveals that the CWs do not affect the crystallinity of the composite. However, in SF/J/G50/C5 composite containing 5% CWs, an additional peak appeared at $2\theta = 15°$, suggesting the incorporation of CWs into the synthesized composite (Figure 3.2.8f). The absence and decrease in intensity of the peaks at $2\theta = 23°$ and $16°$ for CWs was apparent in the X-ray diffractograms of CW loaded (1-5%) crosslinked jute/SF composites. CW was organized differently and lost its structure, such as the unit cell parameters and chain conformation. Because of either vigorous mixing or the presence of SF macromolecules, CW cannot form structures within the composite as in the case of pure CW. A strong diffraction peak for nanoclay at $2\theta = 9°$ and a small peak at $2\theta = 24°$ was observed. The peak at $9°$ corresponds to a $d$-spacing of about 1.2 nm in pure clay [47]. The diffraction peak of the nanoclay tactoids is absent in the X-ray diffractograms for 1% and 3% clay incorporated composites, {curve (h) and (i)}. The $d_{001}$ peak of the clay in the nanocomposites completely disappeared, indicating the formation of a delaminated structure in the nanocomposites. It can be inferred that either the full expansion of the nanoclay gallery occurred, which is not detected by XRD, or the nanoclay layers were delaminated and no crystal diffraction peak appeared. In SF/J/G50/C5/M5 composites, the position of the characteristic peak of nanoclay at $2\theta = 9°$ is found to shift to lower $2\theta$ values, indicating the greater intercalation of resin and CWs due to an increase in interlayer spacing.

### 3.2.5. TEM study

The morphological features of cellulose layered-silicate nanocomposites were examined by TEM investigation. Figure 3.2.9 presents micrographs of samples SF/J/G50, SF/J/ G50/C5, and SF/J/G50/C5/M5. TEM images showed that the nanowhiskers appeared as a network structure (shown by arrow marks). The typical size of the cellulose nanowhiskers as determined by TEM was found to be around 15–40 nm in diameter within the composite. The TEM image of SF/J/ G50/C5 revealed

that the cellulose chains are bundled together randomly to form a network structure. The formation of network structure results from the formation of hydrogen bonds between cellulose nanoparticles during the nanocomposite preparation [48]. The image corresponding to sample SF/J/G50/C5/M5 shows the dispersion of nanoclay in the composite. The threadlike dark lines (indicated by arrows) represent the intersections of the clay layers, and the bright areas denote the jute-based cross-linked SF composite matrix. The appearance of the threadlike lines suggests that the nanoclay was not homogeneously distributed within the composite, indicating the existence of a partial compatibility between the polymer, CWs, and nanoclay surface [49]. Both individual silicate layers along with double or triple layers can be observed in the morphology, and very few tactoids of clay were present in jute based cross-linked SF composite matrix. The TEM image clearly revealed that most of the clay layers lost their stacking structure and dispersed in a disorderly fashion in the jute-based cross-linked SF composite matrix. The results obtained from TEM analysis are in accordance with our XRD analysis. Both sets of results suggested the formation of partially exfoliated nanocomposites.
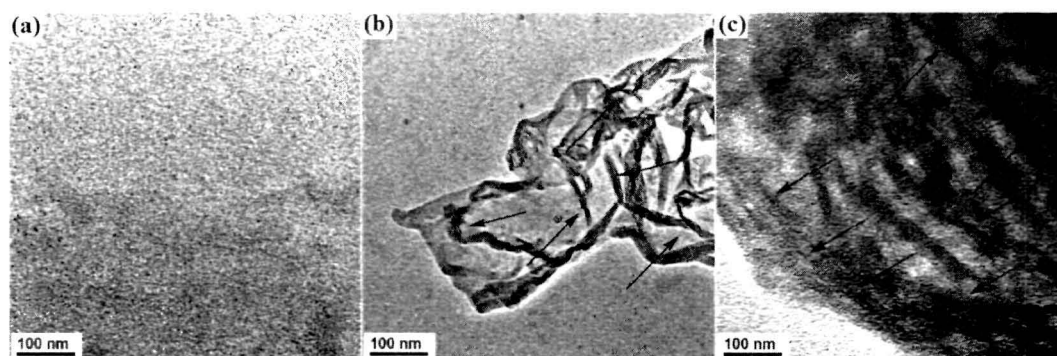


**Figure 3.2.9.** TEM micrograph of (a) SF/J/G50 (b) SF/J/G50/C5 and (c) SF/J/G50/C5/M5.

### 3.2.6. SEM study

Scanning electron microscopy is considered as a strong tool for determining the homogeneity of CWs, the microscale dispersion level of the whiskers, and presence of aggregates of CWs in the composite. SEM images of cellulose powder before and after acid treatment are shown in Figure 3.2.10. It can be observed from Figure 3.2.10 c & d that, after acid hydrolysis, the cellulose microfibrils were swollen and separated into much smaller crystalline cellulose products in the forms such as rods and spheres. These two different forms of cellulose nanocrystals cannot be separated by the common

methods of filtration and centrifugation. The bundles of rod like CWs observed in the SEM image had a width of ~1 $\mu$m. It seems that some aggregation of CW rods took place to form larger bundles during freeze-drying. However, these bundles of CW rods were loosely packed and could easily be separated [50].
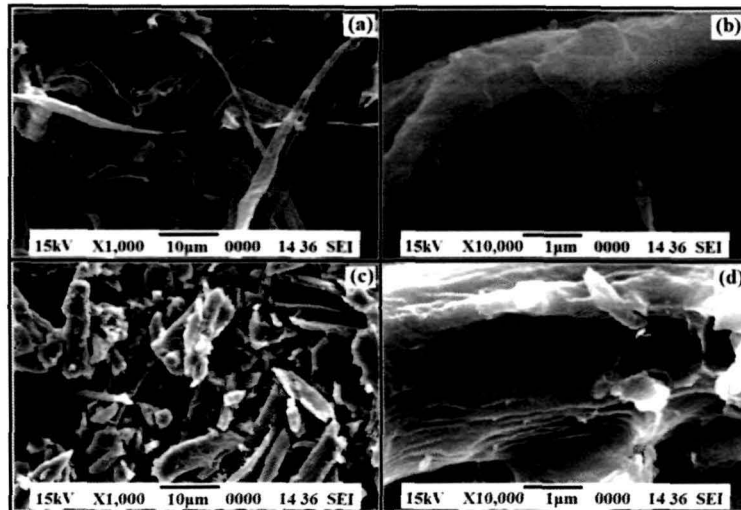


**Figure 3.2.10.** SEM images of Whatman 1 filter paper (a & b) and Cellulose whiskers (c & d).

Figure 3.2.11 shows SEM images of the fracture surfaces of SF/J/G50, SF/J/G50/C1, SF/J/G50/C5, SF/J/G50/C5/M1 and SF/J/G50/C5/M5 composites. The SF/J/G50 sheet shows a relatively smooth surface (Figure 3.2.11a). It is noted that the fracture surface of SF/J/G50/C1 (Figure 3.2.11b) displays homogeneous structure; suggesting a relatively uniform distribution of the CWs in the SF and jute composite. However, as the cellulose content increased, the fracture surface of SF/J/G50/C5 (Figure 3.2.11c) exhibited a relatively rough structure, suggesting relatively high interfacial adhesion among SF, jute and CWs. Compared with the SF/J/G50 sheet, the presence of the CWs in the SF and jute composites can be observed in the synthesized composites. Nevertheless, it is difficult to distinguish the individual filler dispersion because of its small size. Some filler appears as white domains on the fracture surface of the samples. Moreover, upon addition of nanoclay into the SF/J/G50/C5 composite, the roughness was found to increase (Figure 3.2.11d, e). This might be due to the fact that the clay particles increased the interaction with the SF matrix, CWs, and jute surface.
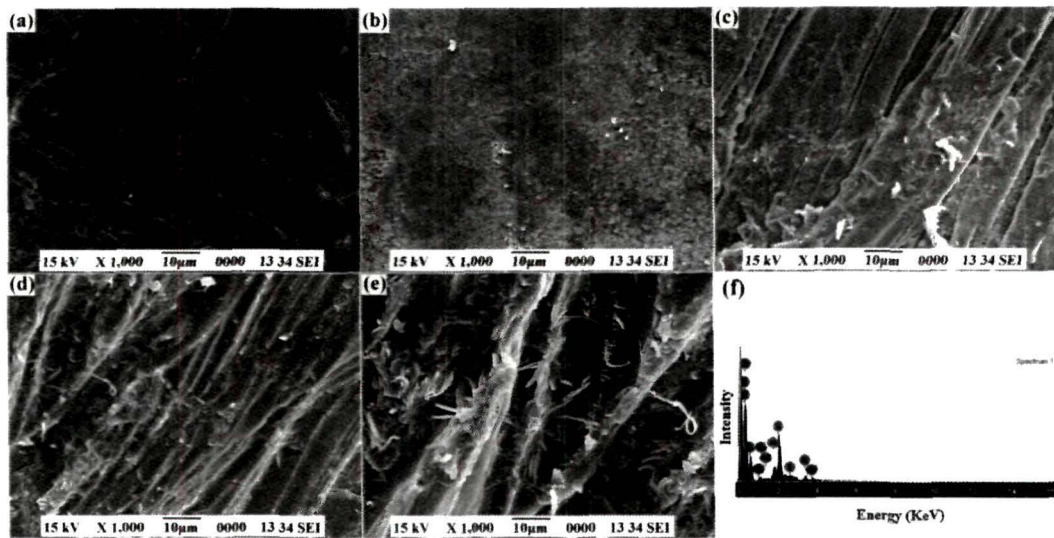
**Figure 3.2.11.** SEM micrographs of (a) SF/J/G50, (b) SF/J/G50/C1, (c) SF/J/G50/C5, (d) SF/J/G50/C5/M1 and (e) SF/J/G50/C5/M5.

Further analysis was done through energy-dispersive X-ray analysis of the nanoparticles observed in the fracture of the clay-loaded composite, as shown in Figure 3.2.11f. Elements such as Al, Na, and Si, which are mainly from the silicate nanoclay, were detected, indicating that the nanoclay had been successfully incorporated into the composite [51].

### 3.2.7. Thermal property study

Thermogravimetric analysis (TGA) was used to study the degradation pattern and the thermal stability of the synthesized bio-nanocomposites. Figure 3.2.12 displays the thermograms for some samples of the SF/J/G50, SF/J/G50/C1, SF/J/G50/C3, SF/J/G50/C5, SF/J/G50/C5/M1, SF/J/G50/C5/M3 and SF/J/G50/C5/M5 composites. Table 3.2.3 (derived from Figure 3.2.12) lists the initial decomposition temperature ($T_i$), maximum pyrolysis temperature ($T_m$), decomposition temperature ($T_d$) at different weight loss percentages, and residual weights (RWs) of the composites at 600°C. All the thermogram shows an initial degradation around 100°C due to the loss of water molecule. It is clearly seen from the thermograms that the $T_i$, $T_m$, $T_d$ at different weight loss percentages, and residual weight (RW, %) were improved upon the addition of CWs. $T_i$ values of the composites were found to be enhanced with increasing CW concentration. On the other hand, nanoclay is often used to enhance the thermal properties of composite material [52]. Significant increase in the decomposition and

char retention were obtained for a range of polymer nanocomposites using nanoclay. This is generally attributed to the ability of nanoclay to function as a mass-transport barrier, hindering the out-diffusion of decomposition products and restricting the thermal motion of the polymer chain at the nanoclay surface [53]. In the CW incorporated nanocomposites, the CWs might restrict the thermal motion of the polymer chain and retard the diffusion of degradable decomposed products through the nanocomposites. Hence, an improvement in thermal stability was observed that is evident from the TGA thermograms as shown in Figure 3.2.12. The increased thermal resistance of the nanoclay-incorporated CW nanocomposites compared to the CW nanocomposites; that is, SF/J/G50/C5/M1, SF/J/G50/ C5/M3, and SF/J/G50/C5/M5 can be attributed to the retarded out-diffusion of decomposition products due to the labyrinth morphology of the exfoliated nanoclay in the matrix [54].
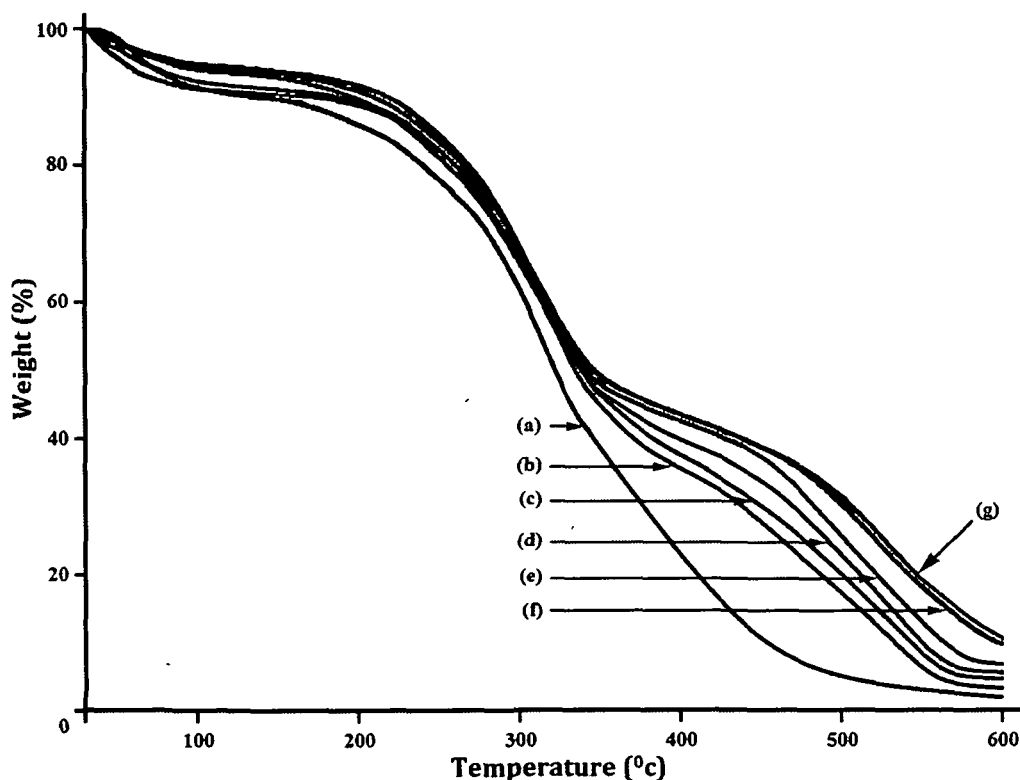


**Figure 3.2.12.** TGA thermograms of (a) SF/J/G50, (b) SF/J/G50/C1, (c) SF/J/G50/C3, (d) SF/J/G50/C5, (e) SF/J/G50/C5/M1, (f) SF/J/G50/C5/M3 and (g) SF/J/G50/C5/M5.

**Table 3.2.3** Thermal Properties of (a) SF/J/G50, (b) SF/J/G50/C1, (c) SF/J/G50/C3, (d) SF/J/G50/C5, (e) SF/J/G50/C5/M1, (f) SF/J/G50/C5/M3 and (g) SF/J/G50/C5/M5.

| Sample Particulars | $T_i$ | $^aT_m$ | $^bT_m$ | Temperature of Decomposition at different weight loss (%) | | | | | RW % at 600 °C |
|---|---|---|---|---|---|---|---|---|---|
| | | | | 20 | 30 | 40 | 50 | 60 | |
| SF/J/G50 | 172 | 212 | 298 | 224 | 265 | 285 | 304 | 337 | 3 |
| SF/J/G50/C1 | 177 | 219 | 304 | 235 | 268 | 290 | 321 | 363 | 5 |
| SF/J/G50/C3 | 183 | 225 | 309 | 243 | 270 | 298 | 327 | 376 | 7 |
| SF/J/G50/C5 | 191 | 234 | 317 | 252 | 272 | 305 | 331 | 395 | 9 |
| SF/J/G50/C5 /M1 | 202 | 243 | 328 | 258 | 279 | 313 | 337 | 430 | 10 |
| SF/J/G50/C5 /M3 | 209 | 249 | 334 | 266 | 281 | 314 | 341 | 441 | 12 |
| SF/J/G50/C5 /M5 | 215 | 253 | 339 | 271 | 286 | 318 | 346 | 448 | 14 |

$^aT_m$ value for $1^{st}$ step; $^b T_m$ value for $2^{nd}$ step.

### 3.2.8. LOI study

LOI values of SF/J composites with different percentage of CWs and nanoclay are given in Table 3.2.4. Form Table 3.2.4 it can be observed that all the samples produced small localised flames and the nanoclay-filled samples generates higher char than those without nanoclay. The LOI test assumes that inherently less flammable materials require greater oxygen concentrations to produce the heat necessary for the continued production of flammable volatiles and flame propagation. It is also observed in Table 3.2.4 that the LOI value increases with increasing percentage of CWs in the composites. CWs form cross-links with SF, jute, and GA and thus restrict the accessibility of oxygen for the production of degradable components from the composites, hence resulting in higher LOI values [55]. Further, the higher the CW concentration, the higher the LOI value. The enhancement in properties might be due to the increase in interactions among SF, jute, GA, and CWs. However, upon addition of nanoclay into the CW-incorporated composites, the LOI value is further enhanced.

From Table 3.2.4, it can be seen that the LOI values of the nanoclay-filled composites are greater than those of the composites without nanoclay. The higher the percentage of nanoclay, the higher the LOI value. Jute and SF are primarily composed of plant materials that require a very small amount of oxygen for the production of flammable volatiles and the propagation of a flame; hence, they show very low LOI values. The incorporation of nanoclay into the synthesized composite produces a silicate char on the surface and, hence, improves their flame resistance properties. The silicate-rich surface has better barrier properties to heat and oxygen transport, resulting in a delay of the ignition of the composite delays [24]. Therefore, with increase in the concentration of clay, the resistance to flame propagation is improved, and hence, higher LOI values are observed.

**Table 3.2.4.** Comparison of the Tensile, Flexural and LOI values of Unfilled and Filled jute based crosslinked SF nanocomposites.

| Composite System | Tensile Properties (MPa) | | Flexural Properties (MPa) | | LOI (%) |
|---|---|---|---|---|---|
| | Strength | Modulus | Strength | Modulus | |
| SF/J/G50 | 9.488 | 937.453 | 14.516 | 1702.369 | 39 |
| | (±0.826) | (±11.500) | (±1.361) | (±7.349) | (±1.0) |
| SF/J/G50/C1 | 14.654 | 1122.644 | 27.473 | 2156.261 | 44 |
| | (±0.931) | (±10.714) | (±1.206) | (±7.141) | (±1.0) |
| SF/J/G50/C3 | 23.420 | 1791.879 | 37.688 | 2874.533 | 48 |
| | (±1.699) | (±8.118) | (±1.430) | (±9.596) | (±3.0) |
| SF/J/G50/C5 | 30.780 | 1877.287 | 46.697 | 3535.505 | 51 |
| | (±1.252) | (±12.848) | (±0.950) | (±8.912) | (±1.0) |
| SF/J/G50/C5/M1 | 32.685 | 1956.118 | 68.334 | 4129.661 | 57 |
| | (±1.179) | (±8.401) | (±1.212) | (±8.890) | (±2.0) |
| SF/J/G50/C5/M3 | 52.591 | 2363.098 | 82.216 | 6232.557 | 62 |
| | (±0.746) | (±11.041) | (±0.745) | (±8.361) | (±1.0) |
| SF/J/G50/C5/M5 | 47.429 | 2113.082 | 76.933 | 5789.353 | 64 |
| | (±1.384) | (±10.487) | (±1.004) | (±7.933) | (±2.0) |

For Tensile and Flexural property each value in the above table represents average of ten samples. Values in the parenthesis represent the standard deviation.

### 3.2.9. Mechanical property study

The nonlinear mechanical properties of jute-based cross-linked SF composites reinforced with CWs and nanoclay were studied at room temperature. From these measurements, the tensile strength, tensile modulus, flexural strength, and flexural modulus were determined. Experimental data are reported in Table 3.2.4. A significant reinforcing effect was observed upon filler addition, as evidenced by the increase in both the modulus and the strength for the filled composites compared to the unfilled composites. A similar effect of reinforcing agents (micro-/ nanosized bamboo fibrils) on the fracture stress and Young's modulus of soy protein was also observed by Huang and Netravali [56]. It was observed that both flexural and tensile modulus, and strength increases with increase in the concentration of CWs. The macroscopic behaviour of CW-based composites depends, as for any heterogeneous materials, on the specific behaviour of each phase, composition (volume fraction of each phase), morphology (spatial arrangement of phases), and interfacial properties. The mechanical properties of such materials mainly depend on three parameters, namely, the geometrical aspect, the processing method, and the matrix structure and the resulting competition between matrix/filler and filler/filler interactions. The mechanical behaviour of CW based composites suggests the formation of a rigid network of whiskers, which should be responsible for the observed reinforcing effect [57]. Considering the 5% concentration of CWs as the optimum, we modified the composites SF/J/ G50/C5/M1, SF/J/G50/C5/M3, and SF/J/G50/C5/M5 with different percentages of nanoclay ranging from 1% to 5% (w/ w) with respect to SF. However, the nanoclay-incorporated composites showed significant improvements in the mechanical properties with respect to those without nanoclay. This enhancement in mechanical properties of clay-loaded composites is because of their intrinsic high modulus. In other words, it can be said that clays act as rigid reinforcement agent to the polymer matrix. However, the incorporation of a material with high modulus cannot be the only reason for such improvement in mechanical properties of the composites. The other reason might be the high aspect ratio of the nanoclay, which generates a large surface area for polymer adsorption. Apart from this, the intercalation of the polymers into the galleries of the nanoclay restricts their mobility. However, such improvement in mechanical properties with the incorporation of nanoclay can be realized only up to a definite nanoclay loading. In our investigation, an enhancement in mechanical properties was found up to clay loading of 3%, and beyond that, these properties declined upon further addition

of nanoclay. It is also observed that the improvement in reinforcement efficiency due to the incorporation of nanoclay occurred when there was a proper transfer of applied stress to the nanoclay platelets. Such a transfer of stress is only possible with suitable adhesion of the polymer matrix on the nanoclay, which allows the platelets of the nanoclay to be load bearing. At higher concentrations of nanoclay, agglomeration of the clay platelets can take place, and therefore, the interaction between the clay–polymer is reduced. This leads to a reduction in the extent of enhancement of reinforcement efficiency with the addition of higher amounts of nanoclay [58].

### 3.2.10. Dimensional stability test

Water vapour absorption onto the composite samples at room temperature (~30° C) and 65% relative humidity for different time periods is shown in Figure 3.2.13. In all cases, the percentage swelling was found to increase with increasing time. Sample SF/J/G50 is hydrophilic in nature, and hence, it adsorbed a high amount of water vapour. The water vapour adsorption decreased in the presence of the dispersed phase of CWs in the composite. The CW particles act as a barrier for water vapour, resulting in a decrease of water vapour transmission through the jute-based SF cross-linked composites. CWs might elongate the path of water particles in the nanocomposites [59]. Water vapour absorption of the nanocomposites is decreased with increasing CW content. The addition of CWs provides an elongated path for the water molecules to traverse. Further, it was observed that nanoclay treated composites swelled less than those of samples that were not treated with nanoclay. The higher the amount of nanoclay, the lower the swelling. This might be due to the fact that the silicate layers of nanoclay provide a tortuous path that hinders the diffusivity of water particles through the nanocomposite [27].
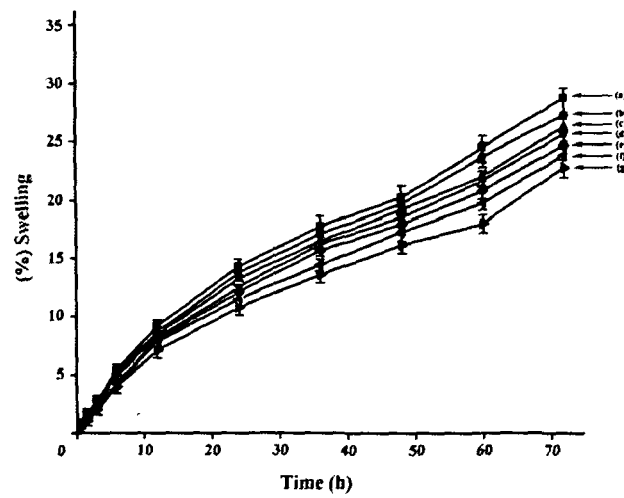
**Figure 3.2.13.** Swelling behaviour of (a) SF/J/G50, (b) SF/J/G50/C1, (c) SF/J/G50/C3, (d) SF/J/G50/C5, (e) SF/J/G50/C5/M1, (f) SF/J/G50/C5/M3 and (g) SF/J/G50/C5/M5.

**Section C: Study on the effect of TiO₂ and nanoclay on jute fabric reinforced soy flour bio-nanocomposites**

Now-a-days, the use of bio based polymer composite has immensely increased due to their several advantages over their synthetic counterparts [60]. The fibre originated from plant is used as a reinforcing agent rapidly to improve the thermal, mechanical as well as other properties of the composite [61]. The properties of SF/J composites can be improved by using nanomaterials [62]. Out of various nanomaterials predecessors, nanoclay is most extensively used for the synthesis of polymer nanocomposite. Besides using nanoclay, different metal oxide nanoparticles *viz.* ZnO, TiO₂, SiO₂ etc. are also used to improve various properties of biopolymer based nanocomposites [63]. In exterior application of biopolymer based materials, UV protection, flame retardancy and weathering resistance are very vital. In recent years, TiO₂ nanopowder is gradually being studied because it is non-toxic, chemically inert, low cost, corrosion resistant and has a high refractive index, UV filtration capacity and high hardness. Reinforcement by TiO₂ also improves electrical, optical, and physiochemical properties at a very low TiO₂ concentration, which make polymer TiO₂ nanocomposites a promising new class of materials [64]. There are limited information regarding the study of the effect of nanoparticles on soy flour based composites. There is enough scope to do further work in this domain.

The part of study is aimed to discuss the effect of TiO₂ nanoparticles alone and in combination with nanoclay (*i.e.* TiO₂ and TiO₂ - nanoclay) on thermal and mechanical properties of SF/J composites. The effect of nanoparticles *viz.* TiO₂ nanoparticles and nanoclay on other properties like UV resistance, dimensional stability, and flame retardancy of the composites has also been studied.

## 3.3. RESULTS & DISCUSSION

The samples, as coded in Table 3.3.1, had been prepared by keeping the weight (%) of the components *viz.* SF, glycerol, jute and GA constant in all the samples where as the percentages (%) of TiO₂ nanoparticles and nanoclay were varied. The weight (%) of the various components used for the synthesis of the composite are provided in Table 3.3.1.

97

**Table 3.3.1.** Codification and filler content of the nanocomposites based on Jute and crosslinked SF with $TiO_2$ nanoparticles and nanoclay (wt %).

| Sample | Starch (S) | Glycerol | Glutaraldehyde (GA) | Jute (J) | $TiO_2$ (T) | Nanoclay (N) |
|---|---|---|---|---|---|---|
| S/J/GA50 | 100 | 5 | 50 | 75 | - | - |
| S/J/GA50/T1 | 100 | 5 | ·50 | 75 | 1 | - |
| S/J/GA50/T3 | 100 | 5 | 50 | 75 | 3 | - |
| S/J/GA50/T5 | 100 | 5 | 50 | 75 | 5 | - |
| S/J/GA50/T5/N1 | 100 | 5 | 50 | 75 | 5 | 1 |
| S/J/GA50/T5/N3 | 100 | 5 | 50 | 75 | 5 | 3 |
| S/J/GA50/T5/N5 | 100 | 5 | 50 | 75 | 5 | 5 |

### 3.3.1. FT-IR study

FT-IR spectra of SF, jute, clay, and $TiO_2$ nanoparticles are presented in Figure 3.3.1A. The spectrum of SF (curve-a in Figure 3.3.1A) shows peaks in the region 1647, 1542 and 1254 cm$^{-1}$ for C = O stretching of amide – I, – NH bending of amide – II and C – N stretching of amide – III [13]. The FT-IR spectrum of jute (curve-b in Figure 3.3.1A) shows the absorption bands around 3440 cm$^{-1}$ for –OH stretching, 1736 cm$^{-1}$ for C=O stretching vibration of ester groups of hemicelluloses, 1643 cm$^{-1}$ for C=O stretching, 1247 cm$^{-1}$ for –C–O–C– bond in cellulose chain and 1057–1116 cm$^{-1}$ for C–O stretching [14]. Clay (curve-c in Figure 3.3.1A) exhibits peaks at 3450 cm$^{-1}$ (–OH stretching), 1619 cm$^{-1}$ (–OH bending), 1030–460 cm$^{-1}$ (oxide bonds of metals like Si, Al, Mg etc.). FT-IR spectrum of $TiO_2$ nanoparticles is presented in curve-d (Figure 3.3.1A). The strong absorbance at 1030–419 cm$^{-1}$ was attributed to the Ti–O–Ti stretching of $TiO_2$. The absorbances at 3435 and 1633 cm$^{-1}$ were assigned to the surface hydroxyl groups of $TiO_2$ [65, 66].

FT-IR spectra for the composite SF/J/GA50, SF/J/GA50/T1, SF/J/GA50/T3, SF/J/GA50/T5, SF/J/GA50/T5/N1, SF/J/GA50/T5/N3, and SF/J/GA50/T5/N5 are shown in Figure 3.3.1B. The FT-IR spectra for all the samples show peaks in the region 3400–3000 cm$^{-1}$, which could be attributed to the –OH and –NH stretching vibrations, respectively. Characteristic peaks of SF in the region of 1647, 1542 and 1254 cm$^{-1}$ were present in all the spectra. Similarly, the peaks appearing in all the spectra at 1247 and 1116–1057 cm$^{-1}$ were the characteristic peaks for jute.
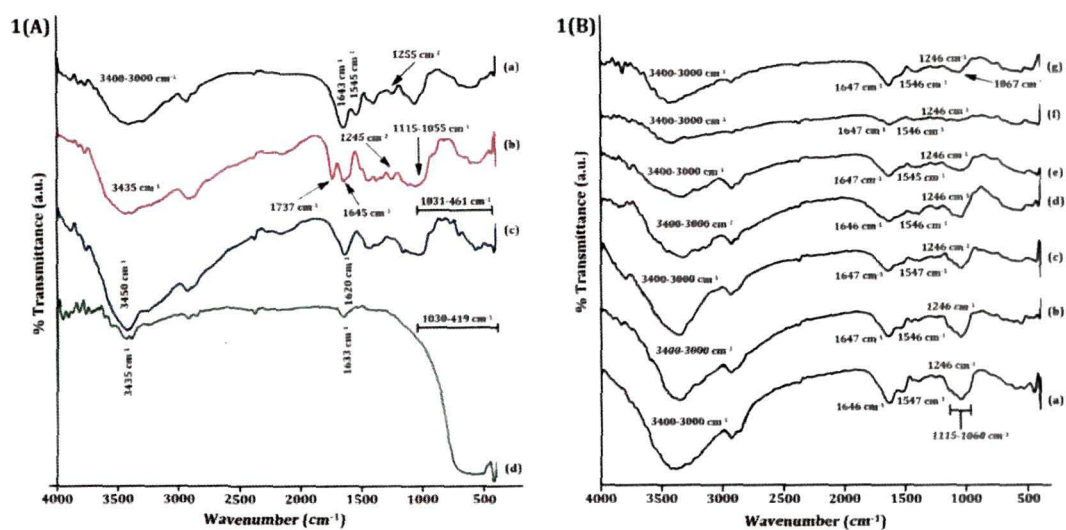
**Figure 3.3.1. (A)** FT-IR spectra of (a) soy flour, (b) jute, (c) nanoclay, and (d) TiO$_2$ nanoparticles. **(B).** FT-IR spectra of (a) SF/J/GA50, (b) SF/J/GA50/T1, (c) SF/J/GA50/T3, (d) SF/J/GA50/T5, (e) SF/J/GA50/T5/N1, (f) SF/J/GA50/T5/N3 and (g) SF/J/GA50/T5/N5.

The intensities of –OH and –NH stretching vibrations in the composites were found to decrease with respect to unfilled composite suggesting the interaction between jute and SF. From the Figure 3.3.1B, it is found that with the increase in concentration of TiO$_2$ nanoparticles, the peak intensities of –OH band were found to decrease. This behaviour could be attributed to the interaction between the free –OH and –NH groups of jute and SF with –OH groups of TiO$_2$ nanoparticles. Upon the addition of nanoclay, the peaks in the ~3400 cm$^{-1}$ further reduce in intensity and are shifted to lower wave number region. The peak intensities in the range of 1030–460 cm$^{-1}$ and 1619 cm$^{-1}$ are found to reduce upto a considerable extent. These results confirm the participation of hydroxyl group of clay with S/J/GA50/T composites [16].

### 3.3.2. SEM study

SEM micrographs of SF/J/GA50, SF/J/GA50/T1, SF/J/GA50/T3, SF/J/GA50/T5, SF/J/GA50/T5/N1, SF/J/GA50/T5/N3, and SF/J/GA50/T5/N5 composites are shown in Figure 3.3.2. The fractured surface of some selective samples was considered for this study. SF/J/GA50 sheet showed a relatively smooth surface (Figure 3.3.2a). Figure 3.3.2b inferred that the fractured surface of SF/J/GA50/T1 displays a homogenous structure suggesting a relatively uniform distribution of the

TiO$_2$ nanoparticles within the composite. However, as the amount of TiO$_2$ nanoparticles was increased, *i.e.*, the fractured surface of SF/J/GA50/T3 and SF/J/GA50/T5 (Figure 2c, d) exhibited a comparatively rough surface, indicating relatively high interfacial adhesion among SF, jute and TiO$_2$ nanoparticles. Furthermore, upon addition of nanoclay into the TiO$_2$ nanoparticles loaded nanocomposites (*i.e.* SF/J/GA50/T5), the roughness was found to enhance (Figure 3.3.2e, f, and g). The enrichment in roughness was due to the fact that clay particles enhance the interaction between the SF macromolecules and jute fibre. Composite having 3 % nanoclay was appeared to be more rough compared with those of the composite prepared with 5 % nanoclay. This indicates that agglomeration of nanoclay particles might have taken place within the composite at higher percentage of nanoclay, the interaction of nanoclay particles with SF and jute are diminished and less rough surface observed.

The fractured surface of TiO$_2$ nanoparticles loaded composites taken for SEM study was also investigated by energy dispersive X-ray elemental analysis (EDX) simultaneously. Figure 3.3.2h shows the EDX analysis of SF/J composite. The presence of Ti and elements such as Al, Na and Si, which are mainly from the silicate nanoclay, along with C and O confirmed the successful incorporation of TiO$_2$ nanoparticles and nanoclay into the composite.
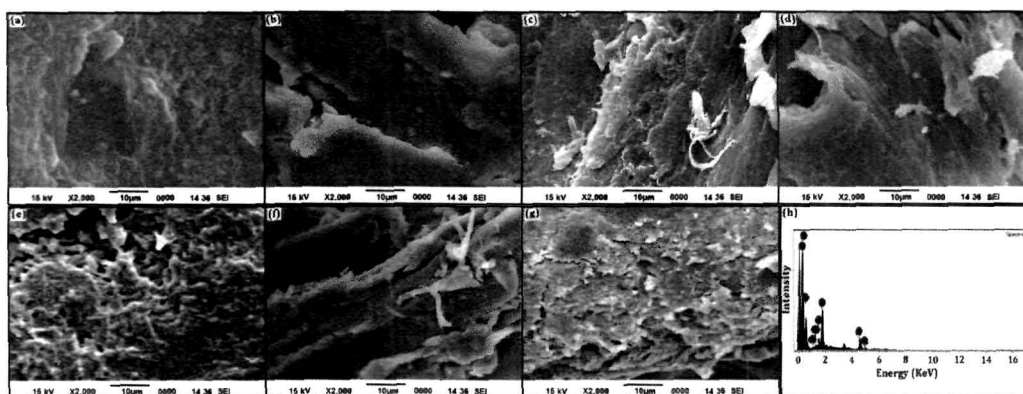


**Figure 3.3.2.** SEM micrographs of (a) SF/J/GA50, (b) SF/J/GA50/T1, (c) SF/J/GA50/T3, (d) SF/J/GA50/T5, (e) SF/J/GA50/T5/N1, (f) SF/J/GA50/T5/N3, (g) SF/J/GA50/T5/N5 and (h) Energy dispersive X-ray analysis of SF/J/GA50/T5/N5.

### 3.3.3. XRD study

Figure 3.3.3A displays the diffractograms of SF, jute, nanoclay, and TiO$_2$ nanoparticles. The diffractogram of SF macromolecules is represented in curve-a. A little wider hump suggesting the amorphous nature of SF macromolecules was observed

at $2\theta$ = 20.2°. Jute (curve-b) shows peaks at $2\theta$ = 21.9° (002 plane of cellulose I) and 19.1° (101 plane of cellulose II) [6]. In Figure 3.3.3A, curve-c, represents the diffractogram of nanoclay. A strong diffraction peak for nanoclay at $2\theta$ = 9.2° and a small peak at $2\theta$ = 24.1° was noticed. The peak at 9.2° resembles to a d-spacing of about 1.2 nm in pure clay. In the diffractogram of bare $TiO_2$ (curve-d), the characteristics peaks appeared at $2\theta$ = 37.8° (004), 48.1° (200), 56.4° (211), and 62.5° (204), and at 27.3° (110), 36.1° (101), 55° (105), were for anatase and rutile phase respectively [67]. All peaks were in good agreement with the standard spectrum (JCPDS no.: 88-1175 and 84-1286).

Figure 3.3.3B represents the diffractograms of SF/J/GA50, SF/J/GA50/T1, SF/J/GA50/T3, SF/J/GA50/T5, SF/J/GA50/T5/N1, SF/J/GA50/T5/N3, and SF/J/GA50/T5/N5 composites. In Figure 3.3.3B, curve-a, represents the diffractograms of SF/J/GA50 (*i.e.* without $TiO_2$ nanoparticles). A small broad diffraction peak corresponding to jute and SF was appeared around $2\theta$ = 20°. Curve (b-d) were the diffractograms of nanocomposites *viz.* SF/J/GA50/T1, SF/J/GA50/T3, and SF/J/GA50/T5 with different percentage of $TiO_2$ nanoparticles (1-5 % w/w of dry SF). The diffraction signals of SF matrix and jute fibre were appeared in the range $2\theta$ = 19° – 22°. However, with higher amount of $TiO_2$ nanoparticles loading, the peaks corresponding to $TiO_2$ nanoparticles appeared with higher intensity. Mina *et al.* [68] reported an increase in peak intensity of $TiO_2$ while studying the X-ray diffraction profile of polypropylene/ titanium dioxide composite. For composites, containing 1% and 3% clay the diffraction peak of the nanoclay tactoids was not observed in the X-ray diffractograms (curve e, f). The $d_{001}$ peak of the nanoclay within the prepared nanocomposites completely disappeared, demonstrating the development of a delaminated structure. It could be said that either the full expansion of the nanoclay gallery take place, which could not be visualized by XRD, or the nanoclay layers were delaminated due to which no crystal diffraction peak appears. In SF/J/GA50/T5/N5 composites, the typical peak of nanoclay was found to appear at $2\theta$ = 7.1° with less intensity representing an existence of agglomeration of nanoclay within the nanocomposite.

Figure 3.3.3. (A) XRD pattern of (a) soy flour, (b) jute, (c) $TiO_2$, and (d) nanoclay. (B) XRD diffractograms of (a) SF/J/GA50, (b) SF/J/GA50/T1, (c) SF/J/GA50/T3, (d) SF/J/GA50/T5, (e) SF/J/GA50/T5/N1, (f) SF/J/GA50/T5/N3 and (g) SF/J/GA50/T5/N5.

## 3.3.4. TEM study

Figure 3.3.4 indicates the TEM micrographs of the SF/J composites with different percentage of nanoclay and $TiO_2$ nanoparticles. Figure 3.3.4a represents the TEM micrographs of composite without $TiO_2$ nanoparticles and nanoclay. The presence of well dispersed black spots (shown by arrow marks) is clearly visualized for $TiO_2$ nanoparticles in SF/J/GA50/T1 and SF/J/GA50/T5 (Figure 3.3.4b, c) [64]. TEM micrographs corresponding to SF/J/GA50/T5/N1 and SF/J/GA50/T5/N3 samples show the dispersion of nanoclay within the nanocomposite (Figure 3.3.4d, e). The threadlike dark lines and black spots (indicated with arrows) signify the intersections of the clay layers and $TiO_2$ particles. It has seen, from the micrographs, that the silicate layers are not homogeneously distributed within the composite indicating the existence of partial compatibility between jute, polymer, $TiO_2$ nanoparticles and nanoclay surface [49]. However, at higher concentration of nanoclay, the thickness of dark slices of nanoclay increases due to agglomeration (Figure 3.3.4f). The results obtained from TEM analysis were in accordance with our XRD findings. Both the results suggest the formation of the partially exfoliated nanocomposites.
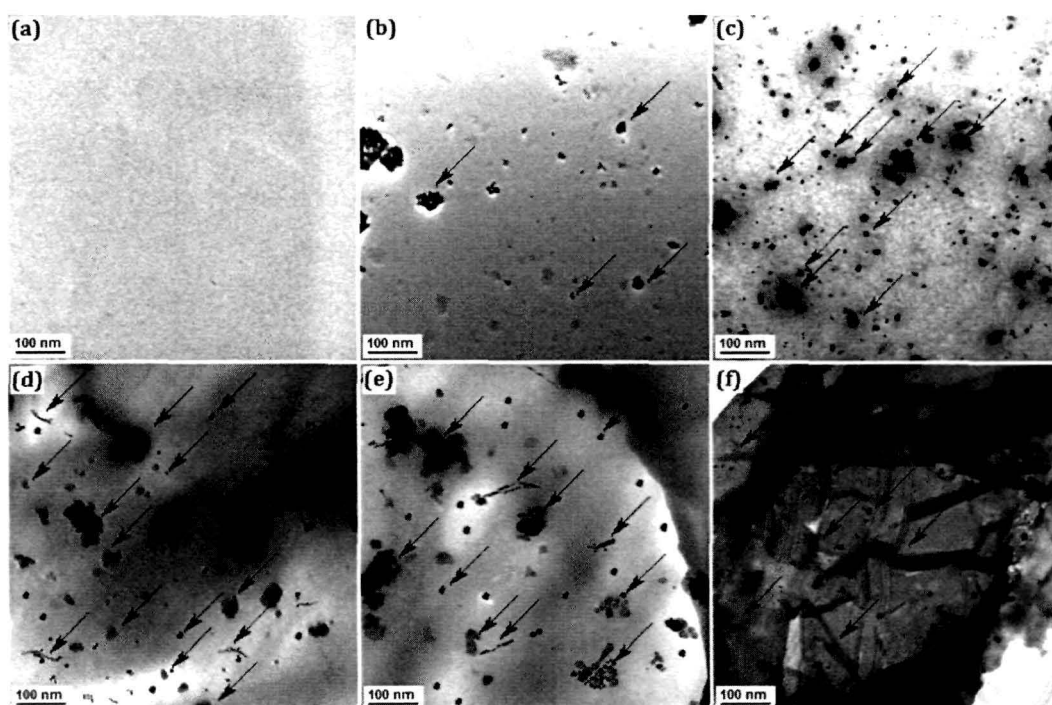
**Figure 3.3.4.** TEM micrograph of (a) SF/J/GA50, (b) SF/J/GA50/T1, (c) SF/J/GA50/T5, (d) SF/J/GA50/T5/N1, (e) SF/J/GA50/T5/N3 and (f) SF/J/GA50/T5/N5.

### 3.3.5. Mechanical property study

The mechanical properties of SF/J composites reinforced with $TiO_2$ nanoparticles and nanoclay were studied at room temperature. Experimental data are presented in Table 3.3.2. A noticeable reinforcing effect was found upon filler addition, which can be anticipated from the increase in both modulus and strength of the composite compared to the unfilled ones. The increase in the percentage of $TiO_2$ nanoparticles might have direct effect in increasing the mechanical properties of the nanocomposites [64]. With increase in the amount of $TiO_2$ nanoparticles, both the tensile and flexural properties of the nanocomposites improves. The interaction of $TiO_2$ nanoparticles with crosslinked SF and jute through its surface hydroxyl group might stiffen the composites and results in enhancement of mechanical properties. Considering the 5 % concentration of the $TiO_2$ nanoparticles as optimum, we had further modified the composites viz. SF/J/GA50/T5/N1, SF/J/GA50/T5/N3 and SF/J/GA50/T5/N5 by incorporating different percentage of nanoclay [1-5 % (w/w of dry SF)]. With the incorporation of nanoclay, composites showed a significant improvement in the mechanical properties compared to nanoclay free composite. The

silicate layers of nanoclay act as a reinforcing agent which binds the polymer chains inside the gallery space and restricts the mobility of the polymer chains.

**Table 3.3.2** Comparison of Tensile and Flexural values of unfilled and filled crosslinked jute based SF nanocomposites before UV treatment.

| Composite | Tensile Properties | | Flexural Properties | |
|---|---|---|---|---|
| System | Strength (MPa) | Modulus (MPa) | Strength (MPa) | Modulus (MPa) |
| SF/J/GA50 | 10.84 (±2.1) | 984.3 (±12.6) | 15.91 (±1.8) | 1777.5 (±11.1) |
| SF/J/GA50/T1 | 16.85 (±1.8) | 1187.8 (±11.5) | 28.98 (±2.2) | 2198.9 (±11.4) |
| SF/J/GA50/T3 | 28.54 (±1.2) | 1819.3 (±12.8) | 40.31 (±1.4) | 2920.3 (±12.5) |
| SF/J/GA50/T5 | 34.25 (±2.6) | 1932.4 (±16.1) | 49.58 (±2.1) | 3631.4 (±12.2) |
| SF/J/GA50/T5/N1 | 39.97 (±1.5) | 2094.1 (±11.3) | 70.93 (±2.5) | 4304.5 (±14.5) |
| SF/J/GA50/T5/N3 | 55.76 (±1.4) | 2443.3 (±12.2) | 88.14 (±1.8) | 6349.8 (±11.3) |
| SF/J/GA50/T5/N5 | 49.13 (±1.3) | 2237.8 (±11.7) | 79.41 (±2.5) | 5866.3 (±12.8) |

Each value in the above table represents average of ten samples. Values in the parenthesis represent the standard deviation.

Faruk *et al.* [69] observed an increase in mechanical properties of wood–plastic composite after the incorporation of nanoclay. However, such improvement in mechanical properties with the incorporation of nanoclay might only be realized up to a certain clay loading. In the present work, the enhancement in mechanical properties was found up to 3 % of clay loading, and beyond that it declines on further addition of nanoclay. At higher concentration of nanoclay, agglomeration of clay particles might have taken place and therefore its interaction with polymer was reduced which led to

the declining trend in the mechanical properties of the composites. TEM study also supported the agglomeration of $TiO_2$ nanoparticles.

### 3.3.6. Thermal property study

Figure 3.3.5 depicts the thermograms of SF/J/GA50, SF/J/GA50/T1, SF/J/GA50/T3, SF/J/GA50/T5, SF/J/GA50/T5/N1, SF/J/GA50/T5/N3, and SF/J/GA50/T5/N5. All the thermograms showed an initial weight loss around 100 °C due to the loss of confined water molecules. It was clearly inferred from the thermograms that all the values of the nanocomposites were found to increase with increase in the amount of $TiO_2$ nanoparticles. The
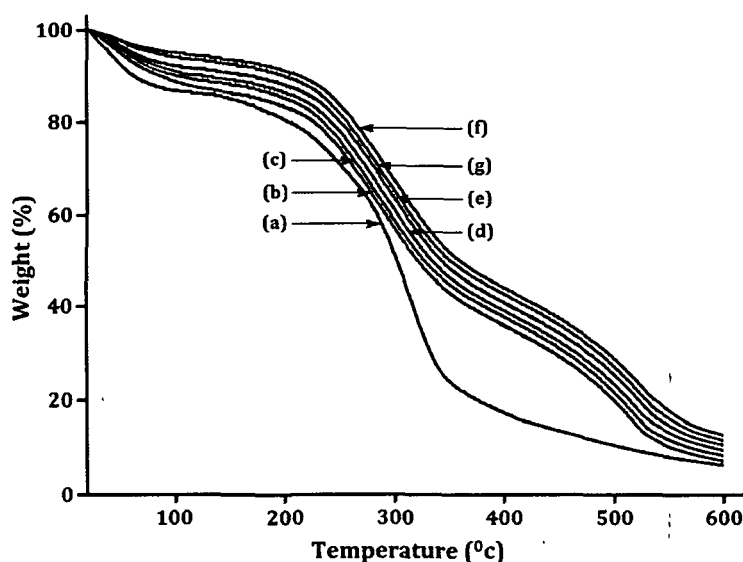


**Figure 3.3.5.** TGA thermograms of (a) SF/J/GA50, (b) SF/J/GA50/T1, (c) SF/J/GA50/T3, (d) SF/J/GA50/T5, (e) SF/J/GA50/T5/N1, (f) SF/J/GA50/T5/N3 and (g) SF/J/GA50/T5/N5.

heat shielding effect of $TiO_2$ nanoparticles were responsible for enhancement in thermal thermal stability [70]. To enhance the thermal stability of composite materials, nanoclay is widely used. After the incorporation of nanoclay, the thermal stability of the $TiO_2$ nanoparticles loaded nanocomposites were further improved. This increase in thermal stability of the prepared nanocomposites is attributed to the hindered diffusion of volatile decomposition products within it. This might also be due to the physico-chemical adsorption of the volatile degradation products on the silicate surface of nanoclay. The volatilization of the degraded products originated by carbon-carbon bond scission in the composite was delayed by tortuous path provided by the silicate layers

[53]. Laachachi *et al.* [71] studied the thermal stability of PMMA by using organoclay and TiO$_2$ and reported significant increase in thermal stability of PMMA due to the synergistic effect of clay/TiO$_2$. With the increase in concentration of clay, the agglomeration of clay probably took place which contributed to the reduction in the thermal stability. Therefore, it is concluded that the thermal stability of SF/J composites was increased on addition of upto a certain amount of TiO$_2$ nanoparticles and nanoclay.

### 3.3.7. UV test results

The weight loss of SF/J/GA50, SF/J/GA50/T1, SF/J/GA50/T3, SF/J/GA50/T5, SF/J/GA50/T5/N1, SF/J/GA50/T5/N3, and SF/J/GA50/T5/N5 are represented in Figure 3.3.6. Weight losses of the samples were determined at room temperature as a



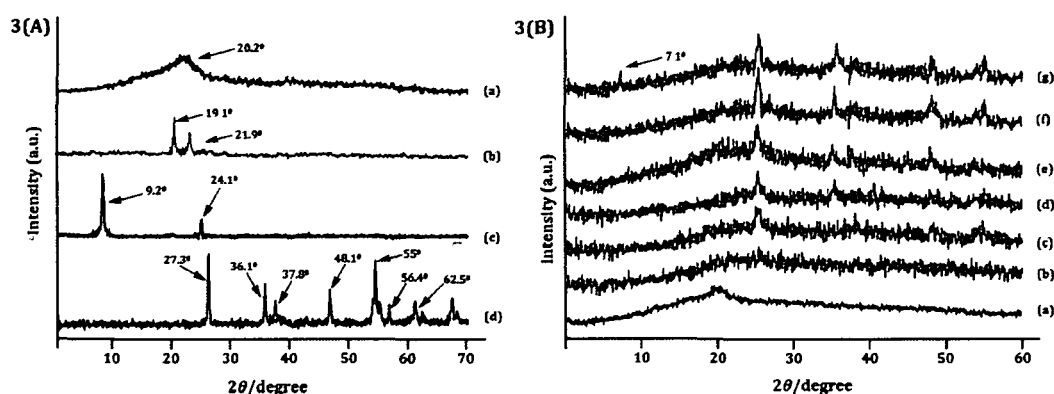**Figure 3.3.6.** Weight loss vs Exposure time for (a) SF/J/GA50, (b) SF/J/GA50/T1, (c) SF/J/GA50/T3, (d) SF/J/GA50/T5, (e) SF/J/GA50/T5/N1, (f) SF/J/GA50/T5/N3 and (g) SF/J/GA50/T5/N5.

function of exposure time and found linear variation with this. Initially a small increase in weight was found due to moisture uptake by the samples, which was greater than the material loss induced by the degradation in the early stage. The rate of weight loss was lowest for SF/J/GA50/T5/N3 followed by SF/J/GA50/T5/N5, SF/J/GA50/T5/N1, SF/J/GA50/T5, SF/J/GA50/T3, SF/J/GA50/T1 and SF/J/GA50. The TiO$_2$ nanoparticles and nanoclay unloaded composite had shown maximum weight losses. After 60 days of exposure time, the weight losses in S/J/GA50, S/J/GA50/T1, S/J/GA50/T3, S/J/GA50/T5, S/J/GA50/T5/M1, S/J/GA50/T5/M3 and S/J/GA50/T5/M5 were 4.82 ±

0.3 %, 4.09 ± 0.2%, 3.51 ± 0.2 %, 2.96± 0.3 %, 2.03 ± 0.2 %, 1.32 ± 0.1 % and 1.66 ±

0.2 % respectively. Result shown was the average of four specimens. The lower weight

loss (%) for SF/J/GA50/T5/N3 composites after UV exposure was due to the UV

shielding ability of TiO$_2$ nanoparticles and nanoclay. On exposure to UV radiation, the

chain scission followed by decrease in the density of the entanglements of the SF

polymer chains occurred. This resulted in the decrease in the weight of the synthesized

composites.

Figure 3:3.7 displays the FT-IR spectra of (a) SF/J/GA50, (b) SF/J/GA50/T1,

(c) SF/J/GA50/T3, (d) SF/J/GA50/T5, (e) SF/J/GA50/T5/N1, (f) SF/J/GA50/T5/N3

and (g) SF/J/GA50/T5/N5 after UV exposure. The carbonyl peak intensity was found
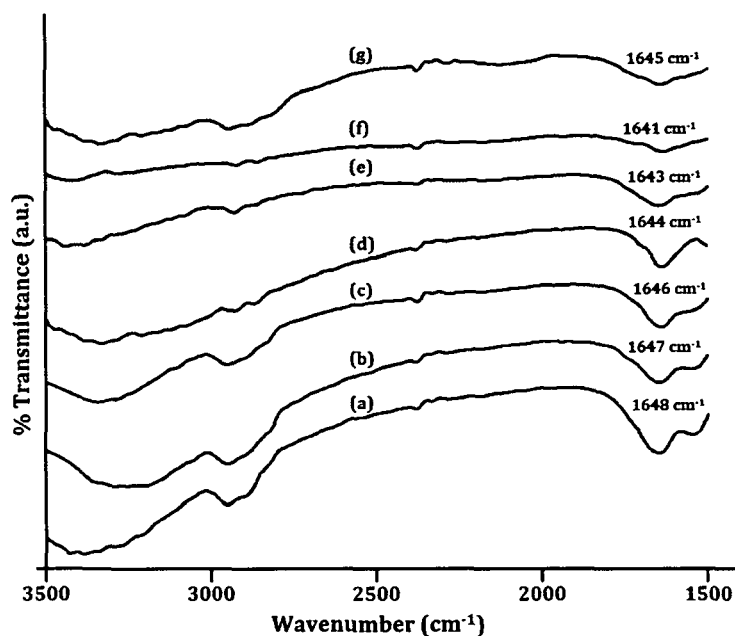


**Figure 3.3.7.** Change in carbonyl peak intensity of (a) SF/J/GA50, (b) SF/J/GA50/T1, (c) SF/J/GA50/T3, (d) SF/J/GA50/T5, (e) SF/J/GA50/T5/N1, (f) SF/J/GA50/T5/N3 and (g) SF/J/GA50/T5/N5.

to increase after irradiation of the samples for 60 days. Upon exposing the samples to

UV-radiation, chain scission of the polymers take place and the carbonyl index value

increases as shown in Figure 3.3.8. SF/J/GA50/T5/N3 had lowest carbonyl index value

whereas SF/J/GA50 had the utmost one. TiO$_2$ nanoparticles played an important role

for stabilizing the SF/J composites by acting as a screen and slowed down the photo

degradation process. TiO$_2$ nanoparticles absorbed the UV radiation and hence reduced

the UV intensity required for the oxidation of the synthesized nanocomposites. Du *et*

*al.* [72] observed an improvement in UV stability of WF/HDPE composite after the incorporation of $TiO_2$. The presence of nanoclay in the composite also has a screening effect which further delays the photo degradation process. Grigoriadou *et al.* [73] had observed an increase in UV stability of HDPE after incorporating montmorillonite clay. SF/J/GA50/T5/N5 exhibits lower protection against UV with respect to SF/J/GA50/T5/N3.
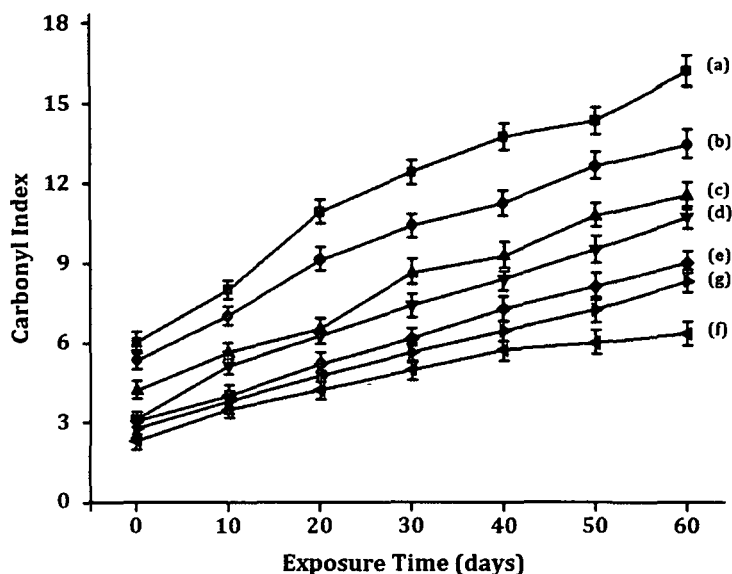


**Figure 3.3.8.** Carbonyl Index value of (a) SF/J/GA50, (b) SF/J/GA50/T1, (c) SF/J/GA50/T3, (d) SF/J/GA50/T5, (e) SF/J/GA50/T5/N1, (f) SF/J/GA50/T5/N3 and (g) SF/J/GA50/T5/N5.

This might be due to the agglomeration of nanoclay particles within the composite material. It is well known that UV-radiation has a deterioration effect on many plastic materials. These materials, when exposed to the outdoor environment, undergo significant changes, namely, photo-degradation, causing loss of mechanical properties. Therefore, the changes in the mechanical properties of the composites after the UV treatment are presented in Table 3.3.3. Both the flexural and tensile properties were reduced after UV treatment. The loss of mechanical properties of unfilled composites was more significant compared to nanoparticles filled composites. SF/J/GA50 was more prone to UV attack and hence it showed maximum loss of mechanical properties. The values presented in Table 3.3.3 suggested that the interfacial interactions among SF, jute, GA, $TiO_2$ nanoparticles and nanoclays were strong enough to decay the massive sheer due to rupture. Therefore, the resistance of SF/J composite

to UV instability, *i.e.*, photodegradation embrittlement, could be improved significantly with the addition of nanoparticles.

**Table 3.3.3.** Changes in the mechanical properties of Unfilled and Filled jute based crosslinked SF nanocomposites after UV Exposure.

| Composite System | Tensile Properties (MPa) | | Flexural Properties (MPa) | |
|---|---|---|---|---|
| | Strength | Modulus | Strength | Modulus |
| SF/J/GA50 | 4.72 (±1.1) | 703.1 (±10.7) | 9.88 (±2.1) | 1422.2 (±12.4) |
| SF/J/GA50/T1 | 9.57 (±1.8) | 972.4 (±12.2) | 24.79 (±1.7) | 1773.3 (±11.3) |
| SF/J/GA50/T3 | 22.46 (±1.8) | 1641.2 (±11.5) | 35.98 (±1.5) | 2611.5 (±11.6) |
| SF/J/GA50/T5 | 29.63 (±1.2) | 1774.3 (±12.1) | 44.89 (±1.9) | 3276.7 (±12.8) |
| SF/J/GA50/T5/N1 | 35.87 (±1.3) | 1837.3 (±11.4) | 65.88 (±2.1) | 3901.2 (±14.3) |
| SF/J/GA50/T5/N3 | 52.56 (±1.4) | 2152.4 (±15.6) | 83.33 (±1.5) | 6140.1 (±12.7) |
| SF/J/GA50/T5/N5 | 45.89 (±1.2) | 1972.3 (±12.7) | 74.72 (±2.6) | 5564.6 (±11.5) |

Each value in the above table represents average of ten samples. Values in the parenthesis represent the standard deviation.

### 3.3.8. Dimensional stability test

The water vapour absorption study was carried out at room temperature (~ 30 °C) with 65 % relative humidity for different time period which is shown in Figure 3.3.9. From the figure, it is seen that for all the composites, the % swelling is increased with the increase in time. Water vapour absorption was found to decrease due to the presence of dispersed phase of $TiO_2$ nanoparticles in the composite system. Water vapour absorption of S/J/GA50/T composites decreased with the increase in $TiO_2$ nanoparticles content. $TiO_2$ nanoparticles act as a barrier to the passage of water as the strong affinity of water molecules towards $TiO_2$ nanoparticles restricts its free motion and reduces the diffusion co-efficient of water. The well dispersed phase of $TiO_2$ nanoparticles improves the resistance of the composite and retards the motion of water molecules through it. Zhu *et al.* [74] reported the increase in barrier property of poly(lactic acid) nanocomposite film after the incorporation of nano-$TiO_2$. The better the distribution of nanoparticles, the higher is the barrier property. Furthermore, the dimensional stability of the SF/J/GA50/T5 composite was improved with the

incorporation of nanoclay. This might be due to the fact that the silicate layers of nanoclay provide a tortuous path which hinders the diffusivity of water molecules through the nanocomposite [27]. As the nanoclay concentration was increased to 5 %, the superfluous filler congregates easily, decreasing the effective content of filler and therefore had little effect on decreasing of water vapour absorption. Nanoclay at higher concentration was found to become agglomerated within the composite which resulted in an increase in water vapour absorption capacity.
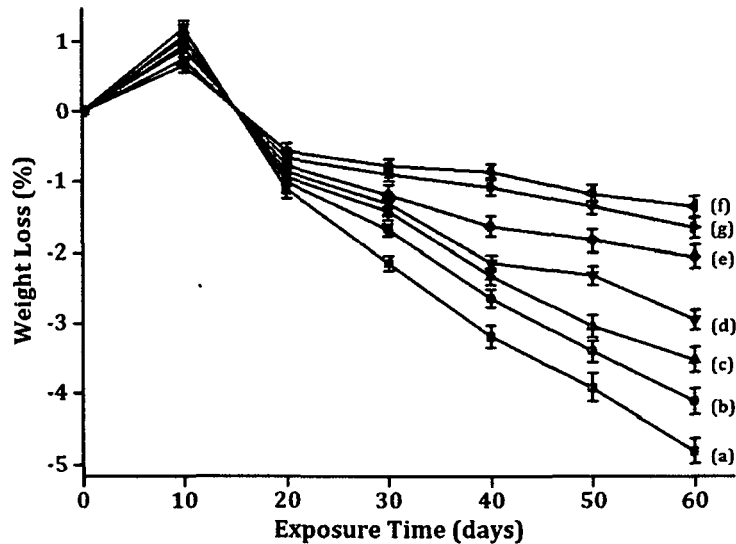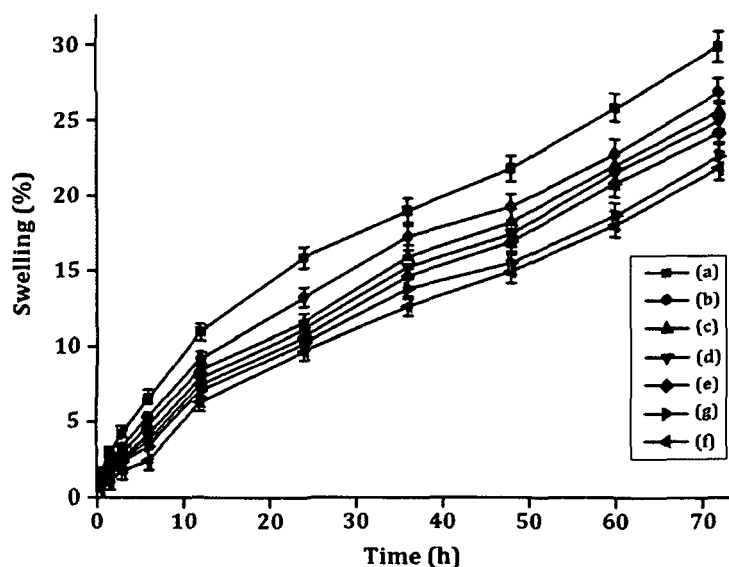


**Figure 3.3.9.** Swelling behaviour of (a) SF/J/GA50, (b) SF/J/GA50/T1, (c) SF/J/GA50/T3, (d) SF/J/GA50/T5, (e) SF/J/GA50/T5/N1, (f) SF/J/GA50/T5/N3 and (g) SF/J/GA50/T5/N5.

### 3.3.9. LOI study

LOI values of jute based SF composites with different percentage of $TiO_2$ nanoparticles and nanoclay are depicted in Table 3.3.4. From the table, it is observed that all the samples produce small localised flame and nanoclay filled composites produce higher char than that of the nanoclay unfilled one. The LOI test assumed that inherently less flammable materials require greater oxygen concentrations to produce the heat necessary for the continuous production of flammable volatiles and flame propagation. This test envisaged that the LOI value increases with the increase in the concentration of $TiO_2$ nanoparticles in the composites. The surface hydroxyl groups of $TiO_2$ nanoparticles may interact with SF, jute and GA and thus restricts the accessibility of oxygen for the production of degradable components from the composites and hence improvement in LOI value was observed [64]. However, on addition of nanoclay into

TiO$_2$ nanoparticles filled composites, further enhancement in LOI value is observed. The incorporation of the nanoclay into the synthesized composite produces a silicate char on the surface of it and hence improves their flame resistance property. The silicate rich surface has better barrier property to heat and oxygen transport due to which ignition of the composite delays [75]. The LOI value is increased upto addition of 3 % of nanoclay. At higher concentration of nanoclay (5 %), the LOI value is decreased. At higher clay loading, the agglomeration of nanoclay results in decrease of interaction with concomitant reduction in barrier property as well as LOI value.

**Table 3.3.4.** LOI and Flaming Characteristics of the prepared composites.

| Samples | LOI (%) | Flame description | Smoke & Fumes | Char |
|---|---|---|---|---|
| SF/J/GA50 | 42 (±0.22) | Small localised flame | Small and black smoke | Little |
| SF/J/GA50/T1 | 45 (±0.41) | Small localised flame | Small and black smoke | Moderate |
| SF/J/GA50/T3 | 49 (±0.63) | Small localised flame | Small and black smoke | Moderate |
| SF/J/GA50/T5 | 52 (±0.33) | Small localised flame | Small and black smoke | Moderate |
| SF/J/GA50/T5/N1 | 58 (±0.21) | Small localised flame | Small and black smoke | Higher |
| SF/J/GA50/T5/N3 | 68 (±0.42) | Small localised flame | Small and black smoke | Higher |
| SF/J/GA50/T5/N5 | 64 (±0.31) | Small localised flame | Small and black smoke | Higher |

* Each value represents average five samples.

**Section D:** **Study on the effect of ZnO and nanoclay on jute fabric reinforced soy flour bio-nanocomposites**

The pollution caused by petroleum based polymeric materials has become a matter of serious concern. The removal of petroleum based polymeric materials is a global awareness and also a demand of legislative authorities. Therefore, the need for greener and more sustainable technologies has profound interest on use of renewable and eco-friendly materials with high performance [28, 76]. Hence, biopolymer based materials have recently dominated the traditionally obtained petroleum based polymer materials. Apart from the various advantages, biopolymer based materials also exhibit certain limitations like poor mechanical properties and water resistivity. Biofibres, have become a promising option for improving the mechanical properties of such materials. Biofibres display significant features like high specific modulus, low density, easily availability also being cost effective and comparatively safe over their conventional counterpart [77]. Moreover, the properties of biopolymer based composites can be improved by using nanoparticles. Out of various nanoparticles predecessors, nanoclay is most extensively used for the synthesis of polymer nanocomposite. In exterior application of biopolymer based materials, UV protection, flame retardancy and weathering resistance are very important. In recent years, ZnO nanoparticles (ZNP) is one of the widely used filler in exterior coatings to improve photostability [78], as a component of UV protection for nanocomposites [79]. Along with the UV-resistance property, ZNP also improve thermal, mechanical and other relevant properties of polymer nanocomposites [80].

This part of study is aimed to discuss the effect of ZNP alone and in combination with nanoclay on thermal and mechanical properties of SF/J composites. We also study the effect of nanoparticles *viz.* ZNP and nanoclay on other properties like UV resistance, flame retardancy, dimensional stability and biodegradation of the composites.

**3.4. RESULTS & DISCUSSION**

The samples, as coded in Table 3.4.1, had been prepared by keeping the weight (%) of the components *viz.* SF, glycerol, jute and GA constant in all the samples where as the percentages (%) of ZNP and nanoclay were varied. The weight (%) of the various components used for the synthesis of the composite are provided in Table 3.4.1.

**Table 3.4.1.** Codification and filler content of the nanocomposites based on jute and crosslinked SF with zinc oxide nanoparticles and nanoclay (wt %).

| Sample | Soy flour (SF) | Glycerol | Glutaraldehyde (GA) | Jute (J) | ZnO (Z) | Nanoclay (N) |
|---|---|---|---|---|---|---|
| SF/J/GA50 | 100 | 5 | 50 | 75 | - | - |
| SF/J/GA50/Z1 | 100 | 5 | 50 | 75 | 1 | - |
| SF/J/GA50/Z3 | 100 | 5 | 50 | 75 | 3 | - |
| SF/J/GA50/Z5 | 100 | 5 | 50 | 75 | 5 | - |
| SF/J/GA50/Z5/N1 | 100 | 5 | 50 | 75 | 5 | 1 |
| SF/J/GA50/Z5/N3 | 100 | 5 | 50 | 75 | 5 | 3 |
| SF/J/GA50/Z5/N5 | 100 | 5 | 50 | 75 | 5 | 5 |

### *3.4.1. FT-IR study*

The interactions among jute, SF, GA, ZNP, and clay were studied by FT-IR spectroscopy. FT-IR spectra of jute, SF, clay, and ZNP are presented in Figure 3.4.1A. The FT-IR spectrum of jute shows the absorption bands around 3440 cm$^{-1}$ for –OH stretching, 1736 cm$^{-1}$ for C=O stretching vibration of ester groups of hemicelluloses, 1643 cm$^{-1}$ for C=O stretching, 1247 cm$^{-1}$ for –C–O–C– bond in cellulose chain and 1057–1116 cm$^{-1}$ for C–O stretching [14]. The spectrum of SF (curve-b in Figure 3.4.1A) shows peaks in the region 1647, 1542 and 1254 cm$^{-1}$ for C = O stretching of amide – I, – NH bending of amide – II and C – N stretching of amide – III [13]. Clay exhibits peaks at 3450 cm$^{-1}$ (–OH stretching), 1619 cm$^{-1}$ (–OH bending), 1030–460 cm$^{-1}$ (oxide bonds of metals like Si, Al, Mg etc.). FT-IR spectrum of ZNP is presented in curve-d Figure 3.4.1A. Absorption peaks at 3429 and 1633 cm$^{-1}$ in the spectra is due to –OH stretching and –OH bending vibrations while the high intensity broad band at approximately 421 cm$^{-1}$ resulting from the stretching of the zinc and oxygen bond [81].
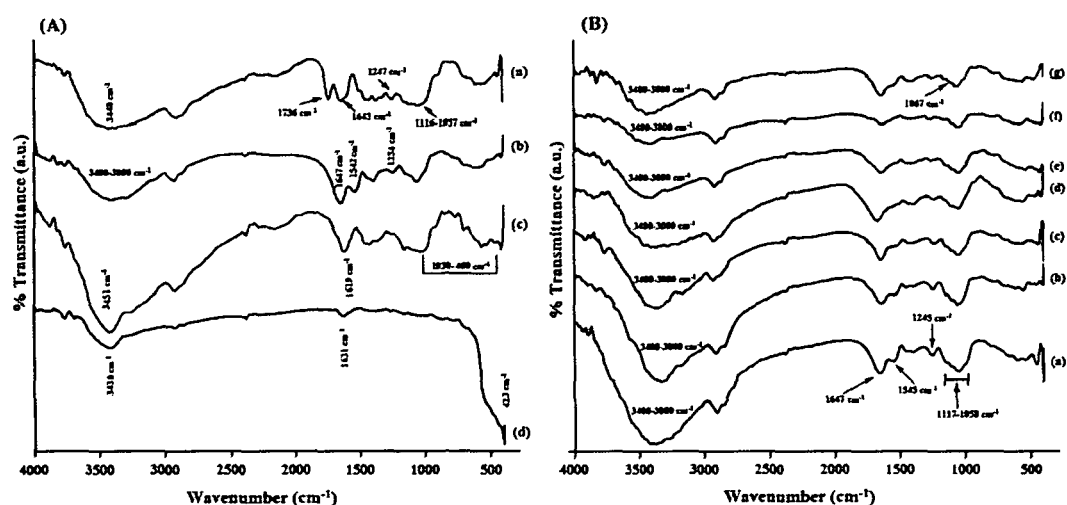
**Figure 3.4.1. (A)** FT-IR spectra of (a) soy flour, (b) jute, (c) nanoclay, and (d) ZNP. **(B).** FT-IR spectra of (a) SF/J/GA50, (b) SF/J/GA50/Z1, (c) SF/J/GA50/Z3, (d) SF/J/GA50/Z5, (e) SF/J/GA50/Z5/N1, (f) SF/J/GA50/Z5/N3 and (g) SF/J/GA50/Z5/N5.

FT-IR spectra for the composite SF/J/GA50, SF/J/GA50/Z1, SF/J/GA50/Z3, SF/J/GA50/Z5, SF/J/GA50/Z5/N1, SF/J/GA50/Z5/N3, and SF/J/GA50/Z5/N5 are shown in Figure 3.4.1B. The FT-IR spectra for all the samples show peaks in the region 3400–3000 cm$^{-1}$, which could be attributed to the –OH and –NH stretching vibrations, respectively. Characteristic peaks of SF in the region of 1647, 1542 and 1254 cm$^{-1}$ for C=O stretching of amide–I, –NH bending of amide –II and C–N stretching of amide – III were present in all the spectra. Similarly, the peaks appearing in all the spectra at 1247 and 1116-1057 cm$^{-1}$ are for –C–O–C– bond in cellulose chain and C–O stretching vibration, which are the characteristic peaks for jute. The entire spectrum shows the peak around 900 cm$^{-1}$ due to the $\beta$-(1→4)-glycosidic linkages. The intensities of –OH and –NH stretching vibrations were found to decrease with respect to unfilled composite suggesting the interaction between jute and SF. From the IR spectrum, it was observed that with the increase in concentration of ZNP, the peak intensities of –OH band were found to decrease and slightly shifted. This behaviour could be attributed to the interaction between the free –OH and –NH groups of jute and SF with –OH groups of ZNPs. The FT-IR spectra indicated the existence of a strong binding but no obvious formation of covalent bonds between the S/J/GA50 composites and ZNP [82]. Upon the addition of nanoclay, the intensity of the peaks in the ~3400 cm$^{-1}$ range was further reduced and shifted to lower wavenumber. The peak intensities in the range of 1030–

460 cm$^{-1}$ and 1619 cm$^{-1}$ are found to reduce upto a considerable extent. These results confirmed the participation of hydroxyl group of clay with S/J/GA50/Zn composites [16].

### 3.4.2. SEM study

As a vital tool for studying surface morphology of composite materials, scanning electron microscopy analysis was performed. Figure 3.4.2 shows SEM micrographs of SF/J/GA50, SF/J/GA50/Z1, SF/J/GA50/Z3, SF/J/GA50/Z5, SF/J/GA50/Z5/N1, SF/J/GA50/Z5/N3, and SF/J/GA50/Z5/N5 composites. The
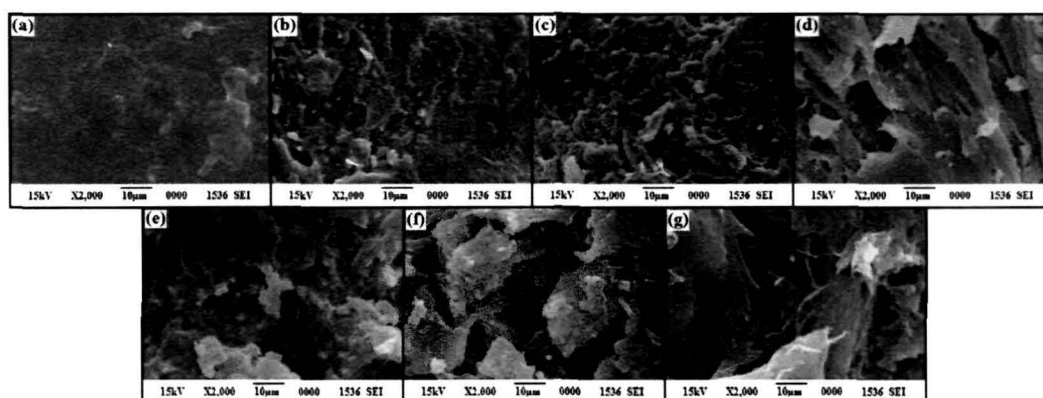


**Figure 3.4.2.** SEM micrographs of (a) SF/J/GA50, (b) SF/J/GA50/Z1, (c) SF/J/GA50/Z3, (d) SF/J/GA50/Z5, (e) SF/J/GA50/Z5/N1, (f) SF/J/GA50/Z5/N3 and (g) SF/J/GA50/Z5/N5.

fractured surface of some selective samples was considered for this study. SF/J/GA50 sheet showed a relatively smooth surface (Figure 3.4.2a). Figure 3.4.2b inferred that the fractured surface of SF/J/GA50/Z1 displays a homogenous structure suggesting a relatively uniform distribution of the ZNP within the composite. However, as the percentage of ZNP increased, *i.e.*, the fractured surface of SF/J/GA50/Z3 and SF/J/GA50/Z5 (Figure 3.4.2c, d) exhibited a relatively rough surface, indicating high interfacial adhesion among SF, jute and ZNP. Moreover, upon addition of nanoclay into the ZNP loaded nanocomposites (*i.e.* SF/J/GA50/Z5), the roughness was found to enrich (Figure 3.4.2e, f, and g). The enrichment in roughness was due to the fact that clay particles enhance the interaction with the SF matrix and jute surface [12]. The roughness of fractured surface of composite having 3 % nanoclay was more compared to those of the composite prepared with 5 % nanoclay. This indicated that

115

agglomeration of nanoclay particles might have taken place within the composite at higher concentration of clay due to which interaction of clay particles with SF and jute are diminished and less rough surface appeared.

The fractured surface of ZNP loaded composites taken for SEM study was also investigated by energy dispersive X-ray elemental analysis (EDX) simultaneously. Figure 3.4.3 shows the EDX analysis of SF/J composite. The presence of Zn along with C and O confirmed the successful incorporation of ZNP into the composite. Elements such as Al, Na and Si, which are mainly from the silicate nanoclay, were also detected (Figure 3.4.3b) along with Zn, indicating the successful incorporation of nanoclay and ZNP into the composite.
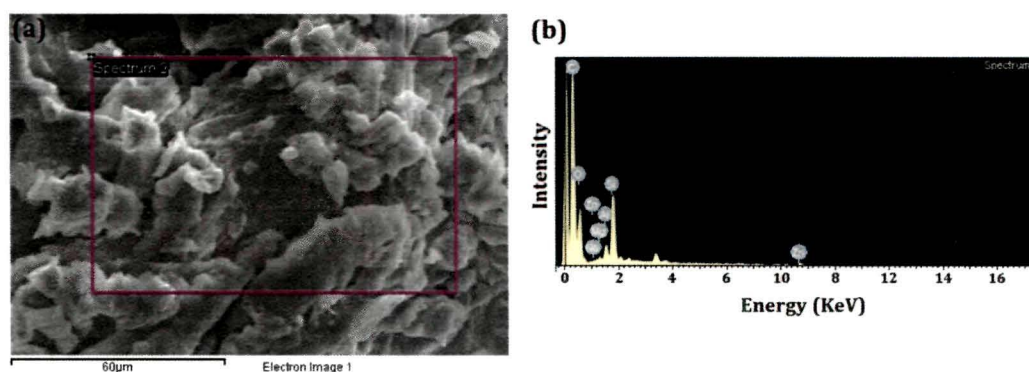


**Figure 3.4.3.** Energy dispersive X-ray analysis of SF/J/GA50/Z5/N5.

### 3.4.3. XRD study

XRD analysis was implemented to obtain comprehensive information regarding crystal structure of the nanoparticles (i.e. ZNP and nanoclay) and the synthesized composites. Figure 3.4.4A represents the diffractograms of SF, jute, ZNP, and nanoclay. In Figure 3.4.4A, curve-a represents the diffractogram of SF macromolecules. A little broader hump suggesting the amorphous nature of SF was noticed at $2\theta = 20°$. Jute (curve-b) shows peaks at $2\theta = 22°$ (002 plane of cellulose I) and 19° (101 plane of cellulose II) [6]. Curve-c shows the X-ray diffraction patterns of bare ZNP. From this, a series of characteristic peaks at $2\theta = 32.1°$ (100), 34.4° (002), 36.6° (101), 47.6° (102), 56.5° (110), 63.1° (103), 66.6° (200), 67.9° (112) and 69.2° (201) was observed and they are in accordance with the zincite phase of ZnO (International Centre for Diffraction Data, JCPDS 5-0664). Curve-d, represents the diffractogram of pure nanoclay. A strong diffraction peak for nanoclay at $2\theta = 9°$ and a

116

small peak at $2\theta = 24°$ was observed. The peak at $9°$ resembles to a d-spacing of about 1.2 nm in pure clay [12].

Figure 3.4.4B depicts the diffractograms of SF/J/GA50, SF/J/GA50/Z1, SF/J/GA50/Z3, SF/J/GA50/Z5, SF/J/GA50/Z5/N1, SF/J/GA50/Z5/N3, and SF/J/GA50/Z5/N5 composites. Curve-a (Figure 3.4.4B) without ZnO (*i.e.* SF/J/GA50) exhibits a small broad diffraction peak corresponding to jute and SF in the $2\theta$ range $10°$ - $20°$. Curve (b-d) are for jute based crosslinked SF nanocomposites (SF/J/GA50/Z1, SF/J/GA50/Z3, and SF/J/GA50/Z5) with different percentage of ZNP (1-5 % $^w/_w$ of dry SF). The diffraction signals of jute and SF appearing in the range $2\theta = 19°$ - $22°$ were found to shrink after the introduction of ZNP in the composite [83]. However, at a higher amount of ZNP loading, the peaks corresponding to ZNP appeared with higher intensity [81]. The diffraction peak of the nanoclay tactoids was absent in the X-ray diffractograms for 1% and 3% clay incorporated composites (curve e, f in Figure 3.4.4B). The $d_{001}$ peak of the clay within the synthesized nanocomposites completely disappeared, indicating the development of a delaminated structure within the nanocomposites. It could be said that either the full expansion of the nanoclay gallery occurs, which could not be identified by XRD, or the nanoclay layers were delaminated due to which no crystal diffraction peak appears. In SF/J/GA50/Z5/N5 composites, the typical peak of nanoclay at $2\theta = 9°$ was found to shift to lower $2\theta$ values (*i.e.* $2\theta = 7°$) with less intensity representing an occurrence of agglomeration of nanoclay within the nanocomposite.
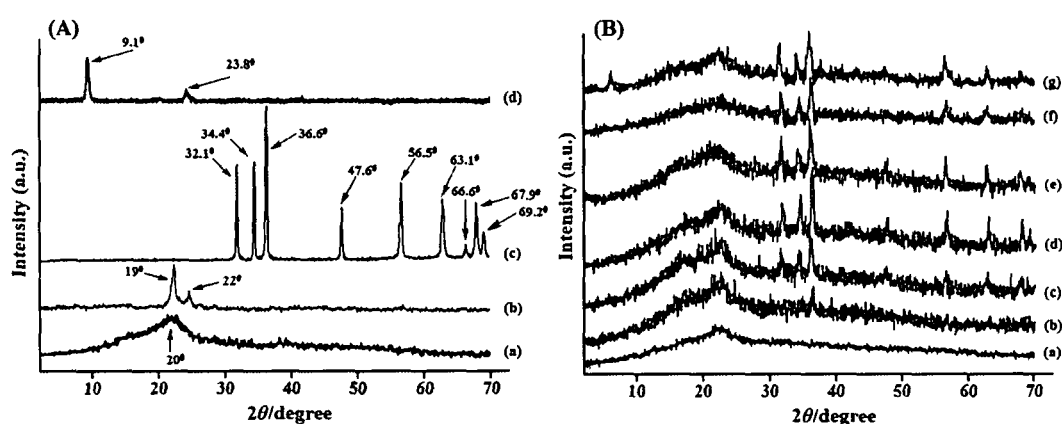


**Figure 3.4.4.** **(A)** XRD pattern of (a) soy flour, (b) jute, (c) ZnO, and (d) nanoclay. **(B)** XRD diffractograms of (a) SF/J/GA50, (b) SF/J/GA50/Z1, (c) SF/J/GA50/Z3, (d) SF/J/GA50/Z5, (e) SF/J/GA50/Z5/N1, (f) SF/J/GA50/Z5/N3 and (g) SF/J/GA50/Z5/N5.

### 3.4.4. TEM study

The morphological features of the synthesized nanocomposites were characterized by HRTEM investigation. Figure 3.4.5 (a-f) are the micrographs of the SF/J/GA50, SF/J/GA50/Z1, SF/J/GA50/Z5, SF/J/GA50/Z5/N1, SF/J/GA50/Z5/N3, and SF/J/GA50/Z5/N5 samples, respectively. Figure 3.4.5a represents the TEM micrographs of composite without ZNPs and nanoclay. The presence of dark spots (shown by arrow marks) is clearly visualized for ZNP in SF/J/GA50/Z1 and SF/J/GA50/Z5 (Figure 3.4.5b, c) [82]. From the micrographs (Figure 3.4.5b, c), it was observed that the nanoparticles were well dispersed within the prepared SF/J nanocomposites. TEM micrographs corresponding to SF/J/GA50/Z5/N1 sample show the dispersion of nanoclay within the nanocomposite (Figure 3.4.5d). The threadlike dark lines (indicated with arrows) signify the intersections of the clay layers, and the bright areas symbolize the composite comprising of jute and SF matrix. From the micrographs, it is seen that the threadlike lines are not homogeneously distributed within the composite indicating the existence of partial compatibility between jute, polymer, ZNP and nanoclay surface [49]. TEM micrographs clearly revealed the loss of stacking structure of clay layers and eventually dictated the disordered dispersion within the composite. However, at higher concentration of nanoclay, the thickness of dark slices of nanoclay increased and as a result agglomeration took place (Figure 3.4.5f). The results obtained from HRTEM analysis are in accordance with our XRD findings. Both the results suggested the formation of the partially exfoliated nanocomposites.
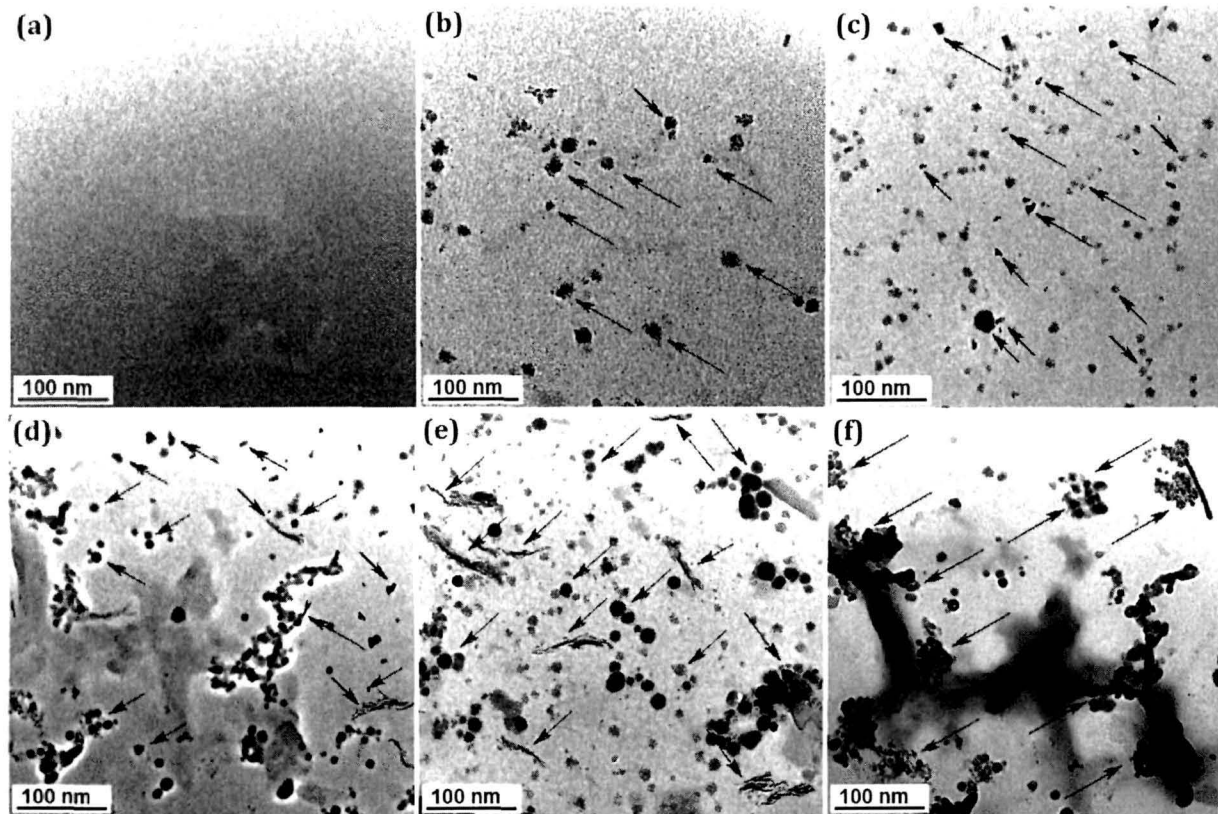
**Figure 3.4.5.** TEM micrograph of (a) SF/J/GA50, (b) SF/J/GA50/Z1, (c) SF/J/GA50/Z5, (d) SF/J/GA50/Z5/N1, (e) SF/J/GA50/Z5/N3 and (f) SF/J/GA50/Z5/N5.

### 3.4.5. Mechanical property study

The mechanical properties data of SF/J composites reinforced with ZNP and nanoclay were presented in Table 3.4.2. A noticeable reinforcing effect was observed upon filler addition, which could be anticipated from the increase in both modulus and strength of the composite compared to the unfilled ones. The increase in the concentration of ZNP might have direct effect in increasing the mechanical properties of the nanocomposites [81]. As the ZNP content increased, both the tensile and flexural properties of the nanocomposites also increased. The interaction of ZnO with crosslinked SF and jute through its surface hydroxyl group might stiffen the composites and results in enhancement of mechanical properties. Considering the 5 % concentration of the ZNP as optimum, we had further modified the composites viz. SF/J/GA50Zn5/N1, while SF/J/GA50/Zn5/N3 and SF/J/GA50/Zn5/N5 with different percentage of nanoclay ranging from 1-5 % ($^w/_w$ of dry SF). With the incorporation of nanoclay, composites showed a significant improvement in the mechanical properties with respect to the nanoclay untreated one. The reason for such improvement in mechanical properties of the composites might be due to the high aspect ratio of the nanoclay which generated a large surface area for the polymer chains absorption. Clay acts as a rigid reinforcement to the polymer matrix. The interaction of the polymer chains into the galleries of nanoclay restricts its mobility [18]. However, such improvement in mechanical properties with the incorporation of nanoclay might only be realized up to a certain clay loading. In present work, the enhancement in mechanical properties was found up to 3 % of clay loading, and beyond that it declined on further addition of nanoclay. At higher concentration of nanoclay, agglomeration of clay particles might have taken place and therefore the interaction between polymer-clay was reduced which led to the declining trend in the magnitude of enhancement of reinforcement efficiency with the addition of higher amount of nanoclay.

**Table 3.4.2.** Comparison of Tensile, Flexural, and LOI values of unfilled and filled crosslinked jute based SF nanocomposites before UV treatment.

| Composite | Tensile Properties (MPa) | | Flexural Properties (MPa) | | LOI (%) |
|---|---|---|---|---|---|
| System | Strength | Modulus | Strength | Modulus | |
| SF/J/GA50 | 10.11 | 982.4 | 15.23 | 1775.7 | 41 (±2) |
| | (±1.56) | (±11.86) | (±2.44) | (±13.37) | |
| SF/J/GA50/Z1 | 15.35 | 1182.6 | 28.35 | 2196.6 | 44 (±1) |
| | (±2.11) | (±12.14) | (±1.89) | (±12.25) | |
| SF/J/GA50/Z3 | 27.85 | 1808.7 | 39.62 | 2917.8 | 58 (±1) |
| | (±1.75) | (±16.96) | (±2.23) | (±11.45) | |
| SF/J/GA50/Z5 | 33.68 | 1926.3 | 48.68 | 3627.9 | 52 (±3) |
| | (±1.65) | (±14.54) | (±1.87) | (±14.57) | |
| SF/J/GA50/Z5/N1 | 39.34 | 2087.7 | 70.23 | 4298.4 | 57 (±2) |
| | (±1.71) | (±12.75) | (±2.23) | (±11.33) | |
| SF/J/GA50/Z5/N3 | 54.48 | 2436.9 | 86.27 | 6345.1 | 64 (±2) |
| | (±1.87) | (±11.52) | (±2.54) | (±12.51) | |
| SF/J/GA50/Z5/N5 | 48.62 | 2232.6 | 77.34 | 5861.1 | 62 (±1) |
| | (±2.25) | (±13.26) | (±3.12) | (±11.13) | |

Each value in the above table represents average of ten samples. Values in the parenthesis represent the standard deviation.

### 3.4.6. Thermal property study

Figure 3.4.6 and Table 3.4.3 displays the initial decomposition temperature ($T_i$), maximum pyrolysis temperature ($T_m$), decomposition temperature ($T_d$) at different weight loss (%) and residual weight (RW, %) thermograms of S/J/GA50, S/J/GA50/Z1, S/J/GA50/Z3, S/J/GA50/Z5, S/J/GA50/Z5/M1, S/J/GA50/Z5/M3, and S/J/GA50/Z5/M5. All the thermograms showed an initial weight loss around 100 °C due to the loss of confined water molecules. It was clearly inferred from the thermograms that all the values of the nanocomposites (Table 3.4.3) were found to increase with increase in the amount of ZNP. This might be attributed to the heat shielding effect of ZNP [84]. To enhance the thermal stability of composite materials,

nanoclay is widely used. After the incorporation of nanoclay, the thermal stability of the ZNP loaded nanocomposites were further improved. This increase in thermal stability of the synthesized nanocomposites is attributed to the hindered diffusion of volatile decomposition products within it. This might also be due to the physico-chemical absorption of the volatile degradation products on the silicate surface of nanoclay. The volatilization of the degraded products originated by carbon-carbon bond scission in the composite was delayed by tortuous path provided by the silicate layers. Clay treated composites showed a subsidiary enhancement in RW values over clay untreated one [53]. With the increase in concentration of clay, the agglomeration of clay probably took place which contributed to the reduction in the thermal stability. Therefore, it may be concluded that the thermal stability of SF/J composites increased on addition of upto a certain concentration of ZNP and nanoclay.
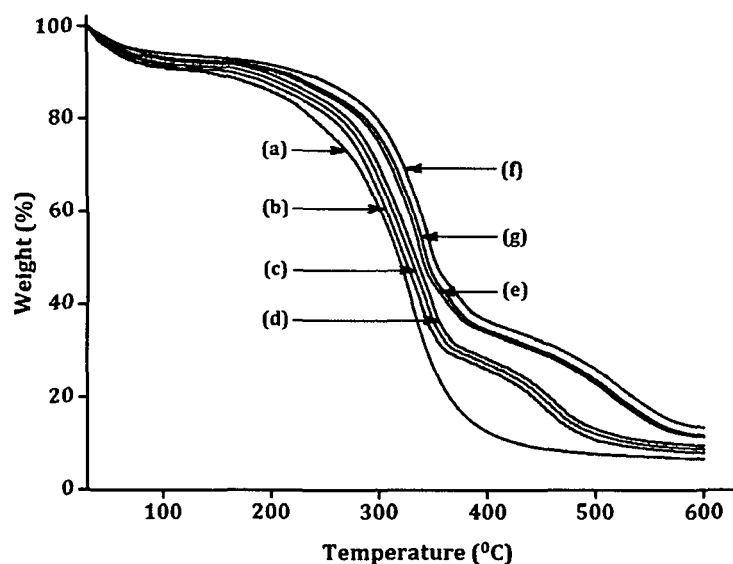


**Figure 3.4.6.** TGA thermograms of (a) SF/J/GA50, (b) SF/J/GA50/Z1, (c) SF/J/GA50/Z3, (d) SF/J/GA50/Z5, (e) SF/J/GA50/Z5/N1, (f) SF/J/GA50/Z5/N3 and (g) SF/J/GA50/Z5/N5.

**Table 3.4.3.** Thermal Properties of (a) SF/J/GA50, (b) SF/J/GA50/Z1, (c) SF/J/GA50/Z3, (d) SF/J/GA50/Z5, (e) SF/J/GA50/Z5/N1, (f) SF/J/GA50/Z5/N3 and (g) SF/J/GA50/Z5/N5.

| Sample Particulars | $T_i$ | $^aT_m$ | $^bT_m$ | Temperature of Decomposition at different weight loss (%) | | | | | RW % at 600 °C |
|---|---|---|---|---|---|---|---|---|---|
| | | | | 20 | 30 | 40 | 50 | 60 | |
| SF/J/GA50 | 187±1 | 223±2 | 307±1 | 242±2 | 290±2 | 304±2 | 318±3 | 331±2 | 7±1 |
| SF/J/GA50/Z1 | 193±1 | 230±2 | 316±1 | 260±3 | 296±1 | 310±2 | 325±2 | 342±1 | 8±2 |
| SF/J/GA50/Z3 | 197±2 | 237±1 | 325±2 | 269±2 | 301±1 | 315±1 | 331±2 | 347±3 | 9±1 |
| SF/J/GA50/Z5 | 204±2 | 245±1 | 331±3 | 277±2 | 309±2 | 319±2 | 336±1 | 351±1 | 10±2 |
| SF/J/GA50/Z5/N1 | 214±3 | 254±2 | 338±2 | 290±1 | 316±1 | 330±1 | 342±1 | 365±2 | 12±2 |
| SF/J/GA50/Z5/N3 | 222±2 | 266±3 | 353±2 | 307±2 | 330±3 | 342±2 | 353±2 | 383±2 | 15±2 |
| SF/J/GA50/Z5/N5 | 217±1 | 259±1 | 344±2 | 295±1 | 322±2 | 337±3 | 347±1 | 371±1 | 13±3 |

$T_i$ : initial decomposition temperature.

$^aT_m$ : maximum pyrolysis temperature value for 1st step.

$^bT_m$ : maximum pyrolysis temperature value for 2nd step.

Each value in the table represents average value of three samples.

## 3.4.7. UV test results

The weight loss of SF/J/GA50, SF/J/GA50/Z1, SF/J/GA50/Z3, SF/J/GA50/Z5, SF/J/GA50/Z5/N1, SF/J/GA50/Z5/N3, and SF/J/GA50/Z5/N5 are presented in Figure 3.4.7. Weight losses of the samples were determined at room temperature as a function of exposure time and found linear variation with this. Initially a small increase of weight was found due to moisture uptake by the samples, which was greater than the material loss induced by the degradation in the early stage. The rate of weight loss was lowest for SF/J/GA50/Z5/N3 followed by SF/J/GA50/Z5/N5, SF/J/GA50/Z5/N1, SF/J/GA50/Z5, SF/J/GA50/Z3, SF/J/GA50/Z1 and SF/J/GA50. The ZNP and nanoclay unfilled composite had shown maximum weight losses. After 60 days of exposure, the weight losses in S/J/GA50, S/J/GA50/Z1, S/J/GA50/Z3, S/J/GA50/Z5, S/J/GA50/Z5/M1, S/J/GA50/Z5/M3 and S/J/GA50/Z5/M5 were 4.61 ± 0.2 %, 3.91 ± 0.1%, 3.32 ± 0.2 %, 2.74± 0.3 %, 1.85 ± 0.3 %, 1.15 ± 0.3 % and 1.45 ± 0.2 % respectively. Results presented were the average of four specimens. The lower weight loss (%) for SF/J/GA50/Z5/N3 composites after UV exposure was due to the UV shielding ability of ZNP and nanoclay. On exposure to UV radiation, the chain scission followed by decrease in the density of the entanglements of the SF polymer chains occurred. This resulted in the decrease in the weight of the synthesized composites.
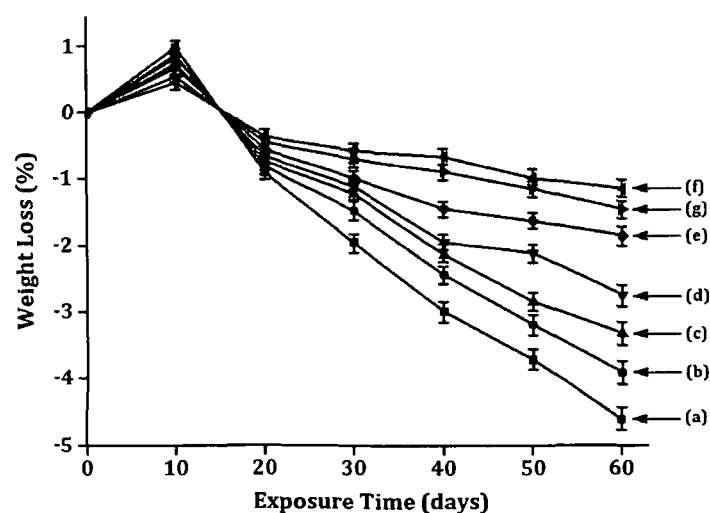


**Figure 3.4.7.** Weight loss vs Exposure time for (a) SF/J/GA50, (b) SF/J/GA50/Z1, (c) SF/J/GA50/Z3, (d) SF/J/GA50/Z5, (e) SF/J/GA50/Z5/N1, (f) SF/J/GA50/Z5/N3 and (g) SF/J/GA50/Z5/N5.

Figure 3.4.8 represents the FT-IR spectra of (a) SF/J/GA50, (b) SF/J/GA50/Z1, (c) SF/J/GA50/Z3, (d) SF/J/GA50/Z5, (e) SF/J/GA50/Z5/N1, (f) SF/J/GA50/Z5/N3 and (g) SF/J/GA50/Z5/N5 after UV exposure. The intensity of the carbonyl peaks was found to increase after irradiation of the samples for 60 days. Upon exposing the samples to UV-radiation, chain scission of the polymers take place and the carbonyl index value increases as shown in Figure 3.4.9. The SF/J/GA50/Z5/N3 had lowest carbonyl index value whereas SF/J/GA50 had the highest one. ZNP played an important
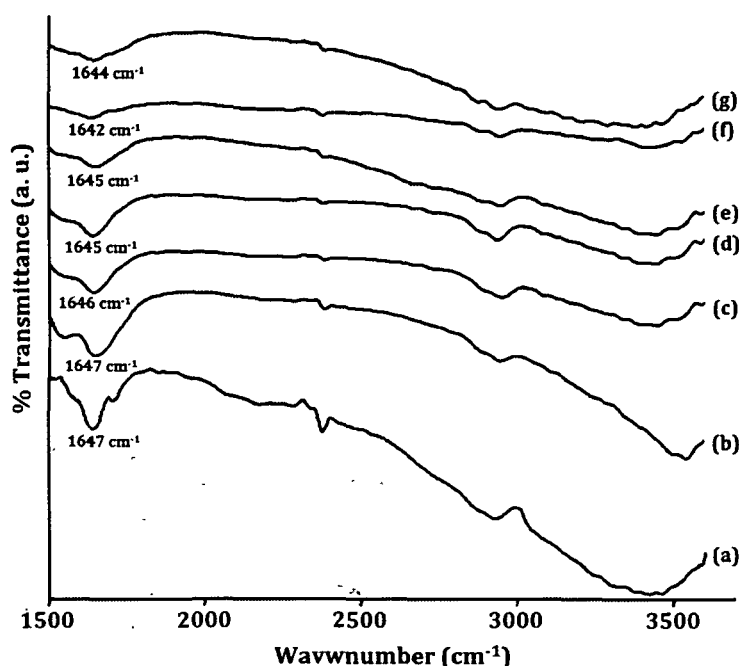


**Figure 3.4.8.** Change in carbonyl peak intensity of (a) SF/J/GA50, (b) SF/J/GA50/Z1, (c) SF/J/GA50/Z3, (d) SF/J/GA50/Z5, (e) SF/J/GA50/Z5/N1, (f) SF/J/GA50/Z5/N3 and (g) SF/J/GA50/Z5/N5.

role for stabilizing the SF/J composites by acting as a screen and slowed down the photo degradation process. ZNP absorbed the UV radiation and hence reduced the UV intensity required for the oxidation of the synthesized nanocomposites [85]. The presence of nanoclay in the composite also had a screening effect which further delayed the photo degradation process. Grigoriadou *et al.* [73] observed an increase in UV stability of HDPE after incorporating montmorillonite clay. SF/J/GA50/Z5/N5 exhibited lower protection against UV with respect to SF/J/GA50/Z5/N3. This might be due to the agglomeration of nanoclay particles within the composite material which is responsible for higher photodegradation.

It is well known that UV-radiation has a deterioration effect on many plastic materials. These materials, when exposed to the outdoor environment, undergo significant changes, namely, photo-degradation, causing loss of mechanical properties. Therefore, the changes in the mechanical properties of the composites after the UV treatment are presented in Table 3.4.4. Both the flexural and tensile properties reduced after UV treatment. The loss of mechanical properties of unfilled composites was more significant compared to nanoparticles filled composites. SF/J/GA50 was more prone to UV attack and hence it showed maximum loss of mechanical properties. The values presented in Table 3.4.4 suggest that the interfacial interactions among SF, jute, GA, ZNP and nanoclays were strong enough to decay the massive sheer due to rupture. Therefore, the resistance of SF/J composite to UV instability, *i.e.*, photodegradation embrittlement, could be improved significantly with the addition of nanoparticles.
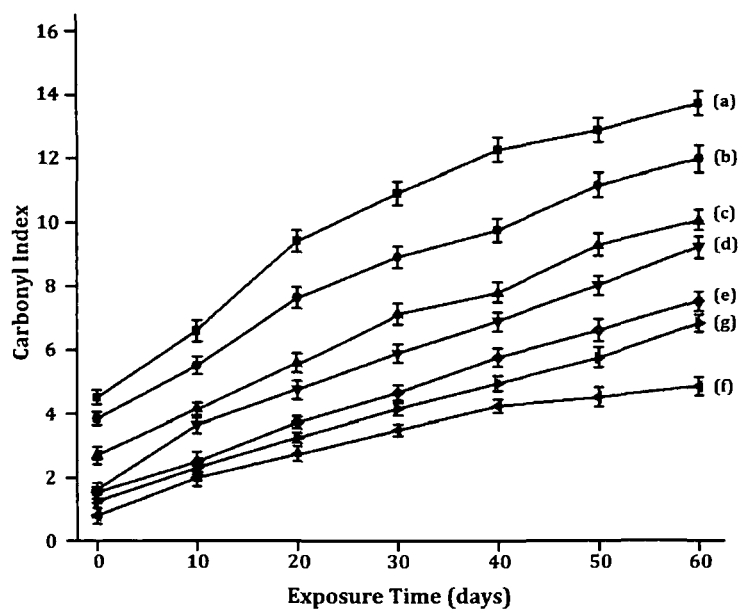


**Figure 3.4.9.** Carbonyl Index value of (a) SF/J/GA50, (b) SF/J/GA50/Z1, (c) SF/J/GA50/Z3, (d) SF/J/GA50/Z5, (e) SF/J/GA50/Z5/N1, (f) SF/J/GA50/Z5/N3 and (g) SF/J/GA50/Z5/N5.

**Table 3.4.4.** Changes in the mechanical properties of Unfilled and Filled jute based crosslinked SF nanocomposites after UV Exposure.*

| Composite System | Tensile Properties | | | Flexural Properties | | |
|---|---|---|---|---|---|---|
| | Strength (MPa) | Changes after UV study (%) | Modulus (MPa) | Strength (MPa) | Changes after UV study (%) | Modulus (MPa) |
| SF/J/GA50 | 4.85 | 52.1 | 721.3 | 9.44 | 18.3 | 1445.3 |
| | (±1.86) | | (±11.52) | (±1.33) | | (±11.58) |
| SF/J/GA50/Z1 | 10.21 | 33.2 | 982.5 | 24.15 | 18.1 | 1796.1 |
| | (±1.31) | | (±10.86) | (±2.16) | | (±12.23) |
| SF/J/GA50/Z3 | 23.12 | 17.3 | 1648.7 | 35.45 | 10.2 | 2625.2 |
| | (±1.63) | | (±12.24) | (±1.34) | | (±10.87) |
| SF/J/GA50/Z5 | 30.32 | 10.1 | 1785.4 | 44.28 | 9.3 | 3289.1 |
| | (±1.56) | | (±13.54) | (±2.23) | | (±11.46) |
| SF/J/GA50/Z5/N1 | 36.71 | 6.7 | 1846.8 | 65.44 | 8.9 | 3916.8 |
| | (±1.42) | | (±15.11) | (±1.89) | | (±15.27) |
| SF/J/GA50/Z5/N3 | 52.14 | 4.3 | 2164.6 | 83.15 | 3.1 | 6156.9 |
| | (±1.38) | | (±11.23) | (±2.62) | | (±11.57) |
| SF/J/GA50/Z5/N5 | 45.56 | 6.3 | 1985.1 | 74.56 | 4.7 | 5584.7 |
| | (±1.81) | | (±10.75) | (±1.35) | | (±13.47) |

*Each value in the above table represents average of ten samples. Values in the parenthesis represent the standard deviation.

### 3.4.8. Dimensional stability study

The water vapour absorption study of the composites are shown in Figure 3.4.10. From the Figure, it is seen that for all the composites, the percentage swelling is increased with increase in time. Water vapour absorption was found to decrease due to the presence of dispersed phase of ZNP in the composite system. Water vapour absorption of S/J/GA50/Z composites decreased with the increase in ZNP content [82]. ZNP act as a barrier to the passage of water as the strong affinity of water molecules towards ZNP restricts its free motion and reduces the diffusion co-efficient of water. The well dispersed phase of ZNP improves the resistance of the composite and retards the motion of water molecules through it. The better the distribution of nanoparticles, the higher is the barrier property. Further, the dimensional stability of the SF/J/GA50/Z5 composite was improved with the incorporation of nanoclay. This might be due to the fact that the silicate layers of nanoclay provide a tortuous path which

hinders the diffusivity of water molecules through the nanocomposite [27]. As the nanoclay concentration was increased to 5 %, the superfluous filler congregates easily, decreasing the effective content of filler and thus had little effect on decreasing of water vapour absorption.
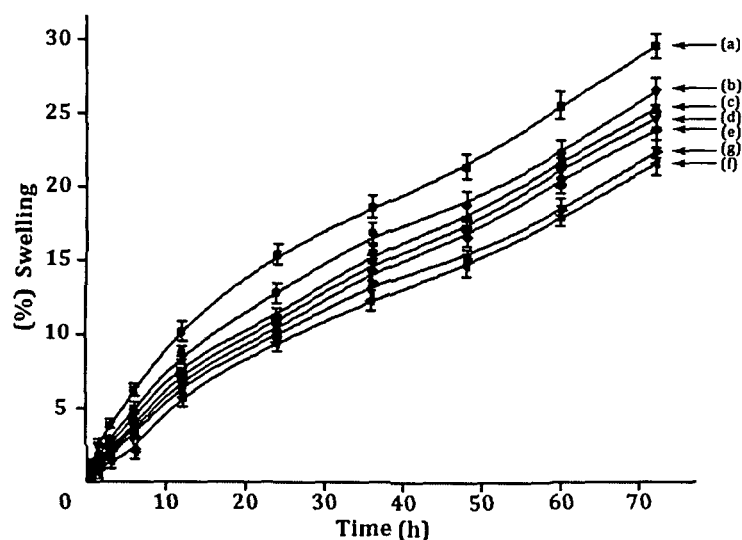


**Figure 3.4.10.** Swelling behaviour of (a) SF/J/GA50, (b) SF/J/GA50/Z1, (c) SF/J/GA50/Z3, (d) SF/J/GA50/Z5, (e) SF/J/GA50/Z5/N1, (f) SF/J/GA50/Z5/N3 and (g) SF/J/GA50/Z5/N5.

### 3.4.9. LOI study

LOI values of jute based SF composites with different percentage of ZNP and nanoclay are depicted in Table 3.4.2. From the table, it is observed that the LOI value increases with the increase in the concentration of ZNP in the composites. The surface hydroxyl group of ZNP may interact with SF, jute and GA and thus restricts the accessibility of oxygen for the production of degradable components from the composites and hence improvement in LOI value was observed [86]. However, on addition of nanoclay into ZNP incorporated composites, further enhancement in LOI value was observed. The incorporation of the nanoclay into the synthesized composite produces a silicate char on the surface of it and hence improves their flame resistance property. The silicate rich surface had better barrier property to heat and oxygen transport due to which ignition of the composite delays [24]. The LOI value was increased upto addition of 3 % of nanoclay, beyond that it decreased. At higher clay loading condition, the agglomeration of nanoclay results in decrease of interaction with concomitant reduction in barrier property as well as LOI value.

### 3.4.10. Biodegradation study

SF/J composites were exposed to cellulolytic bacterial strain directly in broth culture medium for the biodegradation study. After one month of incubation of the samples in broth culture media, the growth of bacteria and degradation of the composite samples was clearly detectable. The bacterial growth of the samples with respect to
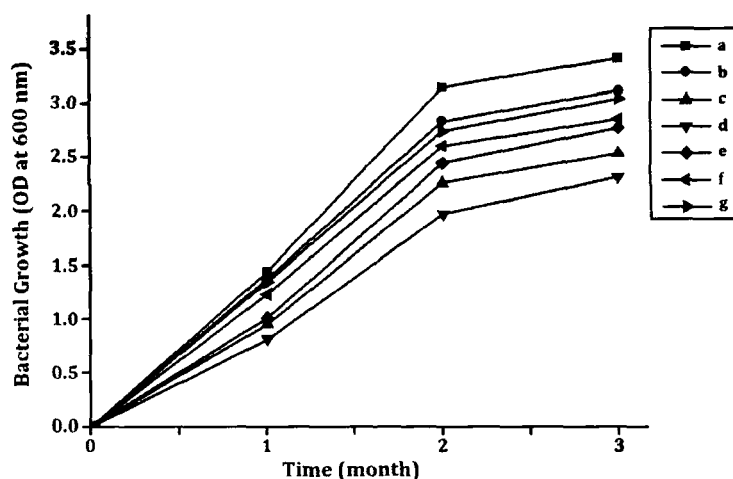


**Figure 3.4.11.** Bacterial growth of (a) SF/J/GA50, (b) SF/J/GA50/Z5/N5, (c) SF/J/GA50/Z5/N3, (d) SF/J/GA50 /Z5/N1, (e) SF/J/GA50/Z1, (f) SF/J/GA50/Z3 and (g) SF/J/GA50/Z5.

time is represented in Figure 3.4.11. The microbial attack was more in case of ZNP free composite compared to the composite filled with ZNP and nanoclay. Initially, the growth of the bacterial strains increased quite steadily with bacterial exposure time, but the rate of growth slightly decreased after 3 month of incubation. As the composites are mainly comprised of SF and jute which are basically carbohydrate and cellulose, these two are very good carbon source for the bacteria due to which higher rate of bacterial growth is observed. The powerful cellulolytic and pectinolytic activity of bacteria could be a reason for the enhancement of bacterial growth [87]. After 3 months, the rate of microbial growth was slightly diminished due to the production of toxic metabolites by the microbes. In our study, the growth of bacteria and degradation of the samples were revealed by SEM study (Figure 3.4.12). SEM was used to observe the extent of physical breakdown of SF/J polymer composites. SEM shows different levels of degradation, colonized nanoclay SF/J composite sometimes only shows superficial degradation whereas, ZNP incorporated SF/J composites show less degradation as ZnO

sometimes acts as a fungicide and protective agent [88]. The degradation was more in the unfilled SF/J composites as SF and jute were gradually breakdown in the broth culture media. The lower biodegradability of filled SF/J nanocomposites was sacrificed considering the enhanced thermal and mechanical properties. However, in case of nanoclay incorporated composites, the rate of degradation increases with increasing the concentration of nanoclay in SF/J composites. In bacterial media the degradation of SF/J polymer composites is a complex process involving four main phenomena: (i) water adsorption, (ii) bond cleavage and formation of oligomer fragments, (iii) solubilisation of oligomer fragments, and finally (iv) diffusion of soluble oligomers by bacteria [89, 90]. Therefore, the factor that increases the hydrolysis tendency of S/J composites eventually controls the degradation of the composites. In case of nanoclay incorporated composites, the presence of unreacted terminal hydroxyl group may be the responsible factor for this behaviour [91].
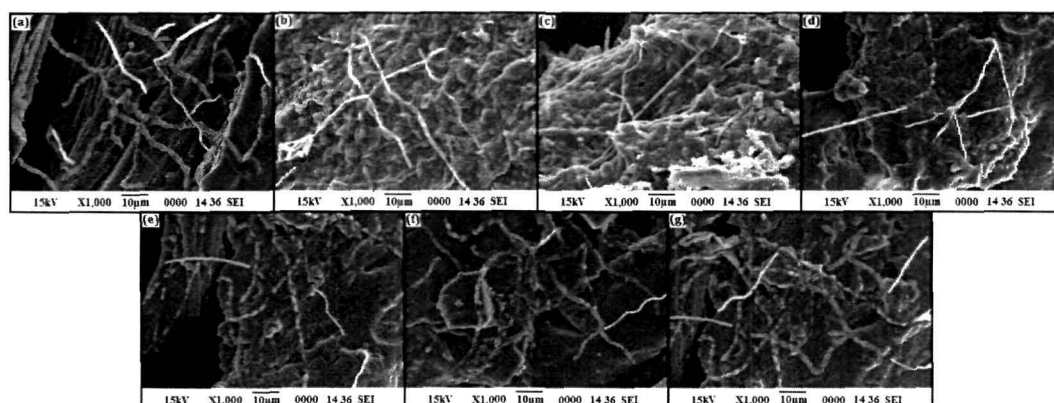


**Figure 3.4.12.** SEM micrographs of samples after microbial test on (a) SF/J/GA50, (b) SF/J/GA50/Z1, (c) SF/J/GA50/Z3, (d) SF/J/GA50/Z5, (e) SF/J/GA50/Z5/N1, (f) SF/J/GA50/Z5/N3 and (g) SF/J/GA50/Z5/N5.

### References

[1] Chabba, S., et al. *Green. Chem.* **7**(8), 576--581, 2005.

[2] Mohanty, A. K., et al. *Macromol. Mater. Eng.* **276/277**(1), 1--24, 2000.

[3] Romhany, G., et al. *Macromol. Mater. Eng.* **288**(9), 699--707, 2003.

[4] Plackett, D., et al. *Compos. Sci. Technol.* **63**(8), 1287--96, 2003.

[5] Kaith, B.S., *J. Macromol. Sci. Part A: Pure Appl. Chem.* **48**(4), 299--308, 2011.

[6] Das, K., et al. *Ind. Eng. Chem. Res.* **49**(6), 2775--2782, 2010.

[7] Huang, X., & Netravali, A. N. *Biomacromolecules* **7**(10), 2783--2789, 2006.

[8] Chen, P.; Zhang, L. *Biomacromolecules* **7**(6), 1700--1706, 2006.

[9] Yoonessi, M., et al. *Macromolecules* **37**(7), 2511--2518, 2004.

[10] Wang, Y., et al. *J. App. Polym. Sci.* **104**(1), 130--136, 2007.

[11] Hillberg, A. L., et al. *Biomaterials* **30**(27), 4463--4470, 2009.

[12] Ray, D., et al. *Macromol. Mater. Eng.* **292**(10/11), 1075--1084, 2007.

[13] Schmidt, V., et al. *Polym. Degrad. Stab.* **87**(1), 25--31, 2005.

[14] Ray, D. & Sarkar, B. K. *J. App. Polym. Sci.* **80**(7), 1013--1020, 2001.

[15] Migneault, I., et al. *BioTechniques.* **37**(5), 790--802, 2004.

[16] Darder, M., et al. *Chem. Mater.* **15**(20), 3774--3780, 2003.

[17] Nam, S. & Netravali, A. N. *J. Adhes. Sci. Technol.* **18**(9), 1063--1076, 2004.

[18] Deka, B.K. & Maji, T.K. *Compos. Sci. Technol.* **70**(12), 1755--1761, 2010.

[19] Saha, A. K., et al. *J. App. Polym. Sci.* **78**(3), 495--506, 2000.

[20] Swain, S. N., et al. *Polym. Int.* **54**(5), 739--743, 2005.

[21] Gilman, J. W., et al. *Chem. Mater.* **12**(7), 1866--1873, 2000.

[22] Zanetti, M., et al. *Macromol. Rapid. Commun.* **22**(3), 176--180, 2001.

[23] Qin, H., et al. *Polym. Degrad. Stab.* **85**(2), 807--813, 2004.

[24] Urbanczyk, L., et al. *J. Mater. Chem.* **20**(8), 1567--1575, 2010.

[25] Sun, J., et al. *J. Mol. Model.* **16**(12), 1809--1818, 2010.

[26] Chabba, S., & Netravali, A. N. *J. Mater. Sci.* **40**(23), 6263--6273, 2005.

[27] Rana, H. T., et al. *AIChE J.* **51**(12), 3249--3256, 2005.

[28] Coates, G. W. & Hillmyer, M. A. *Macromolecules* **42**(21), 7987--7989, 2009.

[29] DeWit, M. A. & Gillies, E. R. *J. Am. Chem. Soc.* **131**(51), 18327--18334, 2009.

[30] Tian, H., et al. *Prog. Polym. Sci.* **37**(2), 237--280, 2012.

[31] Metters, A.T., et al. *Polymer* **41**(11), 3993--4004, 2000.

[32] Nam, J.Y., et al. *Macromolecules,* **36**(19), 7126--7131, 2003.

[33] Tang, X. & Alavi, S. *J. Agric. Food Chem.* **60**(8), 1954--1962, 2012.

[34] Lim, S. T., et al. *Chem. Mater.* **14**(4), 1839--1844, 2002.

[35] Wang, L., et al. *Carbohydr. Polym.* **69**(2), 391--397, 2007.

[36] Pandey, K. K. *Polym. Degrad. Stab.* **90**(1), 9--20, 2005.

[37] Colom, X., et al. *Polym. Degrad. Stab.* **80**(3), 543--549, 2003.

[38] Colom, X. & Carrillo, F. *Eur. Polym. J.* **38**(11), 2225--2230, 2002.

[39] Hinterstoisser, B., et al. *Carbohydr. Res.* **334**(1), 27--37, 2001.

[40] Oh, S. Y., et al. *Carbohydr. Res.* **340**(15), 2376--2391, 2005.

[41] Kataoka, Y. & Kondo, T. *Int. J. Biol. Macromol.* **24**(1), 37--41, 1999.

[42] Gaussian 03, Revision B.05, Frisch, M. J., et al. Gaussian, Inc., Pittsburgh PA, 2003.

[43] Moog, R. S. & Farrell, J. J. *Chemistry: A Guided Inquiry*, Wiley, New York, 2008.

[44] Pavia, D. L., Lampman, G. M., Kriz, G. S. & Vyvyan, J. R. *Spectroscopy*; Cengage Learning India Private Limited, New Delhi, India, 2009.

[45] Sèbe, G., et al. *Biomacromolecules* **13**(2), 570--578, 2012.

[46] Klemm, D., et al. *Angew. Chem. Int. Ed.* **44**(22), 3358--3393, 2005.

[47] Gournis, D., et al. *J. Am. Chem. Soc.* **128**(18), 6154--6163, 2006.

[48] Hashaikeh, R. & Abushammala, H. *Carbohydr. Polym.* **83**(3), 1088--1094, 2011.

[49] Bendahou, A., et al. *Macromol. Mater. Eng.* **296**(8), 760--769, 2011.

[50] Lu, P. & Hsieh, Y. L. *Carbohydr. Polym.* **82**(2), 329--336, 2010.

[51] Cai, X., et al. *Composites Part A* **39**(5), 727--737, 2008.

[52] Kashiwagi, T., et al. *Nat. Mater.* **4**(12), 928--933, 2005.

[53] Pranger, L. & Tannenbaum, R. *Macromolecules* **41**(22), 8682--8687, 2008.

[54] LeBaron, P. C., et al. *Appl. Clay Sci.* **15**(1-2), 11--29, 1999.

[55] Ramaraj, B. *J. Appl. Polym. Sci.* **103**(2), 909--916, 2007.

[56] Huang, X. & Netravali, A. *Compos. Sci. Technol.* **69**(7-8), 1009--1015, 2009.

[57] Favier, V., et al. *Macromolecules* **28**(18), 6365--6367, 1995.

[58] Ojijo, V., et al. *ACS Appl. Mater. Interfaces* **4**(5), 2395--2405, 2012.

[59] Savadekar, N. R. & Mhaske, S. T. *Carbohydr. Polym.* **89**(1), 146--151, 2012.

[60] Ma, X., et al. *Carbohydr. Polym.* **62**(1), 19--24, 2005.

[61] De Rosa, I.M., et al. *Compos. Sci. Technol.* **70**(1), 116--122, 2010.

[62] Sui, G., et al. *Bioresour. Technol.* **100**(3), 1246--1251, 2009.

[63] Chieruzzi, M., et al. *Composites Part A* **45**, 44--48, 2013.

[64] Deka, B.K. & Maji, T.K. *Composites Part A* **42**(12), 2117--2125, 2011.

[65] Zhang, S.L., et al. *Chinese Sci. Bull.* **45**(16), 1533--1536, 2000.

[66] Xu, L. & Yang, M. *J. Appl. Polym. Sci.* **114**(5), 2755--2763, 2009.

[67] Thamaphat, K. *Kasetsart J. (Nat Sci)* **42**(5), 357--361, 2008.

[68] Mina, F., et al. *Polym. Degrad. Stab.* **94**(2), 183--188, 2009.

[69] Faruk, O. & Matuana, L.M. *Compos. Sci. Technol.* **68**(9), 2073--2077, 2008.

[70] Ansari, M.O. & Mohammad, F. *J. Appl. Polym. Sci.* **124**(6), 4433--4442, 2012.

[71] Laachachi, A., et al. *Polym. Degrad. Stab.* **89**(2), 344--352, 2005.

[72] Du, H., et al. *J. Appl. Polym. Sci.* **118**(2), 1068--1076, 2010.

[73] Grigoriadou, I., et al. *Polym. Degrad. Stab.* **96**(1), 151--163, 2011.

[74] Zhu, Y., et al. *Polym. Compos.* **32**(4), 519--528, 2011.

[75] Camino, G., et al. *Polym. Degrad. Stab.* **90**(2), 354--362, 2005.

[76] Espert, A., et al. *Composites Part A* **35**(11), 1267--1276, 2004.

[77] Bledzki, A.K. & Gassan, J. *Prog. Polym. Sci.* **24**(2), 221--274, 1999.

[78] Yu, Y., et al. *Holzforschung*, **64**(3), 385--390, 2010.

[79] Weichelt, F., et al. *Macromol. Mater. Eng.* **295**(2), 130--136, 2010.

[80] Lu, N., et al. *Polym. Int.* **56**(1), 138--143, 2007.

[81] Deka, B.K. & Maji, T.K. *J. Appl. Polym. Sci.* **124**(4), 2919--2929, 2012.

[82] Ma, X., et al. *Carbohydr. Polym.* **75**(3), 472--478, 2009.

[83] Espitia, P.J.P., et al. *Carbohydr. Polym.* **94**(1), 199--208, 2013.

[84] Devi, R.R. & Maji, T.K. *Ind. Eng. Chem. Res.* **51**(10), 3870--3880, 2012.

[85] Zhao, H. & Li, R.K.Y. *Polymer* **47**(9), 3207--3217, 2006.

[86] Wu, N., et al. *Polym. Degrad. Stab.* **95**(2), 2589--2595, 2010.

[87] Clausen, C.A. *Int. Biodeterior. Biodegrad.* **37**(1-2), 101--107, 1996.

[88] Lykidis, C., et al. *Wood Mater. Sci. Eng.* **8**(4), 242--244, 2013.

[89] Lunt, J. *Polym. Degrad. Stab.* **59**(1-3), 145--152, 1998.

[90] Drumright, R.E., et al. *Adv. Mater.* **12**(23), 1841--1846, 2000.

[91] Ray, S.S., et al. *Nano Lett.* **2**(10), 1093--1096, 2002.

# Chapter 4

## *Results & Discussion: Jute based Starch nanocomposites*

***Section A*: Study on the effect of crosslinker and nanoclay on jute fabric reinforced starch bio-nanocomposites**

The growing awareness of the pressing need for greener, more sustainable technologies has focussed attention on use of eco-friendly and cost effective material with high performance [1]. Another aspect, which is receiving more attention, is the use of alternate source prior to the use of the conventional materials [2]. Biopolymers, which exist abundantly worldwide, are one of such promising material. They offer many fundamental and practical advantages of relevance to the chemist as well as to the chemical industries, which are constantly searching for high performing, cost effective and environmentally friendly materials [3, 4]. Besides these, natural fibres with their characteristics properties such as low cost, easy availability, low density, high specific strength, renewability and less abrasive with respect to processing tools, can be added to such class of materials [5, 6].

In this part of study, we have prepared composites by using starch, jute and glutaraldehyde (GA). The composites have been prepared by varying the amount of GA from 30-70% and keeping other components (starch, jute and glycerol) constant. The effect of the crosslinker *i.e.* GA on the physiochemical properties such as mechanical, thermal and dimensional stability have been studied by various techniques. The composites have further been modified by addition of different amount of nanoclay and their effects on various properties of the composites stated above have been studied.

## 4.1. RESULTS & DISCUSSION

The samples, as coded in Table 4.1.1, had been prepared by keeping the weight (%) of the components viz. starch, glycerol and jute constant in all the samples where as the percentages (%) of GA and nanoclay were varied. The weight (%) of the various components used for the synthesis of the composite are provided in Table 4.1.1.

**Table 4.1.1.** Different composition of prepared composite.

| Sample | Starch[a] | Glycerol | GA[b] (Wt. %) | Jute | Nanoclay |
|---|---|---|---|---|---|
| S/J | 100 | 5 | - | 75 | - |
| S/J/G30 | 100 | 5 | 30 (6) | 75 | - |
| S/J/G40 | 100 | 5 | 40 (8) | 75 | - |
| S/J/G50 | 100 | 5 | 50 (10) | 75 | - |
| S/J/G60 | 100 | 5 | 60 (12) | 75 | - |
| S/J/G70 | 100 | 5 | 70 (14) | 75 | - |
| S/J/G50/M1 | 100 | 5 | 50 | 75 | 1 |
| S/J/G50/M3 | 100 | 5 | 50 | 75 | 3 |
| S/J/G50/M5 | 100 | 5 | 50 | 75 | 5 |

[a] 20 g of starch is assumed to be 100.

[b] The percentage of GA with respect to Starch. The values in the parenthesis indicate the amount of GA in gram.

### *4.1.1. FT-IR study*

The interactions between starch, jute, glycerol, clay and glutaraldehyde were studied by FT-IR spectroscopy. FT-IR spectra of starch, jute, clay, S/J, S/J/GA and S/J/GA/M are presented in Figure 4.1.1. The FT-IR spectrum of starch (curve-a) shows the presence of absorption bands at 571, 980, 1160, 1650, 2920 and 3400 cm$^{-1}$ confirming the carbohydrate nature [7]. The typical saccharide bands appeared in the range 1180-950 cm$^{-1}$ was considered as the vibration modes of C–C and C–O stretching and the bending of C–H bonds [8]. Jute (curve-b) shows the presence of peaks in the range 3440-3390 cm$^{-1}$ for –OH stretching, 1738 cm$^{-1}$ for the C=O stretching vibration of ester groups of hemicelluloses, 1640 cm$^{-1}$ for C=O stretching, 1254 cm$^{-1}$ for –C–O–C– bond in cellulose chain and 1057-1116 cm$^{-1}$ for C–O stretching [5]. Clay exhibits (curve-c) peaks at 3465 cm$^{-1}$ (–OH stretching), 1619 cm$^{-1}$ (–OH bending), 1030-460 cm$^{-1}$ (oxide bonds of metals like Si, Al, Mg etc).
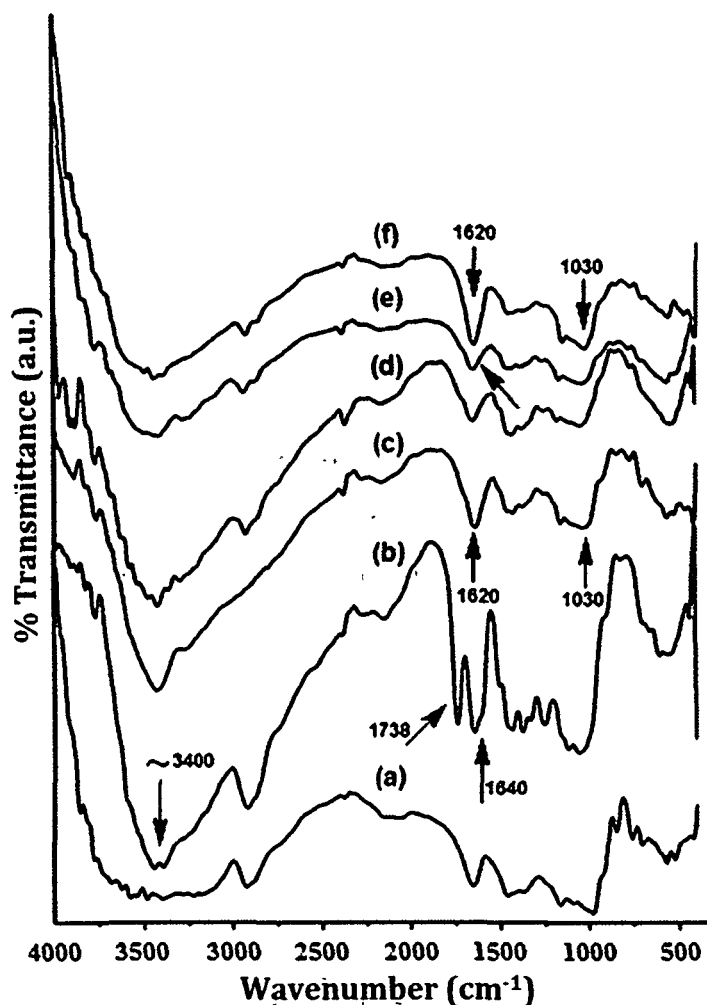
**Figure 4.1.1.** FT-IR spectra of (a) Starch, (b) Jute, (c) clay, (d) S/J, (e) S/J/G50 and (f) S/J/G50/M5.

Characteristics peaks of starch and jute were appeared in the spectrum of S/J composite (curve-d). Curve-e represents the spectrum of glutaraldehyde crosslinked S/J composite. The intensities of –OH and C=O stretching were found to decrease in the crosslinked composites suggesting the formation of covalent bond between jute and starch. The possible interaction between starch, jute and glutaraldehyde are given in Figure 4.1.2. In the spectrum of clay filled (curve-f) S/J composites, the intensity of peak corresponding to –OH had further decreased. The intensities of peaks at 1620 cm$^{-1}$ and 1030 cm$^{-1}$ assigned for Si–O–Si stretching were more pronounced compared to glutaraldehyde crosslinked S/J composites. All this suggested the participation of hydroxyl group of clay in crosslinking reaction with starch and jute [9].

136
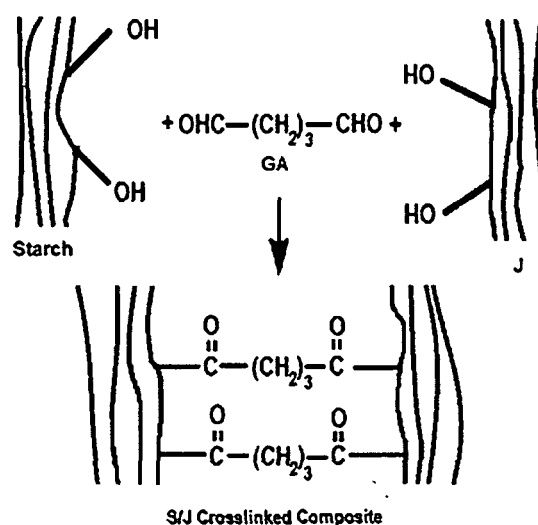
**Figure 4.1.2.** Schematic diagram of glutaraldehyde crosslinked starch/jute composite.

### *4.1.2. XRD study*

The interlayer spacing (d-spacing) of the starch/nanoclay nanocomposites prepared via solution induced intercalation method was detected by X-ray diffraction study. Figure 4.1.3 shows the XRD patterns of Jute, starch, S/J, S/J/G50, clay and the nanocomposites. Clay shows sharp peaks around 2θ = 24 and 9°. The peak around 9° corresponds to a d-spacing of about 1.2 nm in pure clay [10]. Jute shows peaks at 2θ = 22° (002 plane of cellulose I) and 19° (101 plane of cellulose II) [11]. Curve – b represents the diffractograms of starch. A little broader peak around 2θ = 20° was found to appear. Curve – c and d representing the composites without and with crosslinker exhibited no diffraction peak between 1- 10° in the 2θ range, reflecting the absence of any ordered structure of starch and jute in this range. The diffraction peak of the nanoclay tactoids was absent in the X-ray diffractograms for 1% and 3% clay loaded composites (curves-f & g). It could be said that either the full expansion of the MMT gallery occurred, which was not possible to detect by XRD, or the MMT layers became delaminated and no crystal diffraction peak appeared [12]. As shown in the Figure 4.1.3 (curve -h), the peak obtained for pure clay at around 9° was shifted towards left with reduction in intensity in the S/J/G50/M5 composites. This indicated that the layer in clay was delaminated in the aqueous medium by the starch macromolecules [12].

137
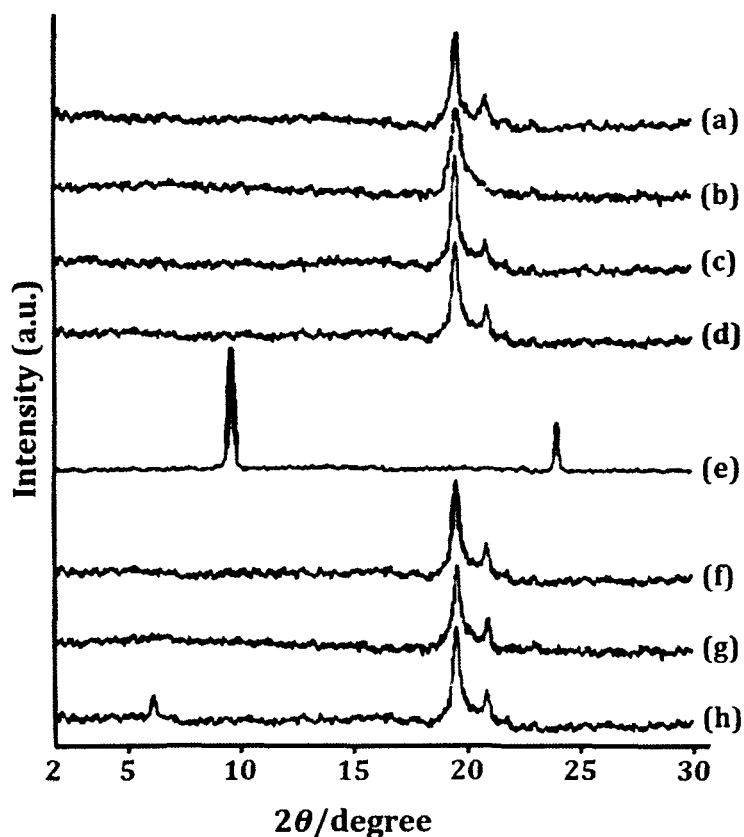
**Figure 4.1.3.** XRD patterns of (a) Jute, (b) Starch, (c) S/J, (d) S/J/G50, (e) Clay (f) S/J/G50/M1, (g) S/J/G50/M3 and (h) S/J/G50/M5.

### 4.1.3. TEM study

TEM analysis was carried out to verify the extent of exfoliation of nanoclay in the synthesized composites. The dispersion of clay layers as dark lines (shown by arrow mark) was observed in both the images. The TEM micrographs of nanoclay incorporated composites are shown in Figure 4.1.4. Figure 4.1.4 {(a) and (b)} represent the TEM micrographs in 100 and 20 nm range. As indicated by TEM micrographs, the clay layers were delaminated into thin lamellas by starch having a dimension of 2~3 nm in thickness. This suggested that the nanoclay were well dispersed and partially exfoliated into starch matrix. This type of partially exfoliated structure of nanoclay was also reported in various literatures and had been considered as a successful intercalation of the nanoclay into the composites [13, 14]. Therefore, from XRD and TEM studies, it could be concluded that S/J/Clay nanocomposites with a delaminated structure could be prepared by solution induced intercalation method in neutral aqueous medium.
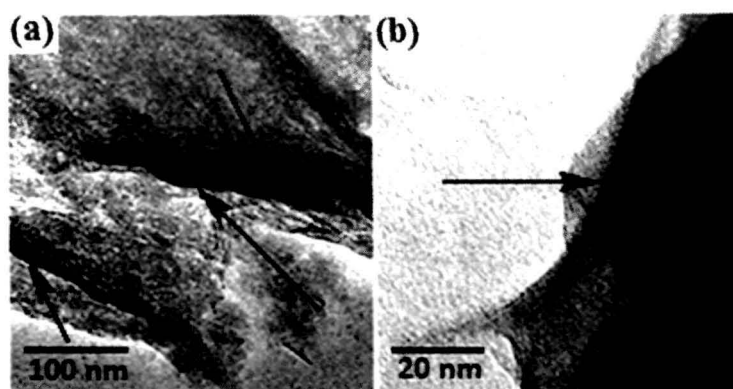
**Figure 4.1.4.** TEM micrographs of S/Clay composite with 5% clay (a) 100 nm and (b) 20 nm scale.

### *4.1.4. SEM study*

SEM micrographs of Jute, starch and the smooth surface and fractured surface of S/J composite without and with clay are presented in Figure 4.1.5. The surface of jute fibres was smooth and regular {Figure 4.1.5 (a)}. The shape of starch particles were irregular compact disc type as shown in the {Figure 4.1.5 (b)} [7]. On addition of GA, S/J composite appeared rough {Figure 4.1.5 (c)} [15]. The roughness was increased with the addition of clay {Figure 4.1.5 (e)}. The
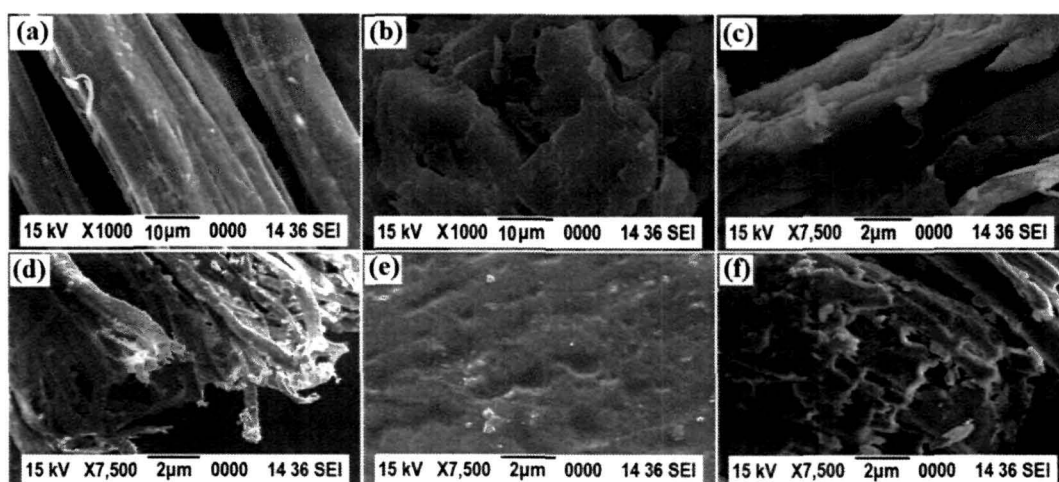


**Figure 4.1.5.** SEM micrographs of (a) jute, (b) starch, (c) S/J/G50 smooth surface, (d) S/J/G50 fracture surface, (e) S/J/G50/M5 smooth surface (f) S/J/G50/M5 fracture surface.

roughness might be due to the adherence of either the starch or the starch/clay to the jute surface. However, on addition of GA into the composite less fibres were found to be the protruded out of the composite {Figure 4.1.5 (d)}. This suggested a failure in the

brittleness of the starch matrix. The resins were found to adhere on some of the fibre surface. Surface of some fibres were smooth as there was no resin. Moreover, on addition of nanoclay into the composite, the brittleness was found to enhance {Figure 4.1.5 (f)}. This might be due to the fact that the clay particles increased the interaction with starch matrix and jute fibre surface which resulted in less pull out of fibres from the fractured surface [16].

Further work was done through energy dispersive X-ray analysis of the nanoparticles observed in the fracture for the clay loaded composite as shown in Figure 4.1.6. Elements such as Al, Na and Si, which are mainly from the silicate nanoclay, were detected indicating that the nanoclay had been successfully incorporated into the composite [17].
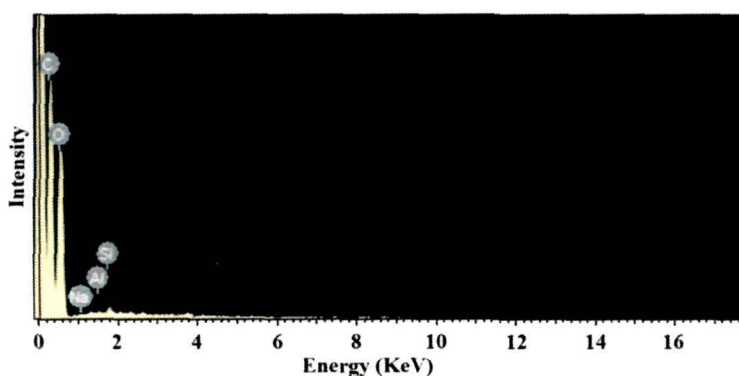


**Figure 4.1.6.** Energy dispersive X-ray analysis of S/J/G50/M.

### *4.1.5. Mechanical property study*

The flexural and tensile properties of composites with varying percentage of glutaraldehyde and clay are shown in Table 4.1.2. The values shown in the table are the mean values of five readings. It was observed that both the flexural and tensile modulus and strength increased with the increase in the concentration of glutaraldehyde. The increase in mechanical properties could be ascribed to the formation of crosslinking between the polar groups of starch and jute by glutaraldehyde as shown in Figure 4.1.2. The mechanical properties of composite were found to increase with the increase in the concentration of GA [18]. It was observed from Table 4.1.2 that except the flexural strength there was no significant enhancement on the properties such as flexural modulus, tensile strength and tensile modulus beyond 50% of GA. This might be due to saturation of crosslinking sites in both starch and jute surface. Since, all these properties together culminate to the overall mechanical strength of the composite.

Hence, considering the 50% concentration of the crosslinker as optimum, we modified the composite (S/J/G50/M1, S/J/G50/M3 and S/J/G50/M5) with different percentage of nanoclay ranging from 1-5% (w/w) of starch. The mechanical properties of the clay treated samples were found better compared to the clay untreated samples. The higher the percentage of clay, the higher was the mechanical properties. The increase in mechanical properties was due to the restriction in the mobility of the intercalated polymer chains present inside the silicate layers of clay [19].

**Table 4.1.2.** Flexural and tensile properties of (a) S/J, (b) S/J/G30, (c) S/J/G40, (d) S/J/G50, (e) S/J/G60, (f) S/J/G70, (g) S/J/G50/M1, (h) S/J/G50/M3 and (i) S/J/G50/M5.

| Composite System | Flexural Properties | | Tensile Properties | |
|---|---|---|---|---|
| | Strength (MPa) | Modulus (MPa) | Strength (MPa) | Modulus (MPa) |
| S/J | 27.67 (±1.22) | 1141.9 (±1.57) | 12.59 (±1.26) | 755.38 (±16.74) |
| S/J/G30 | 28.31 (±1.34) | 1336.2 (±1.16) | 18.62 (±1.84) | 1117.10 (±13.46) |
| S/J/G40 | **37.8** (±2.31) | 1641.6 (±2.11) | 19.88 (±0.96) | 1192.53 (±17.32) |
| S/J/G50 | **39.5** (±2.14) | 2234.0 (±1.96) | 22.54 (±1.03) | 1352.18 (±15.34) |
| S/J/G60 | **45.8** (±1.12) | 2575.6 (±1.32) | 22.65 (±1.31) | 1358.81 (±10.79) |
| S/J/G70 | 51.4 (±1.32) | 2620.1 (±1.13) | 24.64 (±2.07) | 1478.53 (±14.08) |
| S/J/G50/M1 | 69.8 (±1.31) | 3777.0 (±2.09) | 28.42 (±0.74) | 1705.47 (±11.67) |
| S/J/G50/M3 | 82.0 (±1.76) | 4516.3 (±1.54) | 32.40 (±1.37) | 1944.78 (±17.62) |
| S/J/G50/M5 | 90.7 (±2.54) | 6434.1 (±2.09) | 40.53 (±2.31) | 2344.67 (±12.78) |

Each value represents average five samples.

## 4.1.6. Thermal property study

The influence of crosslinker and nanoclay on the thermal properties of the synthesized composites was investigated by TGA, as shown in Figure 4.1.7. Table 4.1.3 (derived from Figure 4.1.7) shows the initial decomposition temperature $(T_i)$, maximum pyrolysis temperature $(T_m)$, decomposition temperature $(T_D)$ at different weight loss (%) and residual weight (RW) of the composites. It was seen clearly from the thermograms that the $T_i$, $T_m$, $T_D$ at different weight loss (%) and residual weight $(RW, \%)$ were improved with the addition of crosslinker.
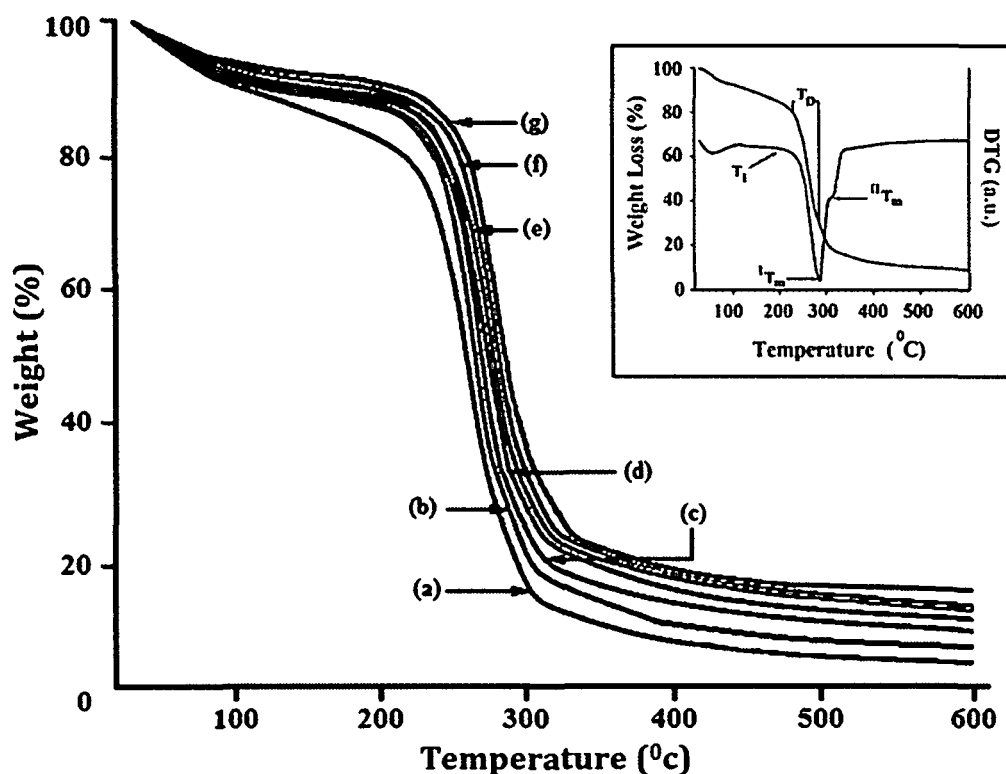


**Figure 4.1.7.** TGA thermograms of (a) S/J, (b) S/J/G30, (c) S/J/G50, (d) S/J/G70, (e) S/J/G50/M1, (f) S/J/G50/M3 and (g) S/J/G50/M5. TGA and DTG for curve-C are shown in the inset.

$T_i$ values of S/J composites were found to enhance with the increase in the percentage of crosslinker concentration. $T_i$ values increased further due to incorporation of clay. The interesting area of TGA of starch based composite is the 250° C to 350° C temperature range. $T_m$ values for both the stages of pyrolysis were found to increase as the percentage of crosslinker increased. $T_D$ values of the crosslinked S/J composite were higher than uncrosslinked S/J composite. The higher the crosslinker concentration, the higher was the $T_D$ value. This might be due to the formation of crosslinking caused by

the interaction between glutaraldehyde and different polar groups present in starch and jute. The $T_D$ values were improved further when clay was added to it. The increase in thermal stability of the synthesized nanocomposites is attributed to the hindered diffusion of volatile decomposition products within it [20]. This might also be due to the physico-chemical adsorption of the volatile degradation products on the silicate surface [21]. The volatilization of the degraded products originated by carbon-carbon bond scission in the composite was delayed by tortuous path provided by the silicates layer [22]. Clay treated composite showed a subsidiary increase in RW values over clay untreated composite. Therefore, it could be concluded that the thermal stability of the S/J composites increased on addition of crosslinker and nanoclay.

**Table 4.1.3.** Thermal properties of starch, jute, glutaraldehyde and nanoclay composite.

| Sample Particulars | $T_i$ | $^I T_m$ | $^{II} T_m$ | Temperature of Decomposition at different weight loss (%) | | | | | | RW % at 600 $^0$C |
|---|---|---|---|---|---|---|---|---|---|---|
| | | | | 20 | 30 | 40 | 50 | 60 | 70 | |
| S/J | 176±1 | 220±1 | 321±2 | 283±1 | 305±2 | 315±1 | 325±1 | 334±2 | 350±2 | 10±1 |
| S/J/G30 | 182±2 | 319±1 | 360±1 | 287±2 | 308±1 | 318±2 | 326±1 | 335±1 | 354±1 | 13±1 |
| S/J/G50 | 196±1 | 322±2 | 365±2 | 291±1 | 309±1 | 319±1 | 327±1 | 338±1 | 355±2 | 15±2 |
| S/J/G70 | 197±2 | 324±2 | 366±1 | 296±2 | 310±2 | 320±1 | 328±1 | 340±2 | 357±1 | 16±2 |
| S/J/G50/M1 | 218±1 | 351±1 | 391±2 | 298±1 | 313±1 | 322±1 | 331±1 | 341±2 | 361±1 | 18±2 |
| S/J/G50/M3 | 219±2 | 354±2 | 393±1 | 299±1 | 314±1 | 323±2 | 332±1 | 341±2 | 361±1 | 20±1 |
| S/J/G50/M5 | 221±2 | 359±1 | 397±1 | 301±2 | 316±1 | 325±1 | 334±1 | 344±2 | 364±1 | 23±2 |

$T_i$: initial decomposition temperature.

$^I T_m$: maximum pyrolysis temperature value for 1$^{st}$ step.

$^{II} T_m$: maximum pyrolysis temperature value for 2$^{nd}$ step.

* Each value represents average three samples.

### 4.1.7. LOI study

The LOI values of the S/J composites with different percentage of crosslinker and clay are presented in the Table 4.1.4. From that table, it was observed that LOI value increased with the increase in the percentage of crosslinker. GA formed crosslinks between jute and starch. The higher the concentration of GA, the higher is the crosslinking [18]. The network structure thus formed would restrict the accessibility of oxygen for the production of degradable components from the composites and hence LOI value would be more. LOI value was further on addition of nanoclay. The LOI

**Table 4.1.4.** LOI and Flaming Characteristics of the prepared composites.

| Samples | LOI (%) | Flame description | Smoke & Fumes | Char |
|---|---|---|---|---|
| S/J | 22 (±2.0) | Candle like Flame | Small and black smoke | Little |
| S/J/G30 | 29 (±1.0) | Small localised flame | Small and black smoke | Little |
| S/J/G40 | 38 (±3.0) | Small localised flame | Small and black smoke | Little |
| S/J/G50 | 39 (±1.0) | Small localised flame | Small and black smoke | Little |
| S/J/G60 | 44 (±2.0) | Small localised flame | Small and black smoke | Little |
| S/J/G70 | 47 (±1.0) | Small localised flame | Small and black smoke | Little |
| S/J/G50/M1 | 51 (±2.0) | Small localised flame | Small and black smoke | Higher |
| S/J/G50/M3 | 56 (±3.0) | Small localised flame | Small and black smoke | Higher |
| S/J/G50/M5 | 61 (±2.0) | Small localised flame | Small and black smoke | Higher |

* Each value represents average five samples.

values of the nanoclay treated composites were found more compared to nanoclay untreated composite. The higher the percentage of nanoclay, the higher was the LOI

value. Jute, primarily composed of plant materials cellulose and lignin, requires a very less amount of oxygen for the production of flammable volatiles and propagation of flame and hence showed very low LOI value. Whereas, the incorporation of the nanoclay particle into the synthesized composite produced a silicate char on the surface of it and hence improved their flame resistance property [23]. The silicate rich surface had better barrier property to heat and oxygen transport due to which ignition of the composite delayed. Therefore, with increase in the concentration of clay, the resistance of flame propagation was improved and hence higher LOI values were observed.

### 4.1.8. Dimensional stability test

The effect of swelling in water vapour at room temperature ($\sim30^0$ C) and 65% relative humidity for the composite samples for different time periods is shown in Figure 4.1.8. In all the cases, the % swelling was found to increase with the increase of time. From the figure, it was observed that the composites having higher percentage of GA showed more reduction in swelling than the composites containing lower percentage of GA [24]. Composites containing higher percentage of GA swelled less due to higher crosslink densities and less availability of the polar groups. Clay treated composites swelled less than those of clay untreated samples. The higher the amount of clay, the lower was the swelling. The silicate layer of clay provided a tortuous path which hindered the diffusivity of water through the composites [25].
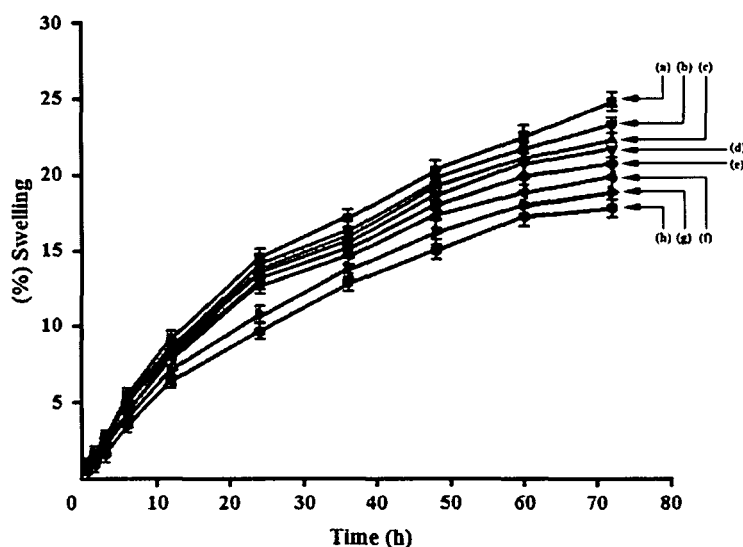


**Figure 4.1.8.** Swelling behaviour of (a) S/J, (b) S/J/G30, (c) S/J/G40, (d) S/J/G50, (e) S/J/G70, (f) S/J/G50/M1, (g) S/J/G50/M3 and (h) S/J/G50/M5.

**Section B**: **Study on the effect of cellulose whisker and nanoclay on jute fabric reinforced starch bio-nanocomposites**

Polymeric materials have generated remarkable influence in our daily life. However, the increasing cost of petroleum based polymeric materials and most importantly the ever-increasing pollution from non-degraded plastic waste have directly threatened human being's survival, health and development [26]. Therefore, the rising concern towards environmental issues lead to the development of commercially viable "green products" based on natural resources for both matrices and reinforcements for a wide range of applications.

This part of work explores the preparation and characterization of bio based polymer nanocomposites comprising of starch, jute, glutaraldehyde, cellulose whiskers and nanoclay with high physical properties.

## 4.2. RESULTS & DISCUSSION

Table 4.2.1 represents the composition of the synthesized nanocomposites and their respective codes. The samples as coded in Table 4.2.1 have been prepared by keeping the weight of the components viz. Starch, glycerol, glutaraldehyde and jute are fixed while varying the percentages of reinforcing agents CWs and nanoclay.

**Table 4.2.1.** Codification and composition of the nanocomposites based on jute and crosslinked starch with CWs and nanoclay (wt %).

| Sample | Starch (S) | Glycerol | Glutaraldehyde (G) | Jute (J) | CWs (C) | Nanoclay (N) |
|---|---|---|---|---|---|---|
| S/J/G | 100 | 5 | 50 | 75 | - | - |
| S/J/G/C1 | 100 | 5 | 50 | 75 | 1 | - |
| S/J/G/C3 | 100 | 5 | 50 | 75 | 3 | - |
| S/J/G/C5 | 100 | 5 | 50 | 75 | 5 | - |
| S/J/G/C5/N1 | 100 | 5 | 50 | 75 | 5 | 1 |
| S/J/G/C5/N3 | 100 | 5 | 50 | 75 | 5 | 3 |
| S/J/G/C5/N5 | 100 | 5 | 50 | 75 | 5 | 5 |

### *4.2.1. XRD study*

Figure 4.2.1 represents the diffractograms of (a) starch, (b) jute, (c) nanoclay and (d) prepared CWs. Curve-a implies the diffractograms of starch macromolecules. A little broader hump connoting the amorphous nature of starch is noticed at $2\theta = 19°$. Jute (curve b) shows peaks at $2\theta = 22°$ (002 plane of cellulose I) and $19°$ (101 plane of cellulose II) [11]. A strong diffraction peak for nanoclay at $2\theta = 9.1°$ (001) and a small peak at $2\theta = 24°$ was observed (curve c). The peak at 9.1 ° resembles to a d-spacing of about ~1.2 nm in pure clay [27]. Curve (d) shows the X-ray diffraction patterns of CWs. From Figure 4.2.1d, shows a series of characteristic peaks at $2\theta = 15.3°$, $16.2°$, $22.4°$ and $34.4°$ which corresponds to the (1-10), (110), (200), and (004) crystallographic planes of CWs is observed [28, 29].
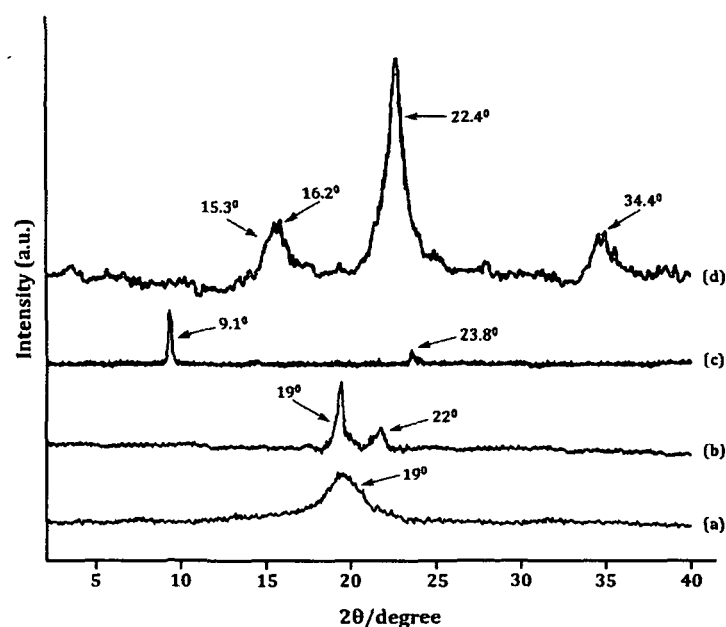


**Figure 4.2.1.** XRD pattern of (a) starch, (b) jute, (c) nanoclay and (d) Cellulose Whiskers.

Figure 4.2.2 shows the XRD patterns of S/J/G composites with or without CWs and nanoclay. In jute reinforced crosslinked starch composite (curve i) the peak at $2\theta = 22°$ (002 plane of cellulose I) is found to shift marginally towards lower angle of the X-ray diffractograms. However, the location of other peaks of starch and jute remained unchanged irrespective of variation of CWs in the composite {curve ii & iii)}. This revealed that incorporation of CWs into the composite did not have a pronounced effect on crystallinity. In S/J/G/C5 composite containing 5 % CWs, the peak at $2\theta = 15.3°$ for CWs was slightly shifted to $2\theta = 14.5°$ (curve iv). However, this peak was absent in

composite containing less than 5 % CWs. In case of the composites containing lower concentration of CWs *i.e.* 1–3 %, CWs may lost its structure such as the unit-cell parameters and chain conformation. Because of either vigorous mixing or the presence of starch macromolecules, CWs could not form crystalline structures within the composite as in the case of pure CW. Hence, the absence or decrease in intensity of the peak at $2\theta = 14.5°$ was observed. This suggested that CWs were well dispersed when its amount is less than 5 %. Upon addition of 1 % and 3 % nanoclay into the CWs incorporated jute reinforced crosslinked starch composites, the diffraction peak of the nanoclay tactoids disappeared {curve (v) and (vi)}. This absence of $d_{001}$ peak of the nanoclay in the nanocomposites indicates the formation of delaminated structure within the nanocomposites. It is envisaged that either the full expansion of the nanoclay gallery takes place within the composite, which is not possible to detect by XRD, or the nanoclay layers became delaminated and no crystal diffraction peak appeared. However, on addition of 5 % nanoclay into the S/J/G/C5 composite a new peak with less intensity emerged at $2\theta = 7.3°$, corresponding to an interlayer distance of 1.26 nm. The appearance of this peak indicated that resin chains had intercalated between the inorganic layers, forming mono and bilayers of polymer chains within the interlayer galleries.
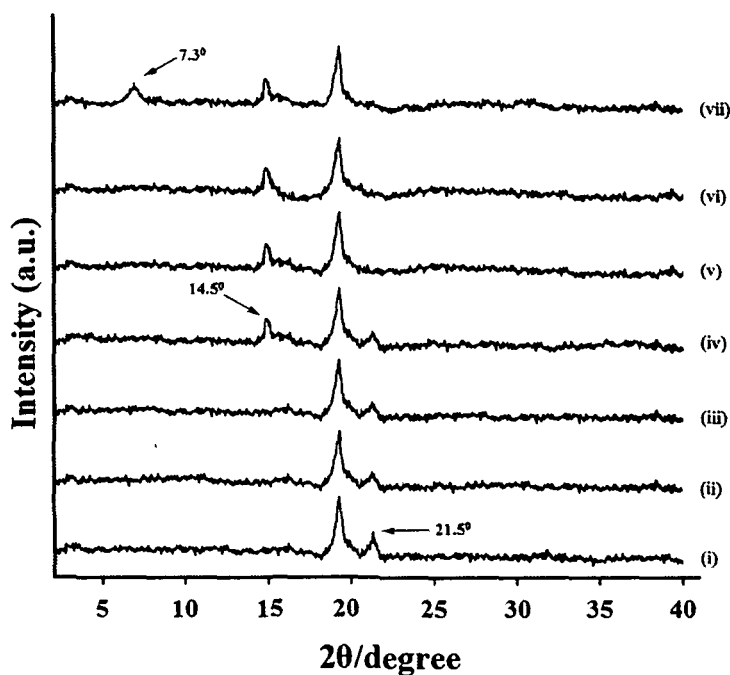


**Figure 4.2.2.** XRD pattern of (i) S/J/G, (ii) S/J/G/C1, (iii) S/J/G/C3, (iv) S/J/G/C5, (v) S/J/G/C5/N1, (vi) S/J/G/C5/N3 and (vii) S/J/G/C5/N5.

### 4.2.2. SEM study

The SEM micrographs of the fracture surface of S/J/G, S/J/G/C5 and S/J/G/C5/N5 composites are shown in Figure 4.2.3 (a-f). Figure 4.2.3 (a-c) represent the SEM micrographs in 50 μm and Figure 4.2.3 (d-f) in 2 μm range. The S/J/G sheet showed a relatively smooth surface [Figure 4.2.3 (a-d)]. It is noted that as the CWs was incorporated into the composite *i.e.* the fracture surface of S/J/G/C5, [Figure 4.2.3 (b-e)] a relatively rough structure was appeared, suggesting relatively high interfacial adhesion between starch, jute and CWs. The existence of the CWs in the starch and jute composites could be observed in the synthesized composites. Nevertheless, it is difficult to distinguish the individual filler dispersion due to its small size. Some filler appeared as white domains (indicated with arrows) on the fracture surface of the samples. Moreover, on addition of nanoclay into the S/J/G/C5 composite, the roughness is found to enhance [Figure 4.2.3 (c-f)]. This may be due to the fact that the clay particles increases the interaction due to the presence of hydroxyl groups with starch matrix, CWs and jute surface.
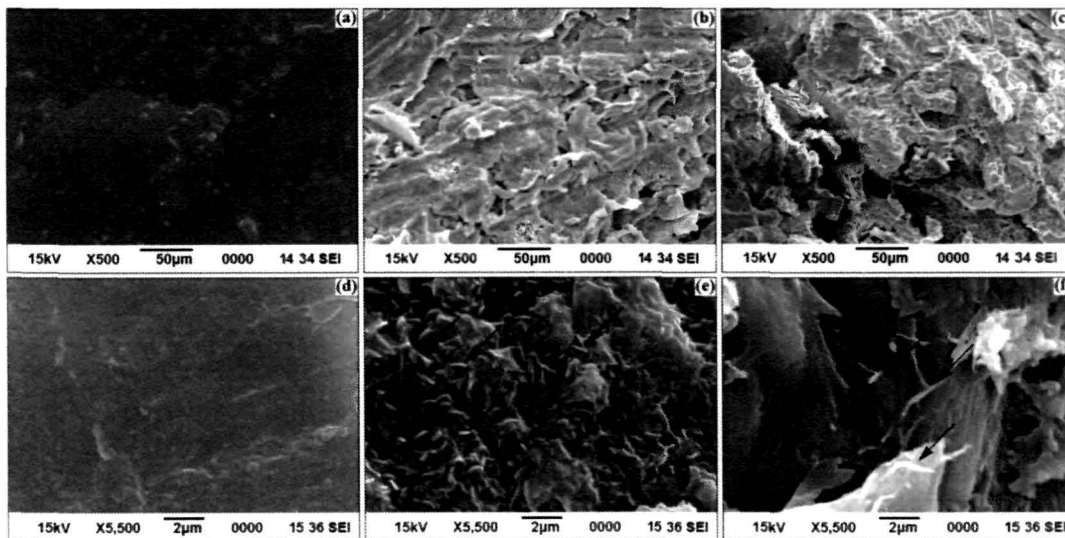


**Figure 4.2.3.** SEM micrographs of (a) S/J/G, (b) S/J/G/C5 and (c) S/J/G/C5/N5 in 50 μm scale and (d) S/J/G, (e) S/J/G/C5 and (f) S/J/G/C5/N5 in 2 μm ranges.

### 4.2.3. TEM study

TEM investigation was carried out to know the morphological features of cellulose layered-silicate nanocomposites. Figure 4.2.4a represents the TEM micrographs without CWs and clay composite in 100 nm range whereas Figure 4.2.4 (b) and 4.2.4 (c) are the micrographs of S/J/G/C5 and S/J/G/C5/N5 samples, respectively. TEM

images showed a good dispersion of the nanowhiskers in the matrix. The representative size of the cellulose nanowhiskers as determined by TEM was found to be ~25 nm in diameters length within the composite. The TEM image of S/J/G/C5 revealed that cellulose chains are bundle together randomly to form a network structure. The formation of network structure results from the formation of hydrogen bonds between cellulose nanoparticles during the nanocomposites preparation [30]. Figure 4.2.4 (c) corresponding to S/J/G/C5/N5 sample shows the dispersion of nanoclay in the composite. The threadlike dark lines (indicated with arrows) represent the intersections of the clay layers, and the bright areas denotes the jute based crosslinked starch composite matrix. Besides this, the nanoclay layers was found to be slightly agglomerated indicating the existence of partial compatibility between polymer, CWs and nanoclay surface [31]. The results obtained from TEM analysis were in accordance with our XRD analysis. Both the results suggested the formation of the partially exfoliated nanocomposites.
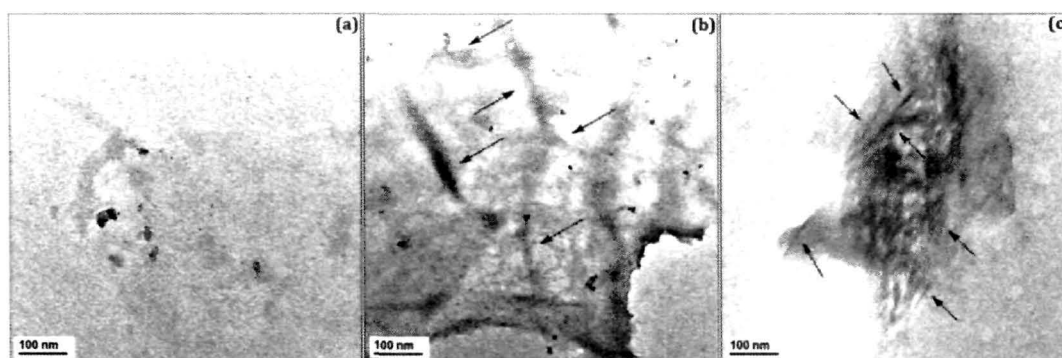


**Figure 4.2.4.** TEM micrographs of (a) S/J/G, (b) S/J/G/C5 and (c) S/J/G/C5/N5.

### 4.2.4. FT-IR study

FT-IR spectra of starch, jute clay and CWs are presented in Figure 4.2.5. The FT-IR spectrum of starch (curve a) showed the absorption bands at 570, 982, 1163, 1655, 2922 and 3450 cm$^{-1}$ indicating existence of the carbohydrate nature [7]. The distinctive saccharide bands appeared in the range 1179-951 cm$^{-1}$ was considered as the stretching mode of C–C and C–O vibration and the bending mode of C–H bond vibration [8]. The peak at 2922 cm$^{-1}$ was due to the C–H stretching vibration of methylene group [32]. Jute (curve b) shows the presence of peaks in the range 3440 cm$^{-1}$ for –OH stretching, 1735 cm$^{-1}$ for C=O stretching vibration of ester groups of hemicelluloses, 1641 cm$^{-1}$ for C=O stretching, 1255 cm$^{-1}$ for –C–O–C– bond in cellulose chain and 1115–1055cm$^{-1}$ for C–O stretching [5]. Clay exhibits peaks at 3450

cm$^{-1}$ (–OH stretching), 1620 cm$^{-1}$ (–OH bending), 1031–459 cm$^{-1}$ (oxide bonds of metals like Si, Al, Mg etc.). FT-IR spectrum of CWs is presented in Figure 4.2.5d. A strong broad band was observed at 3430 cm$^{-1}$ which is attributed to stretching of H-bonded hydroxyl groups. The peak at 2913 cm$^{-1}$ is due to symmetric C-H vibrations. An intense band at 1640 cm$^{-1}$ is assigned to the stretching vibration resulting from H-O-H intermolecular linkages. The bands at 1433 and 1325 cm$^{-1}$ in the spectrum are assigned to the symmetric CH$_2$ bending and wagging, the C-H bending occurs at 1368 cm$^{-1}$, 1255 cm$^{-1}$ [33, 34]. The two bands at 1188 cm$^{-1}$ and 897 cm$^{-1}$ correspond to C-O-C stretching at the $\beta$-(1→4)-glycosidic linkages [35]. The in-plane ring of $\beta$-(1→4)-glycosidic linkages gives a shoulder at 1115 cm$^{-1}$. Strong peaks at 1058 cm$^{-1}$ indicates the C-O stretching at C-3 [36]. In the spectra of CWs, the band occurred at 708 cm$^{-1}$ and 753 cm$^{-1}$ are the characteristic absorption of cellulose I$_\alpha$ and I$_\beta$ [37].
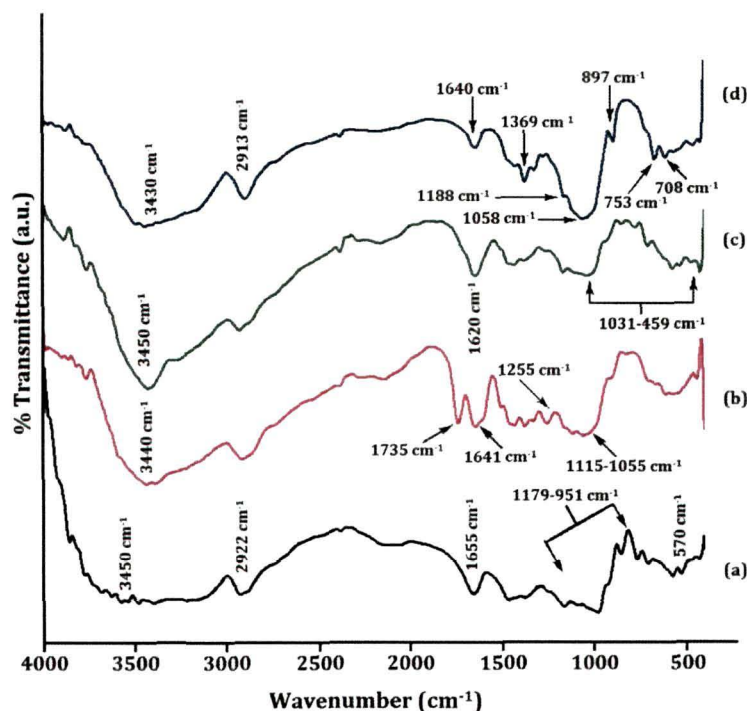


**Figure 4.2.5.** FT-IR spectra of (a) starch, (b) jute, (c) nanoclay and (d) Cellulose Whiskers.

The FT-IR spectra for the composite S/J/G (curve i), S/J/G/C1 (curve ii), S/J/G/C5 (curve iii), S/J/G/C5/N1 (curve iv) and S/J/G/C5/N5 (curve v) are shown in Figure 4.2.6. The FT-IR spectra for all the samples show peaks in the region 3400-3200 cm$^{-1}$, which could be attributed to the –OH stretching vibrations. The typical saccharide bands of starch appeared in the region of 1180-950 cm$^{-1}$. Similarly, the characteristic

peaks for jute appeared in all the spectrum at 1254 and 1116-1057 cm$^{-1}$. The entire spectrum shows the peak around 900 cm$^{-1}$ due to the $\beta$-(1$\rightarrow$4)-glycosidic linkages. The intensities of –OH and C=O stretching were found to decrease with respect to unfilled composite. From the IR spectrum, it was found that increase in CWs concentration, the peak intensities decreases. This may be attributed to the interaction between the free – OH group of jute and starch with –OH group of CWs. On addition of nanoclay, the peak intensity in the 3400-3200 cm$^{-1}$ corresponding to –OH stretching vibrations reduced and sharpened. In the spectrum of clay filled S/J/C composites, the intensity of peak corresponding to –OH was further decreased. The intensities of peaks at 1620 cm$^{-1}$ and 1030 cm$^{-1}$ assigned for Si–O–Si stretching are more pronounced compared to clay untreated composites. All this suggested the participation of hydroxyl group of clay in crosslinking reaction with starch, jute and CWs.
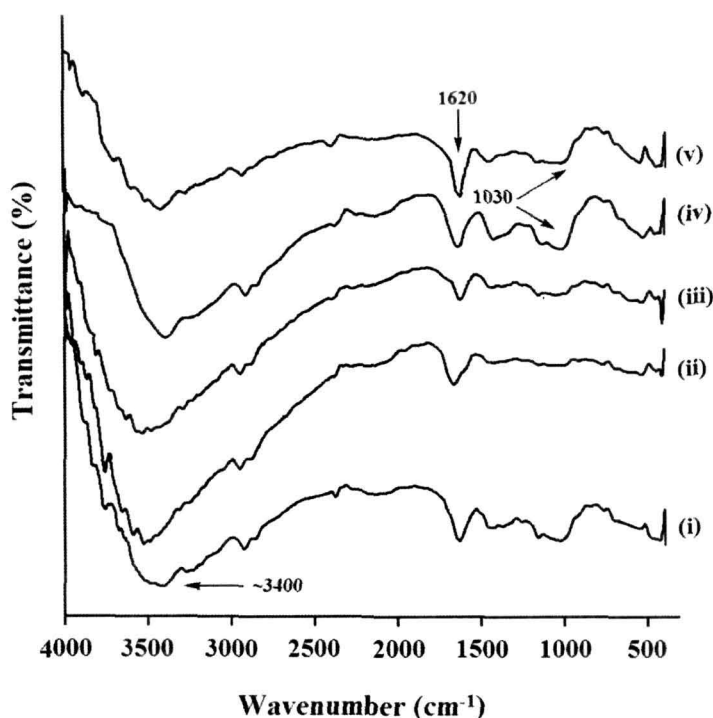


**Figure 4.2.6.** FT-IR spectra of (i) S/J/G, (ii) S/J/G/C1, (iii) S/J/G/C5, (iv) S/J/G/C5/N1 and (v) S/J/G/C5/N5.

### 4.2.5. Thermal property study

The degradation pattern and the thermal stability of the synthesized bio-nanocomposites were studied by using TGA. Figure 4.2.7 displays the weight (%) thermograms for some samples of the S/J/G, S/J/G/C1, S/J/G/C3, S/J/G/C5, S/J/G/C5/N1, S/J/G/C5/N3 and S/J/G/C5/N5. Table 4.2.2 (derived from Figure 4.2.7)

153

shows the initial decomposition temperature (T$_i$), maximum pyrolysis temperature (T$_m$), decomposition temperature (T$_d$) at different weight loss (%) and residual weight (% RW) of the composites at 600 °C. All the thermograms revealed an initial degradation around 100 °C due to the loss of water molecule. It is clearly inferred from the Figure 4.2.7 that the T$_i$, T$_m$, T$_d$ at different weight loss (%) and residual weight (RW, %) are improved with the addition of CWs. T$_i$ values of the composites were found to enhance with the increase in the percentage of CWs concentration. In the CWs incorporated nanocomposites, the CWs might restrict the thermal motion of the polymer chain and retard the diffusion of degradable decomposed products through the nanocomposites. Hence, an improvement in thermal stability was observed. On the other hand, nanoclay was often used to enhance the thermal properties of composite material [38]. Significant increase in the decomposition and char retention was described for a range of polymer nanocomposites using nanoclay. This was generally attributed to the ability of nanoclay to function as a mass transport barrier, hindering the out-diffusion of decomposition products and restricting the thermal motion of the polymer chain at the nanoclay surface [39]. The increased thermal resistance of the nanoclay incorporated CWs nanocomposites compared to CWs nanocomposites *viz.* S/J/G/C5/N1, S/J/G/C5/N3 and S/J/G/C5/N5 may be attributed to the retarded out-diffusion of decomposition products due to the labyrinth morphology of exfoliated nanoclay in the matrix [40].
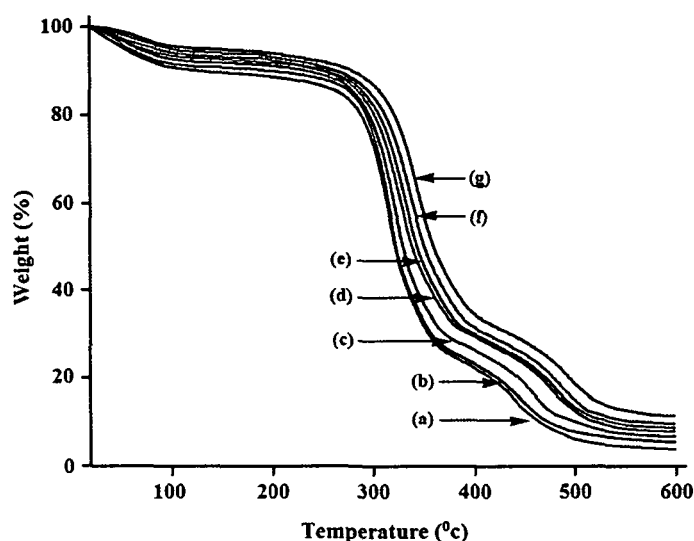


Figure 4.2.7. TGA thermograms of (a) S/J/G, (b) S/J/G/C1, (c) S/J/G/C3, (d) S/J/G/C5, (e) S/J/G/C5/N1, (f) S/J/G/C5/N3 and (g) S/J/G/C5/N5.

**Table 4.2.2.** Thermal Properties of (a) S/J/G, (b) S/J/G/C1, (c) S/J/G/C3, (d) S/J/G/C5, (e) S/J/G/C5/N1, (f) S/J/G/C5/N3 and (g) S/J/G/C5/N5.

| Sample Particulars | $T_i$ | $^a T_m$ | $^b T_m$ | Temperature of Decomposition at different weight loss (%) | | | | | RW % at 600 °C |
|---|---|---|---|---|---|---|---|---|---|
| | | | | 20 | 30 | 40 | 50 | 60 | |
| S/J/G | 198±1 | 319±1 | 363±2 | 288±1 | 302±1 | 312±2 | 321±1 | 334±2 | 5±1 |
| S/J/G/C1 | 201±1 | 321±2 | 367±2 | 291±1 | 303±1 | 315±1 | 324±3 | 336±1 | 7±1 |
| S/J/G/C3 | 205±2 | 325±1 | 369±3 | 294±1 | 305±3 | 317±1 | 327±1 | 339±2 | 9±3 |
| S/J/G/C5 | 209±3 | 327±1 | 371±1 | 297±2 | 308±1 | 323±1 | 331±1 | 348±1 | 11±2 |
| S/J/G/C5/N1 | 216±2 | 334±2 | 378±1 | 302±2 | 312±2 | 338±1 | 347±2 | 356±1 | 11±1 |
| S/J/G/C5/N3 | 220±1 | 339±2 | 384±1 | 313±1 | 321±2 | 347±2 | 351±2 | 367±2 | 12±2 |
| S/J/G/C5/N5 | 226±2 | 347±1 | 393±1 | 321±1 | 335±1 | 358±2 | 366±2 | 384±1 | 14±2 |

$T_i$: initial decomposition temperature.

$^a T_m$: maximum pyrolysis temperature value for 1st step.

$^b T_m$: maximum pyrolysis temperature value for 2nd step.

Each value represents average three samples.

### 4.2.6. Mechanical property study

The mechanical tests results are shown in Table 4.2.3. A significant reinforcing effect is observed upon filler addition, as displayed by the increase of both the modulus and strength for composites compared to the unfilled composites. It was observed that both the tensile and flexural strength and modulus have increased with the increase in the concentration of CWs. The mechanical properties of such materials were mainly dependent on three parameters like, the geometrical aspect, the processing method and finally the matrix structure and the resulting competition between matrix/filler and filler/filler interactions. The mechanical behaviour of CW based composites suggested the formation of a rigid network of whiskers which could be responsible for the observed reinforcing effect [42]. Similarly, Bendhau *et al* [42] found an increase in tensile properties of the natural rubber composite after the incorporation of CWs. Considering the 5 % concentration of the CWs as optimum, the composites were further modified by incorporating nanoclay into it (*i.e.* S/J/G/C5/N1, S/J/G/C5/N3 and S/J/G/C5/N5) with varying percentage of nanoclay ranging from 1 to 5 % (w/w of starch). However, the nanoclay incorporated composites show significant improvement in the mechanical properties with respect to the nanoclay untreated one. This enhancement in mechanical properties of clay loaded composites was due to their high intrinsic modulus. Otherwise, it could be stated that clays act as rigid reinforcement agent to the polymer matrix. The high aspect ratio of nanoclay which generated a large surface area for the polymers adsorption was also a reason for the enhancement in mechanical properties. Apart from this, the intercalation of the polymers into the galleries of nanoclay restricted its mobility. However, such improvement in mechanical properties with the incorporation of nanoclay may only be realized up to a definite nanoclay loading. In this present work, the enhancement in mechanical properties was observed up to a clay loading of 3 %, and beyond that it declined on further addition of nanoclay. At higher concentration of nanoclay, agglomeration of clay platelets took place and as a result the interaction between the clay - polymer was reduced. This has led to the reduction in the extent of enhancement of reinforcement efficiency with the addition of higher amount of nanoclay [43].

**Table 4.2.3.** Comparison of the Tensile, Flexural and Limiting Oxygen Index (LOI) properties of Unfilled and Filled jute based crosslinked Starch nanocomposites.

| Composite System | Tensile Properties | | Flexural Properties | | LOI (%) |
|---|---|---|---|---|---|
| | Strength (MPa) | Modulus (MPa) | Strength (MPa) | Modulus (MPa) | |
| S/J/G | 21.81 (±1.42) | 1222.2 (±11.50) | 41.41 (±0.82) | 2358.7 (±8.64) | 40 (±2.0) |
| S/J/G/C1 | 28.58 (±1.45) | 1612.2 (±15.76) | 48.42 (±1.78) | 2975.5 (±10.34) | 43 (±1.0) |
| S/J/G/C3 | 34.64 (±2.43) | 1789.8 (±11.64) | 59.68 (±2.13) | 3874.8 (±14.74) | 47 (±2.0) |
| S/J/G/C5 | 39.56 (±1.78) | 1917.5 (±19.23) | 69.65 (±1.46) | 4735.4 (±13.43) | 52 (±3.0) |
| S/J/G/C5/N1 | 47.72 (±1.65) | 2178.3 (±13.34) | 81.31 (±1.79) | 5629.2 (±12.82) | 56 (±1.0) |
| S/J/G/C5/N3 | 57.34 (±1.13) | 2572.1 (±16.38) | 98.64 (±1.12) | 6524.3 (±12.37) | 61 (±2.0) |
| S/J/G/C5/N5 | 51.61 (±2.11) | 2341.4 (±15.21) | 88.54 (±1.43) | 5989.6 (±11.52) | 64 (±1.0) |

For Tensile and Flexural property each value in the above table represents average of ten samples. Values in the parenthesis represent the standard deviation.

### 4.2.7. LOI study

The synergistic effect of CWs and nanoclay on Limiting oxygen indices (LOI) values and flaming characteristics of jute based crosslinked starch are shown in Table 4.2.3. It is observed form Table 4.2.3 that the synthesized composites produced small localized flame. It was also found that the nanoclay filled samples generated higher char than the nanoclay unfilled one. The LOI test assumes that inherently less flammable materials require greater oxygen concentrations to produce the heat necessary for the continuous production of flammable volatiles and flame propagation. LOI value was found to increase with the increase in the concentration of CWs in the composites. This may be due to the fact that the –OH groups of CWs form crosslink with starch, jute and glutaraldehyde and restricted the accessibility of oxygen for the production of degradable components from the composites [18]. Further, higher the CWs concentration, higher was the LOI value. The enhancement in properties may be due to the increase in interaction among starch, jute, glutaraldehyde and CWs. However, on addition of nanoclay into CWs incorporated composites, LOI value was further enhanced. The higher the percentage of nanoclay, the higher is the LOI value. Jute and starch primarily composed of plant materials which require a very less amount of oxygen for the production of flammable volatiles and propagation of flame and hence shows very low LOI value. The incorporation of the nanoclay into the synthesized composite produced a silicate char on the surface of it and hence improved their flame resistance property. The silicate rich surface had better barrier property to heat and oxygen transport due to which ignition of the composite delayed [23]. Therefore, with increase in the concentration of clay, the resistance of flame propagation improved and hence higher LOI values were observed.

### 4.2.8. Dimensional stability test

Figure 4.2.8 represents the results of water vapour exclusion study. From the Figure 4.2.8, it was observed that water vapour absorption initially occurred at a rapid rate and finally at a slower rate. In all the cases, water vapour absorption rate increased with the increase in time. S/J/G is hydrophilic in nature and hence it absorbed a high amount of water vapour. The water vapour absorption decreased by the presence of dispersed phase of CWs into the composite. The CWs particles crosslinked with the free –OH groups of jute and starch and reduced the absorption of water vapour. CWs may elongate the diffusion path of water particles in the nanocomposites [44]. Water

vapour absorption of the nanocomposites decreased with the increase in the CWs content. Further, it was observed that nanoclay treated composites absorbed less water than those of nanoclay untreated samples. The higher the amount of nanoclay, the lower is the water absorption. This may be due to the fact that the silicate layers of nanoclay provide a tortuous path which hindered the diffusivity of water particles through the nanocomposites composites [25].
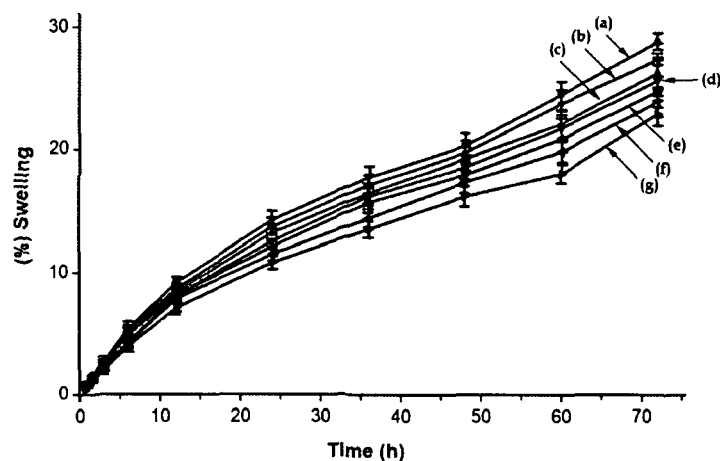


**Figure 4.2.8.** Swelling behaviour of (a) S/J/G, (b) S/J/G/C1, (c) S/J/G/C3, (d) S/J/G/C5, (e) S/J/G/C5/N1, (f) S/J/G/C5/N3 and (g) S/J/G/C5/N5.

**Section C:** **Study on the effect of TiO₂ and nanoclay on jute fabric reinforced starch bio-nanocomposites**

The use of bio based polymer composite has immensely increased due to their several advantages over their synthetic counterparts [1]. The composites reinforced with plant based fibre and bio polymers have shown an excessive development due to their numerous advantages that they possess. They are easily abundant worldwide, their processing is easy, economic, and most importantly they are environmentally benign. The properties of starch/jute (S/J) composites can be improved by using nanomaterials [45]. Out of various nanomaterials predecessors, nanoclay is most widely used for the production of polymer nanocomposite. Besides using nanoclay, different metal oxide nanoparticles *viz.* $ZnO$, $TiO_2$, $SiO_2$ etc. are also used to improve various properties of biopolymer based nanocomposites [46]. In exterior application of biopolymer based materials, UV protection, flame retardancy and weathering resistance are very vital. In recent years, $TiO_2$ nanopowder is gradually being studied because it is non-toxic, chemically inert, low cost, and has a high refractive index, UV filtration capacity and high hardness. Reinforcement by $TiO_2$ also improves electrical, optical, and physiochemical properties at a very low $TiO_2$ concentration, which make polymer $TiO_2$ nanocomposites a promising new class of materials [47].

This part of study is aimed to discuss the effect of $TiO_2$ nanoparticles alone and in combination with nanoclay (*i.e.* $TiO_2$ and $TiO_2$ - nanoclay) on thermal and mechanical properties of S/J composites. The effect of nanoparticles, *viz.* $TiO_2$ nanoparticles and nanoclay on other properties like UV resistance, dimensional stability, and flame retardancy of the composites have also been studied.

## 4.3. RESULTS & DISCUSSION

The samples, as coded in Table 1, had been prepared by keeping constant weight (%) of the components viz. starch, glycerol, jute and GA, where as the percentages (%) of $TiO_2$ nanoparticles and nanoclay were varied. The weight (%) of the various components used for the synthesis of the composite are provided in Table 4.3.1.

160

**Table 4.3.1.** Codification and filler content of the nanocomposites based on Jute and crosslinked Starch with TiO₂ nanoparticles and nanoclay (wt %).

| Sample | Starch (S) | Glycerol | Glutaraldehyde (GA) | Jute (J) | TiO₂ (T) | Nanoclay (N) |
|---|---|---|---|---|---|---|
| S/J/GA50 | 100 | 5 | 50 | 75 | - | - |
| S/J/GA50/T1 | 100 | 5 | 50 | 75 | 1 | - |
| S/J/GA50/T3 | 100 | 5 | 50 | 75 | 3 | - |
| S/J/GA50/T5 | 100 | 5 | 50 | 75 | 5 | - |
| S/J/GA50/T5/N1 | 100 | 5 | 50 | 75 | 5 | 1 |
| S/J/GA50/T5/N3 | 100 | 5 | 50 | 75 | 5 | 3 |
| S/J/GA50/T5/N5 | 100 | 5 | 50 | 75 | 5 | 5 |

### *4.3.1. XRD study*

As an indirect but non-invasive technique, XRD analysis is accomplished to obtain comprehensive information regarding crystallinity of the nanoparticles (*i.e.* TiO₂ and nanoclay) and the synthesized composites. Figure 4.3.1A displays the diffractograms of starch, jute, nanoclay, and TiO₂ nanoparticles. Curve a shows the diffractograms of starch macromolecules. A little broader hump connoting the amorphous nature of starch is noticed at $2\theta = 19.7°$. Jute (curve-b) shows peaks at $2\theta = 22.3°$ (002 plane of cellulose I) and $19.2°$ (101 plane of cellulose II) [11]. In Figure 4.3.1A, curve-c, represents the diffractogram of nanoclay. A strong diffraction peak for nanoclay at $2\theta = 9.2°$ and a small peak at $2\theta = 24.1°$ was noticed. The peak at $9.2°$ resembles to a d-spacing of about 1.2 nm in pure clay [27]. In the diffractogram of bare TiO₂ (curve-d), characteristics peaks appeared at $2\theta = 37.7°$ (004), $48.3°$ (200), $56.7°$ (211), and $62.6°$ (204), and at $27.4°$ (110), $36.3°$ (101), $55.1°$ (105), were for anatase and rutile phase respectively [48]. All peaks were in good agreement with the standard spectrum (JCPDS no.: 88-1175 and 84-1286).

Figure 4.3.1B represents the diffractograms of S/J/GA50, S/J/GA50/T1, S/J/GA50/T3, S/J/GA50/T5, S/J/GA50/T5/N1, S/J/GA50/T5/N3, and S/J/GA50/T5/N5 composites. In Figure 4.3.1B, curve-a, represents the diffractograms of S/J/GA50 (*i.e.* without TiO₂ nanoparticles). A small broad diffraction peak corresponding to jute and starch was appeared around $2\theta = 20°$. Curve (b-d) were the diffractograms of nanocomposites *viz.* S/J/GA50/T1, S/J/GA50/T3, and S/J/GA50/T5 with different

percentage of $TiO_2$ nanoparticles (1-5 % w/w of dry starch). The diffraction signals of starch matrix and jute fibre were appeared in the range $2\theta = 19° - 22°$. However, at a higher amount of $TiO_2$ nanoparticle loading, the peaks corresponding to $TiO_2$ nanoparticles appeared with higher intensity. Mina *et al.* [49] reported an increase in peak intensity of $TiO_2$ while studying the X-ray diffraction profile of polypropylene/ titanium dioxide composite. For composites, containing 1% and 3% clay the diffraction peak of the nanoclay tactoids was absent in the X-ray diffractograms (curve e, f). The $d_{001}$ peak of the nanoclay within the prepared nanocomposites completely disappeared, demonstrating the development of a delaminated structure. It could be said that either the full expansion of the nanoclay gallery took place, which could not be identified by XRD, or the nanoclay layers were delaminated due to which no crystal diffraction peak appeared. In S/J/GA50/T5/N5 composites, the typical peak of nanoclay was found to appear at $2\theta = 7.7°$ with less intensity representing an existence of agglomeration of nanoclay within the nanocomposite.
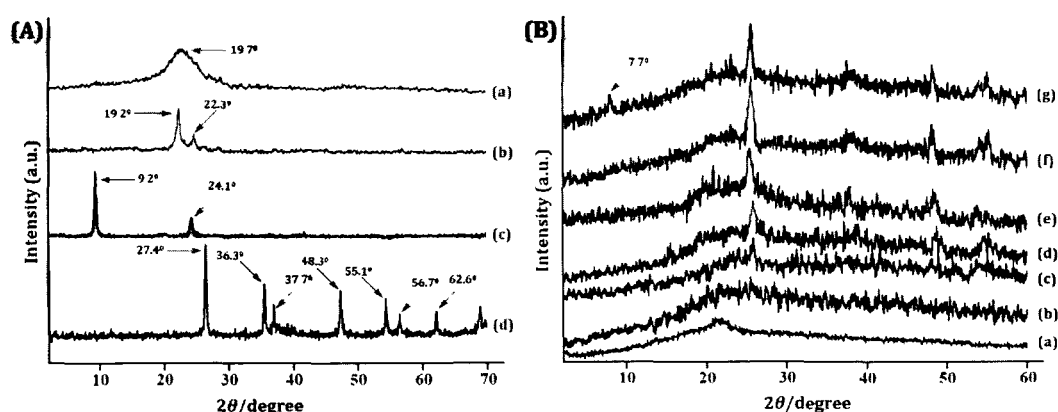


**Figure 4.3.1.** **(A)** XRD pattern of (a) starch, (b) jute, (c) nanoclay, and (d) $TiO_2$ nanoparticles. **(B)** XRD diffractograms of (a) S/J/GA50, (b) S/J/GA50/T1, (c) S/J/GA50/T3, (d) S/J/GA50/T5, (e) S/J/GA50/T5/N1, (f) S/J/GA50/T5/N3 and (g) S/J/GA50/T5/N5.

### 4.3.2. TEM study

Figures 4.3.2 indicates the TEM micrographs of the S/J composites with different percentage of nanoclay and $TiO_2$ nanoparticles. Figure 4.3.2a represents the TEM micrographs of composite without $TiO_2$ nanoparticles and nanoclay. The presence of well dispersed black spots (shown by arrow marks) is clearly visualized for $TiO_2$ nanoparticles in S/J/GA50/T1, S/J/GA50/T3, and S/J/GA50/T5 (Figure 4.3.2b-d)

[47]. TEM micrographs corresponding to S/J/GA50/T5/N1 and S/J/GA50/T5/N3 sample showed the dispersion of nanoclay within the nanocomposite (Figure 4.3.2e, f). The threadlike dark lines and black spots (indicated with arrows) significant the intersections of the clay layers and $TiO_2$ particles. It is inferred, from the micrographs, that the silicate layers were not homogeneously distributed within the composite indicating the existence of partial compatibility between jute, polymer, $TiO_2$ nanoparticles and nanoclay surface [42]. However, at higher concentration of nanoclay, the thickness of dark slices of nanoclay increases due to agglomeration (Figure 4.3.2g). The results obtained from TEM analysis are in accordance with our XRD findings. Both the results suggested the formation of the partially exfoliated nanocomposites.
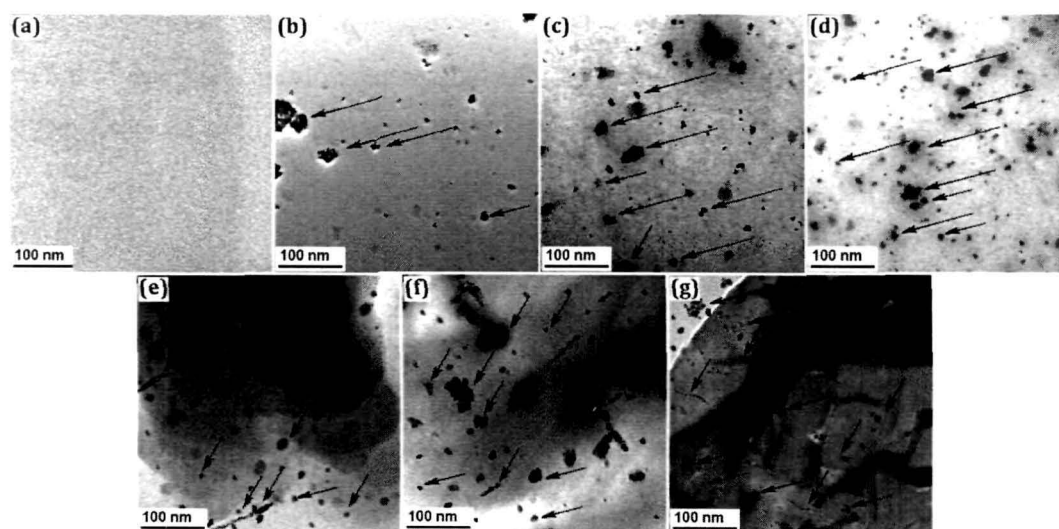


**Figure 4.3.2.** TEM micrograph of (a) S/J/GA50, (b) S/J/GA50/T1, (c) S/J/GA50/T3, (d) S/J/GA50/T5, (e) S/J/GA50/T5/N1, (f) S/J/GA50/T5/N3 and (g) S/J/GA50/T5/N5.

### 4.3.3. FT-IR study

FT-IR spectra of starch, jute, clay, and $TiO_2$ nanoparticles are presented in Figure 4.3.3A. The FT-IR spectrum of jute (curve-a in Figure 4.3.3A) shows the absorption bands around 3436 cm$^{-1}$ for –OH stretching, 1736 cm$^{-1}$ for C=O stretching vibration of ester groups of hemicelluloses, 1644 cm$^{-1}$ for C=O stretching, 1244 cm$^{-1}$ for –C–O–C– bond in cellulose chain and 1056–1114 cm$^{-1}$ for C–O stretching [5]. The FT-IR spectrum of starch shows the absorption bands at 572, 982, 1160, 1652, 2920 and 3452 cm$^{-1}$ confirming the carbohydrate nature [7]. The typical saccharide bands appeared in the range 1182-951 cm$^{-1}$ was considered as the stretching mode of C–C and C–O vibration and the bending mode of C–H bond vibration [8]. The peak at 2920 cm$^{-}$

[1] is characteristic of the C–H stretching vibration of methylene group [32]. Clay (curve-c in Figure 4.3.3A) exhibits peaks at 3448 cm^{-1} (–OH stretching), 1621 cm^{-1} (–OH bending), 1031–462 cm^{-1} range (oxide bonds of metals like Si, Al, Mg etc.). FTIR spectrum of $TiO_2$ nanoparticles is presented in curve-d (Figure 4.3.3A). The strong absorbance at 1029–420 cm^{-1} range was attributed to the Ti–O–Ti stretching of $TiO_2$. The absorbance at 3434 and 1632 cm^{-1} were assigned to the surface hydroxyl groups of $TiO_2$ [50, 51].
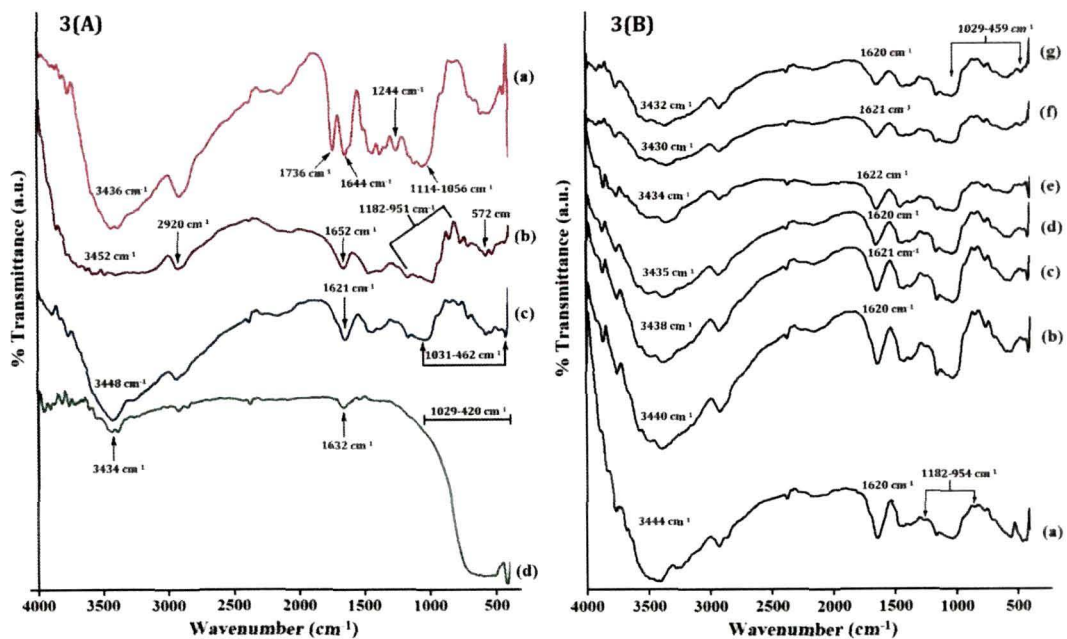


**Figure 4.3.3. (A)** FT-IR spectra of (a) starch, (b) jute, (c) nanoclay, and (d) $TiO_2$ nanoparticles. **(B)** FT-IR spectra of (a) S/J/GA50, (b) S/J/GA50/T1, (c) S/J/GA50/T3, (d) S/J/GA50/T5, (e) S/J/GA50/T5/N1, (f) S/J/GA50/T5/N3 and (g) S/J/GA50/T5/N5.

FT-IR spectra for the composite S/J/GA50, S/J/GA50/T1, S/J/GA50/T3, S/J/GA50/T5, S/J/GA50/T5/N1, S/J/GA50/T5/N3, and S/J/GA50/T5/N5 are shown in Figure 4.3.3B. The FT-IR spectra for all the samples showed peaks in the region 3400–3250 cm^{-1}, which could be attributed to the –OH stretching vibration. Characteristic saccharide bands of starch appeared in the region of 1180–950 cm^{-1} were present in all the spectra. Similarly, the peaks appearing in all the spectra at 1247 and 1116–1057 cm^{-1} were the characteristic peaks for jute. The entire spectra show the band around 900 cm^{-1} due to the $\beta$-(1→4)-glycosidic linkages. The position of –OH and C=O stretching is shifted in the crosslinked composite (S/J/GA50) suggesting the interaction between

jute and starch. From the Figure 4.3.3B, it was found that with the increase in concentration of $TiO_2$ nanoparticles, the peak intensities of –OH band were found to decrease. This behaviour could be attributed due to the interaction between the free – OH groups of jute and starch with –OH groups of $TiO_2$ nanoparticles. Upon the addition of nanoclay, the peaks in the ~3400 cm$^{-1}$ range further reduce in intensity and are shifted to lower wavenumber. The peak intensities in the range of 1029–459 cm$^{-1}$ and 1619 cm$^{-1}$ were also found to reduce upto a considerable extent. These results confirmed the participation of hydroxyl group of clay with S/J/GA50/T composites [52].

### *4.3.4. SEM study*

SEM micrographs of S/J/GA50, S/J/GA50/T1, S/J/GA50/T3, S/J/GA50/T5, S/J/GA50/T5/N1, S/J/GA50/T5/N3, and S/J/GA50/T5/N5 composites are shown in Figure 4.3.4. The fractured surface of some selective samples was considered for this study. S/J/GA50 sheet showed a relatively smooth surface (Figure 4.3.4a). Figure 4.3.4b inferred that the fractured surface of S/J/GA50/T1 displays a homogenous structure suggesting a relatively uniform distribution of the $TiO_2$ nanoparticles within the composite. However, as the amount of $TiO_2$ nanoparticles was increased, *i.e.*, the fractured surface of S/J/GA50/T3 and S/J/GA50/T5 (Figure 4.3.4c, d) exhibited a comparatively rough surface, indicating relatively high interfacial adhesion among starch, jute and $TiO_2$ nanoparticles. Furthermore, upon addition of nanoclay into the $TiO_2$ nanoparticles loaded nanocomposites (*i.e.* S/J/GA50/T5), the roughness was found to enhance (Figure 4.3.4 e-g). The enrichment in roughness was due to the fact that clay particles enhance the interaction with the starch macromolecules and jute fibre. Composite having 3 % nanoclay was appeared to be more rough compared to that of the composite prepared with 5 % nanoclay. This indicated that agglomeration of nanoclay particles might have taken place within the composite at higher percentage of nanoclay.

The fractured surface of $TiO_2$ nanoparticles loaded composites taken for SEM study was also investigated by energy dispersive X-ray elemental analysis (EDX) simultaneously. Figure 4.3.4h shows the EDX analysis of S/J composite. The presence of Ti and elements such as Al, Na and Si, which are mainly from the nanoclay, along with C and O confirmed the successful incorporation of $TiO_2$ nanoparticles and nanoclay into the composite.
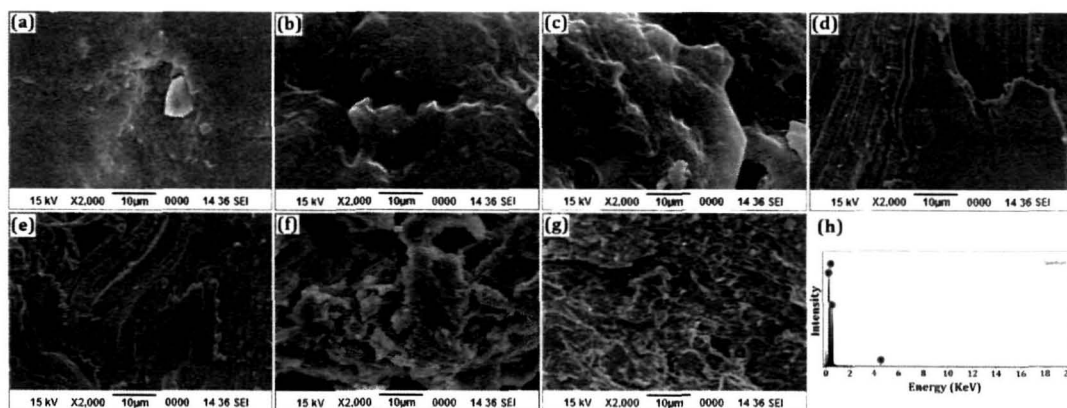
**Figure 4.3.4.** SEM micrographs of (a) S/J/GA50, (b) S/J/GA50/T1, (c) S/J/GA50/T3, (d) S/J/GA50/T5, (e) S/J/GA50/T5/N1, (f) S/J/GA50/T5/N3, (g) S/J/GA50/T5/N5 and (h) Energy dispersive X-ray analysis of S/J/GA50/T5/N5.

### *4.3.5. Thermal property study*

The influence of $TiO_2$ nanoparticles and nanoclay on the thermal properties of the synthesized bio-nanocomposites was investigated by TGA as shown in Figure 4.3.5. Figure 4.3.5 depicts the thermograms of S/J/GA50, S/J/GA50/T1, S/J/GA50/T3, S/J/GA50/T5, S/J/GA50/T5/N1, S/J/GA50/T5/N3, and S/J/GA50/T5/N5. All the thermograms showed an initial weight loss around 100 °C due to the loss of confined water molecules. It was clearly inferred from the thermograms that all the values of the nanocomposites were found to increase with increase in the amount of $TiO_2$ nanoparticles. The heat shielding effect of $TiO_2$ nanoparticles were responsible for enhancement in thermal stability [53]. To enhance the thermal stability of composite materials, nanoclay is widely used. After the incorporation of nanoclay, the thermal stability of the $TiO_2$ nanoparticles loaded nanocomposites (*i.e.* S/J/GA50/T5) were further improved. This increase in thermal stability of the prepared nanocomposites are attributed to the hindered diffusion of volatile decomposition products within it. This might also be due to the physico-chemical absorption of the volatile degradation products on the silicate surface of nanoclay. The volatilization of the degraded products originated by carbon-carbon bond scission in the composite was delayed by tortuous path provided by the silicate layers [39]. Laachachi *et al.* [54] studied the thermal stability of PMMA by using organoclays and $TiO_2$ and found a significant increase in thermal stability of PMMA due to the synergistic effect of clay/$TiO_2$. With the increase in concentration of clay, the agglomeration of clay probably took place which contributed to the reduction in the thermal stability. Therefore, it could be concluded

that the thermal stability of S/J composites was increased on addition of a certain concentration of $TiO_2$ nanoparticles and nanoclay.



**Figure 4.3.5.** TGA thermograms of (a) S/J/GA50, (b) S/J/GA50/T1, (c) S/J/GA50/T3, (d) S/J/GA50/T5, (e) S/J/GA50/T5/N1, (f) S/J/GA50/T5/N3 and (g) S/J/GA50/T5/N5.

### 4.3.6. Mechanical property study

The mechanical properties of S/J composites reinforced with $TiO_2$ nanoparticles and nanoclay were studied at room temperature. Experimental data are presented in Table 4.3.2. A noticeable reinforcing effect was found upon filler addition, which can be anticipated from the increase in both modulus and strength of the composite compared to the unfilled ones. The increase in the percentage of $TiO_2$ nanoparticles might have direct effect in increasing the mechanical properties of the nanocomposites [47]. With the increase in $TiO_2$ nanoparticles content, both the tensile and flexural properties of the nanocomposites also increased. The interaction of $TiO_2$ nanoparticles with crosslinked starch and jute through its surface hydroxyl group might stiffen the composites and results in enhancement of mechanical properties. Considering the 5 % concentration of the $TiO_2$ nanoparticles as optimum, we had further modified the composites *viz.* S/J/GA50/T5/N1, S/J/GA50/T5/N3 and S/J/GA50/T5/N5 by incorporating different percentage of nanoclay [1-5 % (w/w of dry starch)]. With the incorporation of nanoclay, composites showed a significant improvement in the mechanical properties compared to nanoclay free composite. The silicate layers of nanoclay acts as a reinforcing agent which binds the polymer chains inside the gallery

space and restricts the mobility of the polymer chains. However, such improvement in mechanical properties with the incorporation of nanoclay might only be realized up to a certain clay loading. In present work, the enhancement in mechanical properties was found up to 3 % of clay loading, and beyond that it declines on further addition of nanoclay. At higher concentration of nanoclay, agglomeration of clay particles might have taken place and therefore its interaction with polymer was reduced which led to the diminishing trend in the mechanical properties of the composites. TEM study also supported the agglomeration of $TiO_2$ nanoparticles.

**Table 4.3.2.** Comparison of Tensile and Flexural properties of Unfilled and Filled jute based crosslinked starch nanocomposites before UV treatment.

| Composite System | Tensile Properties | | Flexural Properties | |
|---|---|---|---|---|
| | Strength (MPa) | Modulus (MPa) | Strength (MPa) | Modulus (MPa) |
| S/J/GA50 | 23.52 (±1.55) | 1281.1 (±13.42) | 43.24 (±1.76) | 2429.8 (±14.76) |
| S/J/GA50/T1 | 31.54 (±2.36) | 1689.7 (±12.61) | 52.13 (±2.32) | 3082.1 (±11.57) |
| S/J/GA50/T3 | 38.28 (±1.56) | 1863.4 (±11.85) | 62.23 (±1.89) | 3992.6 (±12.42) |
| S/J/GA50/T5 | 42.42 (±1.12) | 2024.3 (±11.53) | 70.16 (±1.56) | 4872.9 (±10.21) |
| S/J/GA50/T5/N1 | 51.64 (±2.43) | 2263.3 (±16.56) | 85.27 (±2.79) | 5796.2 (±15.56) |
| S/J/GA50/T5/N3 | 61.59 (±1.34) | 2655.2 (±14.74) | 100.87 (±2.46) | 6667.2 (±14.37) |
| S/J/GA50/T5/N5 | 55.21 (±1.67) | 2419.2 (±12.22) | 92.76 (±1.75) | 6034.1 (±12.46) |

Each value in the above table represents average of ten samples. Values in the parenthesis represent the standard deviation.

### 4.3.7. UV test results

The weight loss of S/J/GA50, S/J/GA50/T1, S/J/GA50/T3, S/J/GA50/T5, S/J/GA50/T5/N1, S/J/GA50/T5/N3, and S/J/GA50/T5/N5 are represent in Figure 4.3.6. Weight losses of the samples were determined at room temperature as a function of exposure time and found linear variation with this. Initially a small increase in weight was found due to moisture uptake by the samples, which was greater than the material loss induced by the degradation in the early stage. The rate of weight loss was lowest for S/J/GA50/T5/N3 followed by S/J/GA50/T5/N5, S/J/GA50/T5/N1, S/J/GA50/T5, S/J/GA50/T3, S/J/GA50/T1 and S/J/GA50. The $TiO_2$ nanoparticles and nanoclay unloaded composite had shown maximum weight losses. After 60 days of exposure time, the weight losses in S/J/GA50, S/J/GA50/T1, S/J/GA50/T3, S/J/GA50/T5, S/J/GA50/T5/N1, S/J/GA50/T5/N3 and S/J/GA50/T5/N5 were 4.62 ± 0.3 %, 3.93 ± 0.2%, 3.34 ± 0.1 %, 2.75± 0.2 %, 1.87 ± 0.3 %, 1.17 ± 0.2 % and 1.48 ± 0.3 % respectively. Results shown were the average of four specimens. The lower weight loss (%) for S/J/GA50/T5/N3 composites after UV exposure was due to the UV shielding ability of $TiO_2$ nanoparticles and nanoclay. On exposure to UV radiation, the chain scission followed by decrease in the density of the entanglements of the starch polymer chains occurred. This resulted in the decrease in the weight of the synthesized composites.
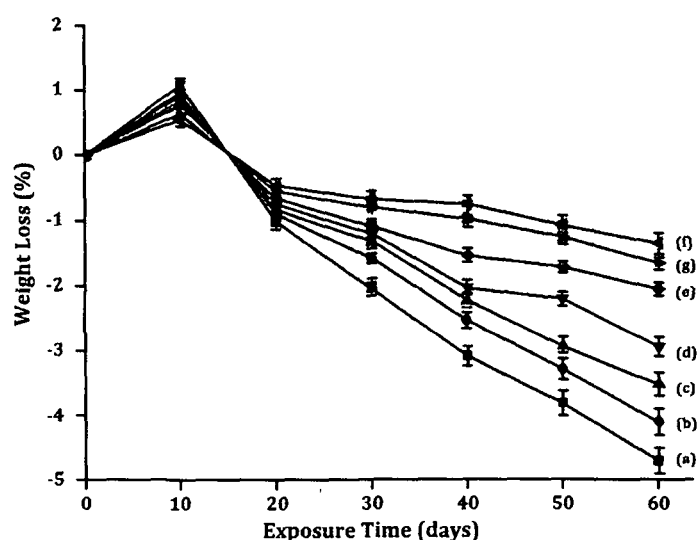


**Figure 4.3.6.** Weight loss vs Exposure time for (a) S/J/GA50, (b) S/J/GA50/T1, (c) S/J/GA50/T3, (d) S/J/GA50/T5, (e) S/J/GA50/T5/N1, (f) S/J/GA50/T5/N3 and (g) S/J/GA50/T5/N5.
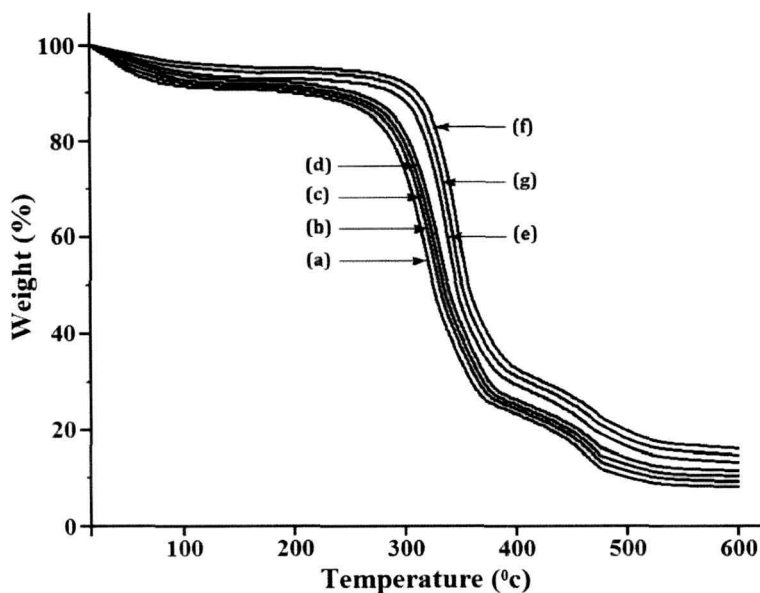
Figure 4.3.7 displays the FT-IR spectra of (a) S/J/GA50, (b) S/J/GA50/T1, (c) S/J/GA50/T3, (d) S/J/GA50/T5, (e) S/J/GA50/T5/N1, (f) S/J/GA50/T5/N3 and (g) S/J/GA50/T5/N5 after UV exposure. The carbonyl peak intensity was found to increase
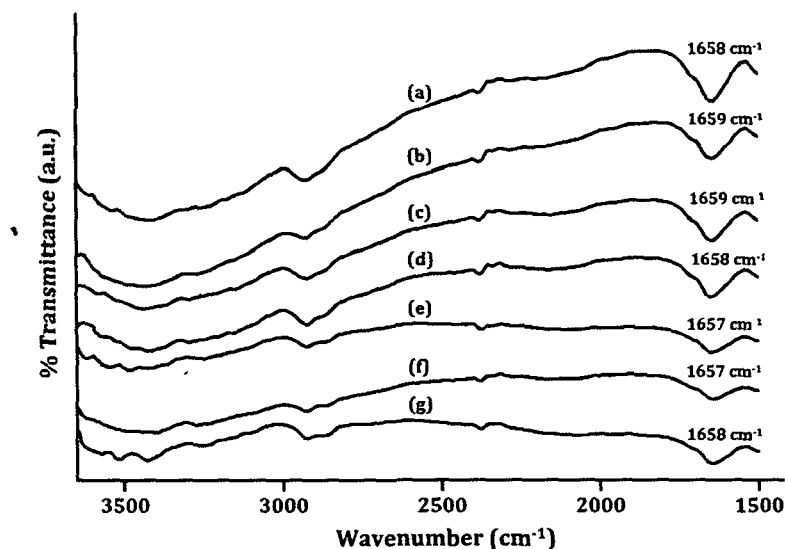


**Figure 4.3.7.** Change in carbonyl peak intensity of (a) S/J/GA50, (b) S/J/GA50/T1, (c) S/J/GA50/T3, (d) S/J/GA50/T5, (e) S/J/GA50/T5/N1, (f) S/J/GA50/T5/N3 and (g) S/J/GA50/T5/N5.

after irradiation of the samples for 60 days. Upon exposing the samples to UV-radiation, chain scission of the polymers took place and the carbonyl index value increased as shown in Figure 4.3.8. S/J/GA50/T5/N3 had lowest carbonyl index value whereas S/J/GA50 had the utmost one. $TiO_2$ nanoparticles played an important role for stabilizing the S/J composites by acting as a screen and slowed down the photo degradation process. $TiO_2$ nanoparticles absorbed the UV radiation and hence reduced the UV intensity required for the oxidation of the synthesized nanocomposites. Du *et al.* [55] observed an improvement in UV stability of WF/HDPE composite after the incorporation of $TiO_2$. The presence of nanoclay in the composite also has a screening effect which further delays the photo degradation process. Grigoriadou *et al.* [56] had observed an increase in UV stability of HDPE after incorporating montmorillonite clay. S/J/GA50/T5/N5 exhibits lower protection against UV with respect to S/J/GA50/T5/N3. This might be due to the agglomeration of nanoclay particles within the composite material.

**Figure 4.3.8.** Carbonyl Index value of (a) S/J/GA50, (b) S/J/GA50/T1, (c) S/J/GA50/T3, (d) S/J/GA50/T5, (e) S/J/GA50/T5/N1, (f) S/J/GA50/T5/N3 and (g) S/J/GA50/T5/N5.

It is well known that UV-radiation has a deterioration effect on many plastic materials. These materials, when exposed to the outdoor environment, undergo significant changes, namely, photo-degradation, causing loss of mechanical properties. Therefore, the changes in the mechanical properties of the composites after the UV treatment are presented in Table 4.3.3. Both the flexural and tensile properties were reduced after UV treatment. The loss of mechanical properties of unfilled composites was more significant compared to nanoparticles filled composites. S/J/GA50 was more prone to UV attack and hence it showed maximum loss of mechanical properties. The values presented in Table 3 suggested that the interfacial interactions among starch, jute, GA, $TiO_2$ nanoparticles and nanoclays were strong enough to decay the massive sheer due to rupture. Therefore, the resistance of S/J composite to UV instability, *i.e.*, photodegradation embrittlement, could be improved significantly with the addition of $TiO_2$ nanoparticles and nanoclays.

**Table 4.3.3.** Changes in the mechanical properties of Unfilled and Filled jute based crosslinked starch nanocomposites after UV Exposure.

| Composite System | Tensile Properties | | Flexural Properties | |
|---|---|---|---|---|
| | Strength (MPa) | Modulus (MPa) | Strength (MPa) | Modulus (MPa) |
| S/J/GA50 | 15.12 (±1.24) | 1025.4 (±11.45) | 35.23 (±1.24) | 2103.3 (±14.32) |
| S/J/GA50/T1 | 26.23 (±2.13) | 1414.6 (±13.42) | 46.12 (±1.64) | 2692.9 (±10.65) |
| S/J/GA50/T3 | 31.44 (±1.57) | 1593.7 (±12.23) | 57.21 (±1.35) | 3559.8 (±11.41) |
| S/J/GA50/T5 | 37.62 (±1.46) | 1803.1 (±11.52) | 66.76 (±2.14) | 4516.1 (±13.28) |
| S/J/GA50/T5/N1 | 45.32 (±1.11) | 1951.2 (±12.34) | 77.31 (±1.87) | 5428.6 (±14.86) |
| S/J/GA50/T5/N3 | 57.47 (±2.17) | 2498.9 (±15.76) | 96.11 (±2.65) | 6399.8 (±12.75) |
| S/J/GA50/T5/N5 | 51.71 (±1.23) | 2127.8 (±14.38) | 86.32 (±1.33) | 5768.2 (±15.34) |

Each value in the above table represents average of ten samples. Values in the parenthesis represent the standard deviation.

### 4.3.8. Dimensional stability test

The water vapour absorption study was carried out at room temperature (~ 30 °C) with 65 % relative humidity for different time period which is shown in Figure 4.3.9. From the figure, it is seen that for all the composites, the % swelling is increased with the increase in time. Water vapour absorption was found to decrease due to the presence of dispersed phase of $TiO_2$ nanoparticles in the composite system. Water vapour absorption of S/J/GA50/T composites decreased with the increase in $TiO_2$ nanoparticles content. $TiO_2$ nanoparticles act as a barrier to the passage of water as the

strong affinity of water molecules towards $TiO_2$ nanoparticles restricts its free motion and reduces the diffusion co-efficient of water. The well dispersed phase of $TiO_2$ nanoparticles improves the resistance of the composite and retards the motion of water molecules through it. The better the distribution of nanoparticles, the higher is the barrier property. Furthermore, the dimensional stability of the S/J/GA50/T5 composite was improved with the incorporation of nanoclay. This might be due to the fact that the silicate layers of nanoclay provide a tortuous path which hinders the diffusivity of water molecules through the nanocomposite [25]. As the nanoclay concentration was increased to 5 %, the superfluous filler congregates easily, decreasing the effective content of filler and therefore had little effect on decreasing of water vapour absorption. Nanoclay at higher concentration were found to become agglomerated within the composite which resulted in an increase in water vapour absorption capacity.
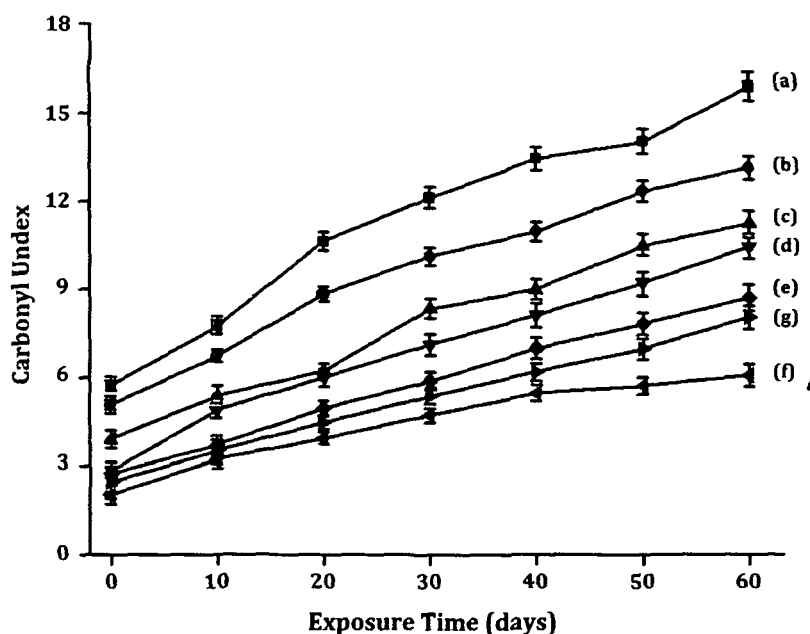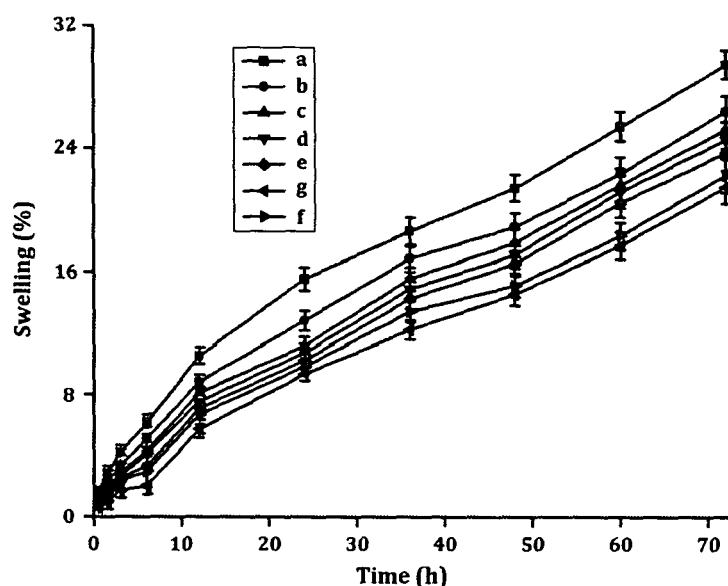


Figure 4.3.9. Swelling behaviour of (a) S/J/GA50, (b) S/J/GA50/T1, (c) S/J/GA50/T3, (d) S/J/GA50/T5, (e) S/J/GA50/T5/N1, (f) S/J/GA50/T5/N3 and (g) S/J/GA50/T5/N5.

### 4.3.9. LOI study

LOI values of jute based starch composites with different percentage of $TiO_2$ nanoparticles and nanoclay are depicted in Table 4.3.4. From the table, it is observed that all the samples produce small localised flame and nanoclay filled composites produce higher char than that of the nanoclay unfilled one. The LOI test assumes that inherently less flammable materials require greater oxygen concentrations to produce the heat necessary for the continuous production of flammable volatiles and flame

propagation. It is also observed that the LOI value increases with the increase in the concentration of $TiO_2$ nanoparticles in the composites. The surface hydroxyl groups of $TiO_2$ nanoparticles may interact with starch, jute and GA and thus restricts the accessibility of oxygen for the production of degradable components from the composites and hence improvement in LOI value was observed. However, on addition of nanoclay into $TiO_2$ nanoparticles filled composites, further enhancement in LOI value is observed. The incorporation of the nanoclay into the synthesized composite produces a silicate char on the surface of it and hence improves their flame resistance property. The silicate rich surface has better barrier property to heat and oxygen transport due to which ignition of the composite delays [57]. The LOI value is increased upto addition of 3 % of nanoclay. At higher concentration of nanoclay (5 %), the LOI value is decreased. At higher clay loading, the agglomeration of nanoclay results in decrease of interaction with concomitant reduction in barrier property as well as LOI value.

**Table 4.3.4.** LOI and Flaming Characteristics of the prepared composites.

| Samples | LOI (%) | Flame description | Smoke & Fumes | Char |
|---|---|---|---|---|
| S/J/GA50 | 40 (±2.0) | Small flame localised | Small and black smoke | Little |
| S/J/GA50/T1 | 44 (±1.0) | Small flame localised | Small and black smoke | Moderate |
| S/J/GA50/T3 | 52 (±1.0) | Small flame localised | Small and black smoke | Moderate |
| S/J/GA50/T5 | 55 (±2.0) | Small . localised flame | Small and black smoke | Moderate |
| S/J/GA50/T5/N1 | 60 (±2.0) | Small flame localised | Small and black smoke | Higher |
| S/J/GA50/T5/N3 | 67 (±1.0) | Small flame localised | Small and black smoke | Higher |
| S/J/GA50/T5/N5 | 63 (±2.0) | Small flame localised | Small and black smoke | Higher |

**Section D: Study on the effect of ZnO and nanoclay on jute fabric reinforced starch bio-nanocomposites**

The current interest on the conservation of natural resources and recycling has encouraged the researchers across the countries to focus more on renewable raw materials. Due to increasing global awareness, environmental legislation has made restriction on the use of traditional composites made of glass, carbon, aramid fibres etc. Therefore, the interest for greener and more sustainable technologies has focused attention in bio-based products and their development to reduce the dependence on fossil fuel and move to a sustainable materials basis [58, 59]. One of such potential material is the biopolymers, which exist abundantly worldwide.

Keeping in mind the advantages of biopolymers, nanofillers and most importantly the increasing demand for greener technologies, herein we demonstrated the preparation and characterization of biopolymer based nanocomposites consisting of starch, jute, glutaraldehyde, ZnO nanoparticle (ZNP), and nanoclay with high thermo-mechanical and UV-resistance property.

**4.4. RESULTS & DISCUSSION**

The codification and compositions of the obtained nanocomposites (each approximately 3 mm thick) are reported in Table 4.4.1. The samples as defined in Table 4.4.1, has been prepared by keeping the weight (%) of the components viz. starch, glycerol, glutaraldehyde and jute fixed while varying the weight percentages of ZNPs and nanoclay.

**Table 4.4.1.** Codification and filler content of the nanocomposites based on Jute and crosslinked Starch with zinc oxide nanoparticles and nanoclay (wt %).

| Sample | Starch (S) | Glycerol | Glutaraldehyde (GA) | Jute (J) | ZnO (Z) | Nanoclay (N) |
|---|---|---|---|---|---|---|
| S/J/GA50 | 100 | 5 | 50 | 75 | - | - |
| S/J/GA50/Z1 | 100 | 5 | 50 | 75 | 1 | - |
| S/J/GA50/Z3 | 100 | 5 | 50 | 75 | 3 | - |
| S/J/GA50/Z5 | 100 | 5 | 50 | 75 | 5 | - |
| S/J/G50/Z5/N1 | 100 | 5 | 50 | 75 | 5 | 1 |
| S/J/G50/Z5/N3 | 100 | 5 | 50 | 75 | 5 | 3 |
| S/J/G50/Z5/N5 | 100 | 5 | 50 | 75 | 5 | 5 |

### 4.4.1. XRD study

As an indirect but non-invasive technique, XRD analysis is accomplished to obtain comprehensive information regarding crystal structure of the nanoparticles (i.e. ZNP and nanoclay) and the synthesized composites. Figure 4.4.1 represents the diffractograms of jute, starch, ZNP, S/J/GA50, nanoclay and the nanocomposites. Jute (curve a) shows peaks at $2\theta = 22°$ (002 plane of cellulose I) and 19° (101 plane of cellulose II) [11]. Curve b implies the diffractograms of starch macromolecules. A little broader hump connoting the amorphous nature of starch is noticed at $2\theta = 19°$. Curve (c) shows the X-ray diffraction patterns of bare ZNPs. From Figure 4.4.1c, a series of characteristic peaks at $2\theta = 32°$ (100), 34.5° (002), 36.4° (101), 47.6° (102), 56.7° (110), 63° (103), 66.5° (200), 68° (112) and 69° (201) are observed and they are in accordance with the zincite phase of ZnO (International Centre for Diffraction Data, JCPDS 5-0664). Curve (d), the diffractograms of composites without ZnO (*i.e.* S/J/GA50) exhibits a small broad diffraction peak corresponding to jute and starch in the $2\theta$ range 1°-20°. Curve (e-g) are for jute based crosslinked starch nanocomposites (S/J/GA50/Z1, S/J/GA50/Z3, and S/J/GA50/Z5) with different percentage of ZNPs (1-5 % w/w of dry Starch). The crystalline peak intensities of jute and starch matrix appeared in the range $2\theta = 19° - 22°$ were found to diminish after the introduction of ZNPs within the composite. With the increase in the concentration of ZNPs, the peak intensity for jute and starch is further decreased [60]. However, at a higher amount of ZNP loading, the peaks corresponding to ZNPs appeared with higher intensity. A strong diffraction peak for nanoclay at $2\theta = 9°$ and a small peak at $2\theta = 24°$ is observed in curve-h. The peak at 9° resembles to a d-spacing of about 1.2 nm in pure clay. The diffraction peak of the nanoclay tactoids is absent in the X-ray diffractograms for 1% and 3% clay incorporated composites (Figure 4.4.1i, j). The $d_{001}$ peak of the clay within the synthesized nanocomposites is completely vanished, signifying the development of a delaminated structure in the nanocomposites. It can be said that either the full expansion of the nanoclay gallery occurs, which is not possible to identify by XRD, or the nanoclay layers are delaminated due to which no crystal diffraction peak appears. In S/J/G50/Z5/N5 composites, the position of the characteristic peak of nanoclay at $2\theta = 9°$ is found to shift to lower $2\theta$ values *(i.e. $2\theta = 7°$)* with less intensity representing an occurrence of agglomeration of clay within the nanocomposite.
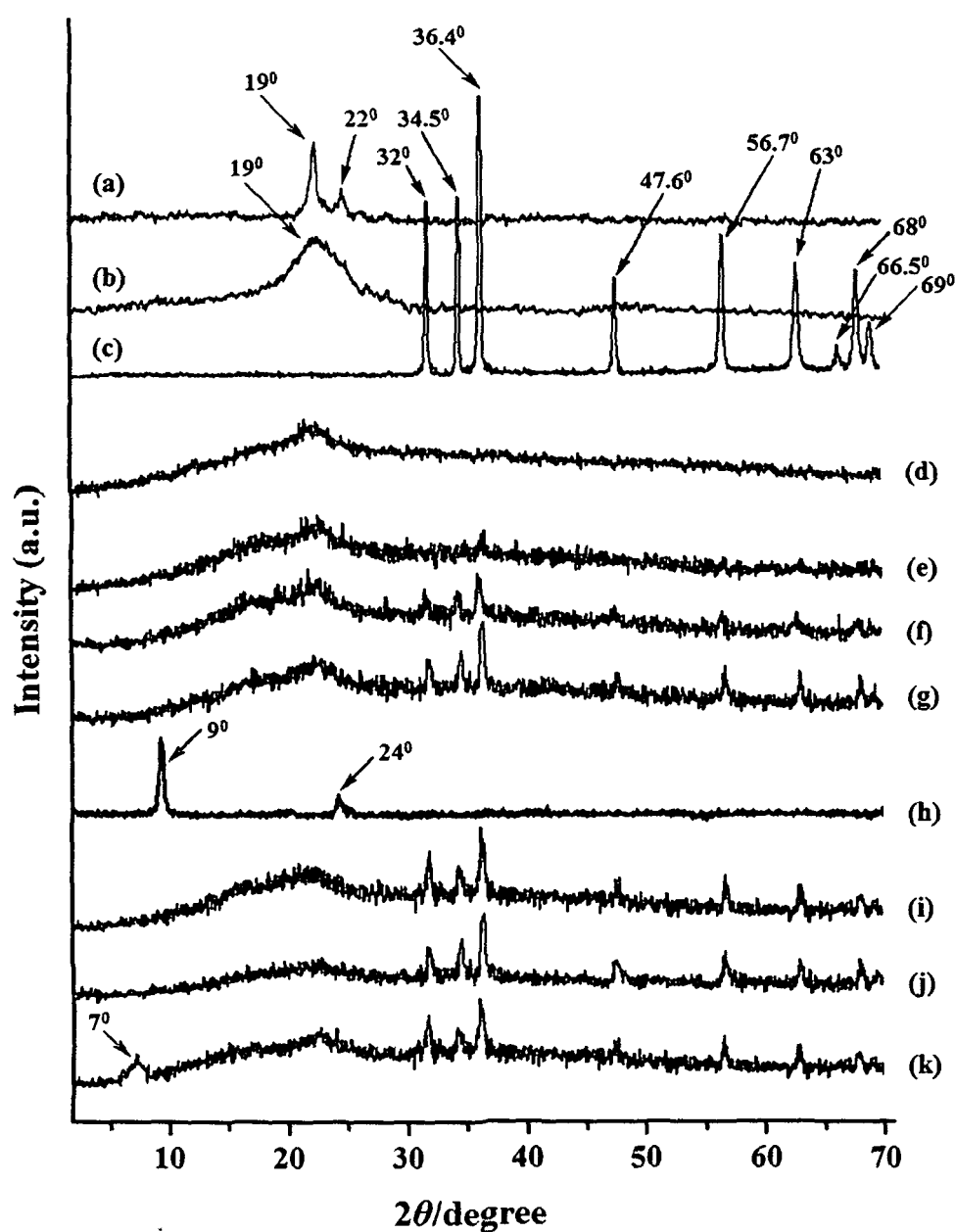
**Figure 4.4.1.** XRD pattern of (a) Jute, (b) Starch, (c) ZnO, (d) S/J/GA50, (e) S/J/GA50/Z1, (f) S/J/GA50/Z3, (g) S/J/GA50/Z5, (h) Nanoclay, (i) S/J/G50/Z5/N1, (j) S/J/G50/Z5/N3 and (k) S/J/G50/Z5/N5.

### 4.4.2. TEM study

The morphological features of the synthesized nanocomposites are provided by HRTEM investigation. Figures 4.4.2 (a-e) are the micrographs of the S/J/GA50, S/J/GA50/Z1, S/J/GA50/Z5, S/J/G50/Z5/N1 and S/J/G50/Z5/N5 samples, respectively. Figure 4.4.2a represents the TEM micrographs of composite without ZNPs and

nanoclay. Dark spots (shown by arrow marks) are appeared for ZNPs (Figure 4.4.2b, c) [61]. From the Figure 4.4.2b, c, it is clearly observed that the nanoparticles are well dispersed within the synthesized nanocomposites comprising of starch, and jute. TEM micrographs corresponding to S/J/G50/Z5/N1 sample shows the dispersion of nanoclay in the composite. The threadlike dark lines (indicated with arrows) signify the intersections of the clay layers, and the bright areas symbolize the S/J composite matrix. The presence of threadlike line suggest that nanoclay is not homogeneously distributed within the composite indicating the existence of partial compatibility between polymer, ZNPs and nanoclay surface. TEM micrographs clearly reveal the loss of stacking structure of clay layers and eventually dictates the disordered dispersion within the composite. However, at higher concentration of the nanoclay, the thickness of dark slices of nanoclay increases and as a result agglomeration takes place (Figure 4.4.2e). The results obtained from HRTEM analysis are in accordance with our XRD analysis. Both the results suggest the formation of the partially exfoliated nanocomposites.
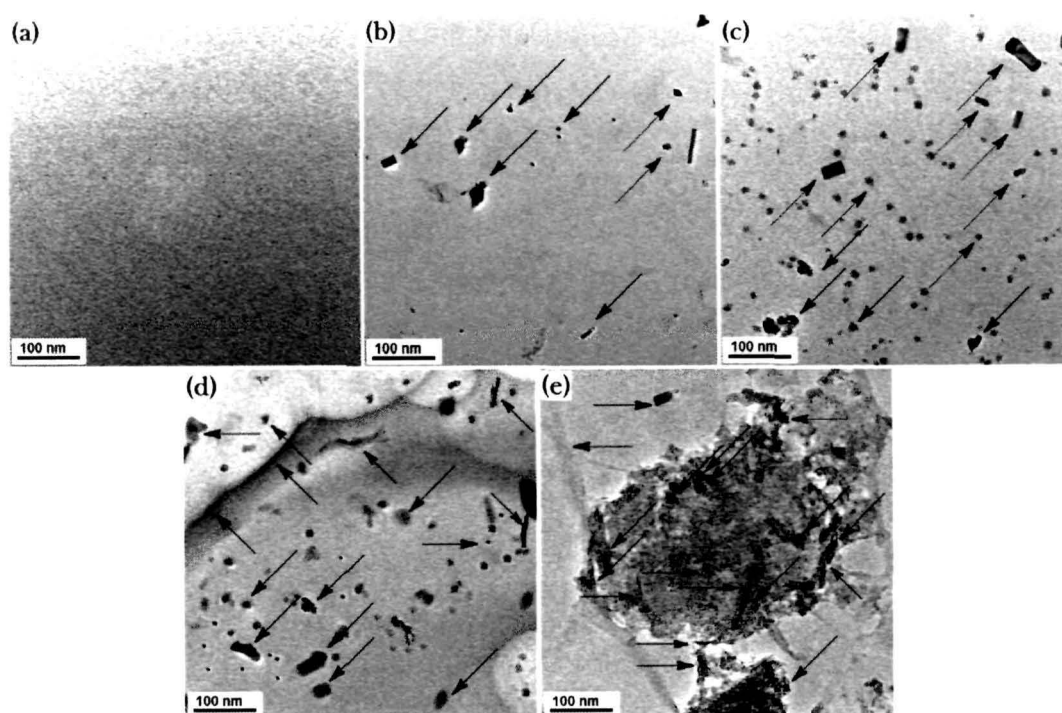


**Figure 4.4.2.** TEM micrograph of (a) S/J/GA50, (b) S/J/GA50/Z1, (c) S/J/GA50/Z5, (d) S/J/G50/Z5/N1 and (e) S/J/G50/Z5/N5.

### 4.4.3. SEM study

Scanning electron microscopy is considered as a vital tool for studying surface morphology of composite materials. Figure 4.4.3 shows SEM micrographs of S/J

composites with or without ZNP and nanoclay, and different percentage of ZNP and nanoclay. The fractured surface of some selective samples is considered for this study. S/J/GA50 sheet shows a relatively smooth surface (Figure 4.4.3a). Figure 4.4.3b inferred that the fracture surface of S/J/GA50/Z1 displays a homogenous structure suggesting a relatively uniform distribution of the ZNPs within the composite. However, as the ZNP content increased, *i.e.*, the fracture surface of S/J/GA50/Z5 containing higher amount of ZNP (Figure 4.4.3c) exhibits a relatively rough surface, indicating relatively high interfacial adhesion among starch, jute and ZNPs. Moreover, upon addition of nanoclay into the ZNP loaded nanocomposites (*i.e.* S/J/GA50/Z5), the roughness is found to enhance (Figure 4.4.3d, e, and f). This might be due to the fact that the clay particles enhance the interaction with the starch matrix and jute surface. The roughness of fractured surface of composite having 3 % nanoclay is more compared with those of composite prepared with 5 % nanoclay. This indicates that agglomeration of nanoclay particles may take place within the composite at higher concentration of clay due to which interaction of clay particles with starch and jute are diminished and less rough surface is appeared.
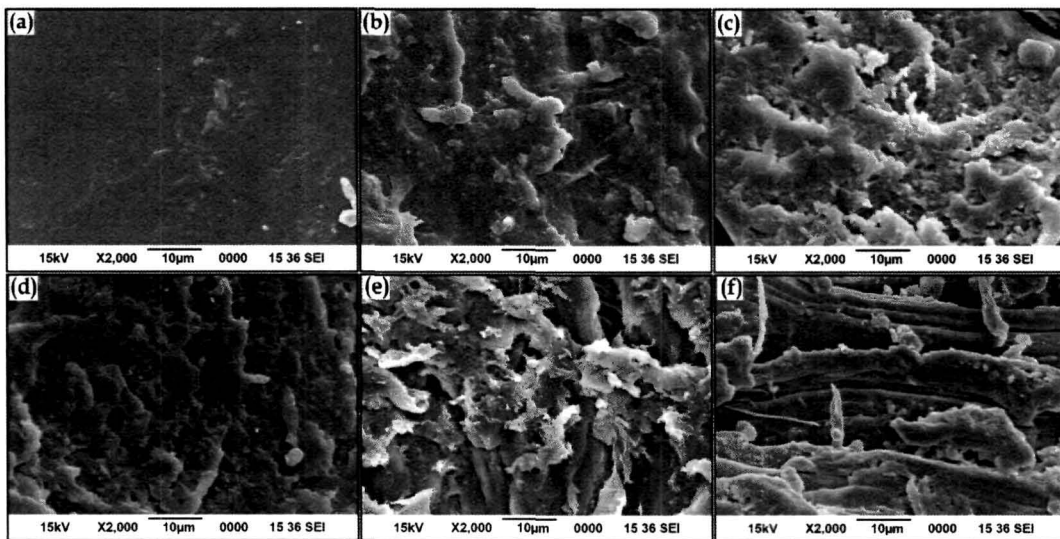


**Figure 4.4.3.** SEM micrographs of (a) S/J/GA50, (b) S/J/GA50/Z1, (c) S/J/GA50/Z5, (d) S/J/G50/Z5/N1, (e) S/J/G50/Z5/N3 and (f) S/J/G50/Z5/N5.

The fracture surface of ZNPs loaded composites taken for SEM study is also investigated by energy dispersive X-ray elemental analysis (EDX) simultaneously. Figure 4.4.4 shows the EDX analysis of jute reinforced starch composite. The presence of Zn along with C and O confirmed the successful incorporation of ZNP into the

composite. Elements such as Al, Na and Si, which are mainly from the silicate nanoclay, are also detected (Figure 4.4.4d) along with Zn, indicating the successful incorporation of nanoclay and ZNPs into the composite.
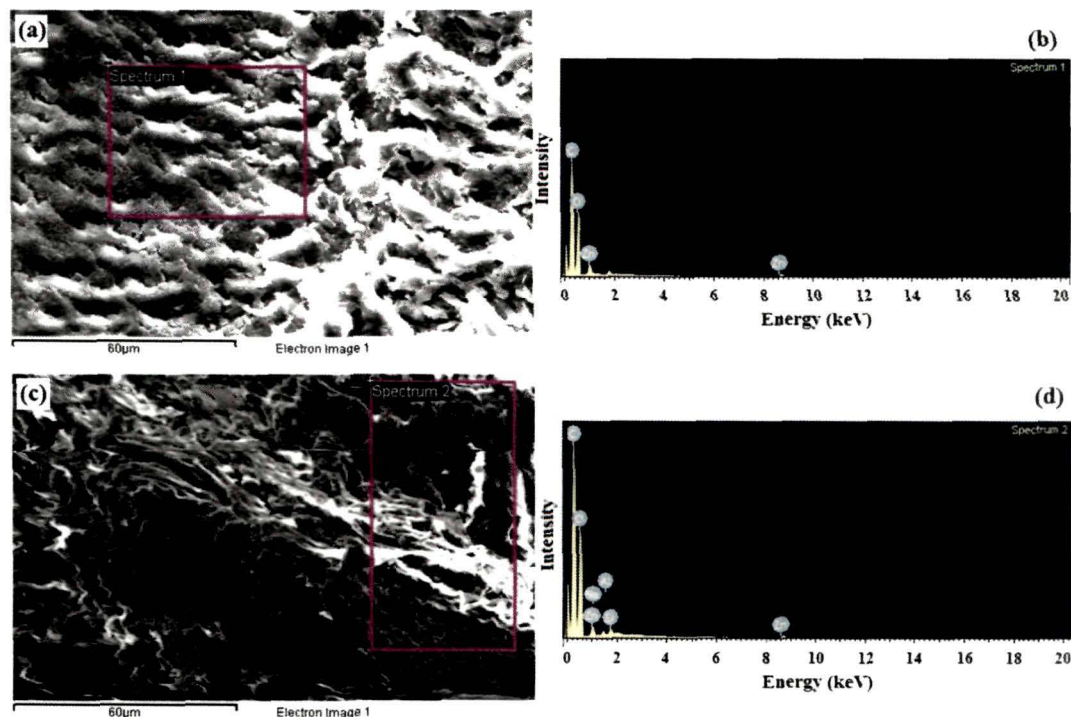


**Figure 4.4.4.** Energy dispersive X-ray analysis of S/J/GA50/Z5 and S/J/G50/Z5/N5.

### 4.4.4. FT-IR study

The interactions among starch, jute, glycerol, GA, ZNPs and clay are studied by FT-IR spectroscopy. FT-IR spectra of starch, jute clay and ZNPs are presented in Figure 4.4.5. The FT-IR spectrum of starch shows the absorption bands at 571, 981, 1161, 1653, 2921 and 3450 $cm^{-1}$ confirming the carbohydrate nature [7]. The typical saccharide bands appeared in the range 1180-950 $cm^{-1}$ was considered as the stretching mode of C–C and C–O vibration and the bending mode of C–H bond vibration [8]. The peak at 2921 $cm^{-1}$ is characteristic of the C–H stretching vibration of methylene group [32]. Jute shows the presence of peaks in the range 3440 $cm^{-1}$ for –OH stretching, 1737 $cm^{-1}$ for C=O stretching vibration of ester groups of hemicelluloses, 1642 $cm^{-1}$ for C=O stretching, 1254 $cm^{-1}$ for –C–O–C– bond in cellulose chain and 1057–1116 $cm^{-1}$ for C–O stretching [5]. Clay exhibits peaks at 3450 $cm^{-1}$ (–OH stretching), 1619 $cm^{-1}$ (–OH bending), 1030–460 $cm^{-1}$ (oxide bonds of metals like Si, Al, Mg etc.). FT-IR spectrum of ZNP is presented in Figure 4.4.5d. Absorption peaks at 3429 and 1633 $cm^{-1}$ in the spectra is due to –OH stretching and –OH bending vibrations while the high intensity

broad band at approximately 421 cm$^{-1}$ resulting from the stretching of the zinc and oxygen bond [62].
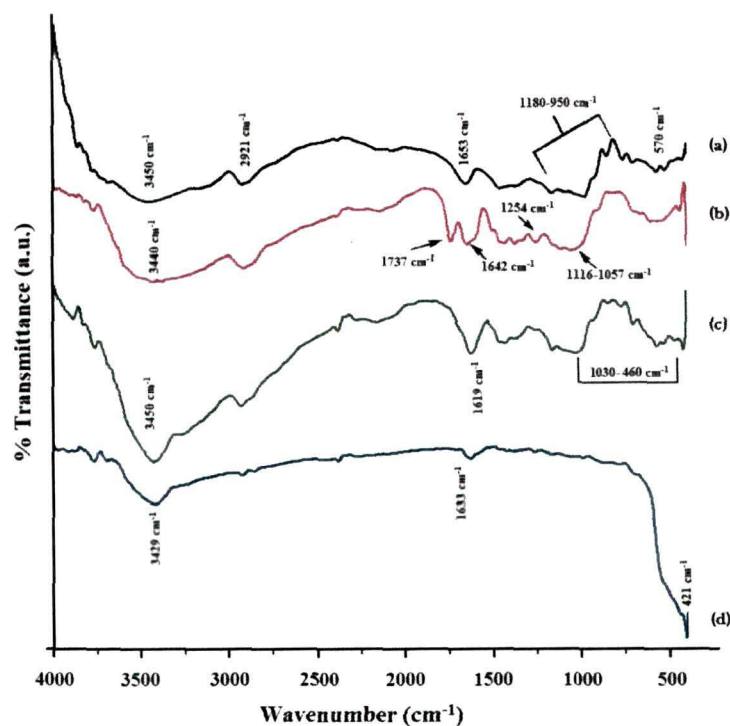


**Figure 4.4.5.** FT-IR spectra of (a) starch, (b) jute, (c) nanoclay and (d) ZNP.

FT-IR spectra for the composite S/J/GA50, S/J/GA50/Z1, S/J/GA50/Z3, S/J/GA50/Z5, S/J/G50/Z5/N1, S/J/G50/Z5/N3 and S/J/G50/Z5/N5 are shown in Figure 4.4.6. The FT-IR spectra for all the samples show peaks in the region 3400–3250 cm$^{-1}$, which could be attributed to the –OH stretching vibrations. The typical saccharide bands of starch appeared in the region of 1180–950 cm$^{-1}$. Similarly the characteristic peaks for jute has been appeared in all the spectrum at 1254 and 1116–1057 cm$^{-1}$. The entire spectra show the band around 900 cm$^{-1}$ which was due to the $\beta$-(1→4)-glycosidic linkages. The position of –OH and C=O stretching is shifted in the crosslinked composite (S/J/GA50) suggesting the interaction between jute and starch. From the IR spectrum, it was found that, with the increase in ZNP concentration the peak intensities of –OH band are decreased and slightly shifted to lower wavenumber. This behaviour could be ascribed to the interaction between the free –OH groups of starch and jute with –OH groups of ZNPs. The FT-IR spectra indicated the existence of a strong binding but no obvious formation of covalent bonds between the S/J/GA50 composites and ZNPs [61]. Upon the addition of nanoclay, the peaks in the ~3400 cm$^{-1}$ range are further

181

reduced in intensity and shifted to lower wavenumber. The peak intensities in the ranges of 1030–460 cm$^{-1}$ and 1620 cm$^{-1}$ are found to be reduced upto a considerable extent. These results confirm the participation of hydroxyl group of clay with S/J/GA50/Zn composites [52].
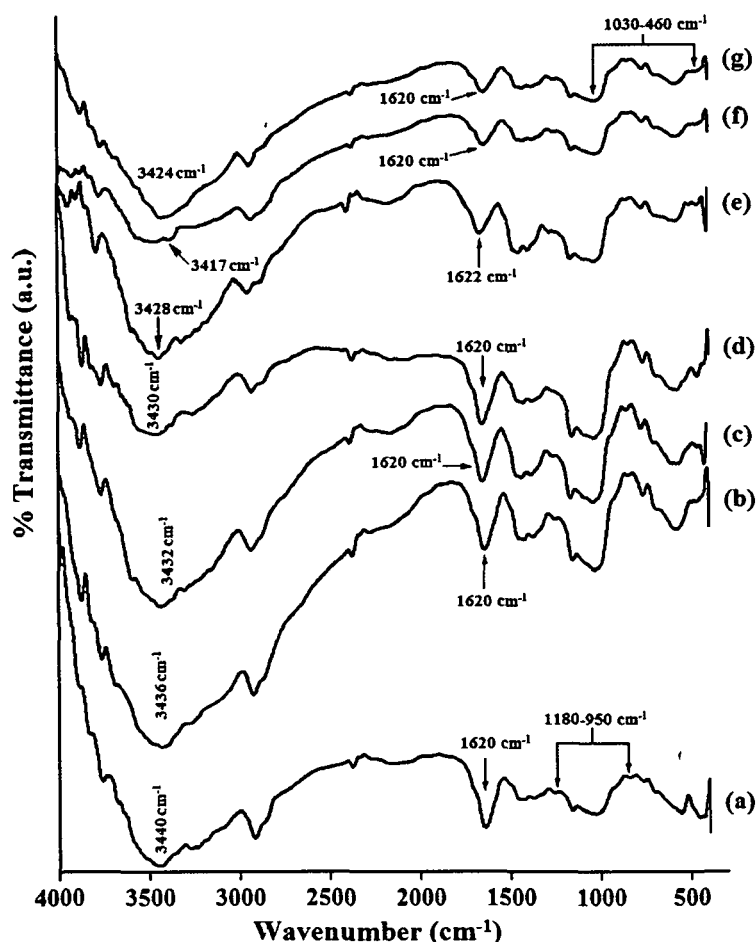


**Figure 4.4.6.** FT-IR spectra of (a) S/J/GA50, (b) S/J/GA50/Z1, (c) S/J/GA50/Z3, (d) S/J/GA50/Z5, (e) S/J/G50/Z5/N1, (f) S/J/G50/Z5/N3 and (g) S/J/G50/Z5/N5.

*4.4.5. Thermal property study*

The influence of ZNP and nanoclay on the thermal properties of the synthesized bio-nanocomposites is investigated by TGA as shown in Figure 4.4.7. Figure 4.4.7 displays the thermograms of S/J/GA50, S/J/GA50/Z1, S/J/GA50/Z3, S/J/GA50/Z5, S/J/G50/Z5/N1, S/J/G50/Z5/N3, and S/J/G50/Z5/N5. Table 4.4.2 (derived from Figure 4.4.7) shows the initial decomposition temperature ($T_i$), maximum pyrolysis temperature ($T_m$), decomposition temperature ($T_d$) at different weight loss (%) and residual weight (RW, %) of the nanocomposites upto 600 °C. All the thermograms show

an initial weight loss around 100 °C due to the loss of trapped water molecules. From the thermograms it is clearly inferred that all the values of the nanocomposites (Table 4.4.2) are found to increase with the increase in ZNPs concentration. This might be ascribed to the heat shielding effect of ZNPs [63]. Nanoclay is widely used to enhance the thermal stability of composite materials. After the incorporation of nanoclay, the thermal stability of the ZNP loaded nanocomposites was further improved. This increase in thermal stability of the synthesized nanocomposites is attributed to the hindered diffusion of volatile decomposition products within it. This might also be due to the physico-chemical absorption of the volatile degradation products on the silicate surface of nanoclay. The volatilization of the degraded products originated by carbon-carbon bond scission in the composite is delayed by tortuous path provided by the silicate layers. Clay treated composites show a subsidiary enhancement in RW values over clay untreated one [39]. At higher concentration of clay, the agglomeration probably decreased the interaction and can give rise to the reduction in the thermal stability. Therefore, it is concluded that the thermal stability of S/J composites is increases on addition of upto a certain concentration of ZNP and nanoclay.
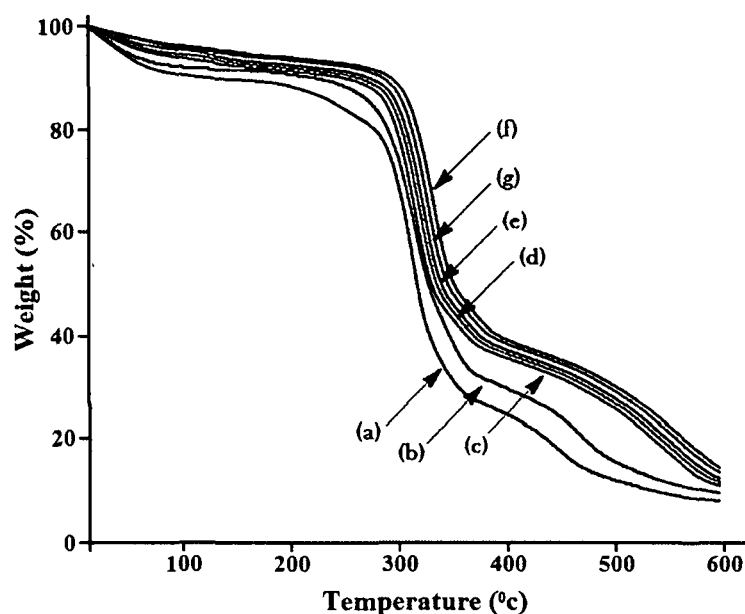


Figure 4.4.7. TGA thermograms of (a) S/J/GA50, (b) S/J/GA50/Z1, (c) S/J/GA50/Z3, (d) S/J/GA50/Z5, (e) S/J/G50/Z5/N1, (f) S/J/G50/Z5/N3 and (g) S/J/G50/Z5/N5.

**Table 4.4.2.** Thermal Properties of (a) S/J/GA50, (b) S/J/GA50/Z1, (c) S/J/GA50/Z3, (d) S/J/GA50/Z5, (e) S/J/GA50/Z5/M1, (f) S/J/GA50/Z5/M3 and (g) S/J/GA50/Z5/M5.

| Sample Particulars | $T_i$ | $^aT_m$ | $^bT_m$ | Temperature of Decomposition at different weight loss (%) | | | | | RW % at 600 °C |
| --- | --- | --- | --- | --- | --- | --- | --- | --- | --- |
| | | | | 20 | 30 | 40 | 50 | 60 | |
| S/J/GA50 | 199±2 | 321±1 | 367±2 | 285±1 | 304±1 | 314±2 | 321±2 | 324±1 | 6±2 |
| S/J/GA50/Z1 | 205±1 | 325±1 | 371±1 | 294±2 | 310±2 | 320±1 | 325±1 | 347±2 | 9±2 |
| S/J/GA50/Z3 | 208±2 | 327±2 | 376±1 | 305±1 | 313±1 | 325±2 | 331±3 | 366±1 | 12±2 |
| S/J/GA50/Z5 | 214±3 | 333±2 | 381±2 | 311±1 | 318±1 | 329±1 | 335±2 | 372±3 | 14±1 |
| S/J/GA50/Z5/N1 | 218±2 | 338±1 | 388±3 | 314±1 | 325±3 | 332±2 | 340±1 | 378±2 | 15±3 |
| S/J/GA50/Z5/N3 | 231±1 | 349±1 | 403±2 | 324±3 | 333±1 | 343±1 | 354±1 | 397±1 | 17±2 |
| S/J/GA50/Z5/N5 | 224±2 | 343±2 | 394±1 | 319±2 | 328±1 | 337±2 | 347±2 | 385±2 | 16±2 |

$T_i$ : initial decomposition temperature.

$^aT_m$ : maximum pyrolysis temperature value for 1$^{st}$ step.

$^bT_m$ : maximum pyrolysis temperature value for 2$^{nd}$ step.

Each value in the table represents average value of three samples.

### 4.4.6. Mechanical property study

The mechanical properties of S/J composites reinforced with ZNPs and nanoclay are studied at room temperature. From these measurements, we have determined the flexural strength, flexural modulus, tensile strength and tensile modulus. Experimental data are deposited in Table 4.4.3. A noticeable reinforcing effect is observed upon filler addition, as displayed by the increase in both the modulus and strength for composite compared to the unfilled composites. The increase in the concentration of ZNP might have the direct effect in increasing the mechanical properties of the nanocomposites [62]. As the ZNPs content increased, both the tensile and flexural properties of the nanocomposites also increased. The interaction of ZnO with crosslinked starch and jute through its surface hydroxyl group may stiffen the composites and results in enhancement of mechanical properties. Considering the 5 % concentration of the ZNPs as optimum, we have further modified the composites viz. S/J/GA50Zn5/M1. S/J/GA50/Zn5/M3 and S/J/GA50/Zn5/M5 having different percentage of nanoclay ranging from 1-5 % ($^w$/$_w$ of starch). With the incorporation of nanoclay, composites show a significant improvement in the mechanical properties with respect to the nanoclay untreated one. The reason for such improvement in mechanical properties of the composites may be the high aspect ratio of the nanoclay which generates a large surface area for the polymer chains absorption. Clay acts as a rigid reinforcement to the polymer matrix. The interaction of the polymer chains into the galleries of nanoclay restricts its mobility [43]. However, such improvement in mechanical properties with the incorporation of nanoclay may only be realized up to a certain clay loading. In our work, the enhancement in mechanical properties is found up to clay loading of 3 %, and beyond that it declines on further addition of nanoclay. At higher concentration of nanoclay, agglomeration of clay particles may takes place and therefore the interaction between polymer-clay is reduced. This led to the reduction in the extent of enhancement of reinforcement efficiency with the addition of higher amount of nanoclay.

**Table 4.4.3.** Comparison of Tensile and Flexural properties of Unfilled and Filled jute based crosslinked starch nanocomposites before UV treatment

| Composite System | Tensile Properties | | Flexural Properties | |
|---|---|---|---|---|
| | Strength (MPa) | Modulus (MPa) | Strength (MPa) | Modulus (MPa) |
| S/J/GA50 | 22.23 (±2.35) | 1272.7 (±14.74) | 42.41 (±1.43) | 2425.2 (±12.47) |
| S/J/GA50/Z1 | 30.45 (±1.63) | 1685.9 (±11.53) | 50.42 (±2.62) | 3076.3 (±09.84) |
| S/J/GA50/Z3 | 36.78 (±1.13) | 1857.4 (±12.22) | 60.68 (±1.78) | 3987.7 (±10.54) |
| S/J/GA50/Z5 | 41.23 (±2.42) | 2019.6 (±16.56) | 68.45 (±0.94) | 4867.8 (±11.67) |
| S/J/GA50/Z5/N1 | 49.57 (±1.86) | 2258.7 (±11.85) | 83.75 (±1.54) | 5789.6 (±14.24) |
| S/J/GA50/Z5/N3 | 59.65 (±2.27) | 2648.3 (±13.42) | 99.57 (±2.25) | 6656.1 (±13.49) |
| S/J/GA50/Z5/N5 | 54.89 (±1.73) | 2414.8 (±12.61) | 90.42 (±2.11) | 6027.3 (±15.32) |

Each value in the above table represents average of ten samples. Values in the parenthesis represent the standard deviation.

### 4.4.7. UV test results

The weight loss of S/J composite and S/J composite loaded with ZNPs and nanoclay is shown in Figure 4.4.8. Weight losses of the samples are determined at room temperature as a function of exposure time and found linear variation with exposure time. Initially a small increase of weight is found due to moisture uptake by the samples, which is greater than the material loss induced by the degradation in the early stage. The rate of weight loss is lowest for S/J/G50/Z5/N3 followed by S/J/G50/Z5/N5, S/J/G50/Z5/N1, S/J/GA50/Z5, S/J/GA50/Z3, S/J/GA50/Z1 and S/J/GA50. The ZNPs and nanoclay unfilled composite shows maximum weight losses. After 60 days of exposure, the weight losses in S/J/GA50, S/J/GA50/Z1, S/J/GA50/Z3, S/J/GA50/Z5, S/J/G50/Z5/N1, S/J/G50/Z5/N3 and S/J/G50/Z5/N5 are −4.41 % ± 0.4 %, −3.76 % ± 0.5 %, −3.12 % ± 0.3 %, −2.54 % ± 0.3 %, −1.67 % ± 0.2 %, −1.02 % ± 0.2 %, and −1.28 % ± 0.2 % respectively. Results presented are the average of four specimens. The lower weight loss (%) for S/J/G50/Z5/N3 composites after UV exposure is due to the UV shielding ability of ZNPs and nanoclay. On exposure to UV radiation, the chain scission followed by decrease in the density of the entanglements of the polymer chains occurred. This lead to the decrease in the weight of the synthesized composites.
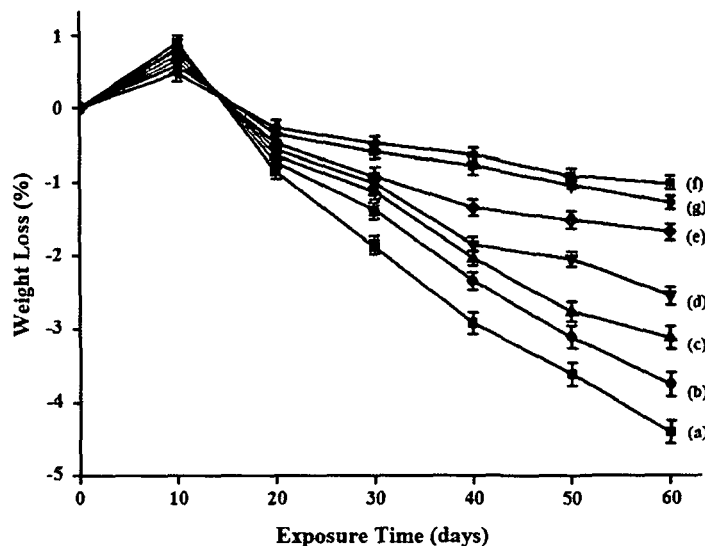


**Figure 4.4.8.** Weight loss vs Exposure time for (a) S/J/GA50, (b) S/J/GA50/Z1, (c) S/J/GA50/Z3, (d) S/J/GA50/Z5, (e) S/J/G50/Z5/N1, (f) S/J/G50/Z5/N3 and (g) S/J/G50/Z5/N5.

Figure 4.4.9 represents the FT-IR spectra of (a) S/J/GA50, (b) S/J/GA50/Z1, (c) S/J/GA50/Z3, (d) S/J/GA50/Z5, (e) S/J/G50/Z5/N1, (f) S/J/G50/Z5/N3 and (g) S/J/G50/Z5/N5after UV exposure, respectively. The intensity of the carbonyl peaks is found to increase after irradiation of the samples for 60 days. Upon exposing the samples to UV-radiation, chain scission of the polymers takes place and the carbonyl index value increases as shown in Figure 4.4.10. The S/J/G50/Z5/N3 has lowest carbonyl index value whereas S/J/GA50 has the highest one. ZNP plays an important role of stabilizing the jute based crosslinked starch composites by acting as screen and slows down the photo degradation process. ZNP absorbs the UV radiation and hence reduces the UV intensity required for the oxidation of the synthesized nanocomposites [64]. The presence of nanoclay in the composite also has a screening effect which further delays the photo degradation process. Grigoriadou *et al.* [56] has observed an increase in UV stability of HDPE after incorporating montmorillonite clay. S/J/G50/Z5/N5 exhibits lower protection against UV with respect to S/J/G50/Z5/N3. This might be due to the agglomeration of nanoclay particles within the composite material which provides lower protection against photodegradation.
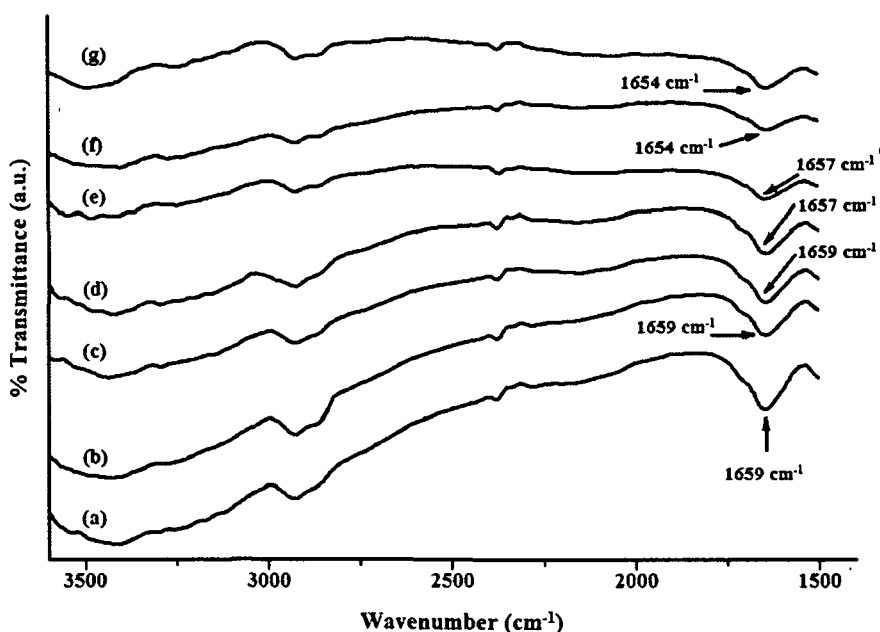


**Figure 4.4.9.** Change in carbonyl peak intensity of (a) S/J/GA50, (b) S/J/GA50/Z1, (c) S/J/GA50/Z3, (d) S/J/GA50/Z5, (e) S/J/G50/Z5/N1, (f) S/J/G50/Z5/N3 and (g) S/J/G50/Z5/N5.

It is well known that UV-radiation has a deterioration effect on many plastic materials. These materials, when exposed to the outdoor environment, undergo significant changes, namely, photo-degradation, causing loss of mechanical properties. Therefore, the changes in the mechanical properties of the composites after the UV treatment are presented in Table 4.4.4. Both the flexural and tensile properties reduced after UV treatment. The loss of mechanical properties of unfilled composites is more significant compared to nanoparticles filled composites. S/J/GA50 is more prone to UV attack and hence it shows maximum loss of mechanical properties. The values presented in Table 4.4.4 suggest that the interfacial interactions among starch, jute, GA, ZNPs and nanoclays are strong enough to decay the massive sheer due to rupture. Therefore, the resistance of jute based crosslinked starch composite to UV instability, *i.e.*, photodegradation embrittlement, can be improved significantly with the addition of nanoparticles.



Figure 4.4.10. Carbonyl Index value of (a) S/J/GA50, (b) S/J/GA50/Z1, (c) S/J/GA50/Z3, (d) S/J/GA50/Z5, (e) S/J/G50/Z5/N1, (f) S/J/G50/Z5/N3 and (g) S/J/G50/Z5/N5.

189

**Table 4.4.4.** Changes in the mechanical properties of Unfilled and Filled jute based crosslinked starch nanocomposites after UV Exposure

| Composite System | Tensile Properties | | | Flexural Properties | | |
|---|---|---|---|---|---|---|
| | Strength (MPa) | Changes after UV study (%) | Modulus (MPa) | Strength (MPa) · | Changes after UV study (%) | Modulus (MPa) |
| S/J/GA50 | 14.05 (±1.11) | 36.8 | 1022.2 (±15.23) | 34.52 (±1.32) | 13.4 | 2099.2 (±12.82) |
| S/J/GA50/Z1 | 25.68 (±1.79) | 15.6 | 1412.2 (±11.24) | 44.34 (±1.57) | 12.5 | 2689.4 (±11.53) |
| S/J/GA50/Z3 | 30.84 (±1.52) | 16.1 | 1589.8 (±13.56) | 55.25 (±1.68) | 10.8 | 3556.2 (±15.67) |
| S/J/GA50/Z5 | 36.56 (±1.78) | 11.3 | 1798.5 (±15.31) | 64.57 (±1.25) | 7.3 | 4511.9 (±10.84) |
| S/J/G50/Z5/N1 | 44.72 (±1.65) | 9.8 | 1948.5 (±11.78) | 76.31 (±1.54) | 6.2 | 5425.7 (±11.48) |
| S/J/G50/Z5/N3 | 56.34 (±1.13) | 5.5 | 2494.2 (±14.54) | 95.58 (±1.11) | 3.9 | 6396.5 (±13.43) |
| S/J/G50/Z5/N5 | 50.61 (±2.11) | 7.7 | 2124.4 (±12.56) | 85.74 (±2.25) | 4.4 | 5765.8 (±12.22) |

Each value in the above table represents average of ten samples. Values in the parenthesis represent the standard deviation.

## 4.4.8. Dimensional stability test

The water vapour absorption study was carried out at room temperature with 65 % relative humidity for different time period is shown in Figure 4.4.11. Form the figure, it is seen that for all the composites, the % swelling is increased with increase in time. Water vapour absorption is found to decrease due to the presence of dispersed phase of ZNPs in the composite system. Water vapour absorption of S/J/GA50/Z composites decreased with the increase in ZNP content [60]. ZNPs act as a barrier to the passage of water as the strong affinity of water molecules towards ZNPs restricts its free motion and reduces the diffusion co-efficient of water. The well dispersed phase of ZNPs improves the resistance of the composite and retards the motion of water molecules through it. The better the distribution of nanoparticles, the higher is the barrier property. Further, the dimensional stability of the S/J/GA50/Z composite is improved with the incorporation of nanoclay. This may be due to the fact that the silicate layers of nanoclay provide a tortuous path which hinders the diffusivity of water particles through the nanocomposite [25]. As the nanoclay concentration is increased to 5 %, the superfluous filler congregates easily, decreasing the effective content of filler and therefore has little effect on decreasing of water vapour absorption.
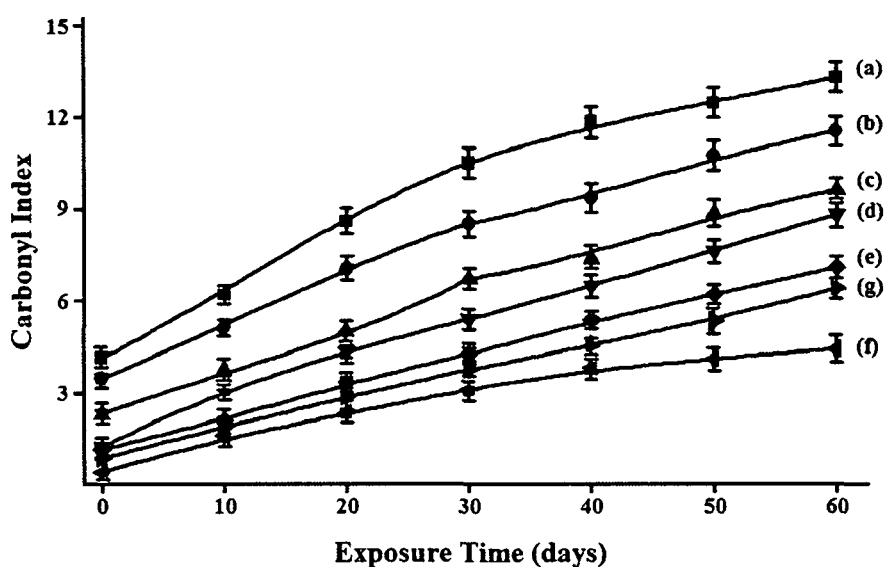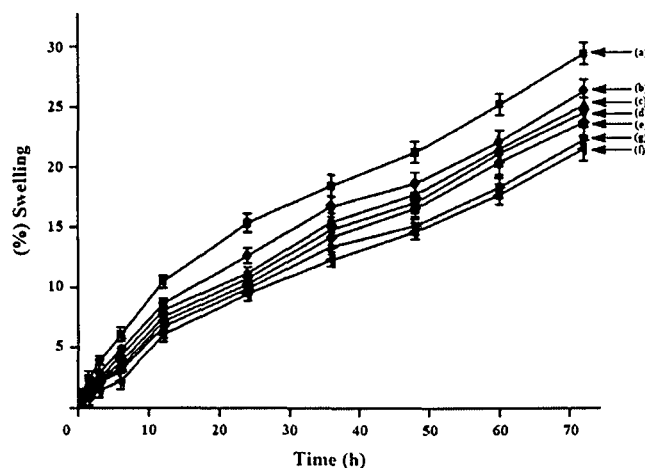


**Figure 4.4.11.** Swelling behaviour of (a) S/J/GA50, (b) S/J/GA50/Z1, (c) S/J/GA50/Z3, (d) S/J/GA50/Z5, (e) S/J/G50/Z5/N1, (f) S/J/G50/Z5/N3 and (g) S/J/G50/Z5/N5.

## 4.4.9. LOI study

LOI values of jute based starch composites with different percentage of ZNP and nanoclay are depicted in Table 4.4.5. From the table, it is inferred that all the samples produce small localised flame and nanoclay filled composites produces higher

char than that of the nanoclay unfilled one. The LOI test assumes that inherently less flammable materials require greater oxygen concentrations to produce the heat necessary for the continuous production of flammable volatiles and flame propagation. It is also observed that the LOI value increases with the increase in the concentration of ZNPs in the composites. The surface hydroxyl group of ZNPs may interact with starch, jute and GA and thus restricts the accessibility of oxygen for the production of degradable components from the composites and hence improvement in LOI value is found [65]. However, on addition of nanoclay into ZNP incorporated composites, further enhancement in LOI value is observed. The incorporation of the nanoclay into the synthesized composite produces a silicate char on the surface of it and hence improves their flame resistance property. The silicate rich surface has better barrier property to heat and oxygen transport due to which ignition of the composite delays [23]. The LOI value is increased upto the addition of 3 % of nanoclay. At higher concentration of nanoclay (5 %), the LOI value is decreased. At higher clay loading condition, the agglomeration of nanoclay results in decrease of interaction with concomitant reduction in barrier property as well as LOI value.

**Table 4.4.5.** LOI and Flaming Characteristics of the prepared composites.

| Samples | LOI (%) | Flame description | Smoke & Fumes | Char |
|---|---|---|---|---|
| S/J/GA50 | 41 (±1.0) | Small localised flame | Small and black smoke | Little |
| S/J/GA50/Z1 | 46 (±2.0) | Small localised flame | Small and black smoke | Higher |
| S/J/GA50/Z3 | 51 (±2.0) | Small localised flame | Small and black smoke | Higher |
| S/J/GA50/Z5 | 56 (±1.0) | Small localised flame | Small and black smoke | Higher |
| S/J/GA50/Z5/N1 | 61 (±3.0) | Small localised flame | Small and black smoke | Higher |
| S/J/GA50/Z5/N3 | 68 (±2.0) | Small localised flame | Small and black smoke | Higher |
| S/J/GA50/Z5/N5 | 64 (±2.0) | Small localised flame | Small and black smoke | Higher |

Each value represents average five samples.

### *4.4.10. Biodegradation study*

S/J composites are exposed to cellulolytic bacterial strain directly in broth culture medium for the biodegradation study. After one month of incubation of the samples in broth culture media, the growth of bacteria and degradation of the composite samples is clearly detectable. The bacterial growth of the samples with respect to time is represented by Figure 4.4.12. The microbial attack is more in case of ZNP free composite compared to the composite filled with ZNP and nanoclay. Initially, the
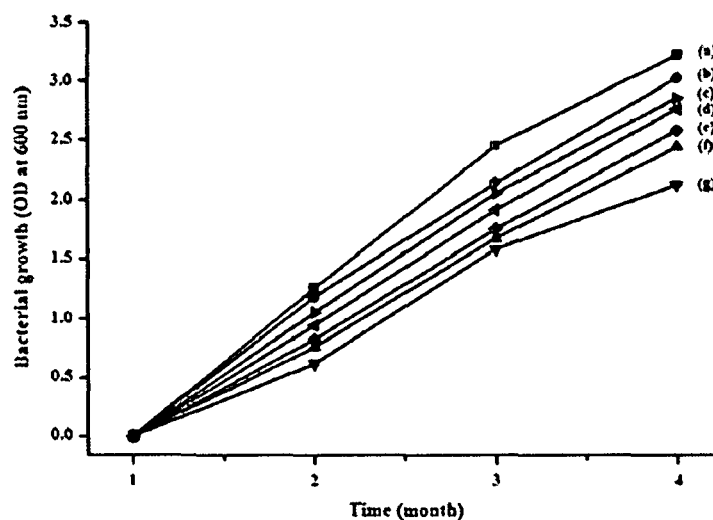


**Figure 4.4.12.** Bacterial growth of (a) S/J/GA50, (b) S/J/G50/Z5/N5, (c) S/J/G50/Z5/N3, (d) S/J/G50/Z5/N1, (e) S/J/GA50/Z1, (f) S/J/GA50/Z3 and (g) S/J/GA50/Z5.

growth of the bacterial strains increased quite steadily with bacterial exposure time, but the rate of growth slightly decreased after 3 month of incubation. As the composites are mainly comprised of starch and jute which are basically carbohydrate and cellulose, these two are very good carbon source for the bacteria due to which higher rate of bacterial growth is observed. The powerful cellulolytic and pectinolytic activity of bacteria could be a reason for the enhancement of bacterial growth [66]. After 3 months, the rate of microbial growth is slightly diminished due to the production of toxic metabolites by the microbes. In our study, the growth of bacteria and degradation of the samples are revealed by SEM study (Figure 4.4.13). SEM is used to observe the extent of physical breakdown of S/J polymer composites. SEM shows different levels of degradation, colonized nanoclay S/J composite sometimes only shows superficial degradation whereas, ZNP incorporated S/J composites show less degradation as ZnO

sometimes acts as a fungicide and protective agent [67]. The degradation is more in the unfilled S/J composites as starch and jute are gradually breakdown in the broth culture media. The lower biodegradability of filled S/J nanocomposites is sacrificed considering the enhanced thermal and mechanical properties. However, in case of nanoclay incorporated composites, the rate of degradation increases with increasing the concentration of nanoclay in S/J composites. The catalytic role plays by the nanoclay may be the cause of this degradation [68, 69]. In bacterial media the degradation of S/J polymer composites is a complex process involving four phenomena: (i) water adsorption, (ii) bond cleavage and formation of oligomer fragments, (iii) solubilisation of oligomer fragments, and finally (iv) diffusion of soluble oligomers by bacteria [70, 71]. Therefore, the factor that increases the hydrolysis tendency of S/J composites eventually controls the degradation of the composites. In case of nanoclay incorporated composites, the presence of unreacted terminal hydroxyl group may be the responsible factors for this behaviour [72].
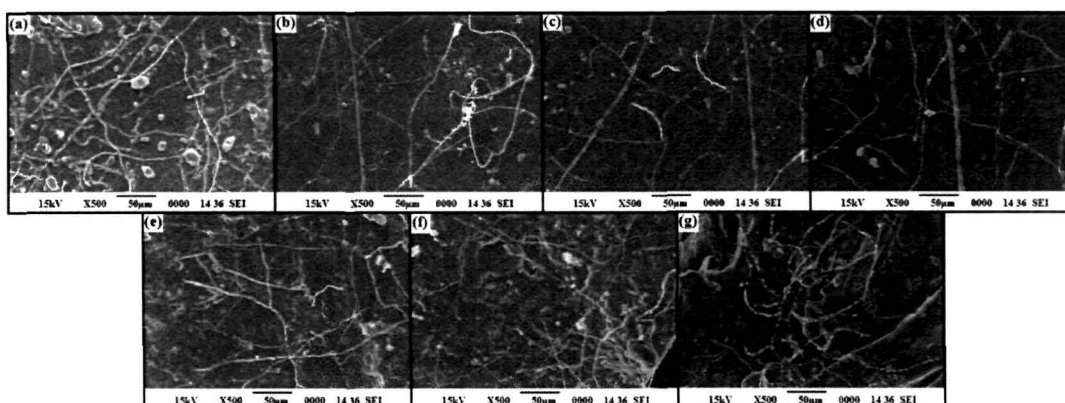


**Figure 4.4.13.** SEM micrographs of samples after microbial test on (a) S/J/GA50, (b) S/J/GA50/Z1, (c) S/J/GA50/Z3, (d) S/J/GA50/Z5, (e) S/J/G50/Z5/N1, (f) S/J/G50/Z5/N3, and (g) S/J/G50/Z5/N5.

## References

[1] Ma, X., et al. *Carbohydr. Polym.* **62**(1), 19--24, 2005.

[2] Satyanarayana, K.G., et al. *Prog. Polym. Sci.* **34**(9), 982--1021, 2009.

[3] Bastioli, C. Starch polymer composites in *Degradable polymers – Principles and Applications*. G. Scott, & D. Gillead, eds., Chapman and Hall, London, 1995, 112—132.

[4] Saheb, D.N. & Jog, J.P. *Adv. Polym. Technol.* **18**(4), 351--363, 1999.

[5] Ray, D. & Sarkar, B. K. *J. App. Polym. Sci.* **80**(7), 1013--1020, 2001.

[6] Plackett, D., et al. *Compos. Sci. Technol.* **63**(8), 1287--96, 2003.

[7] Aboubakar, et al. *J. Food Eng.* **86**(2), 294--305, 2008.

[8] Liu, H., et al. Carbohydr. Polym. **83**(4), 1591--1597, 2011.

[9] Deka, B.K. & Maji, T.K. *Composites Part A* **42**(6), 686--693, 2011.

[10] Huang, X., & Netravali, A. N. *Biomacromolecules* **7**(10), 2783--2789, 2006.

[11] Kvien, I., et al. *J. Mater. Sci.* **42**(19), 8163--8171, 2007.

[12] Lu, W. H., et al. *Forest. Stud. China* **8**(1), 35-40, 2006.

[13] Chen, P. & Zhang, L. *Biomacromolecules* **7**(6), 1700--1706, 2006.

[14] Yoonessi, M., et al. *Macromolecules* **37**(7), 2511--2518, 2004.

[15] Hillberg, A. L., et al. *Biomaterials* **30**(27), 4463--4470, 2009.

[16] Ray, D., et al. *Macromol. Mater. Eng.* **292**(10-11), 1075--1084, 2007.

[17] Cai, X., et al. *Composites Part A* **39**(5), 727--737, 2008.

[18] Ramaraj, B. *J. Appl. Polym. Sci.* **103**(2), 909--916, 2007.

[19] Becker, O., et al. *Macromolecules* **36**(5), 1616--1625, 2003.

[20] Gilman, J. W., et al. *Chem. Mater.* **12**(7), 1866--1873, 2000.

[21] Zanetti, M., et al. *Macromol. Rapid. Commun.* **22**(3), 176--180, 2001.

[22] Qin, H., et al. *Polym. Degrad. Stab.* **85**(2), 807--813, 2004.

[23] Urbanczyk, L., et al. *J. Mater. Chem.* **20**(8), 1567--1575, 2010.

[24] Das, K., et al. *Ind. Eng. Chem. Res.* **49**(5), 2176--2185, 2010.

[25] Rana, H. T., et al. *AIChE J.* **51**(12), 3249--3256, 2005.

[26] Wang, Y., et al. *Macromol. Biosci.* **6**(7), 524--531, 2006.

[27] Chrissopoulou, K., et al. *Macromolecules* **44**(24), 9710--9722, 2011.

[28] Sèbe, G., et al. *Biomacromolecules* **13**(2), 570--578, 2012.

[29] Klemm, D., et al. *Angew. Chem. Int. Ed.* **44**(22), 3358--3393, 2005.

[30] Krishnamachari, P., et al. *Micron* **42**(8), 751--761, 2011.

[31] Bendahou, A., et al. *Macromol. Mater. Eng.* **296**(8), 760--769, 2011.

[32] Fang, J.M., et al. *Carbohydr Polym.* **47**(3) 245--252, 2002.

[33] Colom, X., et al. *Polym. Degrad. Stab.* **80**(3), 543--549, 2003.

[34] Colom, X. & Carrillo, F. *Eur. Polym. J.* **38**(11), 2225--2230, 2002.

[35] Hinterstoisser, B., et al. *Carbohydr. Res.* **334**(1), 27--37, 2001.

[36] Oh, S. Y., et al. *Carbohydr. Res.* **340**(15), 2376--2391, 2005.

[37] Kataoka, Y. & Kondo, T. *Int. J. Biol. Macromol.* **24**(1), 37--41, 1999.

[38] Kashiwagi, T., et al. *Nat. Mater.* **4**(12), 928--933, 2005.

[39] Pranger, L. & Tannenbaum, R. *Macromolecules* **41**(22), 8682--8687, 2008.

[40] LeBaron, P. C., et al. *Appl. Clay Sci.* **15**(1-2), 11--29, 1999.

[41] Favier, V., et al. *Macromolecules* **28**(18), 6365--6367, 1995.

[42] Ma, X., et al. *Carbohydr. Polym.* **62**(1), 19--24, 2005.

[43] Ojijo, V., et al. *ACS Appl. Mater. Interfaces* **4**(5), 2395--2405, 2012.

[44] Savadekar, N. R. & Mhaske, S. T. *Carbohydr. Polym.* **89**(1), 146--151, 2012.

[45] Sui, G., et al. *Bioresour. Technol.* **100**(3), 1246--1251, 2009.

[46] Chieruzzi, M., et al. *Composites Part A* **45**, 44--48, 2013.

[47] Deka, B.K. & Maji, T.K. *Composites Part A* **42**(12), 2117--2125, 2011.

[48] Thamaphat, K. *Kasetsart J. (Nat Sci)* **42**(5), 357--361, 2008.

[49] Mina, F., et al. *Polym. Degrad. Stab.* **94**(2), 183--188, 2009.

[50] Zhang, S.L., et al. *Chinese Sci. Bull.* **45**(16), 1533--1536, 2000.

[51] Xu, L. & Yang, M. *J. Appl. Polym. Sci.* **114**(5), 2755--2763, 2009.

[52] Darder, M., et al. *Chem. Mater.* **15**(20), 3774--3780, 2003.

[53] Ansari, M.O. & Mohammad, F. *J. Appl. Polym. Sci.* **124**(6), 4433--4442, 2012.

[54] Laachachi, A., et al. *Polym. Degrad. Stab.* **89**(2), 344--352, 2005.

[55] Du, H., et al. *J. Appl. Polym. Sci.* **118**(2), 1068--1076, 2010.

[56] Grigoriadou, I., et al. *Polym. Degrad. Stab.* **96**(1), 151--163, 2011.

[57] Camino, G., et al. *Polym. Degrad. Stab.* **90**(2), 354--362, 2005.

[58] Coates, G. W. & Hillmyer, M. A. *Macromolecules* **42**(21), 7987--7989, 2009.

[59] J. K. Pandey, et al. *J. Nanosci. Nanotechnol.* **5**(4), 497--525, 2005.

[60] Espitia, P.J.P., et al. *Carbohydr. Polym.* **94**(1), 199--208, 2013.

[61] Ma, X., et al. *Carbohydr. Polym.* **75**(3), 472--478, 2009.

[62] Deka, B.K. & Maji, T.K. *J. Appl. Polym. Sci.* **124**(4), 2919--2929, 2012.

[63] Devi, R.R. & Maji, T.K. *Ind. Eng. Chem. Res.* **51**(10), 3870--3880, 2012.

[64] Zhao, H. & Li, R.K.Y. *Polymer* **47**(9), 3207--3217, 2006.

[65] Wu, N., et al. *Polym. Degrad. Stab.* **95**(2), 2589--2595, 2010.

[66] Clausen, C.A. *Int. Biodeterior. Biodegrad.* **37**(1-2), 101--107, 1996.

[67] Lykidis, C., et al. *Wood Mater. Sci. Eng.* **8**(4), 242--244, 2013.

[68] Deka, B.K., et al. *Polym. Bull.* **67**(9), 1875--1892, 2011.

[69] Konwar, U. et al., *Polym. Degrad. Stab.* **94**(12), 2221--2230, 2009.

[70] Lunt, J. *Polym. Degrad. Stab.* **59**(1-3), 145--152, 1998.

[71] Drumright, R.E., et al. *Adv. Mater.* **12**(23), 1841--1846, 2000.

[72] Ray, S.S., et al. *Nano Lett.* **2**(10), 1093--1096, 2002.
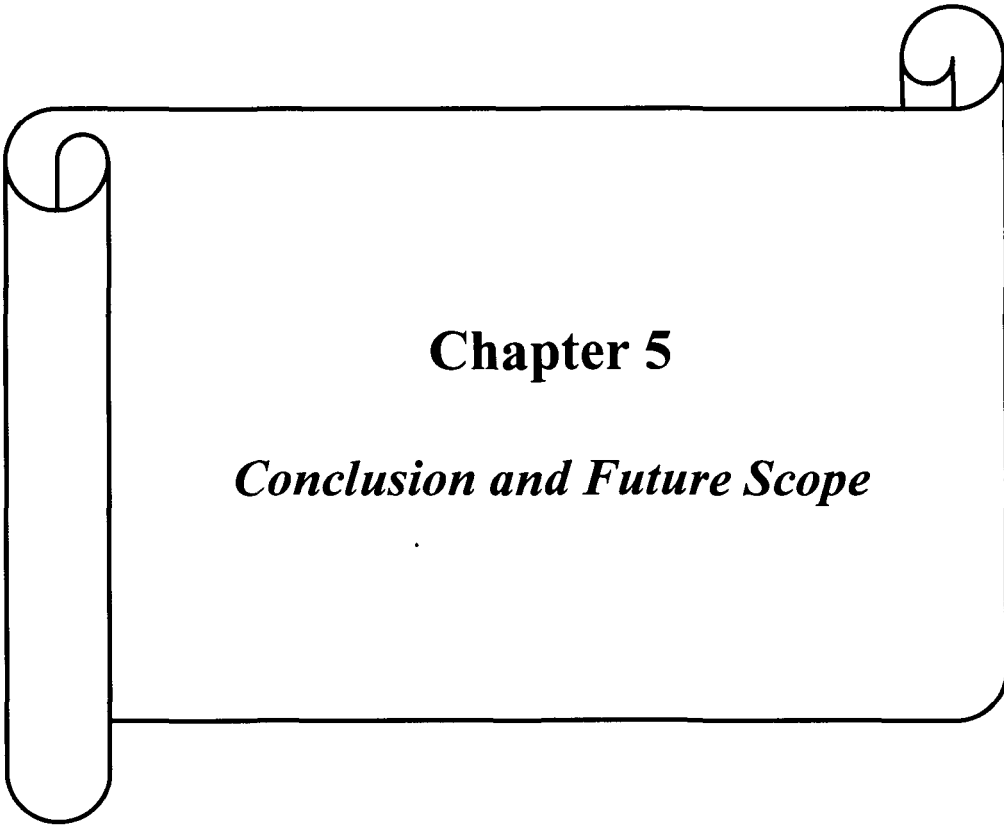
# Chapter 5

## *Conclusion and Future Scope*

## 5.1. Overall Conclusion of the Present Work

Due to several advantages of bio-based polymers over its synthetic counterpart, in recent years much emphasis has been given in the designing of newer bio-based eco-friendly materials. In the present investigation, jute, SF and starch were made value added through the formation of polymer composites. The solution induced intercalation method in combination with the nanotechnology opens up a new aspect to improve numerous properties of bio-based materials like thermal stability, dimensional stability, mechanical properties, flame retardancy, etc.

The significant features that emanates from this thesis work could be summarized as follows-

Composites prepared by using renewable resources such as SF and jute were characterized by various techniques. The effect of the crosslinking agent, GA and the nanoclay particles were studied. The incorporation of the crosslinking agent improved the physicochemical properties such as mechanical, thermal, dimensional stability, and flame retardency *via* a covalent interaction of the aldehydic group of the crosslinker with the hydroxyl and amino group of the jute and SF. The optimum concentration of GA for such improvement on the physical properties of the synthesized composites was found to be 50%. The exfoliation of nanoclay was studied by XRD and TEM. SEM study showed that the surface of the composite became rough due to the presence of nanoclay and SF. The higher the percentage of clay, the higher was the roughness. The presence of the covalent interaction between the crosslinker and S/J composites was confirmed by FTIR analysis which clearly shows an additional peaks at 2230 and 1167 cm$^{-1}$ due to $-N-C=O$ and $C-N$ stretching vibration. On addition of nanoclay to the resultant composites viz. S/J/G50/M1, S/J/G50/M3, and S/J/G50/M5, the mechanical properties, flame retardancy, and dimensional stability were found to improve further. The intrinsic correlation among the three properties namely thermal, mechanical, and LOI study was observed by the regressional analysis. Such type of nanoclay modified composites obtained from renewable sources could be considered eco-friendly compared to the composites obtained from conventional plastics and fibres whose replacement is currently a global concern.

Natural-resource-based green nanocomposites comprising SF, jute, GA, CWs, and nanoclay were synthesized by a solution induced intercalation method. The synthesized nanocomposites were successfully characterized by FT-IR, solid-state $^{13}$C

NMR, and diffuse-reflectance spectroscopies; XRD; TEM; and SEM. The $^{13}$C NMR and DRS study revealed the formation of long chain composite through the cross-linking of SF, jute, GA, CWs, and clay. A plausible mechanism for the cross-linking process is proposed to understand the type of interaction that might be possible among the additives. The formation of C–N linkages caused by the interaction between the aldehydic group of GA and the hydroxyl and amide groups of jute and SF was confirmed by NMR spectroscopy, DRS, and density functional theory. The composite with 5% CWs was found to show better physical properties than those of either bare composites or containing lower percentages of CWs. It is found that the mechanical and thermal properties, LOI, and dimensional stability of the composites were enhanced with increasing interfacial interaction between the filler and matrix. The incorporation of nanoclay resulted in further improvement of the physicochemical properties of the synthesized nanocomposites. Thus, CWs in combination with nanoclay can significantly improve the characteristic properties of natural resource-based composites. Hence, such types of CW- and nanoclay-loaded jute-fabric-based cross-linked SF composites can add a new direction in the field of renewable-resource based industries.

Following the similar methodology, environmentally benign green nanocomposites comprising of SF, jute, GA, TiO$_2$ nanoparticles and nanoclay were fabricated and characterized by various physicochemical and spectroscopic techniques. Effect of nanoparticles (*i.e.* TiO$_2$ and TiO$_2$ - nanoclay) on various properties of the synthesized composites were studied. The incorporation of TiO$_2$ nanoparticles improved the physicochemical properties such as mechanical, thermal, UV-resistance, flame retardancy, and dimensional stability *via* interaction of surface hydroxyl group of TiO$_2$ nanoparticles with hydroxyl group of SF and jute. The composite with 5 % TiO$_2$ nanoparticles was found to exhibit enhanced physical properties in comparison to those of either unfilled composites or composites containing lower amount of TiO$_2$ nanoparticle. The incorporation of nanoclay into TiO$_2$ containing composites, resulted in further improvement of the physicochemical properties of the synthesized material. FT-IR study showed a strong interaction among jute fabric, SF, GA, TiO$_2$ nanoparticles and nanoclay. XRD and TEM studies revealed the distribution of TiO$_2$ nanoparticles and silicate layers of nanoclay in SF/J composites. Composites containing 5 % TiO$_2$ nanoparticles and 3% nanoclay shown maximum improvement in physicochemical properties. Thus, TiO$_2$ nanoparticles in combination with nanoclay could considerably

improve the physical properties of natural resources based composites. Consequently, such kind of $TiO_2$ nanoparticles and nanoclay filled SF/J composites are eco-friendly and can receive applications in newer domains.

In this part, biodegradable nanocomposites comprising of SF, jute, GA, ZnO nanoparticles and nanoclay were fabricated and were characterized by various physicochemical and spectroscopic techniques. Effect of ZnO nanoparticles and nanoclay particles on various properties of the synthesized composites were studied. The incorporation of ZnO nanoparticles improved the physicochemical properties such as thermal, mechanical, flame retardancy, UV-resistance and dimensional stability via interaction of surface hydroxyl group of ZnO nanoparticles with hydroxyl group of SF and jute. The composite with 5 % ZnO nanoparticles was found to exhibit enhanced physical properties in comparison to those of either unfilled composites or composites containing lower amount of ZnO nanoparticle. The incorporation of nanoclay into SF/J/GA50/Z5 composites, results in further improvement of the physicochemical properties of the synthesized material. FT-IR study showed a strong interaction among jute fabric, SF, GA, ZnO nanoparticles and nanoclay. TEM and XRD studies revealed the distribution of ZnO nanoparticles and silicate layers of nanoclay in SF/J composites. Composites containing 5 % ZnO nanoparticles and 3% nanoclay incorporate maximum improvement in several physicochemical properties. Thus, ZnO nanoparticles in combination with nanoclay can considerably improve the physical properties of natural resources based composites. Thus, such kind of ZnO nanoparticles and nanoclay filled SF/J composites are eco-friendly and can obtain applications in newer territories.

In this study, eco-friendly composites made of jute fabric and starch matrix, plasticized with glycerol, were prepared by solution induced intercalation method and characterized by various techniques. Effect of the crosslinking agent, GA and the nanoclay particles were studied. The incorporation of the crosslinking agent improved the physicochemical properties such as mechanical, thermal, flame retardancy and dimensional stability via the interaction of the aldehydic group of the crosslinker with the hydroxyl group of starch and jute. The optimum concentration of GA for obtaining overall improvement in mechanical properties of the synthesized composites was found to be 50%. FTIR study showed a strong interaction among jute fabric, starch, glutaraldehyde and nanoclay. XRD and TEM study showed the exfoliation of nanoclay in the composites. The various properties such as mechanical, thermal, flame retardancy and dimensional stability were found to improve further by the incorporation of the

200

nanoclay to the resultant composites. The adherence of starch and clay particles on the surface of the jute fibre was shown by SEM study. SEM study of fractured surfaces also revealed the intimate bonding between the jute fabric and the matrix material. Therefore, such kind of nanoclay loaded jute fabric reinforced starch composites are eco-friendly and can find applications in newer fields. These synthesized green nanocomposites have the potential for a wider application range such as computer casings, packaging and panels for auto interior. Therefore, these synthesized plant based composites/nanocomposites having optimised properties may add to the rapid development for more sustainable and eco-friendly materials in near future.

CWs had been prepared from Whatman 1 filter paper and characterized by XRD and FT-IR. The prepared CWs were incorporated into crosslinked S/J composite as reinforcing fillers by using solution induced intercalation method. GA was used as crosslinking agent. Various spectrochemical techniques like FT-IR, XRD, TEM and SEM studied reveal the successful incorporation of CWs into the composite. The composite with 5 % CWs showed better physical properties compared to those of either unfilled CWs composite or composites containing lower percentage of CWs. Investigation of thermal, mechanical, LOI and dimensional stability of the composites indicate effective physicochemical properties due to the increase in interfacial interaction between the filler/matrix. At a fixed CW concentration, incorporation of nanoclay results in further improvement of the physicochemical properties of the synthesized nanocomposites. Thus, it indicates that the CWs in combination with nanoclay can significantly improve the characteristics properties of natural resources based composites.

In another study, environmental-friendly green nanocomposites comprising of starch, jute, GA, ZnO nanoparticles and nanoclay were fabricated. The effect of ZnO nanoparticles and nanoclay particles on various properties of the synthesized composites were studied. The incorporation of ZnO nanoparticles improved the physicochemical properties such as flame retardancy, mechanical, thermal, UV-resistance and dimensional stability *via* interaction of surface hydroxyl group of ZnO nanoparticles with hydroxyl group of starch and jute. The composite with 5 % ZnO nanoparticles was found to exhibit enhanced physical properties in comparison to those of either unfilled composites or composites containing lower amount of ZnO nanoparticle. The incorporation of nanoclay into S/J/GA50/Z5 composites, results in further improvement of the physicochemical properties of the synthesized material.

FT-IR study showed a strong interaction among jute fabric, starch, GA, ZnO nanoparticles and nanoclay. TEM and XRD studies revealed the distribution of ZnO nanoparticles and silicate layers of nanoclay in S/J composites. Composites containing 5 % ZnO nanoparticles and 3% nanoclay incorporate maximum improvement in several physicochemical properties. Thus, ZnO nanoparticles in combination with nanoclay can considerably improve the physical properties of natural resources based composites.

Renewable resources based green nanocomposites comprising of starch, jute, GA, ZNPs and nanoclay were developed. Effect of the ZNPs and nanoclay particles were studied. The incorporation of ZNPs improved the physicochemical properties such as thermal, mechanical, flame retardancy, UV-resistance and dimensional stability *via* the interaction of the surface hydroxyl group of ZNPs with the hydroxyl group of starch and jute. The composite with 5% ZNPs was found to exhibit better physical properties than those of either unfilled composites or composites containing lower amount of ZNP. The incorporation of nanoclay resulted in further improvement of the physicochemical properties of the synthesized material. FT-IR study showed a strong interaction among jute fabric, starch, GA, ZNPs and nanoclay. TEM and XRD studies reveal the distribution of ZNPs and silicate layers of nanoclay in S/J composites. Composites containing 5% ZNPs and 3% nanoclay produce maximum improvement in several physicochemical properties. Thus, ZNPs in combination with nanoclay can considerably improve the physical properties of natural resources based composites. Consequently, such kind of ZNP and nanoclay filled S/J composites are eco-friendly and can receive applications in newer domains.

## 5.2. Future Scope

The formation of bio-nanocomposites using SF, starch, jute, and various nanofillers results in overall improvement in properties of the synthesized nanocomposites and can pave a vast area in the field of renewable resources based materials. So the present work can be further extended in the following aspects

❖ The laboratory study of the composites displays a remarkable improvement in various properties. But further study or research is needed for commercial utilization of the product. Fine tuning in the ratio of clay with different nanofillers may be required in order to achieve maximum improvement in properties.

❖ The use of other nanofillers like carbon nanotube and $SiO_2$ either alone or in combination with some other nanoparticles and their effect on various properties of bio-nanocomposites can be studied.

❖ Renewable resources based products finding privilege particularly because of environmental friendliness and dwindling petroleum resources. Biopolymers reinforced with natural fibres have developed significantly over the past two decades because of their significant processing advantages, biodegradability, low cost, low relative density, high specific strength and renewable nature. Unlike many biopolymer products being developed and marketed, very few biodegradable composites have been developed, with most of their technologies still in the research and development stages. This is despite the fact that the environmentally benign composites, where biodegradability is important, provide designers new alternatives to meet challenging requirements.

❖ One of promising interest of research is the production of quality fibre used as reinforcing agent in the composites. The production of quality fibre may be obtained through better cultivation which includes the use of genetic engineering. Exploration of non-traditional fibre as a source of reinforcing agent is another important area. In order to achieve proper reinforcement, the introduction of hybrid nanocomposite may be attempted. The processibility and development of new biodegradable polymers with much improved properties in terms of moisture resistance, mechanical strength, thermal stability and biodegradability are some of the areas which require much attention.

❖ The price of biodegradable polymers for making composites is expected to reduce further in the coming years due to development of raw material, manufacturing techniques and hence it may be considered as a valid alternative to conventional composites. It is also envisaged that further research and development on biodegradable composite may lead to open up new avenues to meet the local as well as global challenges and thus may expand the horizon of applications.

❖ As government is more concerned for assuring resource sustainability and promoting green technology, therefore, a thorough exploration of composites in terms of the biodegradability, fire resistance, pest resistance and low emission of volatile organic compound is also necessary.

# List of Publications

**In Journals**

**1. Iman, M.** and Maji, T. K. Effect of crosslinker and nanoclay on starch and jute fabric based green nanocomposites. *Carbohydr. Polym.* 2012, **89** (1), 290–297.

**2. Iman, M.** and Maji, T. K. Effect of crosslinker and nanoclay on jute fabric reinforced soy flour green composite. *J. App. Polym. Sci.* 2013, **127** (5), 3987–3996.

**3. Iman, M.**, Bania, K. K. and Maji, T. K. Green jute based crosslinked soy flour nanocomposites reinforced with cellulose whiskers and nanoclay. *Ind. Eng. Chem. Res.* 2013, **52** (21), 6969–6983.

**4. Iman, M.**, Manhar, A., Mandal, M. and Maji, T. K. Preparation and characterization of zinc oxide and nanoclay reinforced crosslinked starch/jute green nanocomposites. *RSC Adv.* 2014, **4** (64), 33826–33839.

**5. Iman, M.** and Maji, T. K. Effect of Cellulose Whisker and Nanoclay on Jute reinforced Starch Green Nanocomposites. (Manuscript submitted)

**6. Iman, M.** and Maji, T. K. Synergistic effect of zinc oxide and nanoclay on crosslinked jute reinforced soy flour green nanocomposites. (Manuscript submitted)

**7. Iman, M.** and Maji, T. K. Effect of $TiO_2$ and nanoclay on the ultraviolet degradation and physical properties of crosslinked jute (*Corchorus capsularis L.*) reinforced soy flour green nanocomposites. (Manuscript submitted).

**8. Iman, M.** and Maji, T. K. Property evaluation of $TiO_2$ and nanoclay reinforced jute based starch nanocomposite. (Manuscript submitted).

*Others*

**1.** Banik, N., **Iman, M.**, Hussain, A., Ramteke, A., Boruah, R. and Maji, T. K. Soy flour nanoparticles for controlled drug delivery: effect of crosslinker and montmorillonite (MMT). *New J. Chem.* 2013, **37** (12), 3981–3990.

**2.** Hussain, M. R., **Iman, M.** and Maji, T. K. Determination of degree of deacetylation of chitosan and their effect on the release behaviour of essential oil from chitosan and chitosan-gelatin complex microcapsules. *Int. J. Adv. Eng. App.* 2013, **2** (1), 4–12.

**3. Iman, M.**, Hussain, M. R. and Maji, T. K. *Zanthoxylum Limonella* Oil (ZLO) encapsulated gelatin microcapsules for controlled release of Mosquito Repellent: Effect

of various parameters on microcapsule properties and Mosquito Repellent behaviour. . *Int. J. Adv. Eng. App.* 2013, **2** (5), 151–159.

**In Books**

**1. Iman, M.** and Maji, T. K. Bionanocomposites: A greener alternative for future generation. In *Green Biorenewable Biocomposites: From Knowledge to Industrial Applications,* Thakur, V. K., Kessler, M. R., Eds.; Apple Academic Press, Canada, 30 September, 2014.

**2. Iman, M.** and Maji, T. K. Jute: An interesting lignocellulosic fibres for new generation applications. In *Lignocellulosic Polymer Composites: Processing, Characterization and Properties*, Thakur, V. K., Ed.; John Wiley & Sons, Inc., Hoboken, NJ, USA, 14 November, 2014.

**In Conference**

**1. Iman, M** and Maji, T. K., Effect of Crosslinker and Nanoclay in Jute-reinforced-Starch composite, *National Conference on Smart Nanostructures*, January 18-20, 2011, Tezpur University, Assam, India.

**2. Iman, M** and Maji, T. K., Effect of Crosslinker and Grafting on the properties of Jute-reinforced-Soy flour composite, *National Seminar on Recent Advances in Synthesis and Catalysis*, February 10-12, 2011, Dibrugarh University, Assam, India.

**3. Iman, M** and Maji, T. K., Effect of Nanoclay on the properties of Jute-reinforced-Starch-g-MMA composites, *National Conference on 'Chemistry, Chemical Technology and Society'*, November 11-12, 2011, Tezpur University, Assam, India.

**4. Iman, M** and Maji, T. K., Property Evaluation of Biodegradable Composites based on Cellulose microcrystalline powder and Natural Polymer, *International Conference on Nanomaterials & Nanotechnology*, December 18-21, 2011, University of Delhi, Delhi, India.
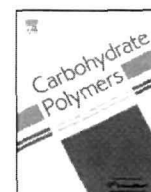
# Effect of crosslinker and nanoclay on starch and jute fabric based green nanocomposites

Murshid Iman, Tarun K. Maji *

Department of Chemical Sciences, Tezpur University, Assam 784028, India

## ARTICLE INFO

## ABSTRACT

'Green' nanocomposites were prepared by solution induced intercalation method using starch, jute, glutaraldehyde, nanoclay and glycerol. The concentration of glycerol was optimised. The synthesized composites were characterized by various physicochemical and spectrochemical techniques such as Fourier transform infrared spectroscopy, X-ray diffractometry, transmission electron microscopy, scanning electron microscopy, and thermogravimetric analysis. Fourier transform infrared spectroscopy study indicated an interaction between the jute, starch and clay. Good adhesion exists between starch and jute surface as revealed by scanning electron microscope study. The extent of exfoliation of clay was studied by X-ray diffraction and transmission electron microscope studies. The addition of glutaraldehyde and nanoclay has been found to improve the thermal stability, flame retardancy, dimensional stability and mechanical strength of the prepared composite.

© 2012 Elsevier Ltd. All rights reserved.

## 1. Introduction

The growing awareness of the pressing need for greener, more sustainable technologies has focussed attention on use of ecofriendly and cost-effective material with high performance (Ma, Yu, & Kennedy, 2005). Another aspect, which is receiving more attention, is the use of alternate source prior to the use of the conventional materials (Satyanarayana, Arizaga, & Wypych, 2009). Biopolymers, which exist abundantly worldwide, are one of such promising material. They offer many fundamental and practical advantages of relevance to the chemist as well as to the chemical industries, which are constantly searching for high performing, cost-effective and environmentally friendly materials (Bastioli, 1995; Pandey & Singh, 2001; Scott, 2000; Shogren, Fanta, & Doanne, 1993). Besides these, natural fibres with their characteristics properties such as low cost, easy availability, low density, high specific strength, renewability and less abrasive with respect to processing tools, can be added to such class of materials (Ray, Sengupta, Sengupta, Mohanty, & Misra, 2007; Saheb & Jog, 1999). Among various natural fibres, jute fibre is cheap and widely available (especially in some Asian countries) (Ray & Sarkar, 2001). Jute, mainly comprising of cellulose and lignin, is an extensively demanding materials in cloth and other such industries (Jahan, Saeed, He, & Ni, 2011; Saha, Das, Basak, Bhatta, & Mitra, 2000). Therefore, with the use of greener methodologies and environmentally

benign materials (such as biopolymers), jute can be modified to a cost-effective and environmentally friendly 'green' products with improved physical properties (Plackett, Anderson, Pedersen, & Nielson, 2003).

One of the most studied and promising raw materials for the production of biodegradable products is starch, a natural, renewable carbohydrate and low cost polymer obtained from a great variety of crops such as corn, wheat, rice and potato (Corre, Bras, & Dufresne, 2010). Starch is basically a mixer of amylose, a linear polymer with molecular weight between 103 and 106 and amylopectin, a branched polymer with a —(1–6)—linked branch points (Dufrense & Vignon, 1998). Native starch commonly exists in a granular structure with about 15–45% crystallinity. Under the action of high temperature and shear, starch can be processed into thermoplastic starch (Forssell, Mikkilä, Moates, & Parker, 1997). Starch based films have significant potential to replace synthetic films such as polyethylene in packaging and agricultural mulching industries (Chen & Patel, 2012). Starch has been investigated widely for the potential manufacture of medical delivery systems and devices (Fishman, Coffin, Konstance, & Onwulata, 2000). However, starch based films have limited applications due to their two main disadvantages such as high hydrophilicity and inherently low moduli of elasticity (Ban, JianguoSong, Argyropoulos, & Lucia, 2006).

Polymer–layered silicate nanocomposites, containing small amounts of inorganic nano phase, have exhibited superior properties like modulus, strength, thermal stability, toughness, gas permeability barrier, and flammability resistance compared to those of the pure polymers (Yoonessi, Toghiani, Kingery, & Pittman, 2004). These unique properties shown by nanocomposites are due

---

* Corresponding author. Tel.: +91 3712 267007x5053; fax: +91 3712 267005.
E-mail address: tkm@tezu.ernet.in (T.K. Maji).

# Effect of Crosslinker and Nanoclay on Jute Fabric Reinforced Soy Flour Green Composite

Murshid Iman, Tarun K. Maji

Department of Chemical Sciences, Tezpur University, Assam 784028, India
Correspondence to: T. K. Maji (E-mail: tkm@tezu.ernet.in)

ABSTRACT: Bio-based composites were prepared by using soy flour, jute, glutaraldehyde (GA), nanoclay, and glycerol. An optimum concentration of glycerol was used as a plasticizer. The synthesized composites were characterized by various techniques such as scanning electron microscopy (SEM), transmission electron microscopy (TEM), X-ray diffractometry (XRD), Fourier transform infrared spectroscopy (FTIR), and thermogravimetric analysis (TGA). The exfoliation of clay layers was detected both by XRD and TEM study. FTIR study showed an interaction between clay, jute, and soy flour. The percentage content of GA and nanoclay was found to have profound influence on various physical properties of the composites. The increase in the concentration of GA and nanoclay improved the thermal stability, flame retardancy, dimensional stability, and most importantly the mechanical properties of the prepared composite. © 2012 Wiley Periodicals, Inc. J. Appl. Polym. Sci. 127: 3987–3996, 2013

## INTRODUCTION

Conventional polymers which are obtained from petrochemicals are non-renewable and environment unfriendly.[1,2] The environmental impact of polymeric waste is increasing global concern, and alternative disposal methods are limited. Besides this, the earth has finite resources in terms of fossil originated fuel. So, there is a need to reduce the use of such conventional polymers by using bio-degradable composite materials which are produced from renewable resources such as agricultural and biological origin. Various bio-degradable polymers such as starch, soy protein, whey protein, wheat gluten, zein, polyhydroxy butyrate-co-valerate (PHBV), etc., have been used with bio-fibres (like jute, hemp, flax, ramie, etc.) as matrix and reinforcing materials to form eco-friendly product, with minimum impact on the environment.[1] Moreover, the use of natural fibres to reinforce thermoplastics such as polypropylene and polyethylene as an alternative to synthetic or glass fibres has been and continues to be the subject of research and development.[3,4] The fibre reinforcement of biopolymers such as PLA can produce composites with suitable mechanical properties for light weight construction materials. Placket et al. have found that the tensile strength and stiffness of PLA can be approximately doubled when jute fibre as reinforcement is used.[5]

Bio-fibres offer several advantages such as low cost, easy availability, low density, high specific strength, and renewability. Apart from these advantages, bio-fibres have some disadvantages like variation in mechanical properties which depend on several factors such as moisture content, cultivation area, processing methods, and poor thermal stability. These fibres in combination with the bio-degradable matrices can produce environmentally friendly "green" products with improved properties.[6–10] Jute, a kind of natural fibre, is widely available and can be used for making composites. Surface modification like dewaxing and mercerization of jute fabrics are essential before their use for composite preparation. Surface modification will not only decrease the moisture absorption property but also concomitantly increase the wettability of fabrics with matrix polymer and the interfacial bond strength. Both are critical factors for obtaining better mechanical properties of the composites.

Soy protein is one of the less expensive bio-polymers abundant worldwide. It was first introduced by Henry Ford in automobile manufacturing as alternating source for plastics and fibers.[11] Its purification process is benign and environment friendly. This protein can also be used as resin due to its ability to form ductile and viscous polymers. Out of different varieties available commercially, defatted soy flour (SF) is the least expensive one. SF contains approximately 55% protein and 32% carbohydrate.

# Green Jute-Based Cross-Linked Soy Flour Nanocomposites Reinforced with Cellulose Whiskers and Nanoclay

Murshid Iman, Kusum K. Bania, and Tarun K. Maji*

Department of Chemical Sciences, Tezpur University, Assam -784028, India

Ⓢ Supporting Information

**ABSTRACT:** A practical procedure for extracting cellulose whiskers (CWs) from ordinary filter paper by acid hydrolysis has been developed. The extracted CWs alone and in combination with nanoclay were used as reinforcing agents for the preparation of green nanocomposites based on jute fabric and glutaraldehyde (GA) cross-linked soy flour (SF). A solution-induced intercalation method was implemented for the successful fabrication of the nanocomposites. The formation of nanocomposites was confirmed by various physicochemical and spectroscopic techniques and by DFT calculations. The results of the various analyses suggest a strong interfacial interaction between the filler and the matrix. The properties of nanoparticle-filled SF/jute nanocomposites were compared with those of unfilled composites. Furthermore, the mechanical strength, thermal stability, flame retardancy, and dimensional stability of the filled composites were found to be much better than those of the unfilled composites, allowing the processing of high-performance green nanocomposites.

## ■ INTRODUCTION

Biopolymer-based materials containing immobilized nanoparticles have recently dominated the traditionally obtained petroleum-based polymer materials.[1,2] Because of their outstanding mechanical properties and biodegradability, biobased polymer nanocomposites are currently considered to be promising materials These materials have the potential to overcome the disadvantages of materials obtained commercially from the petrochemical supply chain. Moreover, the use of biobased polymer nanocomposites plays a vital role in sustainable development and the development of newer methods for the production of environmentally benign "greener" products [3-7]

Of the different types of commercially available soy proteins, soy flour (SF), a natural biodegradable polymer, is inexpensive and readily available.[8-10] The presence of various polar and reactive amino acids such as cystine, arginine, lysine, and hystidine in the structure of SF enable them to cross-link with a cross-linking agent such as glutaraldehyde, thereby improving the tensile and thermal properties of the polymer.[11,12] However, the potential of such material has been less explored in the synthesis of biobased composites. In addition to having various advantages, SF-based materials also exhibit certain disadvantages For example, soy-protein-based plastics have poor flexibility and water resistance. Although several plasticizers such as glycerol, polyethylene glycol, and sorbitol have been used to improve the flexibility of SF but have been found to yield lower mechanical strength and high water sensitivity.[8-13] In this respect, biofibers have become a promising option for improving the mechanical strength of such materials [14] The salient features of natural fibers over their conventional counterparts include comparatively low cost, low weight, high specific modulus, comparative safety, and copious and renewable resources. The applications of natural fibers in sectors such as automobiles, furniture, packing materials, and construction are now highly demanding. Currently, kenaf,

bamboo, and palm-tree fibers are used as reinforcing agents at the micro- and macroscale levels to improve the thermal and mechanical properties of natural biodegradable polymers.[15] Huang and Netravali used micro-/nanosized bamboo fibrils (MBFs) and a modified soy protein resin to fabricate environmentally friendly composites. They reported a significant increase in the fracture stress and Young's modulus of the soy protein concentrate upon incorporation of MBFs Similarly, palm tree and kenaf natural fibers were used as reinforcing agents for the development of self-bonded polymer biocomposites [16] Aside from the already mentioned natural fibers, jute fiber can also be used as a reinforcing agent and for the synthesis of polymer composites Jute, mainly comprising cellulose and lignin, is an extensively used material in cloth and other such industries [1] The most attractive features of jute fibers are that they are inexpensive and widely available and, most importantly, that they can be modified into cost-effective and environmentally friendly green products with improved physical properties such as thermal and mechanical properties.[18]

The combination of SF polymer and jute fibers cross-linked with glutaraldehyde can lead to biobased polymer composites whose properties can be improved by dispersing nanofillers into their matrix.[19-24] Among the various nanofillers, cellulose whiskers (CWs) and clays with surface areas in the ranges of 150−170 and 750 $m^2/g$, respectively, are extensively used for the modification of conventional polymer composites.[25] The immobilization of nanoclays and CWs results in a high interfacial area between the matrix and the filler. This, in turn, endows the polymer nanocomposites with high thermomechanical performance [26]

CrossMark
←click for updates

# Preparation and characterization of zinc oxide and nanoclay reinforced crosslinked starch/jute green nanocomposites

Murshid Iman,[a] Ajay K. Manhar,[b] Manabendra Mandal[b] and Tarun K. Maji[*a]

In the present work, ZnO nanoparticles (ZNP) and ZNP in combination with nanoclays are reported as reinforcing agents for the preparation of 'Green' nanocomposites based on glutaraldehyde (GA) crosslinked starch/jute fabric. A solution-induced intercalation method has been used for the successful fabrication of the nanocomposites. Both ZNP and nanoclay are successfully incorporated into the composite as revealed by X-ray diffractometry (XRD), transmission electron microscopy (TEM), scanning electron microscopy (SEM), and Fourier-transform infrared spectroscopy (FT-IR). The thermal and mechanical properties of the nanocomposites are studied using thermogravimetric analysis (TGA) and mechanical tests, respectively. The study reveals significant changes in the observed properties of the synthesized composites with the amount of nanofillers. Interestingly, the flame retarding properties, UV-resistance, and dimensional stability of the nanoparticle filled composites are found to be much better than those of the unfilled one. The study reveals a strong interfacial interaction between the filler and the matrix within the synthesized green nanocomposites.

## 1. Introduction

The current interest in the conservation of natural resources and recycling has encouraged researchers in different countries to focus more on renewable raw materials. Due to the increasing global awareness, environmental legislation has resulted in restriction on the use of traditional composites made of glass, carbon, aramid fibres, *etc.* Therefore, the interest for greener and more sustainable technologies has focused attention in bio-based products and their development to reduce the dependence on fossil fuel and move to a sustainable materials basis.[1–3] One of such potential material is the biopolymers, which exist abundantly worldwide. Biopolymers provide several fundamental and practical advantages such as they are organic in nature and a host for other useful materials and chemicals, particularly for the production of "greener" materials.[4]

Among the various biodegradable polymers, starch is one of the most exciting and promising raw material for the production of biodegradable products. Starch is produced by many plants as a source of storage energy. In global scenario, it is also the second most abundant biomass material.[5] Starch mainly comprises of two key polysaccharides, amylose and amylopectin along with some minor components such as lipids and proteins. Amylose is defined as a linear polymer of (1 → 4)-linked α-D-glucopyranosyl units with minor amount of (1 → 6)-α-branches. Amylopectin is a highly branched molecule composed of chains of α-D-glucopyranosyl residues linked together mainly by (1 → 4)-linkages along with (1 → 6)-linkages at the branched points.[6] Starch based films are widely used in food packaging, agricultural mulching industries, foamed materials for loose-fill packing and most importantly in health sciences.[7–9] Besides having various advantages, starch based materials exhibit certain disadvantages too such as high hydrophilicity and low moduli of elasticity which reduces its industrial applications.[10] Starch plastics possess good biodegradability but their application is limited due to their poor flexibility. However, plasticizer like glycerol has been used to improve the flexibility of starch but is reported to produce lower mechanical and high water sensitivity.[11] Glutaraldehyde (GA) can be used as a crosslinking agent, thereby improving its thermo mechanical properties and also reducing its hydrophilicity.[12] Moreover, biofibres evolved as one of the potential materials in improving the mechanical strength of such material. The noteworthy advantage of biofibres over their conventional counterparts include comparatively low cost and weight, high specific modulus, easy availability, comparative safety and less abrasive with respect to processing tools. The applications of biofibres in furniture, packing materials, construction, and automobiles sectors are now highly demanding.[13] Among different types of biofibres, jute fibre can also be used as a reinforcing agent for the synthesis of polymer composites. Jute, which consists of cellulose and lignin, is an extensively used material in textile and other such industries. The most

[a]Department of Chemical Sciences, Tezpur University, Assam – 784028, India. E-mail: tkm@tezu.ernet.in; Fax: +91 3712 267005; Tel: +91 3712 267007 ext. 5053
[b]Department of Molecular Biology and Biotechnology, Tezpur University, Assam – 784028, India

# NJC

## PAPER

# Soy flour nanoparticles for controlled drug delivery: effect of crosslinker and montmorillonite (MMT)

Nibedita Banik,[a] Murshid Iman,[a] Anowar Hussain,[b] Anand Ramteke,[b] Ratan Boruah[c] and Tarun K. Maji*[a]

Soy flour (SF)–Montmorillonite (MMT) nanoparticles crosslinked with glutaraldehyde (GA) have been made and used as a carrier for isoniazid. The nanoparticles have been characterized by fourier transmission infra-red spectroscopy (FTIR), X-ray diffractometry (XRD), scanning electron microscopy (SEM) and transmission emission microscopy (TEM). The effects of MMT and glutaraldehyde on the nanoparticles have been assessed with regard to swelling, encapsulation efficiency and consequently, the release of isoniazid in different mediums. The drug release mechanism has been studied for different time periods by UV-Vis spectroscopy. Cytotoxicity testing has been performed by MTT assay analysis. The results imply that the nanoparticles can be exploited as a potential drug carrier for controlled release applications.

## 1 Introduction

In the present scenario of pharmaceutical research, polymers have been extensively used as an active agent for drug delivery. They can control the release of a drug over an extended period by forming a matrix or membrane, or by forming (nano) carriers and thus avoiding repetitive dosing.[1] Pharmaceutical developments are gradually giving more attention to delivery systems which enhance desired therapeutic objectives while lowering side effects.[2] Nowadays, biodegradable polymers are preferred to synthetic polymers as controlled drug delivery systems due to their low toxicity, easy availability and cell biocompatibility.[3] Soy flour (SF) is one such natural biodegradable polymer which can be explored for controlled drug delivery applications. Soy flour is derived from soybean which is a renewable resource and found in nature in abundance. Soybeans are classified as oil seeds, a stable food of nutritional value and a rich source of protein. Soy flour has easy availability, good processability and is non toxic.[4-7] The uses of soy flour as a drug delivery device have not been explored much.

Nanoparticles have evoked much interest recently for the delivery of drugs such as peptides, proteins and genes due to their ability to protect these from degradation in the gastrointestinal tract by proteolytic enzymes.[8,9] Different bioactive agents have been successfully encapsulated within polymers and have been tested for their therapeutic activity.[10] Nanoparticles can be prepared from a variety of

materials such as proteins, polysaccharides and other natural polymers. The selection of matrix materials is dependent on many factors including size of nanoparticles required, inherent properties of the drug, e.g., aqueous solubility and stability, surface charge and permeability, degree of biodegradability, biocompatibility and cytotoxicity, the desired drug release profile, and antigenicity of the final product.[11]

Montmorillonite (MMT) clay is smectite clay having two silica tetrahedral sheets layered between one alumina octahedral sheet. MMT is a clay mineral with a large specific surface area, exhibits good adsorbability, cation exchange capacity, excellent mucoadhesive properties and drug-carrying capability.[12] Due to its good physical and chemical properties, MMT has received considerable attention in recent years for drug delivery systems applications.[13]

Isoniazid is an antituberculosis drug which can be used as a model drug. Isoniazid normally has three $pK_a$ values: 1.8 based on hydrazine nitrogen, 3.5 based on pyridine nitrogen and 10.8 based on acidic group. In pH 1.2, the $pK_a$ of isoniazid is found to be around 2 due to protonation of hydrazine nitrogen whereas in basic pH of 7.4 it is found to be around 12.[14] The main preparation processes of protein nanoparticles are the emulsification process,[15] desolvation method[16] and templating synthesis.[17] Desolvation method is more apt for nanoparticle preparation as it eliminates the use of organic solvents, and provides removal both of the oily residues of the preparation process and of surfactants required for emulsion stabilization.[11] Varieties of crosslinkers are reported to be used for controlling the release behavior of drugs.[18-20] Glutaraldehyde, a crosslinker of synthetic origin, has been used as a successful crosslinking agent in many studies to cross link biopolymers like SF, starch etc.[21]

But, to the best of our knowledge, there is no report for synthesizing drug loaded SF–MMT nanoparticles by using this

[a] Department of Chemical Sciences, Tezpur University, Assam, 784028, India.
E-mail: tkm@tezu.ernet.in; Fax: +91 3712 267005; Tel: +91 3712 267007 ext. 5053
[b] Department of Molecular Biology and Biotechnology, Tezpur University, Assam, 784028, India
[c] Department of Physics, Tezpur University, Assam, 784028, India

# Determination of Degree of Deacetylation of Chitosan and Their effect on the Release Behavior of Essential Oil from Chitosan and Chitosan-Gelatin Complex Microcapsules

**Md Rabiul Hussain, Murshid Iman and Tarun K. Maji***
Department of Chemical Sciences, Tezpur University, Assam - 784028, India
* Corresponding author  Tel  +91 3712 267007, Extn  5053, Fax  +91 3712 267005
E-mail address  tkm@tezu.ernet.in (T K Maji)

**Abstract** - Deacetylation of chitosan was performed by alkali treatment for different time periods  Degree of deacetylation (DDA) was determined by using FTIR spectrophotometer, potentiometric titration and CHN analyzer  The higher the duration of alkali treatment, the higher was the DDA and lower was the molecular weight  At low crosslinking concentration, the oil loading, loading efficiency and release rate of essential oil from deacetylated chitosan or deacetylated chitosan-gelatin matrix decreased as DDA increased  At higher crosslinker concentration, the trends were opposite  Swelling decreased as DDA increased  SEM study indicated that degree of deacetylation and crosslinking controlled the surface smoothness of the microcapsules
**Keywords** - chitosan, gelatin, degree of deacetylation, genipin, essential oil, release studies

## 1 INTRODUCTION

Chitosan, a natural polysaccharide comprising copolymer of glucosamine and N-acetylglucosamine, is obtained on industrial scale by alkaline partial deacetylation of chitin. the second most abundant natural polymer after cellulose (Jana et al., 2013 and Mukhopadhyay et al., 2013).  Chitosan can also be produced by the enzymatic deacetylation of chitin.  It exhibits innumerable applications in a wide range of fields such as agriculture, packaging, food biotechnology, cosmetics, medicinal and pharmaceuticals etc.  Chitosan can be characterized by degree of deacetylation (DDA), molecular weight and their distribution. residue protein etc.  But the most important parameter for characterizing a given chitosan specimen is the degree of deacetylation (Jana et al.. 2013).

The degree of deacetylation (DDA) influences the physical, chemical and biological properties of chitosan, such as acid base and electrostatic characteristics, biodegradability, self aggregation, sorption properties, and the ability to chelate metal ions.  In addition, the degree of deacetylation. which determines the content of free amino groups in the polysaccharide (Li et al., 1992). can be employed to differentiate between chitin and chitosan.  The process of deacetylation involves the removal of acetyl group from the molecular chain of chitin, leaving behind a complete amino group ($-NH_2$) and chitosan versatility depends mainly on this high degree of chemical reactive amino groups.  There are various methods available to increase or decrease the degree of deacetylation.  An increase in either temperature or strength of sodium hydroxide solution can enhance the removal of acetyl groups from chitin, resulting in a range of chitosan molecules with different properties and hence its applications (Baxter et al., 1992).  Since the degree of deacetylation (DDA) depends mainly on the method of purification and reaction conditions (Baxter et al.. 1992 and Li et al.. 1997). it is, therefore. essential to characterize chitosan by determining its DDA prior to its utilization.

The degree of deacetylation (DDA) allows one to define the terms chitin and chitosan. that is. chitosan is usually defined as the derivative that is soluble in dilute acidic solutions (Balázs and Sipos, 2007).  The lowest DDA corresponding to chitosan varies in literature and ranges from 40% to 60%. The majority of the commercial chitosan samples have average DDAs of 70-90%. For some special biological applications. chitosan of higher DDA (> 95%) may be prepared via further deacetylation steps which not only increases the cost of the preparation but also often results in partial depolymerization (Tolaimatea et al., 2003).

Several methods have been used to determine the degree of deacetylation (DDA) of chitosan.  These methods included ninhydrin test (Curotto and Aros. 1993). infrared spectroscopy (IR) (Brugnerotto et al. 2001, Sabnis and Block, 1997 and Domszy and Roberts, 1985), linear potentiometric titration (LPT) (Balázs and Sipos. 2007, Ke and Chen. 1990 and Jiang et al.. 2003) circular dichroism spectroscopy (Domard 1987), hydrogen bromide titrimetry (Baxter et al.. 1992 and Domszy and Roberts. 1985), GPC (Aiba, 1986), ultraviolet (UV) spectroscopy (Muzzarelli, 1985 and Tan et al.. 1998). nuclear magnetic resonance spectroscopy (NMR) (Shigemasa et al., 1996. Lavertu et al.. 2003 and Zhang et al.. 2005), enzymatic determination (Nanjo et al., 1991) and elemental analysis (Shigehiro et al., 1981, Gong et al., 2003, Kasaai et al.. 2000 and Gupta and Jabrail, 2006).  Some of the methods are too tedious, costly for routine analysis or destructive to the sample.  The choice of the method appears to be arbitrary and often does not correlate with others.  A standard method used to determine the DDA of chitosan is essential, if wider exploitation of chitosan is to be realized.  The method has to be simple. rapid, cost effective and reliable yet tolerate the presence of impurities.  Chitosan has multiple applications such as drug carrier, wound healing, implantation and gene therapy. Chitosan is insoluble either in water or organic solvents. The extent of solubility depends on DDA, concentration, type of acid and pH.

4

# Zanthoxylum Limonella Oil (ZLO) encapsulated gelatin microcapsules for controlled release of Mosquito Repellent: Effect of Various Parameters on Microcapsule Properties and Mosquito Repellent behavior

**Murshid Iman, Md Rabiul Hussain and Tarun K. Maji***

*Department of Chemical Sciences, Tezpur University, Assam - 784028, India*
* Corresponding author Tel +91 3712 267007, Extn 5053, Fax +91 3712 267005
*E-mail address* tkm@tezu ernet in (T K Maji)

**Abstract:** Microcapsules properties were found to be dependent on the conditions of preparation Microcapsules prepared at higher pH exhibited lower rate of release of oil Microcapsules prepared at higher stirrer speed showed higher rate of release of oil compared to those of prepared at lower stirrer speed The higher the temperature of the release medium, the higher was the release rate Higher stirrer speed produced higher proportion of smaller and better shaped microcapsules DSC results revealed a low compatibility in thermal properties between oil and gelatin The mosquito repellency behavior of microcapsules based formulation was similar to that of standard synthetic repellent based formulation
*Keywords* Gelatin, microcapsule, ZLO, DEET, mosquito repellent

## 1. INTRODUCTION

Plant and plant-derived substances have been used to repel or kill mosquitoes and other domestic pest insects for a long time before the advent of synthetic chemicals (Curtis et al., 1990). A review on the uses of botanical derivatives against mosquitoes has been cited in literature (Sukumar et al.. 1991). Essential oils of a large number of plants have been found to have repellent properties against various haematophagous arthopods; some have formed the basis of commercial repellent formulations (Curtis et al.. 1990, Mark and Fradin, 1998). The oils, which have been reported as potential sources of insect repellents, include citronella. cedarwood. verbena, penny royal, geranium, lavender, pine, cajeput, cinnamon. Rosemary. basil, thyme, allspice, garlic, peppermint, neem, eucalyptus, etc. Currently a lemon eucalyptus extract which comes from the plant *Eucalyptus maculata citridion* with the principal active ingredient p-menthane-3, 8-diol (PMD) has shown particularly good results in its mosquito repellent properties when tests were carried out under laboratory conditions. This repellent has been found to be effective against mosquitoes, midges, ticks and the stable fly (Curtis et al., 1990, Collins and Brady, 1993, Trigg and Hill. 1996, Trigg. 1996, Govere et al., 2000). Studies on the mosquito repellent activity of 38 essential oils against mosquito under laboratory conditions using human subjects are reported (Trongtokit et al., 2005). It has been reported that undiluted oils of *cymbopogon nardus* (citronella), *pogostemon cablin* (patchuli), *syzygium aromaticum* (clove) and *Zanthoxylum limonella* ( thai name: makaen) are most effective and provided 2 h of complete repellency.

Plant essential oils are widely used as fragrances in cosmetics, food additives, household products and medicines. The US Food and Drug Adminstration (FDA) generally recognizes these as safe. The essential oil obtained from *Zanthoxylum limonella* has found to possess mosquito repellent properties against different mosquito vectors (Das et al., 2003, Trongtokit et al.. 2005). Itthipanichong et al. (Itthipanichong et al.. 2002) have reported the chemical compositions of the essential oil distilled from the fruit of *Z Limonella* in Thailand and found the presence of 33 chemical components. Limonene (31.1%), terpin-4-ol (13.9%) and sabinene (9.1%) have been found to be the major components. They have also reported that the essential oil from the fruit of this plant possessed a stimulatory effect on smooth muscle preparations by non-specific mechanisms.

Although plant based essential oil fulfill important criteria as mosquito repellents, their repellency is lower in terms of efficacy and duration of protection when compared to their synthetic counterparts such as DEET (N,N-diethyl-m-toluimide) (Isman et al., 2006). On the other hand. essential oils undergo undesirable deterioration by heat, humidity, light and oxygen (Edris and Bergnstahl, 2001). High volatility of essential oil components has resulted in short protective duration against mosquitoes and so protection period provided by essential oils against mosquito can be improved by developing a formulation that would fix the oil onto skin for an appropriate time (Pitasawat et al., 2007). Improved efficacy of plant-derived topical repellent product after formulation with some bases or fixative materials such as paraffin (Oyedele et al., 2002). vanillin (Tawatsin et al., 2001), mustard and coconut oils (Das et al., 1999), salicyluric acid (Stuart and Estambale, 2003) has been reported. Various formulations such as the ones based on creams, polymer mixtures. or microcapsules for controlled release have been found to increase the duration of repellency (Gupta and Rutledge. 1989, Gupta and Rutledge, 1991, Sharma and Ansari. 1994. Dua et al., 1996, Nentwig, 2003).

Controlled release by microencapsulation seems to be the best way to protect essential oil from environmental damage and thus ensuring a longer shelf life and consequently longer duration of protection against mosquito vectors. Microencapsulation is a growing field that is finding application in many technological disciplines. A wide range of core materials have been encapsulated. These include adhesives, liquid crystals. repairing agents, phase change materials (PCMs), agrochemicals, catalysts, living cells, flavor oils, pharmaceuticals, vitamins, and water (Rosenberg et al.. 1990, Hussain and Maji, 2008, Augustin et al., 2001, Heinzen, 2002). There are

151